Fakultät Maschinenbau
fortschritt studieren

RUHR UNIVERSITÄT BOCHUM

RUB

Critical Assessment and Investigation of the Ti-Al-X (X = Si, Zr, O) Systems

Dissertation
zur
Erlangung des Grades
Doktor-Ingenieurin

der

Fakultät für Maschinenbau

der Ruhr-Universität Bochum

von

Zahra Kahrobaee

aus

Semnan, Iran

Bochum 2023

Acknowledgments

Author contribution statement

The chapters of this thesis are based on published papers and extended abstracts, in which the contributions of authors are as follows:

1. **Kahrobaee, Z.**; Palm, M.: Experimental Investigation of Ti–Al–Si Phase Equilibria at 800-1200 °C. Journal of Alloys and Compounds 924, 166223 (2022). https://doi.org/10.1016/j.jallcom.2022.166223

   - Corresponding author: **Zahra Kahrobaee**; data curation, conducting experiments and analyses, writing original draft, and visualization.
   - Martin Palm: Conceptualization, validation, writing review, supervision, project administration and funding acquisition.

2. *Extended abstract:* **Kahrobaee, Z.;** Palm, M.: Determination of phase equilibria in the Ti–Al–Si system at 800–1200 °C. In: Proceedings Intermetallics 2021, pp. 78 - 79. Intermetallics 2021, Bad Staffelstein, Germany, October 04, 2021 - October 08, (2021). IM2021_Proceedings.pdf (intermetallics-conference.de)

   - Contributions same as above (item 1).

3. **Kahrobaee, Z.**; Palm, M.: Critical Assessment of the Al–Ti–Zr System. Journal of Phase Equilibria and Diffusion 41, pp. 687 - 701 (2020). https://doi.org/10.1007/s11669-020-00837- x. Selected as the **Editor's Choice Awards** for 2020

   - Corresponding author: **Zahra Kahrobaee**; assessment of the literature, writing original draft, visualization and analyses.
   - Martin Palm: Conceptualization, validation, writing review, and supervision.

4. **Kahrobaee, Z.**; Rashkova, B.; Hauschildt, K.; Palm, M.: Experimental Investigation of Phase Equilibria in the Ti–Al–Zr system at 1000-1300 ° C, Crystals 12, pp. 1184 (2022). https://doi.org/10.3390/cryst12091184

   - Corresponding author: **Zahra Kahrobaee**; data curation, performing experimental investigations and conducting analyses, writing original draft, and visualization.
   - Boryana Rashkova: TEM analyses, review and editing, and project administration.
   - Katja Hauschildt: HE-XRD investigations and analyses, review and editing.

- Martin Palm: Conceptualization, validation, writing review, supervision, project administration and funding acquisition.

5. *Extended abstract:* **Kahrobaee, Z**.; Stein, F.; Palm, M.: Experimental evaluation of the isothermal section of the Ti–Al–Zr ternary system at 1273 K. In: Proceedings Intermetallics 2019, pp. 174 - 175. Intermetallics 2019, Bad Staffelstein, Germany, September 30, 2019 - October 04, (2019). IM2019_Proceedings.pdf (intermetallics-conference.de)

   - Corresponding author: **Zahra Kahrobaee**; assessment of the literature, writing original draft, visualization and analyses.
   - Frank Stein: Review, editing, and project administration.
   - Martin Palm: Conceptualization, validation, writing review, supervision, project administration and funding acquisition.

6. Ilatovskaia, M.; **Kahrobaee, Z.**; Omar, N. A. B.; Palm, M.; Schmitt, L.-Y.; Yang, Y.; Dreval, L.: Al–O–Ti Ternary Phase Diagram Evaluation, MSI Eureka, Watson, A. (Ed.) MSI, Materials Science International Services GmbH, Stuttgart (2022), pp 3-57.
   10.7121/msi-eureka-10.15250.2.9

   No corresponding author; manuscript supervised by Martin Palm and divided into sections, in which authors contributions are as follows:
   - Assessment of the literature, choice and discussion of binaries, writing and revising were done by all authors.
   - M. Ilatovskaia: Leading the assessment of the O-rich corner at temperatures > 1200 °C and section on vertical sections.
   - **Z. Kahrobaee**: Leading the assessment of the metal part at temperatures <1200 °C.
   - Yang Yang: Leading the assessment of thermodynamic data.
   - L.-Y. Schmitt: Leading the properties section.
   - N. A. B. Omar, L. Dreval: writing review and editing.

Abstract

New alloys that could operate at higher temperatures while having less weight are in ever-increasing demand, particularly in the transportation market. Advanced TiAl-based alloys are employed in the low-pressure turbine of advanced aircraft engines and in automobiles. Due to their lower density than Ni-base superalloys, which they have replaced, fuel consumption and emissions could be substantially reduced. However, to increase the engine operating temperature and thus overall efficiency even more, these alloys should be further improved.

The efficient development of alloys relies on the knowledge of phase equilibria in dependence on temperature. CALPHAD (CALculation of PHAse Diagram) modeling is a widely used method by which phase diagrams and phase transitions can be modelled. The present thesis was carried out in the framework of the ADVANCE project with contribution of four parties, i.e., Thermo-Calc Software AB, Max-Planck-Institut für Eisenforschung GmbH, Helmholtz-Zentrum Hereon (formerly known as Helmholtz-Zentrum Geesthacht), and Montanuniversität Leoben.

Utilizing the scanning electron microscopy (SEM), electron probe microanalysis (EPMA), conventional and high-energy X-ray diffraction ((HE-)XRD), differential thermal analysis (DTA), transmission electron microscopy (TEM), and atom probe tomography (APT) techniques on alloys heat treated at temperatures between 800-1300 °C, a new understanding of phase equilibria in the Ti–Al–X (X= Si, Zr, and O) systems has been established.

Five partial isothermal sections of the Ti–Al–Si system up to 70 at. % Al and 40 at. % Si have been experimentally determined between 800 and 1200 °C. Seven alloys were heat-treated for 24–1504 h and characterized. No ternary phase was found, and Ti_3Si was not detected in any of the alloys. In this temperature range αTi, βTi, Ti_3Al, TiAl, TiAl (One-dimensional Anti-Phase Structure (1d-APS)), $TiAl_2$, and $TiAl_3$ are in equilibrium with Ti_5Si_3. A partial vertical section at 9 at% Si shows that all determined data are consistent with each other. The precise solid solubilities of Al in Ti_5Si_3 and Si in the Ti–Al phases have been established which were the main unsettled points in the literature. Based on the results, the precise solid solubilities and therefore phase fractions at higher and lower temperatures can be extrapolated with CALPHAD calculations, specifically for Ti_5Si_3, which is essential in strengthening the alloys at high temperature

Investigation of the Ti–Al–Zr system started with a thorough assessment of the literature. Two partial isotherm sections at 800 and 1000 °C were assessed. However, more recent CALPHAD modellings show large discrepancies with the available experimental evidence. Therefore, new

experimental investigations were necessary. Four partial isothermal sections of the Ti–Al–Zr system up to 60 at. % Al and 30 at. % Zr were experimentally established between 1000–1300 °C. Six heat-treated alloys were analysed. Phase equilibria were determined between B2-ordered (β_0), βTi,Zr, αTi, Ti_3Al, TiAl, and $ZrAl_2$. The results give a new understanding of phase equilibria in the Ti–Al–Zr system between 1000 and 1300 °C. Phase equilibria at all temperatures are different from the ones established before. While previous isothermal sections showed a large solid solubility of Ti in Zr_5Al_3, it is now clear that this phase is stabilized by impurities, especially oxygen. Additionally, it is now clear that B2-ordered β_0 already exists at 1000 °C and remains stable up to at least 1300 °C. The new findings can now be used for improving the CALPHAD database, specifically for precisely modelling the solid solubility of Zr in TiAl and Ti_3Al, which is essential for the development of new TiAl-based alloys.

Knowledge of the Ti–Al–O system is crucial also for all other Ti–Al–X systems because oxygen has a strong effect on phase equilibria in the Ti–Al system. Therefore, an assessment of the complete system has been carried out in in the framework of Materials Science International Team´s (MSIT) Ternary Evaluation Program (http://www.msiport.com/msi-research/ternary-evaluations/), which provides four partial assessed isothermal sections from 945-1200 °C. However, comparison of the newly assessed isothermal sections with those calculated with the existing version of the CALPHAD database showed discrepancies and emphasized the necessity of new experimental investigations. Five alloys were produced and heat-treated between 800-1100 °C. However, it was found that the oxygen content in the Ti–Al phases cannot be measured by EPMA. As APT could only be employed to measure one sample, the experimental investigations concentrated on alloys heat treated at 1100 °C. From the established results and current data reported in the literature it was still possible to revise the assessed isothermal section at 1100 °C, most prominently that the solubility of oxygen in TiAl is substantially lower than anticipated.

By implementing the outcome of the present ADVANCE project into the CALPHAD database, the phase stability and phase transformation temperatures, window for thermomechanical processing can be better predicted, thereby providing a roadmap for the development of future products.

Table of content

Table of figures

List of Tables

List of Abbreviations

Abb./Acronym	Description
APB	**A**nti-**P**hase **B**oundary
APT	**A**tom **P**robe **T**omography
BSE	**B**ack **S**cattered **E**lectron
BCC	**B**ody **C**entered **C**ubic
BF	**B**right-**F**ield
CALPHAD	**Cal**culation of **PHA**se **D**iagrams
DFT	**D**ensity **F**unctional **T**heory
DESY	**D**eutsches **E**lektronen **SY**nchrotron
DTA	**D**ifferential **T**hermal **A**nalysis
ED	**E**lectron **D**iffraction
EPMA	**E**lectron **P**robe **M**icro**A**nalyses
EDS	**E**nergy-**D**ispersive X-ray **S**pectroscopy
FIB	**F**ocused **I**on **B**eam
GE	**G**eneral **E**lectric
HEMS	**H**igh-**E**nergy **M**aterials **S**cience
HE-XRD	**H**igh-**E**nergy **XRD**
ICP-OES	**I**nductively **C**oupled **P**lasma **O**ptical **E**mission **S**pectroscopy
ICDD	**I**nternational **C**entre for **D**iffraction **D**ata
LDE	**L**ayered **D**iffracting **E**lements
LPT	**L**ow-**P**ressure **T**urbine
Mac	**M**ass **a**bsorption **c**oefficient
MSI(T)	**M**aterials **S**cience **I**nternational (**T**eam)
MTU	**M**otoren und **T**urbinen **U**nion GmbH
1d-APS	**One**-**d**imensional **A**nti-**P**hase **S**tructure
PETRA III	**P**ositronen-**E**lektronen-**T**andem-**R**ing-**A**nlage **III**
PHA	**P**ulse-**H**eight **A**nalyser
RT	**R**oom **T**emperature
SEM	**S**canning **E**lectron **M**icroscopy
SXES	**S**oft **X**-ray **E**mission **S**pectroscopy
TCSAB	**T**hermo-**C**alc **S**oftware **AB**

Abb./Acronym	Description
TNB	**T**i–45Al–(5-10) **N**b–(0-0.5)**B**, C at. % commercial alloy
TNM	**T**i–43.5Al–4**N**b–1**M**o–0.1B at. % commercial alloy
TEM	**T**ransmission **E**lectron **M**icroscopy
WDS	**W**avelength **D**ispersive **S**pectroscopy
XRD	**X**-**R**ay **D**iffraction

1. Introduction

The world is changing at an ever-increasing pace, and along with that concerns are arising with unprecedented climate changes and volatile energy crises. We require rapid developments in designs, technologies and innovative materials in different fields to face the emerging challenges.

Only air transport, as of 2018, generates about 895 million tons CO_2 emissions and accounts for about 3 % of total man-made climate impact when considering CO_2 and non-CO_2 emissions, i.e. NO_x, water vapor, and sulfate particles [1]. To decrease their environmental effect, further investigations are needed to develop energy-efficient and clean aero engines, which consume less fuel and emit less contamination. It is known that the efficiency of a gas turbine is closely related to its operating temperature. For instance, the operating efficiency increases by over 1 % for every 10 K increase in the turbine inlet temperature [2]. Therefore, investigations focus on developing alloys that tolerate higher service temperatures and reduce the weight of engine components [2, 3].

Intermetallic materials based on titanium aluminides are an attractive class of structural materials primarily due to their low density (3.9-4.2 g/cm^3), high specific yield strength, good oxidation and creep resistance, along with resistance against ignition [2, 3]. Therefore they are good candidates for weight saving in the hot sections of jet engines up to 1000 °C by replacing Ni-base superalloys of almost twice the density (7.7 - 9.0 g/cm^3) [4, 5].

The Ti–Al phase diagram (**Figure 1.1**) shows the existence of several intermetallic phases. Structural materials of interest are alloys that contain 42-48 Al at. %, which comprise TiAl (γ) (ordered face-centered tetragonal $L1_0$), and Ti_3Al (α_2) (ordered hexagonal $D0_{19}$) [2, 6] microstructures. According to the phase diagram (**Figure 1.1**), these alloys solidify through βTi (body-centered cubic A2), αTi (hexagonal close-packed A3) or peritectic transformation. The solidification path is very sensitive dependent on the composition, in that already small differences in the Al content can alter the solidified microstructure and texture. Additionally, in these alloys βTi and/or αTi occur at high temperatures, which can yield different microstructures depending on the cooling rate [2]. These features allow to attain various microstructures based on alloy composition, processing route and applied heat treatments [3, 6]. Tailoring the microstructure, thus improving the mechanical properties, is the main idea behind developing TiAl (γ)-based alloys.
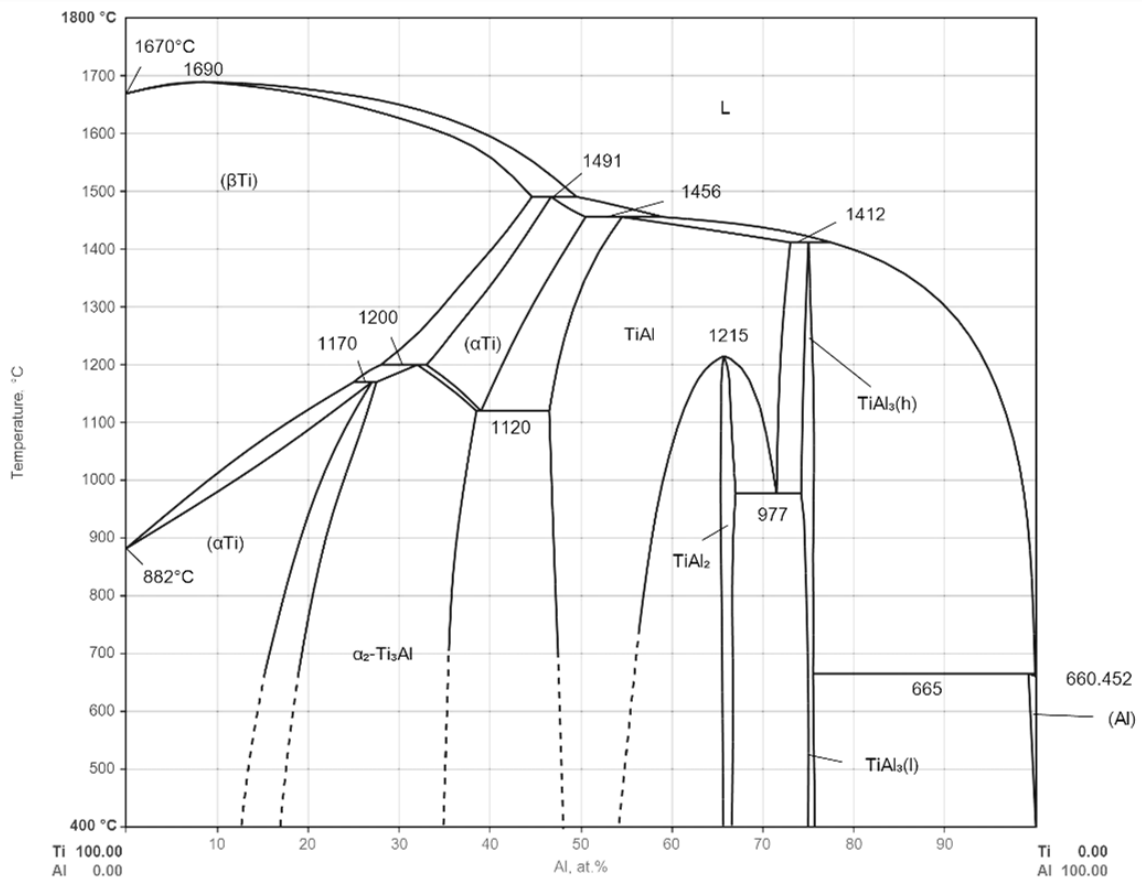
Figure 1.1. The assessed Ti–Al phase diagram from [7].

The development of TiAl-based alloys for commercial aero engines started more than thirty years ago [8]. As the early TiAl-based alloys had no or little ductility at room temperature or at moderate temperatures, i.e. from 20 to about 550 °C, their application was restricted [5]. In 1989 Huang [9] from General Electric (GE) invented new TiAl-alloys by alloying with Nb and Cr [9], later being famous as Ti-48(Al)-2(Nb)-2(Cr) and classified as the second generation of TiAl-based alloys [3, 8, 10]. These alloys, which mainly consisted of the two-phase microstructure TiAl (γ) + Ti$_3$Al (α_2) [6], showed an improved ductility (1-3 %) compared to common TiAl-based alloys at low temperatures [5], making industrial fabrication possible. Ninety-eight cast low-pressure turbine (LPT) blades of this composition were used in the test engine CF6-80C and succeeded 1500 engine cycles, by that initiating the implementation of TiAl-alloys in aero engines [11]. In 2006, GE implemented 48-2-2 LPT blades in commercial GEnx^{TM} aero engines [8]. By the year 2016, there were approximately 119,000 48-2-2 TiAl-LPT blades flying daily on different aircrafts [8] and contributed a significant reduction of 20 % in fuel consumption, 80 % in NO$_x$ emission, and 50 % reduction in perceived noise [8].

The second generation of TiAl-alloys yielded better room temperature ductility, and fracture toughness [3]. However, demand for more efficiency required alloys, which could be operated at even higher temperatures. As a result, the third generation of TiAl-alloys with higher Nb contents and additional alloying elements was developed [8, 10]. Among them, the very well-known alloys are TNM (Ti–43.5Al–4Nb–1Mo–0.1B at. %) [12] and TNB (Ti–45Al–(5-10) Nb–(0-0.5)B, C at. %) [2]. When applying proper thermo-mechanical processing and heat treatment, these class of TiAl-based alloys could reach strength levels of higher than 1000 MPa at room temperature [3]. Compared to the second generation of TiAl-based alloys, third generation alloys exhibit about 66% higher specific strength (approx. 250 MPa/gr.cm^{-3}) while maintaining their mechanical properties up to 850 °C [13, 14]. In 2015, MTU Aero Engines declared the implementation of the third generation of TiAl-based alloys produced by Leistritz Turbinentechnik GmbH in commercial Airbus A320neo engines for the last LPT stage of the new geared turbofan (GTF™) engine [15, 16].

Besides for application in aero engines, TiAl-based alloys have attracted attention in the automotive industry for a longer time. Primarily, TiAl-based alloys are employed in turbochargers in order to improve the combustion efficiency, which ultimately mitigates toxic emissions from the exhaust system [17]. Because the turbo wheel is exposed to high centrifugal stress during rotation, a material with high specific strength is desirable to facilitate rotation and thereby improving engine response [17]. By the end of the 20th century, Mitsubishi replaced the Ni-based superalloy Inconel 713C with TiAl-based alloys for the manufacturing of passenger vehicle turbochargers in their Lancer 6 sports cars [18]. Currently, TiAl-based turbochargers are only used in diesel engines, where application temperatures are up to 800-850 °C. In order to use TiAl-based alloys in gasoline engines, they should be further developed to endure higher temperatures, i.e. 900-950 °C [19, 20]. Also, for many years thermo-mechanically produced valves were employed in formula one racing, however, the production of TiAl-based valves by this route was far too expensive for passenger vehicles. Since then, attempts have been undertaken to develop cast TiAl-based valves, however, they were never commercially implemented [21].

As stated above, to extend the use of TiAl-based alloys, further improvements are needed to develop alloys that can be applied at temperatures above 850 °C, which emphasizes on particularly increasing the creep and oxidation resistance of the current alloys [10].

Advanced TiAl-based alloys are mainly produced by ingot or powder metallurgy followed by thermomechanical working and subsequent heat treatments [3]. To attain desired mechanical properties, the microstructure has to be carefully tailored. For instance, Ti-48Al at. % heat-treated at 1300 °C comprises a duplex microstructure, i.e. a combination of TiAl (γ) grains with fine lath of TiAl (γ)/ Ti$_3$Al (α_2), and yields about 2 % plastic fracture strain at room temperature. If the same composition is heat-treated only 50 °C lower, it consists of single-phase TiAl (γ) grains and the alloy shows no plastic fracture strain [22]. Therefore, for the design of a microstructure which yields the desired mechanical behavior, the knowledge of phase equilibria is crucial, i.e. the stability of individual phases and phase transformations in dependence on composition and temperature.

However, commercial TiAl-alloys can contain up to eight alloying elements [6], and each alloying element alters the phase equilibria. Fortunately, with the development of the CALPHAD method (CALculation of PHAse Diagram) by Kaufman and Ansara in the 1970s, phase equilibria of higher order systems can be attained from thermodynamic calculations [23].

In the CALPHAD method, thermodynamic properties such as the Gibbs energy of each phase are described by a mathematical model with adjustable parameters. The models are constructed based on the available experimental data. The parameters are then adjusted by optimizing the fit of the model to the experimental results, e.g. the constituent phases, their phase fractions, and the compositions of coexisting phases at a certain temperature. With optimized parameters, one can calculate all phase equilibria and extrapolate them to compositions and temperatures, at which no experimental results are available. Therefore, the reliability of CALPHAD-type calculations is inevitably dependent on the availability and reliability of experimental data [24].

A very good example, where knowledge of the phase diagram and application of the CALPHAD method assisted and speeded up the evolution of advanced TiAl-based alloys, is the development of TNM^{TM} alloys by Clemens et al. [6, 12]. The CALPHAD method was employed for the prediction and "expressing trends" of the constituent phases and transition temperatures in different compositions. Constituent phases and phase fractions were optimized to improve the workability at elevated temperatures. However, as stated by these authors and reported in several studies [10, 25-27], current CALPHAD databases cannot describe transition temperatures and phase proportions quantitatively in the third generation of TiAl-based alloys.

One of the strengths of the CALPHAD method is that it can utilize the thermodynamic descriptions of subsystems and extrapolate them to higher order systems, and it is usually

sufficient to have the correct description of the ternary systems [28]. Therefore, it is essential to have accurate and reliable experimental data of the ternary sub-systems to adjust the thermodynamic parameters in the CALPHAD database. The deficiencies in CALPHAD modelling of higher-order Ti–Al–X–Y–… systems therefore stem from missing or unreliable experimental data in the underlying Ti–Al–X systems [10].

Generating experimental data for Ti–Al–X systems is exceptionally challenging. Some of the difficulties for instance are:

- Ti–Al–(X) phase equilibria are extremely sensitive to contaminations (i.e. O, N, C), especially oxygen. Contaminations can shift/change the phase equilibria, particularly those involving βTi, αTi or Ti$_3$Al [29-31]. **Figure 1.2** shows the effect of various oxygen contents on phase equilibria among βTi and αTi. As Ti–Al–(X) alloys are prone to oxygen uptake, this can easily occur during casting and heat treatments at elevated temperatures.

- Some phase transformations cannot be suppressed even by quenching, e.g. βTi $\rightarrow$ αTi or αTi $\rightarrow$ Ti$_3$Al [29]. As phase characterizations are usually performed at room temperature, identifying the phases that were present at high temperature requires complementary experiments.

- Some microstructures are "destroyed" through massive transformation during cooling to room temperature, e.g. αTi $\rightarrow$TiAl or βTi $\rightarrow$ O-phase (orthorhombic phase) [29, 32].
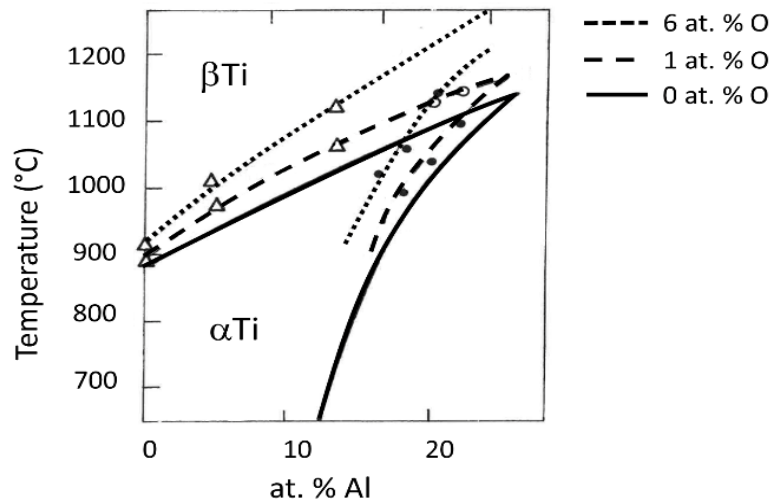
Figure 1.2. Phase equilibria among binary βTi and αTi and in dependence on different oxygen contents according to [31].

In view of the above-mentioned challenges the project ADVANCE was proposed in 2018. ADVANCE is a large-scale international collaborative project between Thermo-Calc Software AB (TCSAB), Sweden, Max-Planck-Institut für Eisenforschung GmbH, Germany, Helmholtz-Zentrum Hereon (formerly Helmholtz-Zentrum Geesthacht), Germany, and Montanuniversität Leoben, Austria [33]. The objective of ADVANCE is to optimize the CALPHAD database for Ti–Al-based alloys. A critical analysis of the then existing cutting-edge CALPHAD database TCTI1 [34] supplied by TCSAB, identified the missing or unreliable data for several important Ti–Al–X(–Y) systems. Based on this critical analysis, eight ternary and two quaternary systems, i.e. Ti–Al–X (X = Nb, Mo, W, O, B, Zr, C, Si)–Y (X = Nb, Y = Mo, W) were chosen for detailed investigation. Experimental investigations focused on the Ti–Al side of the systems and the generated data are used to update the existing thermodynamic database for the development of TiAl-based alloys. The ADVANCE project was performed within the Clean Sky 2 initiative [35], a European joint undertaking which aims to reduce aircraft noise, CO_2 and NO_x emissions by 20 to 30 % compared to the state-of-the-art aircrafts entering into service as of 2014.

Within this thesis, the results for the Ti–Al-rich sides of the three ternary systems Ti–Al–X (X = Si, Zr and O) are presented. Work on all systems started with performing a critical assessment of the system. This does not only include a literature review, but also a critical judgement of all available experiments, critical analysis of the existing isothermal and vertical sections, e.g. whether they contain violations of thermodynamic rules which indicate problems in the underlying data, and then establishing new isotherms and isopleths from the analyzed data,

which are updated to the accepted binaries [36]. The outcome of such an assessment are the standard reference phase diagrams for that system for the upcoming years, which also can be used for optimizing a CALPHAD database.

The Ti–Al–Si system has been the subject of studies for many years. The system was thoroughly assessed within the MSI Ternary Phase Diagram Evaluation scheme [37, 38], in which references up to the year 2002 have been considered, and later on by Raghavan [39, 40], covering references up to 2008. Because of the industrial importance of Al–Si casting alloys, many investigations focused on the Al-rich side of the system. Only in the last decades with the emergence of TiAl-based alloys, the Ti-rich side of the system became attractive. Si has a limited solid solubility in the Ti–Al phases, and therefore the formation of silicides is encouraged [2]. Through proper heat treatments, silicides precipitate incoherently at the Ti_3Al/TiAl lamellar interfaces, thereby improving the creep resistance [41, 42]. The stable silicide that forms at the Ti-rich side of the Ti–Al–Si system is hexagonal Ti_5Si_3 (space group $P6_3$/mmc). Excess amounts of Si lead to the formation of large hexagonal Ti_5Si_3 precipitates, which deteriorate the ductility and creep resistance of the alloy [2]. To attain fine precipitates, that are evenly dispersed in the microstructure, the phase fraction of Ti_5Si_3 at individual temperatures has to be carefully adjusted. Phase fractions in two-phase microstructures are calculated by applying the lever rule and in order to be able to do this, knowledge of the precise compositions of the phase at a certain temperature is a prerequisite [43]. Hence, the solid solubility of Si in the Ti–Al phases and the Al solid solubility in Ti_5Si_3 have to be accurately known. Despite numerous studies, there are still discrepancies between phase equilibria established in different studies and also for the solid solubilities in individual phases. For instance for the solid solubility of Si in TiAl at 1000 °C, reported data vary between 0.1 [44] and about 3 at.% [45, 46] and data for the solid solubility of Al in Ti_5Si_3 were reported between 2 [47] and up to more than 20 at. % [48-50]. Therefore, new experimental results are necessary to settle these discrepancies. **Chapter 3** is dedicated to the Ti–Al–Si system, in which the literature is debated and where the new experimental results for phase equilibria up to 70 at. % Al and 40 at. % Si are presented and discussed.

The addition of Zr to Ti–Al alloys can stabilize disordered βTi, which improves the strength and corrosion resistance [51]. In addition, solid solution hardening of TiAl increases strength at all temperatures [52] and therefore Zr was introduced in the newly developed TNM AM alloy (TNM alloys adopted for additive manufacturing (AM)) [53]. Of the three systems investigated within this study, Ti–Al–Zr is the one for which the least experimental results are

available. The last assessment of the literature of the Ti–Al–Zr system was done a long time ago in the framework of MSIT by Tretyachenko, covering the literature up to 2003 [54]. From 2014 onwards, complete isothermal sections for the Ti–Al–Zr system have been determined. Before then, there had been several investigations, but those results are in contradiction with the more recently published isothermal sections. The main reason is that establishing phase equilibria within this system is even more challenging, as Zr is highly susceptible to oxygen uptake and, as it has a high melting point and low diffusivity, quite long annealing times are necessary to attain equilibrium even at high temperatures [55, 56]. And the fact that even "high-purity" Zr contains comparable high amounts of impurities [57, 58], specifically Hf, is most of the time neglected. As the last assessment was performed more than fifteen years ago, a new critical assessment of the Ti–Al–Zr system is presented in **chapter 4.1**. The critical assessment clarified the gaps in the previous experimental results, which are partially covered by the new experimental work presented in **chapter 4.2**.

Titanium aluminides have attractive properties at high temperatures and therefore reactions and phase equilibria with oxygen are an important issue [2]. In practice, a mixture of $TiO_2 + Al_2O_3$ forms the oxide scale on the TiAl-based alloys [59]. To achieve a good oxidation resistance, development of a continuous layer of dense α-Al_2O_3 (alumina) is essential and the formation of titanium oxides, which grow quickly and give very poor protection, should be avoided. In order to design oxidation resistant alloys, the stability of oxides in equilibrium with the binary Ti–Al system must be known. Oxygen also has a strong influence in shifting certain phase boundaries (**Figure 1.2**) and it is also therefore that the solid solubility of oxygen in individual phases has to be precisely known.

The Ti–Al–O system has been evaluated by Hoch & Lin [60], covering references up to 1988. The only other assessment of the system [61] covers references up to 1998. Through a collaboration with MSIT, an assessment of the complete Ti–Al–O system has been conducted. The part of this assessment that has been led by the present author and which includes phase equilibria of the Ti–Al phases with Al_2O_3 are shown in **chapter 5**.**1**. Experimental results and specific difficulties in determining the exact oxygen content in the Ti–Al phases are discussed within **chapter 5.2.**

2. Materials and Methods

2.1. Materials synthesis

From elements of high purity (Ti: 99.995 %; Al: 99.999 %; Si: 99.99 %; Zr: 99.95 %; HMW Hauner GmbH and Co. KG; and TiO: 99.92 Patinal® Merck KGaA) seven alloys in the Ti–Al–Si system, six alloys in the Ti–Al–Zr system, and five alloys in the Ti–Al–O system were prepared by crucible-free levitation melting (Fives Celes Groups) [30] or advanced arc melting (PINK GmbH Vakuumtechnik). These techniques have been chosen in view that phase equilibria in Ti–Al(–X) are crucially affected by impurities, especially oxygen [29]. Melting was performed under Ar flow, which was purified using Oxy- and Hydrosorb (ZPure M™ 3800cc, Chromatography Research Supplies) to remove remaining oxygen and moisture. In contrast to conventional arc melters, the advanced device is equipped with a manipulator which allows overturning the solidified material without opening the device, thereby maintaining a good vacuum during the whole melting process. This allows re-melting the alloy for multiple times to ensure chemical homogeneity. Moreover, the alloys do not solidify on the cold copper hearth but are cast into a Cu mold. Advanced arc melting has been used for alloys S2, S3, and the Ti–Al–O alloys (**Table 2.1**), which could not be fully molten by levitation melting. The alloys nomenclatures are given in **Table 2.1**; in which, the Si containing alloys were called S, the Zr containing Z, and the oxygen containing O. Intact rods of 15-18 mm in diameter and 150 mm in length were produced by both methods by casting into cold copper molds. However, the Ti–Al–O alloys were rather brittle and especially the alloys O6 and O8 broke into smaller pieces during cooling.

Overall compositions of the alloys and impurity contents have been determined by wet-chemical analysis, employing inert gas fusion (NCS Fusion Master ONH) for oxygen and nitrogen, combustion gas analysis (NCS Combustion Master CS) for carbon, and inductively coupled plasma optical emission spectroscopy (PerkinElmer Optima 8300 ICP-OES) for all other elements. The results are summarized in **Table 2.1**. Typical carbon contents are between 70-160 wt. ppm and nitrogen is below the detection limit of 50 wt. ppm. Oxygen contents vary between different systems. The average oxygen uptake in the Ti–Al–Zr alloys (290 wt. ppm) is somewhat higher than in the Ti–Al–Si alloys (170 wt. ppm). The difference stems from the higher affinity of Zr to oxygen compared to Si. In order to check the homogeneity of cast alloys, wet-chemical analysis of slices taken from the top and bottom of selected alloys were carried out, which showed that alloys were usually homogeneous within standard error (**Table 2.1**).

For heat treatments at 800-1100 °C, slices of the alloys were encapsulated in high-purity quartz capsules back-filled with Ar and using Ti as a getter. Heat treatments at 1200 °C, where quartz capsules are not any longer gas-tight [62], were performed under flowing dry Ar using a double-crucible technique [30, 63]. After annealing all samples were quenched in brine to room temperature (RT) by breaking the ampule/crucible. The durations of individual heat treatments in the various systems are listed in **Table 2.2**.

After heat treatment, wet-chemical analyses were performed on selected samples to check the impurity uptake, which revealed only small increases in the oxygen content (**Table 2.3**). Additionally, overall compositions of some samples were measured after heat treatment, specifically to inspect for preferential evaporation of Al, which in fact did not occur (**Table 2.3**). The difference in the Zr content in alloy Z4 between analyses of the as-cast (**Table 2.1)** and the two heat-treated samples (**Table 2.3**) hints to some inhomogeneity within this alloy, which has been considered when determining phase equilibria.

Table 2.1. Nominal compositions and wet-chemical analyses of the as-cast alloys; the column "Device" indicates if the alloy is produced by levitation melting (Lev.) or advanced arc melting (Arc). For alloys indicated by asterix (*), analyzed compositions are an average of two measurements from slices cut from the top and bottom of the alloy

Alloy	Nominal comp. (at. %)			Device	Analyzed comp. (at. %)			Impurity (wt. ppm)		
	Ti	Al	Si		Ti	Al	Si	O	N	C
S1	40	50	10	Lev.	37.5	55.0	7.5	110	<50	92
S2	45	45	10	Arc	43.5	47.4	9.1	260	<50	100
S3	50	40	10	Arc	50.7	40.4	8.9	430	<50	120
S4	60	30	10	Lev.	60.2	32.7	7.1	85	<50	75
S5	70	20	10	Lev.	71.0	20.4	8.6	70	<50	97
S6*	75	15	10	Lev.	75.8 ± 0.06	14.7 ± 0.04	9.5	105	<50	110 ± 22
S7*	80	10	10	Lev.	80.7 ± 0.1	9.7 ± 0.04	9.6 ± 0.1	130	<50	129 ± 1

Alloy	Nominal comp. (at. %)			Device	Analyzed comp. (at. %)			Impurity (wt. ppm)		
	Ti	Al	Zr		Ti	Al	Zr	O	N	C
Z1	70	20	10	Lev.	69.3	20.6	10.1	350	<50	110
Z2	62.5	27.5	10	Lev.	63.2	27.4	9.4	370	<50	160
Z4	45	40	15	Lev.	44.0	40.8	15.2	340	<50	137
Z5*	50	45	5	Lev.	48.8 ± 0.2	46.1 ± 0.3	5.1 ± 0.01	110 ± 30	<50	127 ± 10
Z6	45	45	10	Lev.	44.7	45.1	10.2	400	<50	120
Z7	40	45	15	Lev.	37.0	47.3	15.7	180	<50	79

Alloy	Nominal comp. (at. %)			Device	Analyzed comp. (at. %)			Impurity (wt. ppm)		
	Ti	Al	O		Ti	Al	O		N	C
O3	45	42.5	12.5	Arc	55.5	37.2	7.3		<50	120
O4	55	40	5	Arc	55.7	38.8	5.5		<50	120
O5	75	20	5	Arc	75.0	19.5	5.5		<50	71
O6	70	20	10	Arc	69.2	19.2	11.6		<50	110
O8	67.5	17.5	15	Arc	65.8	16.4	17.8		<50	110

Table 2.2. Duration of heat treatments within individual systems

Annealing temp. (°C)	800	900	1000	1100	1200	1300
System			Duration (h)			
Ti–Al–Si	1000	1000-1504	1000	200	24	24
Ti–Al–Zr	-	-	100-1000	200	24	24
Ti–Al–O	1000	500	100	200	-	-

Table 2.3. Wet-chemical analyses of the alloys after various heat treatments; n.d.: not determined

Alloy	Condition	Ti (at. %)	Al (at. %)	Si (at. %)	O wt. ppm	N wt. ppm	C wt. ppm
S1	1100 °C/ 165 h	n.d.	n.d.	n.d.	440	<50	110
S6	800 °C/ 1000 h	75.2	15.2	9.6	190	<50	120
S6	900 °C/ 1000 h	n.d.	n.d.	n.d.	230	<50	130
S7	800 °C/ 1000 h	80.2	10.1	9.7	180	<50	118
S7	900 °C/ 1000 h	n.d.	n.d.	n.d.	140	<50	100

Alloy	Condition	Ti (at. %)	Al (at. %)	Zr (at. %)	O wt. ppm	N wt. ppm	C wt. ppm
Z2	1000 °C/100 h	61.8	28.4	9.8	510	<50	147
Z4	1000 °C/100 h	38.8	44.7	16.5	455	<50	111
Z4	1300 °C/24 h	40.6	43.3	16.1	300	<50	89
Z5	1000°C/100 h	48.8	46.1	5.1	200	<50	100
Z6	1300 °C/24 h	45.1	44.6	10.3	480	<50	89
Z7	1300 °C/24 h	38.1	46.6	15.3	240	<50	77

2.2. Materials characterizations

Microstructures were inspected using a SEM (Zeiss LEO 1550 VP) on metallographically prepared samples. The samples were hot embedded (PolyFast, Struers) and ground with abrasive SiC paper from 220 to 4000 grit. They were then polished with polishing cloth 3/1 µm using diamond suspension followed by final vibro-polishing (VibroMet™ 2 Vibratory Polisher, Buehler) employing non-crystallizing colloidal silica polishing suspension (MasterMet2, Buehler). The SEM was operated at 15 kV with varying working distance of 6-8 mm.

Phases were identified by XRD (Bruker Advance D8-A25-X1-1) using powders. Quenched samples were crushed in a steel mortar and sieved to obtain a particle size of <90 μm. The powder was then fixed to a glass slab with hairspray, which does not give any additional reflections. XRD measurements were performed in Bragg-Brentano geometry in the range of $20° < 2θ < 120°$ using Co-Kα ($λ = 0.178897$ nm) radiation. Using a Lynxeye 1D detector, the intensity of the diffracted beam was measured. Phases were identified using the X'Pert HighScore software together with the Powder Diffraction File ^{TM} (PDF-2) provided from the International Center for Diffraction Data (ICDD) [64]. Lattice constants were calculated using the software TOPAS (Bruker AXS-Version 5).

Compositions of the coexisting phases were established with EPMA (JEOL JXA-8100) using metallographic sections. To check the presence of any impurities, qualitative analyses were performed at 15 kV, 400 nA with a beam width of 3 μm. For quantitative analysis, in case of Ti–Al–Si/ –Zr samples, standards of the pure elements have been used and analyses were performed at 15 kV, 20 nA with a focused beam. At least 12 measurements for each phase were carried out on at least five different places of the samples. Final compositions were obtained through ZAF matrix correction. Analyses were discarded if the total mass of Ti + Al + Si/ Zr was not in the range of 99 to 101 mass %. In a few cases, specifically for samples in the Ti–Al–Si system annealed at 800 °C, phases were so fine-scaled that within the spatial resolution of the EPMA a fraction of the measured composition may come from neighboring or underlying grains of another phase. In those cases, all analyses were plotted in a Gibbs triangle and only those data, which corresponded to the very end of a tie-line or the corners of a tie-triangle, i.e. the extreme values, were considered as equilibrium compositions. For these extreme values, no standard deviation can be given.

The EPMA measurements of samples in the Ti–Al–O system are discussed in more details in **section 5.2.2**. Prior to EPMA measurements of these samples, in order to prevent the formation of an instant oxide skin, Ar ion cleaning was done using a plasma cleaner (PECS Model 682 by Gatan) at 2 kV, 32μA, and 5 bar argon pressure, for five minutes.

Dr. Qing Ting from Max-Planck-Institut für Eisenforschung performed atom probe tomography (APT) on alloy O4 (heat-treated at 1100 °C/ 200h); a FEI Helios Nanolabs 600i FIB was used to prepare needle-like specimens from TiAl and Ti_3Al phases in this two-phase alloy. The APT specimens were sharpened with Ga-ions down to a ~50 nm radius, using a final energy of 5 kV and a current of 16 pA to remove regions severely implanted in Ga. APT was

conducted using a CAMECA LEAP® 5000 XS at following operating conditions: base temperature of 40 K, laser pulse energy of 40 pJ, pulse repetition rate of 200 kHz, and evaporation rate of up to 1.0%.

Phase transformation temperatures were measured on bulk samples by DTA (NETZSCH STA 449 F3 Jupiter, NETZSCH DSC 404C) under a stream of pure Ar and using alumina crucibles. Samples in as-cast and heat-treated condition were heated up to a maximum of about 1450 °C for at least two times and cooled down to room temperature at 10 K/min. Though all heating/cooling cycles were analyzed, reported transformation temperatures were usually evaluated from the first heating cycle. By calibration through the melting points of pure Al, Au and Ni, the experimental uncertainty was established to be ± 1 °C.

High-energy XRD (HE-XRD) was used to characterize phases in some Ti–Al–Zr samples in addition to XRD, specifically in case of low phase fractions. Ex-situ HE-XRD experiments were conducted at the High-Energy Materials Science (HEMS) beam-line [65] at DESY's synchrotron storage ring PETRA III in Hamburg, Germany, supervised by Dr. Katja Hauschildt from Helmholtz-Zentrum Hereon. With a photon energy of 100 keV (λ = 0.0124 nm) and a beam size of 1 mm^2, samples with a thickness of 5 mm were measured in transmission. The samples were rotated during the exposure time (100 s), by 20° or 180° to acquire better grain statistics. Diffraction patterns were recorded with a 2D PerkinElmer (Waltham, MA, USA) flat panel detector XRD 1621. Data evaluation was carried out by Dr. Katja Hauschildt. Data were integrated over 360° azimuthal angle using the program Fit2d [66]. The data were analyzed using the MAUD software package [67].

Transmission Electron Microscopy (TEM) was done at Montanuniversität Leoben by Dr. Boryana Rashkova on a few samples in the Ti–Al–Si and Ti–Al–Zr systems. Conventional TEM was applied using a Philips CM12 operated at 120 kV. Additionally, the chemical compositions of the phases were determined by energy dispersive X-ray spectroscopy (EDS) microanalysis using an EDAX system. TEM lamellae were prepared by ion milling carried out in a focused ion beam (FIB) Versa 3D from FEI (Thermo Fisher). The techniques are described in detail in [68, 69].

3. Ti–Al–Si system

Already at the beginning of the development of TiAl-based alloys it became clear that the addition of silicon improves the creep resistance of titanium aluminides [41, 42]. By fine Ti_5Si_3 precipitates, which pin the dislocations at the lamellar interface of the Ti_3Al and TiAl lamellae, the creep resistance is enhanced [41, 42]. Even low amounts of Si promote the formation of hexagonal Ti_5Si_3 through the eutectic reaction L $\leftrightarrow$ Ti_5Si_3 + βTi [45]. Ti_5Si_3 coexists with Ti–Al-rich phases from the early stages of solidification and also forms by various solid-state transformations in the system [45]. By proper heat treatments the desired microstructure with an optimum volume fraction of silicide can be obtained. For the design of an optimum microstructure, precise knowledge of the phase equilibria between Ti_5Si_3 and the binary Ti–Al phases, i.e. the exact solid solubility of Al in Ti_5Si_3 and of Si in Ti_3Al and TiAl in dependence on temperature, must be known.

For the experimental investigation of phase equilibria, it is important that the volume fraction and size of the phases in the equilibrated alloys is large enough, e.g. to be measured by EPMA. Therefore, alloys were investigated, which have higher Si contents compared to e.g. TNM alloys, which may have Si contents below 1 at. % Si [2, 10, 41]. However, alloys with higher Si contents solidify with primary Ti_5Si_3, which precipitates already at 2130 °C [45, 70] and grows in the melt during further cooling, resulting in coarse, idiomorphic hexagonal-shaped Ti_5Si_3 particles. The combination of strong bonding in Ti_5Si_3 and the complex hexagonal structure leads to low diffusion rates during solid-state transformations and therefore it is difficult to equilibrate or dissolve these coarse Ti_5Si_3 particles even during prolonged heat treatments. It is therefore that despite many investigations of the system especially for the precise solid solubilities of the coexisting phases contradictory results were reported.

In view of settling the phase equilibria in the Ti–Al–Si system, the phase equilibria between 800-1200 °C were investigated and the results are presented and discussed in the following chapter. The chapter is based on a published paper and an extended abstract by the current author [71, 72]. The introduction (**section 3.1**) points out the reasons why Si addition to the Ti–Al system became of interest and is followed by a thorough review of the literature focusing on Ti–Al-rich compositions (**Section 3.1.1**). The results of the present investigation are reported in **Section 3.2**, in which the chosen binary reference systems are also introduced and discussed. The investigations at fixed temperatures yielded partial isothermal sections between 800-1200 °C (**Sections 3.2.1** to **3.2.4**). Transformation temperatures determined by DTA yield

information for phase transformations and invariant reactions between the partial isothermal sections and at higher temperatures. Measured temperatures and how they were allocated to certain reactions are described in **Section 3.2.5**. From the combination of all the results and relevant data from the literature, a vertical section at 9 at. % Si between 800-1600 °C is established in **Section 3.2.6**, which also serves as a consistency check for all the obtained results. The specific focus of this study was to precisely determine Si solid solubilities in the Ti–Al-rich phases and of Al in Ti_5Si_3, that are discussed in **Sections 3.2.7-3.2.8**. For the Al solid solubility in Ti_5Si_3 calculated lattice constants in dependence on Al contents are plotted, which helps to solve the discrepancies between the current work and the literature. Finally, in **Section 3.2.9** the main findings of the present experimental investigation are summarized.

Sections 3.1 to 3.3 were published in Kahrobaee and Palm [71]. **Section 3.1** has been slightly shortened to fit the content of the chapter.

3.1. Introduction

The application of TiAl-based alloys in aero engines successfully decreased the amount of fuel consumption and gas emissions. This success was achieved due to the low density of TiAl-based alloys at application temperatures between 600-800 °C compared to Ni-based superalloys, which they have replaced [3]. However, as mentioned earlier, in order to enable even higher application temperatures, their creep and high-temperature oxidation resistance have to be improved which can be achieved through tailoring the microstructure and alloying [3, 59].

The oxide scale which forms on TiAl-based alloys is a multilayer that consists of TiO_2 and Al_2O_3 [3]. TiO_2 is porous and therefore cannot inhibit the metal surface from further oxidation. Alloying with Si can improve the oxidation resistance through different mechanisms. Si refines TiO_2 particles, which results in the formation of a more compact oxide scale [59]. Si also facilitates Al diffusion in the scale and hinders the outward diffusion of Ti^{4+}, thereby prohibiting further formation of TiO_2. About 10 at. % Si are sufficient for the preferential formation of Al_2O_3, which forms a protective oxide scale [73]. Even higher Si contents promote the formation of SiO_2 in the oxide scale. It is assumed that the lower diffusion coefficient of oxygen in SiO_2 compared to TiO_2 and the formation of a TiN layer between the base material and the oxide scale lead to a decrease in the oxidation rate [74, 75].

Moreover, Si is known to be beneficial in improving the creep resistance through the formation of fine-scaled Ti_5Si_3 precipitates [41, 42]. Adding about 0.3 at. % Si can lead to the formation of Ti_5Si_3 at the Ti_3Al/TiAl lamellar interface. Ti_5Si_3 particles substantially increase the creep resistance by hindering the movement of dislocations. For an alloy with about 0.6 at. % Si, a ten times lower creep rate has been achieved compared to its Si-free counterpart [41, 42]. On the other hand, a small excess amount of Si deteriorates the microstructure, thus reducing fracture toughness and creep resistance [41]. Though there is an apparent discrepancy between the optimum Si contents for improving creep and oxidation resistance at the same time only by Si, it was observed recently that of two alloys produced by powder metallurgy and containing 21 and 28 at. % Si, the alloy with the higher amount of Si showed a lamellar structure coupled with larger silicides, which yielded a better toughness [76].

The results of a reliable CALPHAD modeling can be used to predict e.g. compositions, which yield a specific volume fraction of Ti_5Si_3 for improving the creep resistance, or windows for thermomechanical processing or heat treatments to generate individual microstructures.

3.1.1. Literature review

The Ti–Al–Si system has been thoroughly assessed within the MSI Ternary Phase Diagram Evaluation scheme [37, 38], considering references for the ternary system up to 2002 and has been reviewed by Raghavan [39, 40], covering references up to 2008. In the following, a summary of investigations focusing on phase equilibria in the Ti-rich part of the system is given.

Bulanova et al. [77, 78] established three partial isothermal sections at 1250, 1270 and 1300 °C, a liquidus and solidus diagram for the complete Ti–Al–Si system, four vertical sections at 5 and 10 at. % Si, 50 at. % Ti, 40 at. % Al and a reaction scheme using metallography, DTA, XRD, and EPMA of annealed and as-cast alloys. Based on XRD of samples annealed for 6 to 12 h, Schob et al. [79] established a complete isothermal section at 1200 °C. Turner and Crossley [80, 81] established partial isothermal sections of the Ti corner at 600, 800, 900, 1000, 1100, and 1200 °C and two partial vertical sections for 2 and 6 wt. % Al from light optical microscopy. Li et al. [44, 82] established a partial vertical section for 0.3 at. % Si from EPMA measurements showing the Ti$_3$Al/TiAl and αTi/TiAl phase boundaries between 1000-1250 °C. Azevedo and Flower [47, 83, 84] carried out a comprehensive study of the Ti-rich part of the system employing XRD, SEM, and TEM, combined with EDS. They established partial isothermal sections at 700, 800, 900, and 1100 °C [47] and calculated partial isothermal sections for the temperature range 700-1200 °C [83, 84]. From XRD and EPMA results of a single sample and data from literature Viala et al. [85] created a simplified isothermal section at 1000 °C. Gupta [46] studied the phase equilibria in the temperature range 700-1000 °C employing ternary diffusion couples between pure titanium and a eutectic Al–Si alloy. Compositions of the phases were established through EPMA. An isothermal section at 1000 °C was constructed and phase equilibria at the remaining temperatures were discussed. Liu et al. [45] established an isothermal section at 1000 °C and a partial isothermal section at 900 °C focusing on the Al-rich side utilizing EDS measurements of heat-treated alloys. Additionally, they determined the liquidus surface by performing DTA up to 1500 °C. A complete isothermal section at "about 700 °C" was determined employing metallography and XRD of annealed alloys by Raman & Schubert [86]. Apparently, the term "about" was chosen because the authors realized that annealing times of 48 -120 h may have been too short to attain equilibrium in all investigated alloys. Based on the work of Raman & Schubert [86], Gröbner et al. [87] calculated the isothermal section at 700 °C. More recently, a complete isothermal section at 700 °C has been established by XRD and EDS on alloys that were homogenized at 1100 °C for

40 h and then equilibrated at 700 °C for 1080 h [88]. Based on a number of experimental data from Al–Si-rich alloys, complete isothermal sections at 550, 585, 590, 650, 727 and 900 °C were calculated by Li et al. [89]. A complete isothermal section at 550 °C was established by Wang et al. [90] using SEM, EDS and XRD on annealed alloys. Finally, a complete isothermal section at 20 °C was presented by Kamei et al. [91] from microstructures and XRD of as-cast alloys.

Despite all the investigations mentioned above, data on phase equilibria are at least partially controversial. For instance for the solid solubility of Si in TiAl at 1000 °C, reported data vary between 0.1 [44] and about 3 at.% [45, 46] and data for the solid solubility of Al in Ti_5Si_3 vary between 2 [47] and 11 at. % [45]. It is noted that in alloys produced through powder metallurgy even much higher Al contents up to more than 20 at. % Al have been observed in Ti_5Si_3 [48-50], but it is assumed that these compositions are metastable [50]. However, the knowledge of the precise solid solubilities of both phases in dependence on temperature is essential for the design of more creep resistant TiAl-based alloys, because this information yields the volume fraction of Ti_5Si_3 at a certain temperature for a given composition.

As a part of the ADVANCE project [33], phase equilibria between the Ti–Al phases and Ti_5Si_3 between 800-1200 °C, the temperature range where the alloys are processed and maybe applied, were experimentally investigated.

3.2. Results and discussion

To establish the partial isothermal sections, compositions of the phase boundaries in the binary systems were taken from recent assessments. For Ti–Al the updated version [7] of the comprehensive assessment by Schuster & Palm [29] is chosen. The update settles the dispute about the peritectoid or congruent formation of Ti_3Al. While experiments show a peritectoid formation of Ti_3Al, all CALPHAD calculations predict a congruent formation of Ti_3Al. As detailed in [7], also the CALPHAD calculations show the peritectoid reaction $\alpha Ti + \beta Ti \leftrightarrow Ti_3Al$ at 1200 °C, if substitutional vacancies are included in the CALPHAD calculations. In consequence, the phase field of αTi is interrupted between 1170 to 1200 °C by the equilibrium $\beta Ti + Ti_3Al$, i.e. no continuous phase field of αTi exists up to the melt. The Ti–Si binary was adopted from the latest thermodynamic assessment by Fiore et al. [70]. They conclude that the long ongoing debate whether the line compound Ti_3Si exists between the Ti solid solution and Ti_5Si_3 or whether this phase is stabilized by impurities cannot be settled from the existing

evidence. The Al–Si binary is taken from Lukas & Lebrun [92]. It is a simple eutectic system containing no intermetallic phases.

The partial isothermal sections determined here comprise compositions up to 70 at. % Al and 40 at. % Si. The crystallographic data of the solid phases observed within this composition range are listed in **Table 3.1**. No ternary phase was detected within the investigated temperature and composition range. Additionally, Ti_3Si (tp32, $P4_2/n$ [70, 93]), whose existence is still under debate [70], was not detected in the present investigation. This phase was observed in the Ti–Al–Si system by Li et al. [88] and Gupta [46], but not in other studies [50, 77, 78, 80, 81, 90, 94]. Nevertheless, investigated compositions in the present work could be outside the composition range where equilibria with this phase may occur. Therefore, phase equilibria with Ti_3Si are indicated by dashed tie-triangle.

Comparison with the liquidus projection [45] shows that all alloy compositions (**Table 2.1**) are located within the primary field of high-melting Ti_5Si_3 ($T_m = 2130$ °C), except S7. Therefore, S1-S6 contained varying amounts of large idiomorphic grains of primary Ti_5Si_3 in the as-cast state. These grains are too big to equilibrate within reasonable annealing times. Therefore, all compositions measured by EPMA were obtained from small, spherical Ti_5Si_3 grains, which are assumed to have formed at the annealing temperatures.

Table 3.1. Crystallographic data of solid phases

Phase	Pearson Symbol, Space Group, Prototype	Lattice Constants (nm)	Ref.
βTi	cI2, Im$\bar{3}$m, W	a_0= 0.33112	[95]
αTi	hP2, P6$_3$/mmc, Mg	a_0 = 0.29503, c_0 = 0.46810	[95]
Ti$_3$Al	hP8, P6$_3$/mmc, Ni$_3$Sn	a_0 = 0.5765 , c_0 = 0.4625	[96]
TiAl	tP4, P4/mmm, AuCu	a_0 = 0.4000, c_0 = 0.4075	[97]
TiAl (1d-APS)	one-dimensional, tetragonal ordered superstructures of AuCu P4/mmm, tP28, Ti$_2$Al$_5$	a_0 = 0.39053, c_0 = 2.91921	[98]
TiAl$_2$	tI24, I4$_1$/amd, HfGa$_2$	a_0 = 0.3971, c_0 = 2.4312	[99]
TiAl$_3$ (h)	tI8, I4/mmm, TiAl$_3$ (h)	a_0 = 0.3849, c_0 = 0.8610	[100]
Ti$_5$Si$_3$	hP16, P6$_3$/mmc, Mn$_5$Si$_3$	a_0= 0.7452, c_0=0.5142	[101]

3.2.1. Partial isothermal section at 1200 °C

Figure 3.1 depicts the partial isothermal section at 1200 °C. All investigated alloys are located within two-phase fields at this temperature. The compositions of coexisting phases measured with EPMA are summarized in **Table 3.2** and identification of the phases by XRD is shown in **Table 3.3**. All binary Ti–Al phases show a limited solid solubility for Si, while the maximum Al content observed in Ti$_5$Si$_3$ is about 8 at. %. It is noted that in alloys where βTi is stable at 1200 °C, αTi is observed at room temperature, instead. The βTi ↔ αTi transformation in Ti–Al alloys cannot be suppressed even by quenching [63, 96, 102] and also not in Ti–Al–Si alloys [37, 47]. Likewise, the ordering reaction αTi ↔ Ti$_3$Al (α_2) cannot be suppressed during cooling in binary Ti–Al alloys, even by quenching the alloys to room temperature [96, 103]. The same has been observed for the Ti–Al–Si alloys [47]. Finally, Al-rich TiAl cannot be preserved by quenching, but forms a sequence of long-periodic one-dimensional antiphase domain structures during cooling, denoted as 1d-APS [104]. Depending on the composition, different crystallographic structures are observed at room temperature, identified as Ti$_2$Al$_5$ in the present case.

In **Figure 3.2** the present isothermal section is compared with previously reported data. The outline of the βTi phase field at 1200 °C has been investigated before [47, 79, 81] and the present investigation agrees with the previous ones in that the solid solubility for Si in βTi decreases with increasing Al content. Quantitatively, the solid solubility for Si in βTi is

somewhat higher than previously determined, e.g. 2.0 at. % Si at about 20 at. % Al compared to about 1.5 at. % Si [47, 79]. Only Schob et al. [79] investigated a more extended composition range at 1200 °C. They observed an extended homogeneity range for Ti_3Al, denoted as $Ti_{3-2}Al$ in their investigation, which showed a solid solubility of up to about 6 at. % Si. However, by now it is clear that Ti_3Al exists only below 1200 °C, as it forms at that temperature on cooling by the peritectic reaction $\beta Ti + \alpha Ti \leftrightarrow Ti_3Al$ [7, 29]. Instead of Ti_3Al, αTi is stable in that composition range at 1200 °C and its solubility for Si at that temperature is limited to about 0.5 at. % (**Figure 3.1**). Additionally, as $TiAl_2$ had not been considered, phase equilibria in the more Al-rich part differ in [79] from present work (**Figure 3.2**).
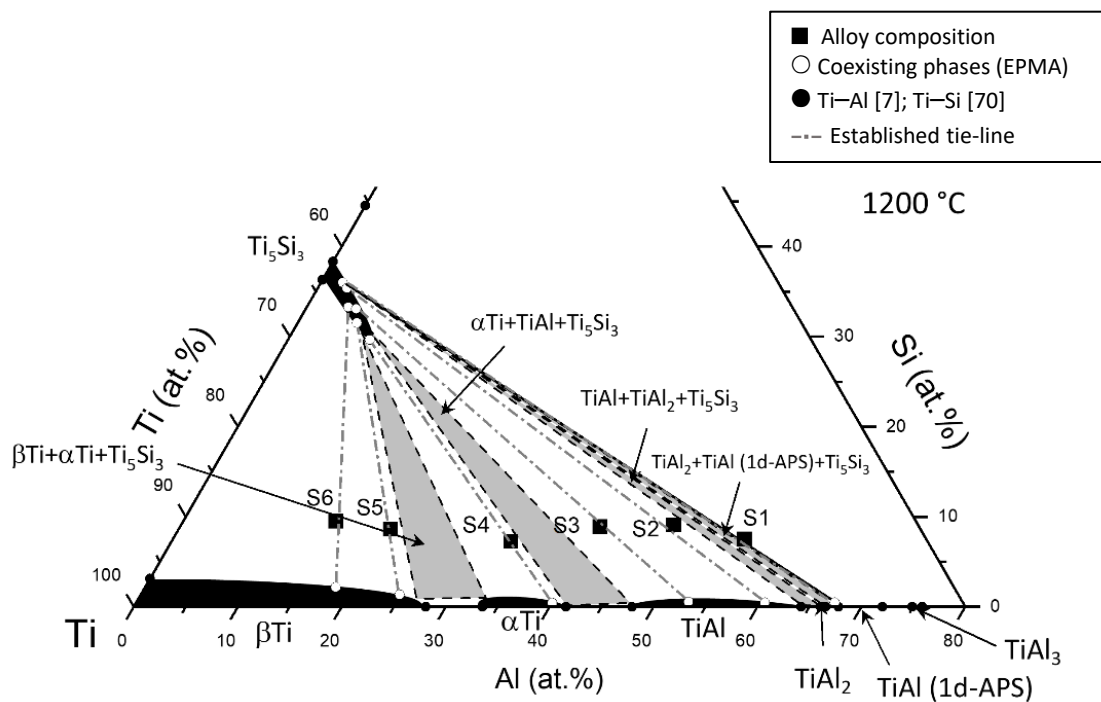
Figure 3.1. Partial Ti–Al–Si isothermal section at 1200 °C.
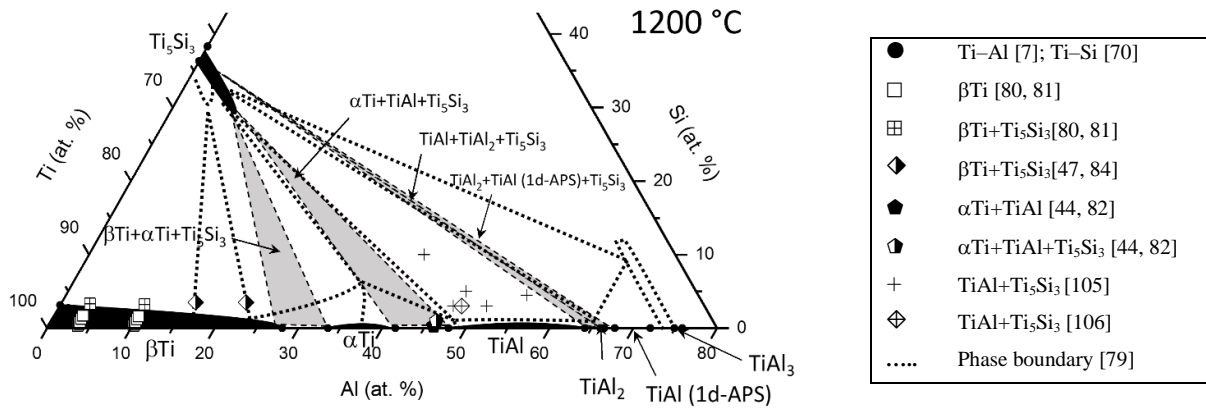
Figure 3.2. Partial Ti–Al–Si isothermal section at 1200 °C in comparison to experimental results from literature.

3.2.2. Partial isothermal section at 1100 °C

The partial isothermal section at 1100 °C is shown in **Figure 3.3a**. At this temperature, alloys S1, S2, and S4 show three-phase equilibria (**Table 3.2**). Compared to the isothermal section at 1200 °C, Ti_3Al is present at 1100 °C and is in equilibrium with Ti_5Si_3, like βTi, TiAl, and $TiAl_2$. No equilibrium between αTi and Ti_5Si_3 is observed, in agreement with the DTA results, which show that αTi + Ti_5Si_3 does not exist between 1095 °C – 1152 °C (see below). This finding is in agreement with Azevedo & Flower [47, 84], who observed the three-phase equilibrium βTi + Ti_3Al + Ti_5Si_3 at 1100 °C. **Figure 3.3b** shows an enlarged section of the respective composition range. At 1100 °C previous data concentrated on the Ti corner [44, 47, 80-82, 84] and **Figure 3.4** shows that these are in good agreement with the present ones.
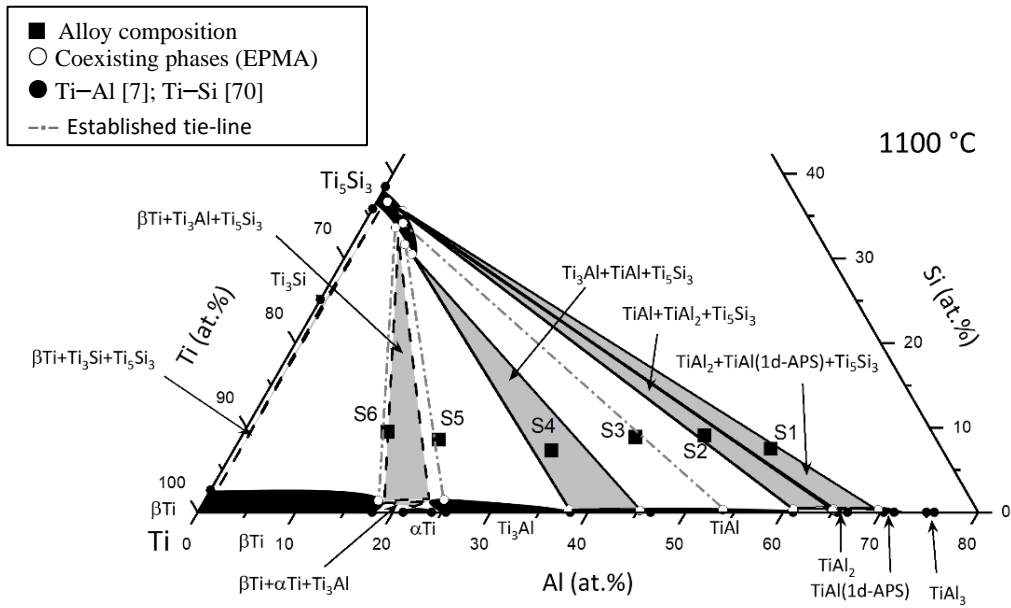
Figure 3.3a. Partial Ti–Al-Si isothermal section at 1100 °C.
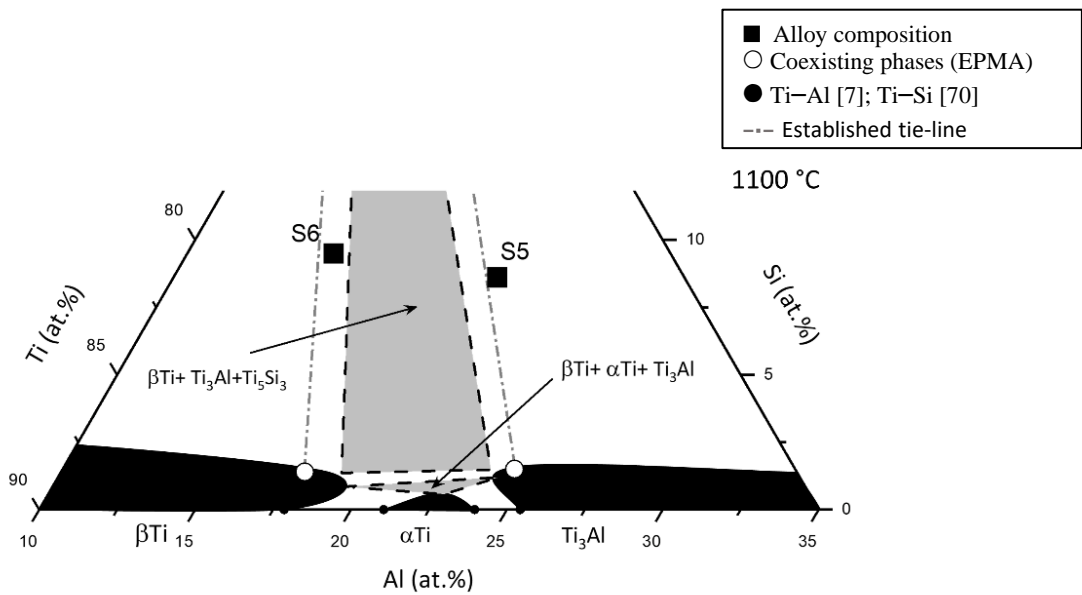
Figure 3.3b. Enlarged part of the 1100 °C isotherm showing phase equilibria with αTi.
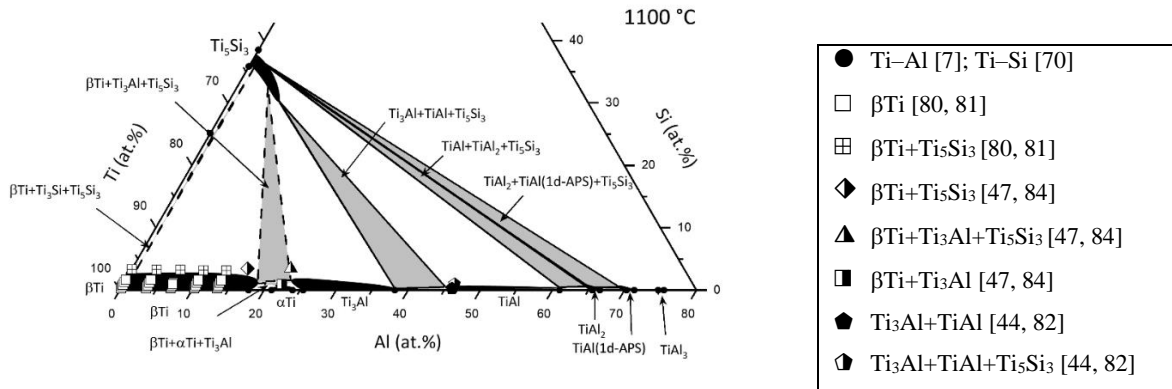
Figure 3.4. Partial Ti–Al–Si isothermal section at 1100 °C with additional experimental results from literature.

3.2.3. Partial isothermal section at 1000 °C

For the determination of the phase equilibria at 1000 °C samples had initially been heat treated only for 100 h. This duration was too short to reach equilibrium and therefore all alloys were annealed for 1000 h, from which the partial isothermal section in **Figure 3.5** was established. Microstructures and XRD analyses of the alloys heat-treated at 1000 °C/ 1000 h are shown in **Figure 3.6**, **3.7**. In alloys S1-S4 (**Figure 3.6**) large, idiomorphic grains of Ti_5Si_3 are observed. These are primary precipitates, which formed in the melt (**Figure 3.6**). As described above, no EPMA was performed on these primary grains, because they are still not in equilibrium after annealing for 1000 h, and hence measurements were only performed on small, spherical Ti_5Si_3 grains which are present in the alloys besides the large idiomorphic grains (**Figure 3.6b**).
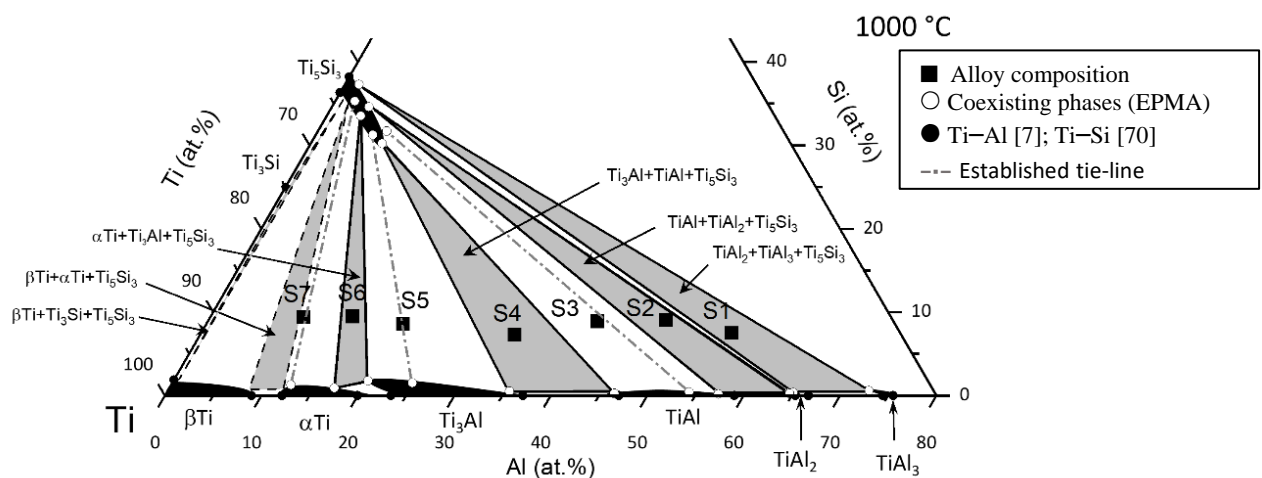
Figure 3.5. Partial Ti–Al–Si isothermal section at 1000 °C.
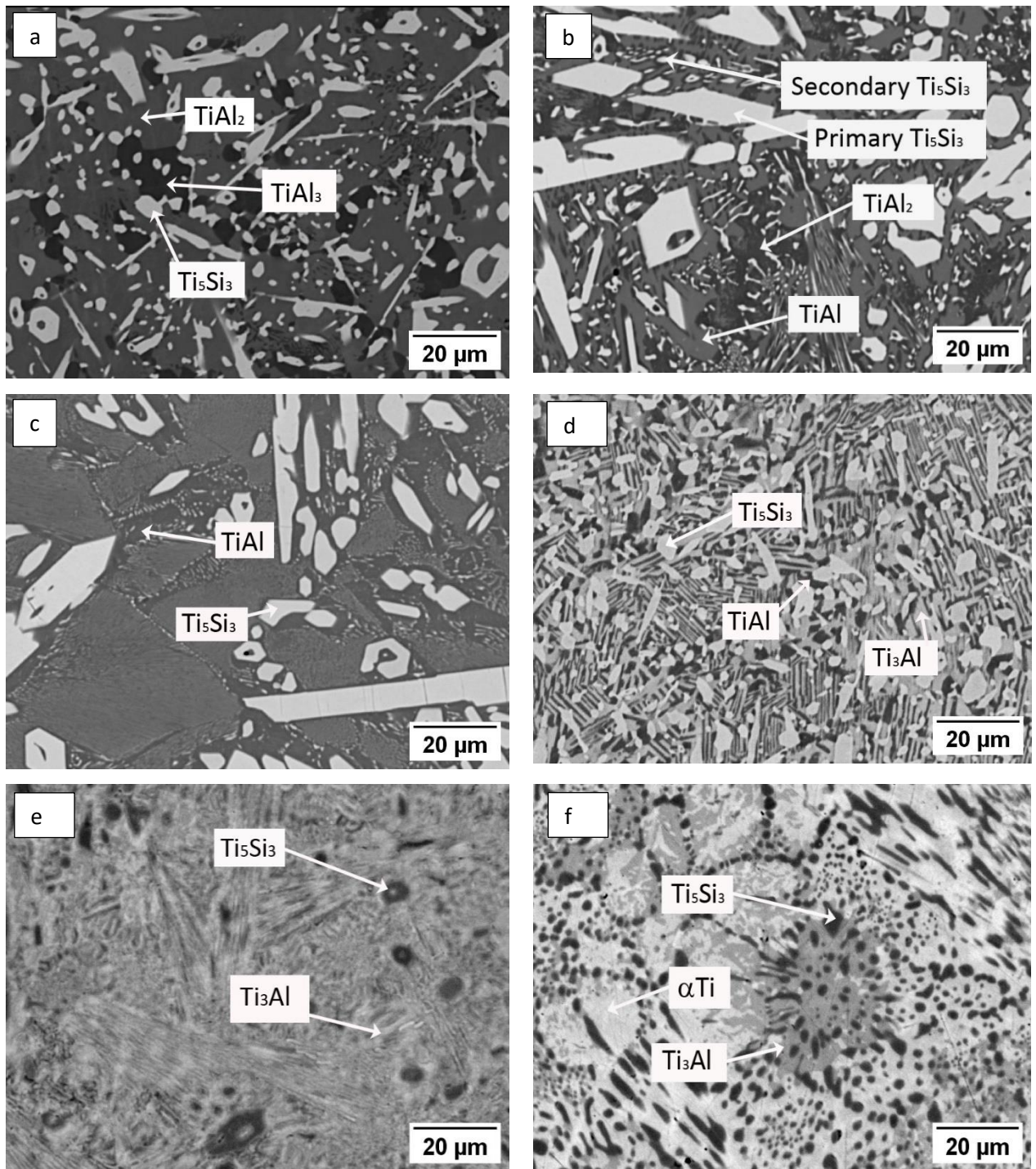
Figure 3.6. Microstructures of the alloys heat-treated 1000 °C/1000 h

a) S1; Ti–55Al–7.5Si (at. %), b) S2; Ti–47.4Al–9.1Si,

c) S3; Ti–40.4Al–8.9Si, d) S4; Ti–32.7Al–7.1Si,

e) S5; Ti–20.4Al–8.6Si, f) S6; Ti–14.7Al–9.5Si,
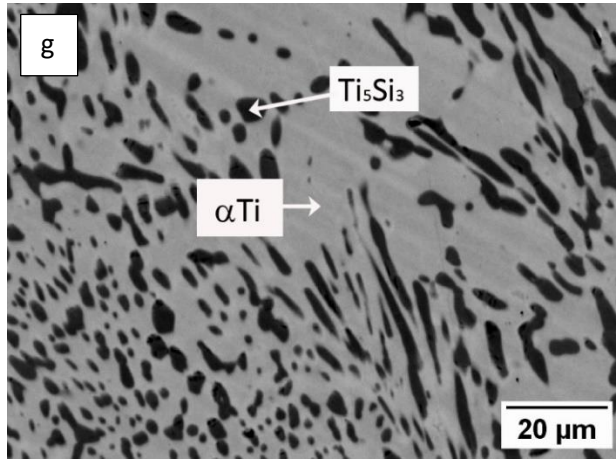
(Continue) Figure 3.6. Microstructures of the alloys heat-treated 1000 °C/1000 h g) S7; Ti–9.7Al–9.6Si.
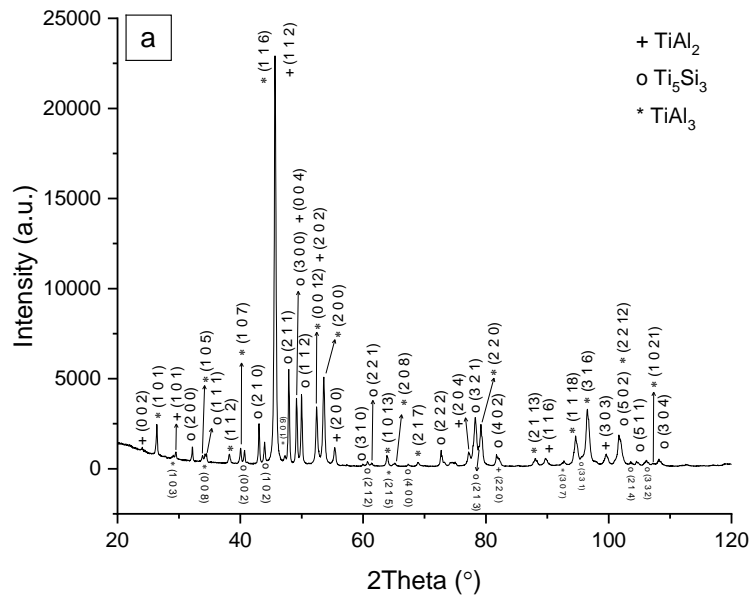
Figure 3.7. XRD analysis of a) S1; Ti–55Al–7.5Si (at. %), heat-treated 1000 °C/1000 h.
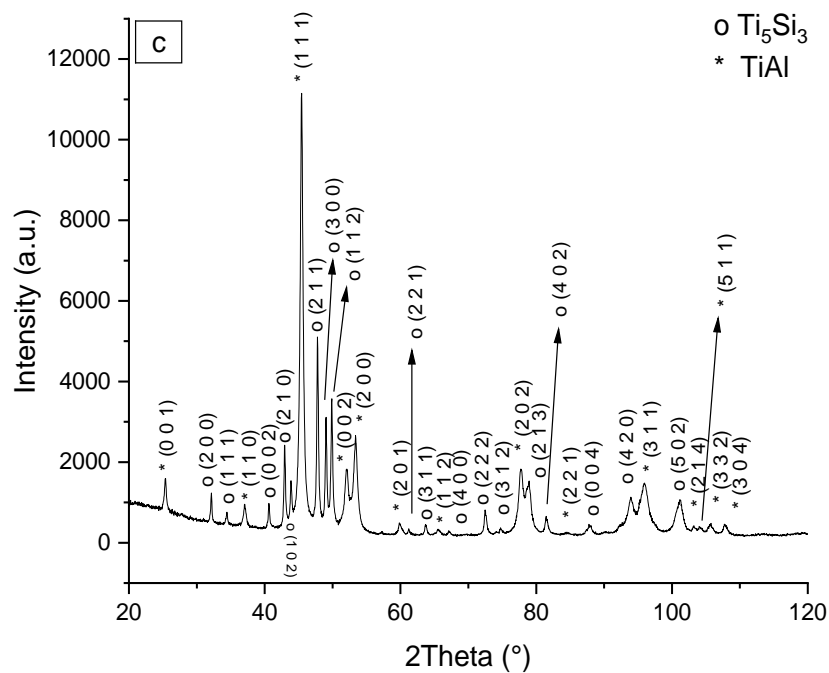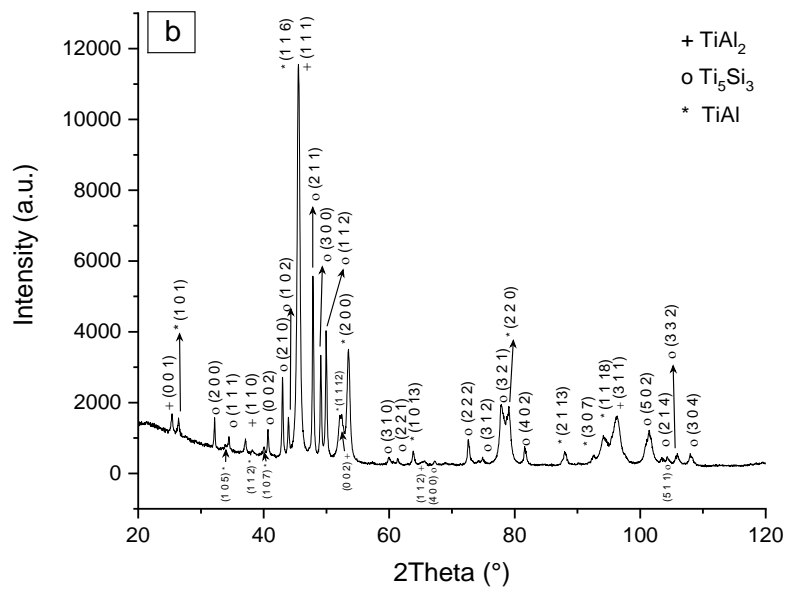
Figure 3.7. XRD analyses of b) S2; Ti–47.4Al–9.1Si (at. %), and c) S3; Ti–40.4Al–8.9Si (at. %) heat-treated 1000 °C/1000 h.
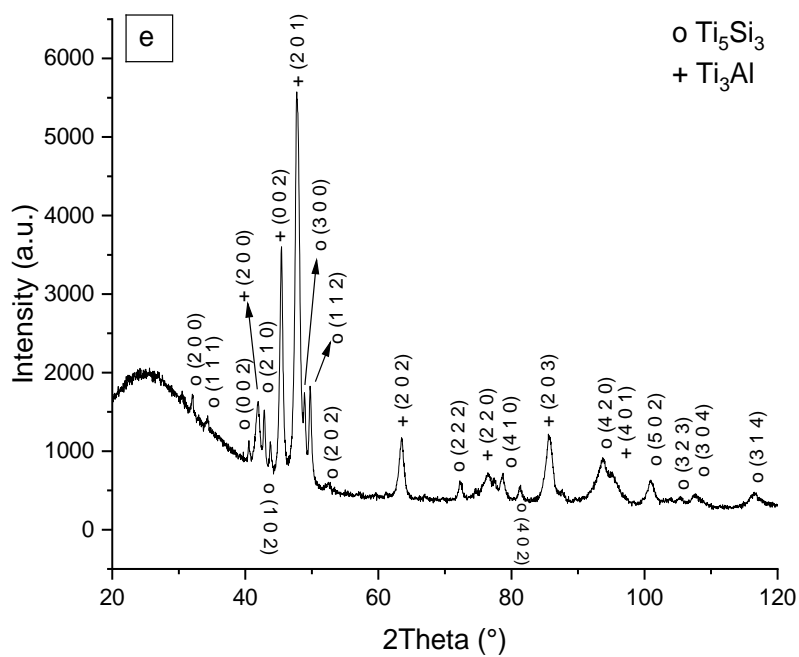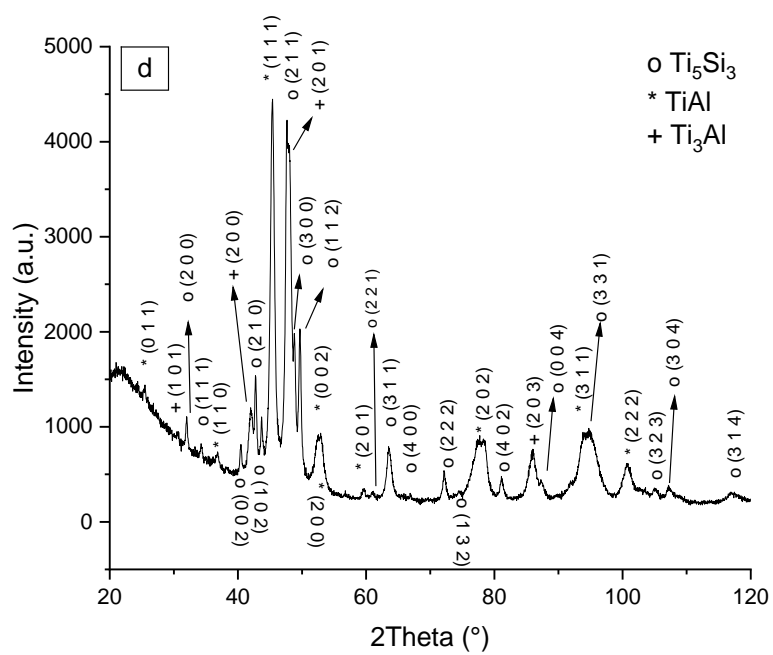
Figure 3.7. XRD analyses of d) S4; Ti–32.7Al–7.1Si (at. %), and e) S5; Ti–20.4Al–8.6Si (at. %) heat-treated 1000 °C/1000 h.
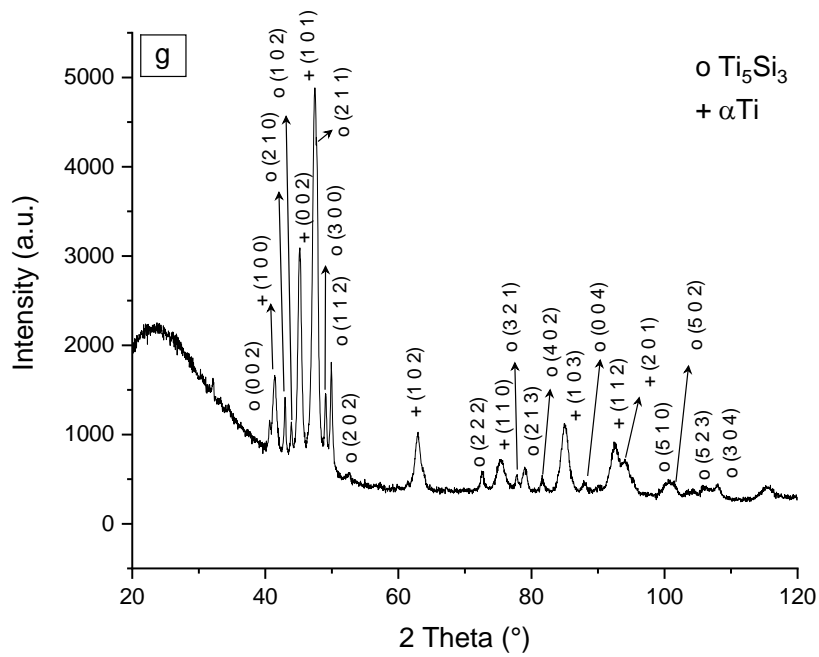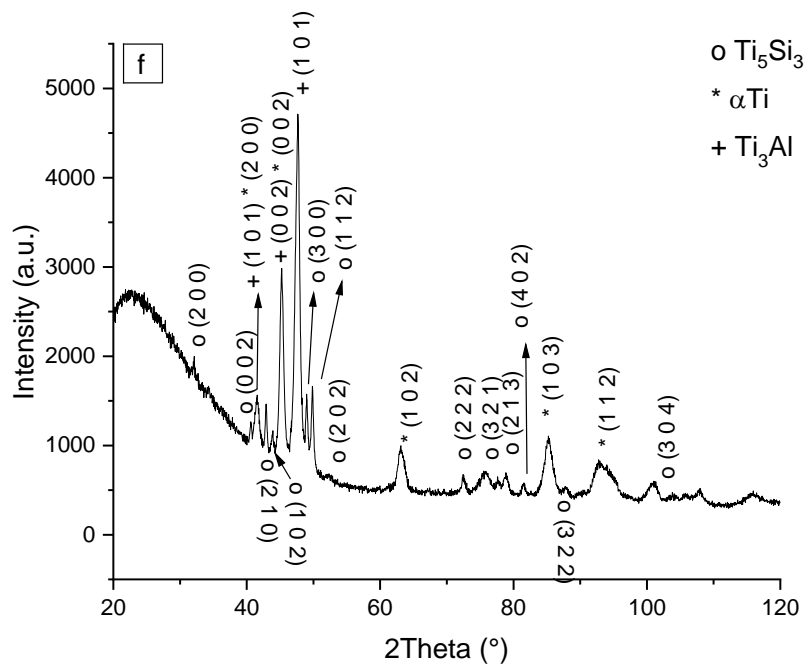
Figure 3.7. XRD analyses of f) S6; Ti–14.7Al–9.5Si (at. %), and g) S7; Ti–9.7Al–9.6Si (at. %) heat-treated 1000 °C/1000 h.

The partial isothermal section in **Figure 3.5** agrees qualitatively with the one determined by Liu et al. [45]. However, phase equilibria among the phases Ti_5Si_3, βTi, αTi, Ti_3Al, and $TiAl$ were not determined in [45] and were therefore shown by dashed lines. Liu et al. [45] reported a solid solubility of Al of 11 at. %. in Ti_5Si_3, which is only about 7 at. % according to the present investigation. Additionally, the shape of the Ti_5Si_3 single-phase field in [45] is different in that it stretches along a constant Ti:Si ratio, while the one shown in **Figure 3.5** is more inclined towards the Ti–Al side, indicating a more pronounced substitution of Si by Al than assumed in [45]. That the present finding is more likely is corroborated by the fact that the measured Al content in Ti_5Si_3 at the three-phase equilibrium $Ti_5Si_3 + TiAl_2 + TiAl_3$ was 2.5 to 3.9 at. % in [45] (1.5 at. % Al determined in here), while, due to the shape of their single-phase field, it is shown at 10 at. % Al in their isothermal section.

The isothermal section established from diffusion couples by Gupta [46] differs considerably from the established partial isothermal section in **Figure 3.5**. Gupta [46] found αTi, Ti_3Al and $TiAl$ in equilibrium with Ti_3Si. There have been two other investigations of the Ti–Al–Si system at 1000 °C, both focusing on the Ti corner. As in the present investigation, they also found αTi, Ti_3Al and $TiAl$ in equilibrium with Ti_5Si_3 instead of Ti_3Si (**Figure 3.5**) [47, 77, 78, 84]. Additionally, Gupta observed Ti_9Al_{23}, which is no binary Ti–Al phase [29]. According to compositions reported in [46, 107] it seems that this "phase" lies within the extended solid solubility range of $Ti(Al,Si)_3$.

3.2.4. Partial isothermal sections at 900 °C and 800 °C

The partial isothermal sections at 900 °C (**Figure 3.8**) and 800 °C (**Figure 3.10**) show the same phase equilibria as at 1000 °C. Alloys S1, S2, S4, and S6 all lie within different three-phase fields from which the tie-triangles were determined. It is noted that in S1 annealed at 900 °C $TiAl_3$ was observed by EPMA and identified by XRD (**Table 3.2**), but that all particles were too small for quantitative EPMA.

For 900 °C phase equilibria are in qualitative agreement with previous investigations of the Ti corner at this temperature [47, 77, 78, 84]. In the Ti/Al–Si diffusion couple analyzed by Gupta at 900 °C, no Ti_3Si was observed, while Ti_9Al_{23} was detected again [46]. More recently, complete isothermal sections were calculated for the temperature range 450-900 °C [89, 108]. In **Figure 3.9** the calculated isothermal section for 900 °C by Li et al. [89] is compared to the present one. calculated and experimentally determined phase equilibria are in qualitative agreement. As the calculation is based on a different description of the binary Ti–Al system

and as except for βTi no solid solubility ranges for the third component, specifically not for Al in Ti₅Si₃, have been calculated, calculated and experimental determined phase equilibria are somewhat shifted against each other (**Figure 3.9**). The most prominent difference is the extent of αTi + βTi + Ti₃Si, which has not been determined in the present investigation, but which should be positioned much nearer to the Ti–Si side than shown in the calculation according to [81], who studied the respective composition range at 900 °C in much detail, there αTi and βTi in equilibrium with Ti₅Si₃, but otherwise phase equilibria are again in qualitative agreement with those shown in **Figure 3.8**.

At 800 °C Ti₃Si was again observed in a diffusion couple and therefore the existence of a three-phase field TiAl + Ti₃Al + Ti₃Si had been proposed [46]. According to the present investigation (**Figure 3.9**), phase equilibria with Ti₅Si₃ are observed instead. This is in accordance with the investigation of the Ti corner at 800 °C [77, 78] where also αTi + Ti₅Si₃ was observed, which rules out any phase equilibria of Ti₃Si with more Al-rich phases.
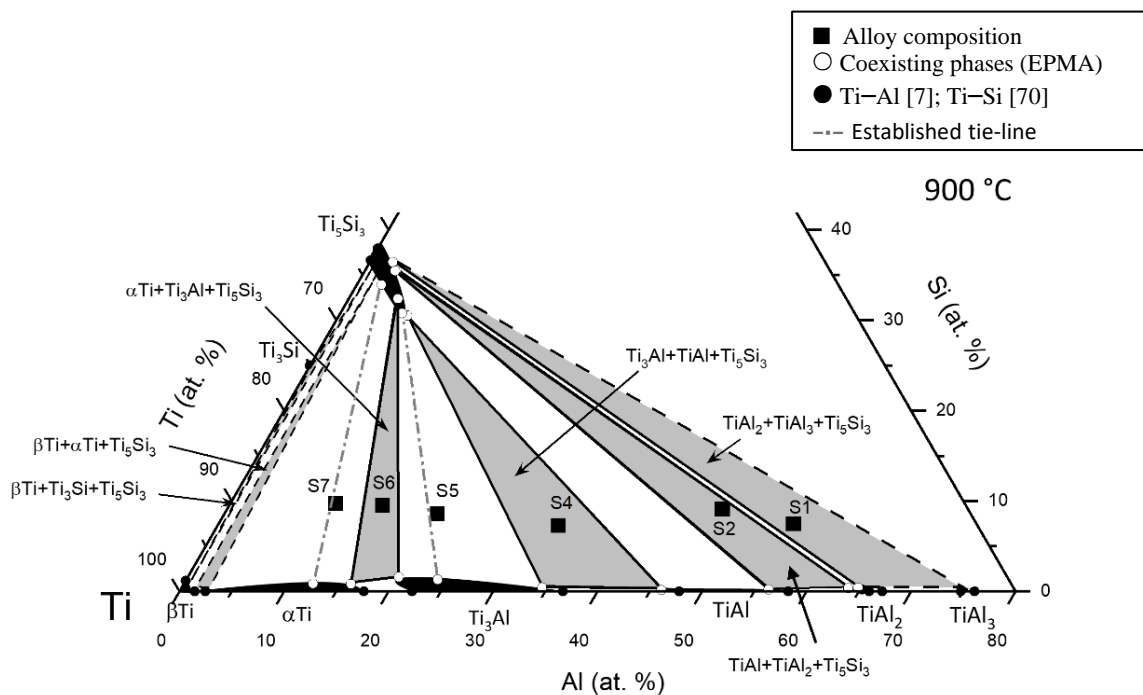
**Figure 3.8.** Partial Ti–Al–Si isothermal section at 900 °C.
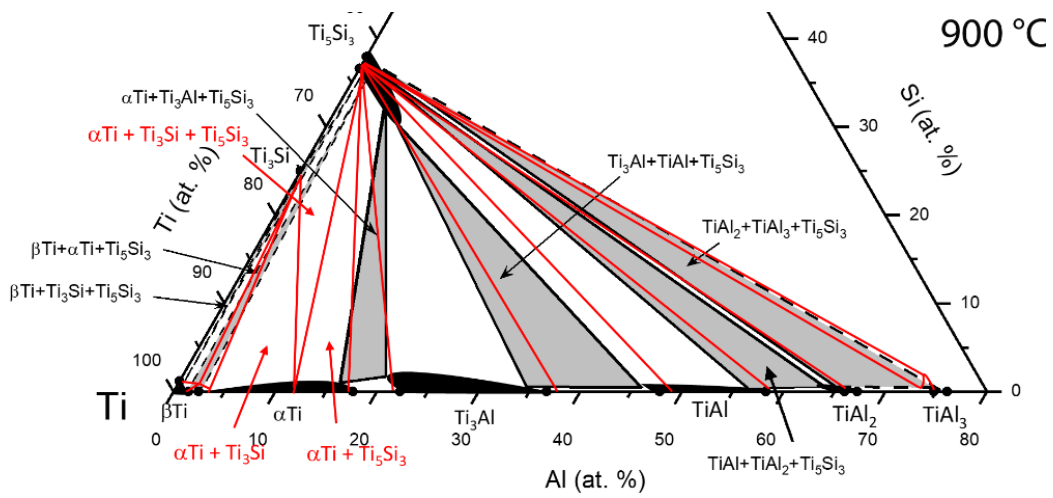
Figure 3.9. Partial Ti–Al–Si isothermal section at 900 °C compared to the calculated one (in red) from [89].
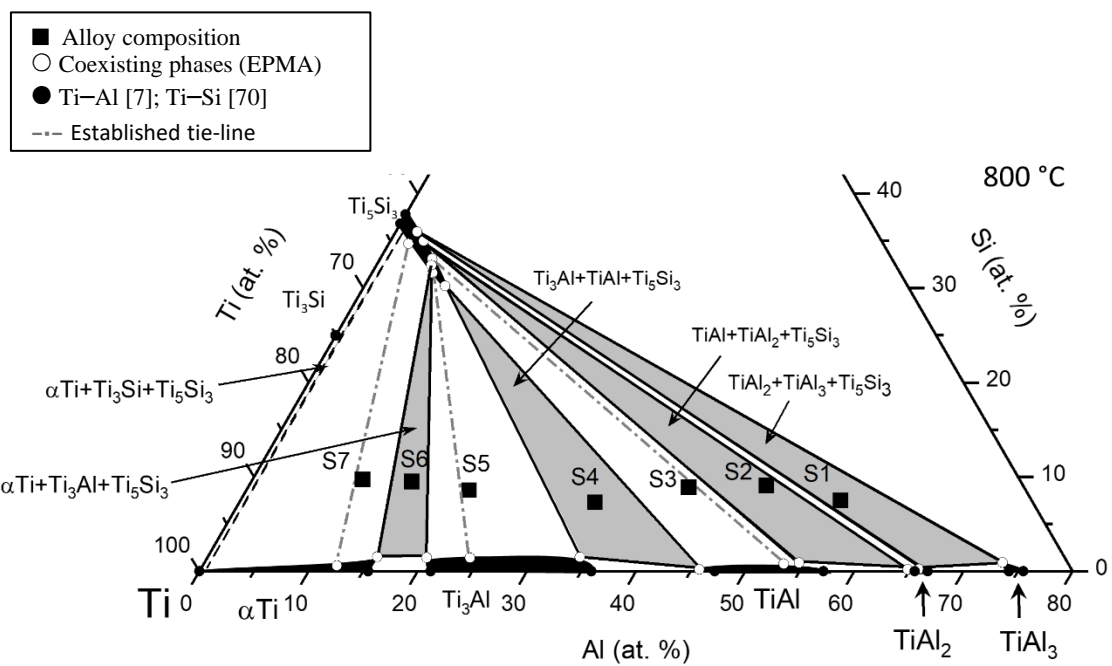
Figure 3.10. Partial Ti–Al–Si isothermal section at 800 °C.

Table 3.2. Compositions of coexisting phases measured with EPMA; figures for HT denote length of heat treatment and figures shown in bold are extreme values (see text); n.d.: not determined

Temp.	1200 °C				1100 °C				1000 °C			
Alloy	Phases	Ti (at. %)	Al (at. %)	Si (at. %)	Phases	Ti (at. %)	Al (at. %)	Si (at. %)	Phases	Ti (at. %)	Al (at. %)	Si (at. %)
HT (h)	24				165				1000			
	Ti_5Si_3	61.9 ± 0.4	2.1 ± 0.4	36.0 ± 0.4	Ti_5Si_3	62.2 ± 0.2	1.1 ± 0.3	36.7 ± 0.2	Ti_5Si_3	61.2 ± 0.2	1.5 ± 0.4	37.3 ± 0.5
S1	TiAl (1d-APS)	32.3 ± 0.6	67.2± 0.6	0.5 ± 0.1	TiAl (1d-APS)	30.1 ± 0.2	69.6 ± 0.2	0.3 ± 0.04	$TiAl_3$	26.7 ± 0.5	72.7 ± 0.7	0.6 ± 0.2
					$TiAl_2$	34.6 ± 0.2	65.0 ± 0.2	0.4 ± 0.04	$TiAl_2$	34.6 ± 0.4	65.0 ± 0.4	0.4 ± 0.1
HT* (h)	24				200				1000			
	Ti_5Si_3	61.8 ± 0.3	2.8 ± 0.6	35.4 ± 0.5	Ti_5Si_3	61.2 ± 0.5	3.2 ± 0.5	35.6 ± 0.2	Ti_5Si_3	61.5 ± 0.5	3.9 ± 0.7	34.6 ± 0.5
S2	TiAl	39.0 ± 0.4	60.5 ± 0.4	0.5 ± 0.06	$TiAl_2$	34.8 ± 0.5	65.0 ± 0.5	0.2 ± 0.1	$TiAl_2$	35.1 ± 0.5	64.6 ± 0.6	0.3 ± 0.1
					TiAl	38.8 ± 0.4	60.8 ± 0.4	0.4 ± 0.1	TiAl	42.3 ± 0.4	57.5 ± 0.4	0.2 ± 0.1
HT* (h)	24				200				1000			
	Ti_5Si_3	62.1 ± 0.3	4.9 ± 0.5	33.1 ± 0.5	Ti_5Si_3	61.8 ± 0.2	4.0 ± 0.2	34.2 ± 0.3	Ti_5Si_3	61.2 ± 0.5	7.1 ± 0.7	31.7 ± 0.7
S3	TiAl	46.4 ± 0.3	53.1 ± 0.4	0.5 ± 0.2	TiAl	46.0 ± 0.3	53.7 ± 0.3	0.3 ± 0.04	TiAl	45.5 ± 0.3	54.1 ± 0.3	0.4 ± 0.1
HT* (h)	24				200				1000			
S4	Ti_5Si_3	62.5 ± 0.2	7.7 ± 0.6	29.8 ± 0.6	Ti_5Si_3	62.8 ± 0.3	6.7 ± 0.6	30.5 ± 0.6	Ti_5Si_3	62.4 ± 0.3	7.4 ± 0.5	30.2 ± 0.3

αTi	59.6 ± 0.3	40.0 ± 0.3	0.4 ± 0.04	TiAl	54.6 ± 0.6	45.2 ± 0.6	0.2 ± 0.01	TiAl	53.3 ± 0.3	46.5 ± 0.3	0.2 ± 0.1
				Ti$_3$Al	61.8 ± 0.4	37.8 ± 0.4	0.4 ± 0.04	Ti$_3$Al	64.0 ± 0.7	35.5 ± 0.7	0.5 ± 0.1
HT* (h)	24			200				1000			
	Ti$_5$Si$_3$	62.8 ± 0.4	5.7 ± 0.2	31.5 ± 0.5	Ti$_5$Si$_3$	62.9 ± 0.2	5.4 ± 0.2	31.7 ± 0.3	Ti$_5$Si$_3$	62.8 ± 0.4	5.9 ± 0.2	31.3 ± 0.5
S5	βTi	73.8 ± 0.3	24.9 ± 0.2	1.3 ± 0.3	Ti$_3$Al	74.0 ± 0.4	24.5 ± 0.3	1.5 ± 0.2	Ti$_3$Al	73.6 ± 0.4	24.9 ± 0.2	1.5 ± 0.5
HT* (h)	24			200				1000			
	Ti$_5$Si$_3$	62.7 ± 0.3	4.0 ± 0.4	33.3 ± 0.5	Ti$_5$Si$_3$	62.9 ± 0.2	3.5 ± 0.3	33.6 ± 0.4	Ti$_5$Si$_3$	63.0 ± 0.2	3.5 ± 0.8	33.5 ± 0.8
S6									Ti$_3$Al	78.1 ± 0.6	20.1 ± 0.7	1.8 ± 0.2
	βTi	79.7 ± 0.4	18.3 ± 0.4	2.0 ± 0.3	βTi	80.8 ± 0.4	17.8 ± 0.4	1.4 ± 0.04	αTi	82.0 ± 0.5	17.1 ± 0.5	0.9 ± 0.03
HT* (h)								1000			
S7								Ti$_5$Si$_3$	62.7 ± 0.4	2.0 ± 0.3	35.3 ± 0.5
								αTi	86.3 ± 0.2	12.4 ± 0.2	1.3 ± 0.1

Temp.	900 °C				800 °C			
Alloy	Phases	Ti (at. %)	Al (at. %)	Si (at. %)	Phases	Ti (at. %)	Al (at. %)	Si (at. %)
HT* (h)	1000				1000			
	Ti$_5$Si$_3$	61.4 ± 0.4	2.2 ± 0.5	36.4 ± 0.4	Ti$_5$Si$_3$	**62.1**	**2.0**	**35.9**
S1	TiAl$_3$	n.d.	n.d.	n.d.	TiAl$_3$	**26.0**	**73.1**	**0.9**
	TiAl$_2$	34.6 ± 0.3	65.2 ± 0.3	0.2 ± 0.1	TiAl$_2$	**34.0**	**65.8**	**0.2**
HT* (h)	1504				1000			
	Ti$_5$Si$_3$	61.8 ± 0.2	2.9 ± 0.1	35.3 ± 0.2	Ti$_5$Si$_3$	**61.9**	**3.1**	**35.0**
S2	TiAl$_2$	35.7 ± 0.2	64 ± 0.2	0.3 ± 0.1	TiAl$_2$	**35.0**	**64.8**	**0.2**
	TiAl	43.5 ± 0.3	56.3 ± 0.3	0.2 ± 0.1	TiAl	44.6 ± 0.2	54.5 ± 0.5	0.9 ± 0.2
HT* (h)	1504				1000			
S3	Ti$_5$Si$_3$				Ti$_5$Si$_3$	62.5 ± 0.1	5.1 ± 0.3	32.4 ± 0.3
	TiAl				TiAl	46.1 ± 0.2	53.1 ± 0.3	0.8 ± 0.1
HT* (h)	1000				1000			
	Ti$_5$Si$_3$	63.0 ± 0.3	6.5 ± 0.3	30.5 ± 0.4	Ti$_5$Si$_3$	62.6 ± 0.2	8.0 ± 0.7	29.4 ± 0.8
S4	TiAl	53.8 ± 0.5	46.0 ± 0.6	0.2 ± 0.1	TiAl	**54.1**	**45.7**	**0.2**
	Ti$_3$Al	65.1 ± 0.4	34.5 ± 0.5	0.4 ± 0.2	Ti$_3$Al	**64.4**	**34.1**	**1.5**
HT* (h)	1000				1000			
S5	Ti$_5$Si$_3$	63.3 ± 0.3	5.9 ± 0.4	30.8 ± 0.5	Ti$_5$Si$_3$	62.8 ± 0.3	5.6 ± 0.2	31.6 ± 0.4
	Ti$_3$Al	74.6 ± 0.5	24.1 ± 0.5	1.3 ± 0.1	Ti$_3$Al	74.5 ± 0.3	24.1 ± 0.3	1.4 ± 0.1
HT* (h)	1000				1000			
	Ti$_5$Si$_3$	62.9 ± 0.2	4.7 ± 0.4	32.4 ± 0.4	Ti$_5$Si$_3$	62.0 ± 0.2	4.7 ± 0.1	33.3 ± 0.2
S6	Ti$_3$Al	78.2 ± 0.3	20.2 ± 0.3	1.6 ± 0.1	Ti$_3$Al	**78.5**	**20.1**	**1.4**
	αTi	83.2 ± 0.3	16.0 ± 0.2	0.8 ± 0.1	αTi	**83.0**	**15.5**	**1.5**
HT* (h)	1000				1000			
S7	Ti$_5$Si$_3$	63.7 ± 0.8	2.4 ± 0.3	33.9 ± 0.8	Ti$_5$Si$_3$	63.5 ± 1.1	1.8 ± 0.4	34.7 ± 1.1
	αTi	86.8 ± 0.2	12.4 ± 0.2	0.8 ± 0.1	αTi	87.1 ± 0.7	12.3 ± 0.7	0.6 ± 0.1

Table 3.3. Lattice constants of the constituent phases; αTi* denotes formation from βTi during quenching to room temperature

Alloy	1200 °C			1100 °C			1000 °C		
	Phase	Lattice constant (nm)		Phase	Lattice constant (nm)		Phase	Lattice constant (nm)	
		a_0	c_0		a_0	c_0		a_0	c_0
S1	Ti_5Si_3	0.74596 (1)	0.51470 (2)	Ti_5Si_3	0.74545(2)	0.51478(1)	Ti_5Si_3	0.74533 (2)	0.51495 (2)
	Ti_2Al_5	0.393519 (1)	2.8932 (1)	Ti_2Al_5	0.39158(2)	2.9125(3)	$TiAl_3$	0.38523 (2)	0.86009 (6)
				$TiAl_2$	0.39704(3)	2.4310(7)	$TiAl_2$	0.397041(7)	2.43098(7)
S2	Ti_5Si_3	0.74641(1)	0.51520 (1)	Ti_5Si_3	0.74644(1)	0.51521(2)	Ti_5Si_3	0.74688(2)	0.51554(2)
	$TiAl$	0.39782(1)	0.40593 (2)	$TiAl_2$	0.39848(3)	2.4373(6)	$TiAl_2$	0.39737(2)	2.4317(2)
				$TiAl$	0.4020(5)	0.3974(3)	$TiAl$	0.39882(3)	0.40796(3)
S3	Ti_5Si_3	0.74794 (1)	0.51637 (2)	Ti_5Si_3	0.74778(5)	0.51611(4)	Ti_5Si_3	0.74767 (2)	0.51605 (2)
	$TiAl$	0.39846 (1)	0.40773 (2)	$TiAl$	0.40412(6)	0.3978 (1)	$TiAl$	0.39855 (2)	0.40844 (3)
S4	Ti_5Si_3	0.74991 (2)	0.51824 (2)	Ti_5Si_3	0.75062(9)	0.51816(8)	Ti_5Si_3	0.75053 (2)	0.51768 (2)
	$αTi$	0.29138(1)	0.46222(2)	$TiAl$	0.4030(1)	0.3955(1)	$TiAl$	0.40650(4)	0.39795(3)
				Ti_3Al	0.57691(8)	0.4628 (1)	Ti_3Al	0.56160(7)	0.46279(3)
S5	Ti_5Si_3	0.74790 (2)	0.51721(1)	Ti_5Si_3	0.74878(9)	0.51695(8)	Ti_5Si_3	0.74958(8)	0.51737(8)
	$α\mathbf{Ti^*}$	0.28974 (1)	0.46384 (2)	Ti_3Al	0.5770 (1)	0.4646 (2)	Ti_3Al	0.57913(6)	0.46403(4)
S6	Ti_5Si_3	0.74758 (3)	0.51629 (2)	Ti_5Si_3	0.7483(1)	0.5164(1)	Ti_5Si_3	0.74818 (3)	0.51566 (3)
	$α\mathbf{Ti^*}$	0.28997 (1)	0.46465 (2)	$α\mathbf{Ti^*}$	0.29157 (5)	0.4658 (1)	Ti_3Al	0.5796 (1)	0.4648(7)
							$αTi$	0.29171(5)	0.4673 (1)
S7							Ti_5Si_3	0.74771 (2)	0.51543 (2)
							$αTi$	0.29231 (1)	0.46629 (3)

Table 3.3. (continue) Lattice constants of the constituent phases in the annealed Ti–Al–Si alloys

Alloy	900 °C			800 °C		
	Phase	Lattice constant (nm)		Phase	Lattice constant (nm)	
		a_0	c_0		a_0	c_0
S1	Ti_5Si_3	0.74522 (1)	0.51473 (2)	Ti_5Si_3	0.74533 (5)	0.51529(6)
	$TiAl_3$	0.38510(7)	0.86017 (5)	$TiAl_3$	0.38524(7)	0.86050(5)
	$TiAl_2$	0.39682(1)	2.43124 (7)	$TiAl_2$	0.39701 (7)	2.43147(2)
S2	Ti_5Si_3	0.74531(4)	0.51500(4)	Ti_5Si_3	0.74695(4)	0.51569(4)
	$TiAl_2$	0.37579(2)	2.56815(8)	$TiAl_2$	0.39791(3)	2.4425(3)
	TiAl	0.39701(2)	0.40527(3)	TiAl	0.39835(5)	0.40544(9)
S3	Ti_5Si_3	0.74675(4)	0.51548(4)	Ti_5Si_3	0.74806(6)	0.51642(6)
	TiAl	0.39800(2)	0.40708(4)	TiAl	0.39919(3)	0.40768(5)
S4	Ti_5Si_3	0.75022(5)	0.51792(5)	Ti_5Si_3	0.75078(5)	0.51828(5)
	TiAl	0.40073(4)	0.40579(6)	TiAl	0.40080(4)	0.40622(6)
	Ti_3Al	0.57690(5)	0.46295(6)	Ti_3Al	0.57760(5)	0.46354(7)
S5	Ti_5Si_3	0.74954(7)	0.51713(6)	Ti_5Si_3	0.74997(7)	0.51753(7)
	Ti_3Al	0.57951(5)	0.46424(4)	Ti_3Al	0.57921(5)	0.46423(4)
S6	Ti_5Si_3	0.74704 (2)	0.51609(2)	Ti_5Si_3	0.7486(3)	0.5169(3)
	Ti_3Al	0.5787(2)	0.4646(1)	Ti_3Al	0.58072(3)	0.46641(3)
	αTi	0.29188(5)	0.4668(2)	αTi	0.29131(1)	0.46396(2)
S7	Ti_5Si_3	0.74713(6)	0.51555(6)	Ti_5Si_3	0.74711(8)	0.51557(8)
	αTi	0.29274(2)	0.46651(3)	αTi	0.29272(3)	0.46648(4)

3.2.5. DTA analyses

DTA was performed on all alloys in the as-cast condition and, where results have been ambiguous, additionally on samples equilibrated at 900 °C. **Table 3.4** summarizes observed temperatures, allocation to certain reactions, and references for invariant reactions. Temperatures given in **Table 3.4** are evaluated from the first heating if not noted otherwise, but those, for which error limits are given, have also been observed in second heating and/or cooling cycles.

S1 showed melting at 1386 °C, in excellent agreement with 1391 °C [45] and 1380-1390 °C [77] observed for alloys of comparable composition. The temperature has been attributed to the invariant reaction L + TiAl $\leftrightarrow$ TiAl$_3$ + Ti$_5$Si$_3$ (U$_3$ in [45]). The strong signal at about 1100 °C is attributed to the reaction TiAl (1d-APS) + Ti$_5$Si$_3$ $\leftrightarrow$ TiAl$_2$ + TiAl$_3$ + Ti$_5$Si$_3$. That the signal observed in the DTA is always stronger on cooling is in line that it stems from the eutectoid decomposition of TiAl (1d-APS). This reaction is listed in the reaction scheme in [77] as "U$_{12}$". No temperature for "U$_{12}$" had yet been determined, but as indicated in [77], the temperature should be higher than 977 °C as in the binary system [7], presumably because TiAl$_3$ is the only binary Ti–Al phase which shows a substantial solid solubility for Si [45, 79]. The present investigation now shows that indeed the temperature is about 120 K higher than in the binary system. The signal observed in S1 on heating of the equilibrated sample at about 1194 °C is associated with the transition from the three-phase field TiAl (1d-APS) + TiAl$_2$ + Ti$_5$Si$_3$ to the two-phase field TiAl (1d-APS) + Ti$_5$Si$_3$, as the annealed sample consisted mainly out of TiAl$_2$, in agreement with **Figure 3.8**. The temperature is also in good agreement with the dissolution temperature of TiAl$_2$ in the binary system (1215 °C [7]), which should not be much lower in the ternary system, as the solid solubility for Si in TiAl$_2$ is very limited and actually 1216 °C have been observed for the stoichiometric ternary composition [90].

For S2 no signals were recorded during first heating (**Table 3.4**). A weak signal observed at 1143 °C during the second heating could indicate transition from TiAl + TiAl$_2$ + Ti$_5$Si$_3$ to TiAl + Ti$_5$Si$_3$. No signals were observed for S3 up to 1400 °C. In S4 the eutectoid reaction αTi + Ti$_5$Si$_3$ $\leftrightarrow$ Ti$_3$Al + TiAl + Ti$_5$Si$_3$ is observed at 1110 °C, which is in excellent agreement with 1100 °C [45] and 1107 °C [77]. The two signals at 1325 °C and 1295 °C should be associated with the transition from βTi + Ti$_5$Si$_3$ to αTi + Ti$_5$Si$_3$ on cooling.

In S5, the peritectoid formation of Ti$_3$Al on cooling is observed at 1152 °C, which was observed at 1158 °C in [45]. A signal observed at 1170 °C in an alloy of nearly the same composition may stem from the same reaction [45]. The signal in S6 at about 1095 °C is associated with the

peritectoid formation of αTi and a signal observed at 1090 °C in [45] in an alloy of nearly identical composition should be related to the same reaction. The signals in S7 at about 1080 °C and about 1030 °C are associated with crossing the αTi + βTi two-phase field, i.e. the formation of αTi and the dissolution of βTi on cooling, respectively.

Table 3.4. DTA results; reactions are listed with decreasing temperature; strength of the signals is indicated by ss (very strong), s (strong), and w (weak)

Alloy	Al (at. %)	Si (at. %)	Condition	Heated to °C	Signal (°C); strength	Reaction	Ref.
S1	55	7.5	900 °C/1504 h	1400	1386; ss	$L + TiAl + Ti_5Si_3 \leftrightarrow TiAl_3 + Ti_5Si_3$	[45, 77]
					~1194; s	$TiAl(1d\text{-}APS) + Ti_5Si_3 \leftrightarrow TiAl(1d\text{-}APS) + TiAl_2 + Ti_5Si_3$	
					1110 ± 10; s	$TiAl(1d\text{-}APS) + Ti_5Si_3 \leftrightarrow TiAl_2 + TiAl_3 + Ti_5Si_3$	[77]
			As-cast	1300	1100 ± 1; s	$TiAl(1d\text{-}APS) + Ti_5Si_3 \leftrightarrow TiAl_2 + TiAl_3 + Ti_5Si_3$	[77]
S2	47.4	9.1	900 °C/1504 h	1350	1143; w	$TiAl + Ti_5Si_3 \leftrightarrow TiAl + TiAl_2 + Ti_5Si_3$	
			As-cast	1300	--		
S3	40.4	8.9	As-cast	1400	--		
S4	32.7	7.1	900 °C/1000 h	1400	1325 ± 4; s	$\beta Ti + Ti_5Si_3 \leftrightarrow \alpha Ti + \beta Ti + Ti_5Si_3$	
					1295 ± 5; s	$\alpha Ti + \beta Ti + Ti_5Si_3 \leftrightarrow \alpha Ti + Ti_5Si_3$	
					1110 ± 5; s	$\alpha Ti + Ti_5Si_3 \leftrightarrow Ti_3Al + TiAl + Ti_5Si_3$	[45, 77]
			As-cast	1300	1109 ± 1; s	$\alpha Ti + Ti_5Si_3 \leftrightarrow Ti_3Al + TiAl + Ti_5Si_3$	[45, 77]
S5	20.4	8.6	As-cast	1300	1152 ± 2; s	$\beta Ti + \alpha Ti + Ti_5Si_3 \leftrightarrow Ti_3Al + Ti_5Si_3$	[45]
S6	14.7	9.5	900 °C/1000 h	1300	1091 ± 5; s	$\beta Ti + Ti_3Al + Ti_5Si_3 \leftrightarrow \alpha Ti + Ti_5Si_3$	
			As-cast	1300	1098 ± 1; s	$\beta Ti + Ti_3Al + Ti_5Si_3 \leftrightarrow \alpha Ti + Ti_5Si_3$	
S7	9.7	9.6	900 °C/1000 h	1350	1080 ± 5; w	$\beta Ti + Ti_5Si_3 \leftrightarrow \beta Ti + \alpha Ti + Ti_5Si_3$	
					1031; s	$\beta Ti + \alpha Ti + Ti_5Si_3 \leftrightarrow \alpha Ti + Ti_5Si_3$	
			As-cast	1400	1081; w	$\beta Ti + Ti_5Si_3 \leftrightarrow \beta Ti + \alpha Ti + Ti_5Si_3$	
					1027 ± 5; s	$\beta Ti + \alpha Ti + Ti_5Si_3 \leftrightarrow \alpha Ti + Ti_5Si_3$	

3.2.6. Vertical section at 9 at. % Si

In order to check the consistency of the determined phase equilibria, a partial vertical section (**Figure 3.11**) has been established from the intersections of the phase boundaries at 9 at. % Si in **Figures 3.1, 3, 5, 8,** and **10** and the DTA results. It is noted that the actual Si content in the alloys deviates slightly from 9 at. % Si (**Table 2.1**). Hence, some phase boundaries shown in **Figure 3.11** do not exactly match the temperatures determined by DTA (**Table 3.4**). Results from [45, 77, 78, 109] for alloys with about 8 – 10 at. % Si have been added for comparison and also to show continuation of phase boundaries up to the liquidus.

Comparison of the vertical section and the actual phase content shows that only for one out of thirty-three samples there seems to be a discrepancy. According to **Figure 3.11**, S4 should contain a minor amount of TiAl at 1200 °C, which could not be detected by EPMA or XRD. However, the composition of S4 is close to the $\alpha Ti + Ti_5Si_3/\alpha Ti + TiAl + Ti_5Si_3$ phase boundary and as S4 is the alloy with the lowest Si content (7.1 at., **Table 2.1**), the shift with respect to the vertical section at 9 at. % Si should account for this discrepancy.

The outline of the vertical section resembles that of the binary Ti–Al system. The same invariant reactions are observed except that Ti_5Si_3 is additionally present in the ternary system. In **Table 3.5** the determined temperatures of the invariant reactions are compared to those of the binary system. The peritectoid formation of Ti_3Al and of αTi occur at substantially lower temperatures than in the binary system, the eutectoid decomposition of TiAl(1d-APS) takes place at a much higher temperature in the ternary system, while the temperature of the eutectoid decomposition of αTi is little affected by the addition of Si.

Table 3.5. Temperatures of invariant reactions in Ti–Al–Si compared to those in binary Ti–Al [7, 29]

Reaction	Ti–Al–Si	Ti–Al [7, 29]
$\beta Ti + \alpha Ti (+ Ti_5Si_3) \leftrightarrow Ti_3Al (+ Ti_5Si_3)$	1152 °C	1200 °C
$\alpha Ti (+ Ti_5Si_3) \leftrightarrow Ti_3Al + TiAl (+ Ti_5Si_3)$	1110 °C	1120 °C
$TiAl(1d\text{-}APS) (+ Ti_5Si_3) \leftrightarrow TiAl_2 + TiAl_3 (+ Ti_5Si_3)$	1100 °C	977 °C
$\beta Ti + Ti_3Al (+ Ti_5Si_3) \leftrightarrow \alpha Ti (+ Ti_5Si_3)$	1095 °C	1170 °C

Results from literature [45, 77, 78, 94, 109] have been added to the vertical section. It is noted that data taken from literature also do not always lie exactly on this vertical section, as many of the investigated alloys contained 10 at. % Si. However, nearly all of the results for equilibrated samples [77, 78] are in agreement with the phase boundaries shown in **Figure 3.11**.

Bulanova et al. [78] presented a partial vertical section at 10 at. % Si for Al contents between 10 – 40 at. %, which differs in two points from the present one. Besides showing phase equilibria with Ti_3Si, though this phase was not detected in any of their samples, they show a continuous phase field for $\alpha Ti + Ti_5Si_3$. Obviously, the continuous phase field was assumed in agreement with the shape of the αTi phase field in the then-accepted Ti–Al binary system. However, in order to fit with their DTA results, they had to draw S-shaped phase boundaries, which is thermodynamically improbable. The DTA results from [78] would fit with the vertical section shown in **Figure 3.11**, however assuming different phase transitions in some of the alloys.

Data from [45, 77, 94] were used in **Figure 3.11** to show how phase boundaries may continue up to the liquidus. 1570 °C for the temperature of the invariant reaction L (+ Ti_5Si_3) $\leftrightarrow$ βTi (+ Ti_5Si_3) and 18 at. % Al for the composition of L for the intersection of the eutectic line at 9 at. % Si were adopted from [78]. This composition matches quite well with that calculated for a partial liquidus line (21 at.% Al) [94] but is somewhat higher than 15 at. % Al found in [45].

It is noted that phase boundaries extrapolated to lower temperatures are in good agreement with the isothermal section from Li et al. [88] at 700 °C.
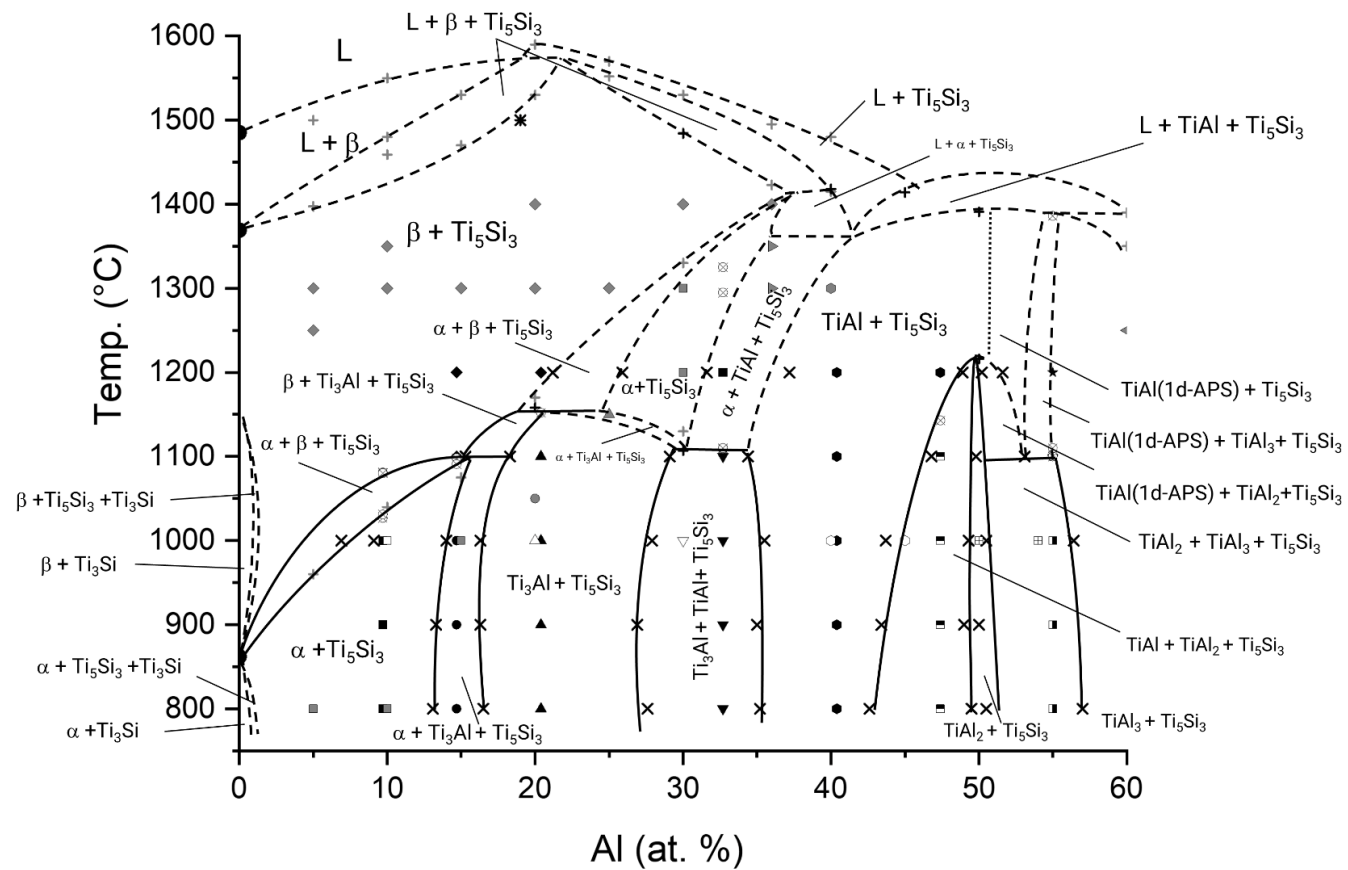
Figure 3.11. Vertical section of Ti–Al–Si system at 9 at. % Si; own data are shown in black while grey and open symbols denote data from literature (see legend for detailed references).

Legend for **Figure 3.11.**

Binary Ti–Si (Si=9 at. %) [70]	▲ Ti$_3$Al+Ti$_5$Si$_3$	◨ TiAl$_2$+TiAl$_3$+Ti$_5$Si$_3$	▲ Ti$_3$Al+Ti$_5$Si$_3$[78]
✕ Phase boundary in Fig 1, 3, 5, 7 & 8	▼ Ti$_3$Al+TiAl+Ti$_5$Si$_3$	⬓ TiAl+TiAl$_2$+Ti$_5$Si$_3$	▼ Ti$_3$Al+TiAl+Ti$_5$Si$_3$[78]
■ αTi+Ti$_5$Si$_3$	⬢ TiAl+Ti$_5$Si$_3$	■ αTi+Ti$_5$Si$_3$ [78]	▶ αTi+TiAl+Ti$_5$Si$_3$[78]
● αTi+Ti$_3$Al+Ti$_5$Si$_3$	★TiAl(1d-APS)+Ti$_5$Si$_3$	● αTi+Ti$_3$Al+Ti$_5$Si$_3$ [78]	⬡ TiAl+Ti$_5$Si$_3$[78]
◆ βTi+Ti$_5$Si$_3$	⬠ TiAl(1d-APS)+TiAl$_2$+Ti$_5$Si$_3$	◆ Ti+Ti$_5$Si$_3$ [78]	◀ TiAl$_3$+Ti$_5$Si$_3$ [77]
□ αTi+Ti$_5$Si$_3$ [45]	▽ Ti$_3$Al+TiAl+Ti$_5$Si$_3$[45]	⊗ DTA	✳ DTA [109]
○ αTi+Ti$_3$Al+Ti$_5$Si$_3$ [45]	⊞ TiAl$_2$+TiAl$_3$+Ti$_5$Si$_3$ [45]	✚ DTA [77, 78]	
△ Ti$_3$Al+Ti$_5$Si$_3$[45]	⬡ TiAl+Ti$_5$Si$_3$[45]	✚ DTA [45]	

3.2.7. Solid solubility of Si in the binary Ti–Al phases

One of the main tasks of the current undertaking was to settle the discrepancy in published data about the solid solubility of Si in the binary Ti–Al phases. The comparison of the partial isotherms in **Figures 3.1, 3, 5** and **8** shows that the solid solubility for Si in βTi increases with increasing temperature. At all temperatures, the solid solubility decreases with increasing Al content, in agreement with [77-81], and therefore the highest solid solubility is observed in binary Ti–Si at all temperatures. Also, the solid solubility of Si decreases steadily with increasing Al content, ruling out the thermodynamically improbable S-shape of the βTi phase boundary calculated in [83, 84].

Figure 3.12 illustrates the solid solubility of Si in αTi, Ti$_3$Al, TiAl, and TiAl$_2$ in dependence on temperature. **Figure 3.12** shows those compositions, for which no marked change in the Al content in dependence on temperature is observed. For αTi with about 12 at. % Al (S7), the solid solubility for Si increases from 0.8 at. % Si at 800 °C to 1.3 at. % at 1000 °C. These data are in perfect agreement with those data determined by [80, 81] for αTi with about 10 at. % Al. The solid solubility of Si in αTi at a given temperature does also not change with the Al content, as shown in [80, 81] for lower Al contents, and by comparison with data determined at higher

Al contents for αTi in alloy S6. However, calculated isotherms in [47, 84] show slight variations of the solubility for Si with the Al content.

Data for S5 show that the solid solubility of Si in Ti_3Al with about 25 at. % Al is about 1.4 at. % and that it does not change with temperature. It is therefore somewhat higher than in disordered αTi. The data are in excellent agreement with those measured in [47] and notably smaller than determined in [45, 79].

In alloy S3 the solid solubility of Si in TiAl is about 0.5 at. % and independent of temperature. This value agrees with compositions determined for TiAl in alloys S2 and S4. From the shape of the single-phase field in **Figures 3.1, 3, 5, 8,** and **10** it is evident that 0.5 at. % Si should also correspond to the maximum solid solubility of Si in TiAl. This value agrees with data measured for TiAl in as-cast alloys [78] and in a directionally solidified alloy [110], but is considerably lower than found in most previous studies, where 1 to 4 at. % Si at 550 °C [90], 0.8 at. % Si at 700 °C [88], 2 to 3 at. % Si at 700 °C [86] and at 1000 °C [45], 1 at. % Si at 1200 °C [79], and 1 to 1.5 at. % Si in diffusion couples annealed between 700 and 1000 °C [46] were reported. On the other hand, no Si was detected by TEM-EDS in TiAl in a two-phase $TiAl + Ti_5Si_3$ alloy annealed at 1200 °C [106, 111].

Data for S1 and S2 show that the solid solubility for Si in $TiAl_2$ is only about 0.3 at. %, independent of temperature. This value is much smaller than any of those measured before, i.e. 1.4 at. % Si at 550 °C [90], 1.5 at 700 °C [88], 1.8 at. % Si at 900 °C [46], and 0.7 at. % Si at 1000 °C [45]. $TiAl_3$ is the only binary Ti–Al phase with a marked solid solubility for Si, which exceeds 10 at. % in equilibrium with $TiSi_2$ [45, 46, 77, 79, 85, 88, 109]. As no adequate alloy compositions have been studied, no additional information can be gained from the current investigation.
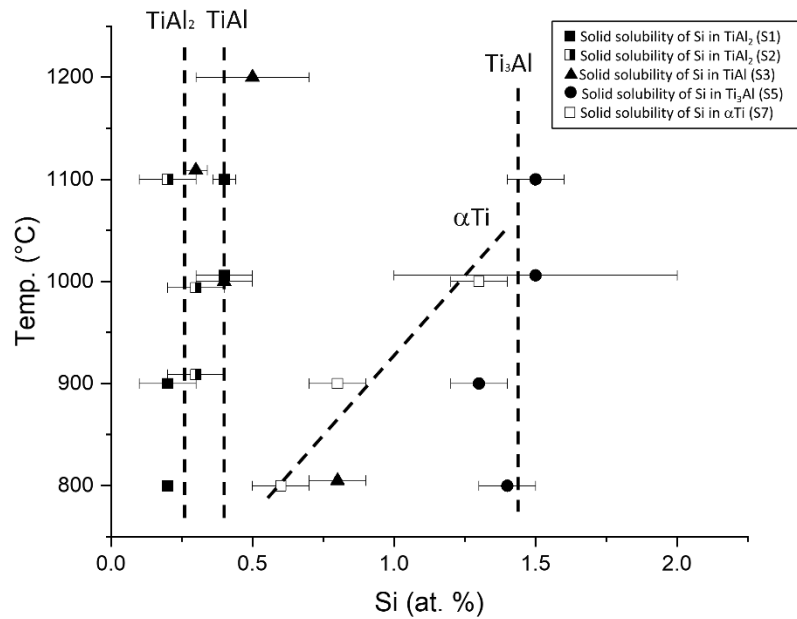
Figure 3.12. The solid solubility of Si in αTi, Ti₃Al, TiAl, and TiAl₂ in dependence on temperature in alloys S7, S5, S3, S2 and S1 respectively.

3.2.8. Solid solubility of Al in Ti₅Si₃

As detailed above, establishing the actual Al content of Ti₅Si₃ is difficult because it is not possible to equilibrate large, primary Ti₅Si₃ grains within reasonable annealing times. The established partial isothermal sections show that the maximum solid solubility for Al is always attained at the three-phase equilibrium Ti₅Si₃ + αTi or Ti₃Al + TiAl (**Figures 3.1, 3, 5, 8,** and **10**), which is observed in alloy S4. The data for S4 in **Table 3.2** show a solid solubility of about 7 at. % Al in Ti₅Si₃ at all investigated temperatures. Though there is some scatter in the data, the solid solubility for Al does only little, if at all, change with temperature. The maximum solid solubility of about 7 at. % Al corresponds to the value reported by Manesh & Flower [94] for "fine silicides" extracted from the eutectic in an as-cast alloy. A similar value for the maximum solid solubility has also been reported in the 1200 °C isotherm by Schob et al. [79], however for the equilibrium βTi + Ti₃Al ("Ti₃₋₂Al") + Ti₅Si₃. Otherwise, mostly higher values have been measured, e.g., 10.9 at. % Al for an alloy equilibrated at 1000 °C [45], 15 to 20 at. % Al in samples prepared by self-propagating high-temperature synthesis (SHS) [49] or by ball milling [48, 50]. However, for the latter case it has been shown that such high Al contents indicate metastable compositions of Ti₅Si₃ [50]. Higher solid solubilities of either 9.2 [111] or

13.4 at. % Al [106] measured by TEM-EDS in Ti_5Si_3 after annealing for 12 h at 1200 °C are possibly due to a too short annealing time.

Significantly lower values for the maximum solid solubility of Al in Ti_5Si_3 were shown in the 1000 °C isotherm by Gupta [46] (3 at. % Al) and in the 700 °C isotherm by Raman & Schubert [86] (5 at.% Al). In both cases the maximum solid solubility is shown for phase equilibria with $TiAl_3$. According to the partial isothermal sections shown in **Figures 3.1, 3, 5, 8,** and **10** such low Al contents are reasonable for Ti_5Si_3 in equilibrium with $TiAl_3$, but do not correspond to the maximum solid solubility for Al, which is attained for Ti_5Si_3 + Ti_3Al + TiAl at these temperatures according to the present partial isothermal sections.

Zhang & Flower [112] showed that Al substantially increases the lattice constants of Ti_5Si_3, which was confirmed in [48, 49], while according to Zha et al. [49] the addition of Al has almost no effect on the lattice constants of Ti_5Si_3 and Bulanova et al. [78] showed a graph, where a_0 of Ti_5Si_3 first decreases, then increases and then decreases again with increasing Al content. To solve this conflicting evidence, lattice constants measured in samples annealed at 800-1200 °C are plotted in **Figure 3.13(a,b)**. Both figures show a steady increase of the lattice constants with increasing Al content. For samples annealed at 1200 °C the increase is even linear (**Figure 3.13; solid symbols**), while for other temperatures there is more scatter of the data (**Figure 3.13; open symbols**). Comparing the data for different temperatures in **Figure 3.13,** there is no evident dependence between annealing temperature and lattice constants. It is noted that, though lattice constants of Ti_5Si_3 show a strong dependence on Al content, they will also vary in dependence on Si content. However, data for Ti_5S_3 in S3 heat-treated at 1000 °C show the largest deviation in **Figure 3.13**, which suggests that Ti_5Si_3 should actually have a lower Al content than the measured value in **Table 3.3**. A lower Al content would indeed fit much better to those Al contents measured for Ti_5Si_3 in S3 at all other temperatures.

The discrepancy in previous data is explained in [48, 49, 78], where lattice constants were shown in dependence on the overall composition of the alloys and not on the actual Al content of Ti_5Si_3. The present results are therefore consistent with results by Kasraee et al. [48], who observed an increase of the lattice constants in "stoichiometric alloys" when they contained up to 7.5 at. % Al, while no further increase was observed for higher Al contents. All samples in Zha et al. [49] were actually located in the three-phase field $TiAl_3$ + Ti_5Si_3 + Ti_5Si_4. Therefore it can be expected that the composition of Ti_5Si_3 is the same in all samples, hence, the lattice constants do not change with increasing Al content. Lattice constants in Bulanova et al. [78] were taken from alloys annealed at about 1300 °C, in which Ti_5Si_3 is in equilibrium with

different phases. It is presumably therefore that lattice constants show a "sinus curve behaviour" in dependence on the Al content.
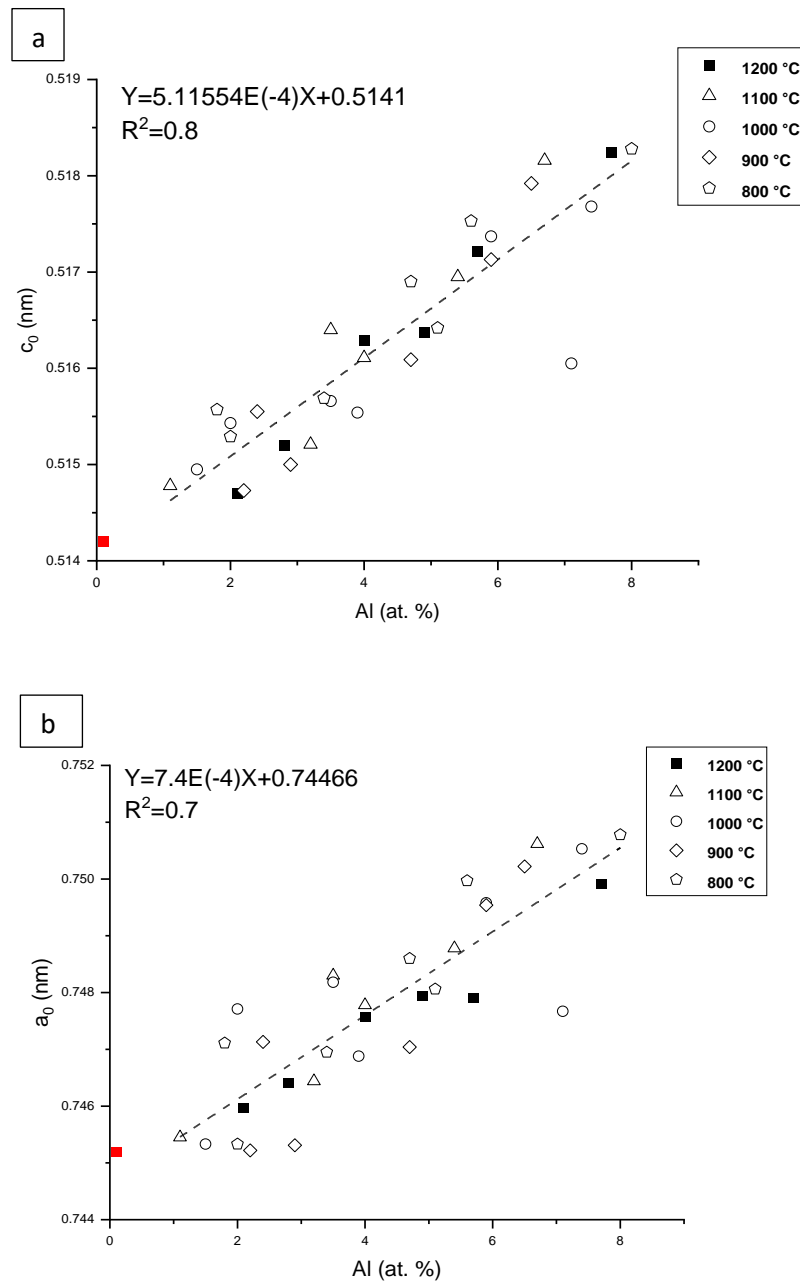
Figure 3.13a, b) Lattice constants of Ti_5Si_3 in relation to Al content; samples have been quenched from 800-1100 °C given as open symbols. Samples have been quenched from 1200 °C given as solid symbols, ■current work, ■ Ti_5Si_3 from binary Ti–Si [101].

3.3. Conclusion

Knowledge of the precise solid solubilities of Al in Ti_5Si_3 and Si in the Ti–Al phases is a perquisite for tailoring the microstructures and thereby the mechanical properties of TiAl-based alloys. From SEM, EPMA, XRD, TEM and DTA investigations, five partial isothermal sections between 800-1200 °C have been established.

No ternary phase was found and Ti_3Si was not detected in any of the alloys. The solid solubilities of Al in Ti_5Si_3 and Si in TiAl, $TiAl_2$ and Ti_3Al do not change in dependence on temperature. Lattice constants of Ti_5Si_3 for all heat-treated samples were calculated and results show that both lattice constants increase with increasing Al content. The partial vertical section of Si 9 at. % shows that all established data are consistent. These data can now be employed to set up the next generation of advanced CALPHAD databases for the development of TiAl-based alloys with improved properties.

4. Ti–Al–Zr system

First attempts of alloying TiAl-based alloys with Zr date back to the 1950s. When TiAl-based alloys were considered for structural applications, it was soon realized that room temperature ductility is an issue for their further development. Attempts have been made to reduce the c/a ratio of TiAl (ordered face-centered tetragonal $L1_0$) to unity by adding Zr [113, 114]. However, though tetragonality could be reduced ductility was not improved and Zr was not considered as an alloying element in commercial TiAl-based alloys. At the beginning of the 21st century, the introduction of the new class of β-stabilized TiAl-based alloys attracted interest in alloying elements which tend to partition to βTi; among them Zr [3, 115]. But it is only recently that Zr was implemented into the novel TiAl-based TNM AM alloys [53]. Nevertheless, the phase equilibria in the Ti–Al–Zr system are not well studied. The last assessment of the system covers the literature up to 2003 [54]. At that time, there were not enough experimental or thermodynamic data to realize any isothermal section and Tretyachenko [54] could only report phase equilibria among αTi, βTi and TiAl at 1200 and 1300 °C. Since then, many new experimental investigations have been carried out and complete, however somewhat contradicting, isothermal sections were established. As the information on phase equilibria in the Ti–Al–Zr system has substantially increased, it is crucial to perform a critical assessment considering all the newly published results.

In the following chapter (**chapter 4.1**) a complete assessment of all literature on the Ti–Al–Zr system up to the year 2020 is presented. This chapter is based on the two publications by the author [116, 117]. The introduction (**section 4.1.1**) gives an overview of the Ti–Al–Zr system and highlights the necessity of conducting a new assessment and details the specific challenges concerning the investigation of phase equilibria in this system. The underlying binary systems, i.e. Ti–Al, Ti–Zr, and Al–Zr are updated compared to the previous assessment in **section 4.1.2**. Discussion about the existence of a ternary phase and stabilization of $β_0$ (ordered body-centered cubic) are addressed in **section 4.1.3**. From critical evaluation of the existing literature, newly assessed isothermal sections at 1000 °C and 800 °C are presented in **sections 4.1.4 and 4.1.5**, respectively. As data were insufficient to establish any isothermal sections below 800 and above 1000 °C, only the respective literature is critically assessed in **sections 4.1.6 and 4.1.7**. A significant number of early publications from the 1960s from the former USSR reported vertical sections that were not thoroughly discussed in the previous assessment [54] and, therefore, are discussed in **section 4.1.8**. Finally, in **section 4.1.9** the literature on thermodynamic

calculations and CALPHAD-type modellings is assessed. Especially these recent publications, which use the more recent experimental data in their calculations, show that substantial discrepancies between experiments and calculations exist, which stem from the deficiencies of reliable experimental data.

In view of the necessity for sound thermodynamic data **chapter 4.2** comprises the experimental investigation of phase equilibria in the Ti–Al–Zr system at 1000-1300 °C. The chapter is based on the author's recent publication [118]. It starts with the introduction (**section 4.2.1**), in which the importance of new investigations of phase equilibria in the Ti–Al–Zr system for the development of TiAl-based alloys is detailed. **Sections 4.2.2** explains why certain references were chosen for the binary reference systems. The partial isothermal sections between 1000-1300 °C and how they were established from the current experiments are shown in **sections 4.2.3** to **4.2.6**. Transformation temperatures determined by DTA yield information for phase transformations and invariant reactions between the partial isothermal sections and at higher and lower temperatures. Measured temperatures and how they were allocated to certain reactions are described in **section 4.2.7**. In view of the extended research regarding the effect of Zr on the lattice parameters for TiAl and the partly contradicting results, lattice parameters obtained for TiAl from current work are illustrated and discussed in **section 4.2.8**. Finally, **section 4.2.9** sums up the main findings of the current experimental investigation and presents a comparison of the partial isothermal sections at 1000 °C established from the assessment of the literature in **section 4.1.4** and from the current experiments.

Sections 4.1.1. to **4.1.9.** were published in Kahrobaee and Palm [116]. **Sections 4.2.1.** to **4.2.9.** were published in Kahrobaee et al. [118]. Compared to the original publication [118], the introduction (**section 4.2.1**) has been substantially shortened to avoid repetition, while a comparison of the assessed isothermal section at 1000 °C (**section 4.1.4.** and the newly determined one (**section 4.2.3.**) has been added now in **section 4.2.9**.

4.1. Critical assessment of the Ti–Al–Zr system

4.1.1. Introduction

In view of applications, different parts of the Ti–Al–Zr system are of interest and investigation of phase equilibria over the decades reflects these interests. With the development of Ti-base alloys, the extension of the homogeneity ranges of βTi,Zr and αTi,Zr within the ternary system in dependence of temperature have been investigated [119-121]. In the Al corner of the system precipitation of (Ti,Zr)Al$_3$ has been investigated for strengthening Al alloys at higher temperatures [122-125] and for grain refining [126-128]. As ductility may improve if instead of tetragonal TiAl$_3$ (D0$_{22}$) or ZrAl$_3$ (D0$_{23}$) metastable (Ti,Zr)Al$_3$ with cubic L1$_2$ structure forms, quite some effort has been spent on establishing phase stability in the Al-rich part of the system [129-135]. With the industrialization of TiAl based alloys, phase equilibria among the Ti–Al based phases in this system came into focus [58, 115, 136-139]. While all these activities were limited to specific parts of the system, studies of full isothermal sections have been performed only very recently [55, 56].

Though of some practical importance, experimental difficulties in investigating Ti–Al(–X) systems at high temperatures make the determination of phase equilibria difficult. High susceptibility to impurities, specifically oxygen, which can have a pronounced effect on phase equilibria, reactions of melts with crucibles or preferential evaporation of Al are some of these problems [29, 140]. The addition of Zr does not improve things, as it is also highly susceptible to oxygen uptake and because of its high melting point and low diffusivity, quite long annealing times are necessary to attain equilibrium even at high temperatures [55, 56]. And the fact that even "high-purity" Zr contains comparable high amounts of impurities [57, 58], specifically Hf, is most of the time neglected.

The key for any aimed alloy development is a sound knowledge of phase equilibria in dependence of temperature and composition. In this regard, assessments play an important role as they collect all the available evidence and critically evaluate it. This is specifically true for the Ti–Al–Zr system, where until recently only scattered information had been available. The current work continues previous assessments by Ansara et al. [141] and Tretyachenko [54], which have been performed in the framework of MSIT.

4.1.2. Binary systems

The binary Al–Zr system is accepted from [142]. The different assessments of the Al–Zr system [142-144] and the thermodynamic modelling [145-147] are in good agreement with each other. According to them, ten stable intermetallic phases, all with restricted homogeneity ranges, exist: Zr_3Al, Zr_2Al, Zr_5Al_3, Zr_3Al_2, Zr_4Al_3, Zr_5Al_4, $ZrAl$, Zr_2Al_3, $ZrAl_2$, and $ZrAl_3$. Their crystallographic structures, lattice parameters and stability ranges are listed in **Table 4.1**. For $ZrAl_3$ it has been shown more recently that the phase forms by the peritectic reaction $L + ZrAl_2 \leftrightarrow ZrAl_3$ [148] in agreement with a previous modelling [149], rather than being a congruent melting compound [142, 144]. The temperatures above which, the phases Zr_5Al_3 and Zr_5Al_4 become stable and the temperature below which, Zr_3Al_2 is stable, are uncertain [142]. Also the liquidus and solidus of βZr have not been precisely determined, while the $\beta Zr/(\beta Zr + Zr_3Al)$ and $\beta Zr/(\beta Zr + \alpha Zr)$ phase boundaries were determined in [150]. The Ti–Zr system, which is accepted from Malfliet et al. [151], shows complete miscibility in the liquid and in the solid. The Ti–Al system has been assessed more recently in [29, 152, 153]. Here both versions by [7, 29] are accepted. While no substantial new experimental results have become available since [29], modelling may yield some insight in two existing controversies about phase equilibria in the Ti–Al system [7, 29]. The first one regards the possible B2 ordering in βTi. Wang et al. [154] combined ab-initio calculations with CALPHAD modelling and showed that in the "pure" Ti–Al system no B2 ordering is observed. However, if substitutional vacancies and anti-site defects are considered in B2, then ordered βTi is observed, thereby stabilising βTi at higher Al contents. As a consequence, B2-ordered βTi (β_0) forms an equilibrium with Ti_3Al, whereby the homogeneity range of αTi gets interrupted by the two invariant reactions $\beta Ti + \alpha Ti \leftrightarrow Ti_3Al$ at about 1200 ± 10 °C and $\beta Ti + Ti_3Al \leftrightarrow \alpha Ti$ at 1170 ± 10 °C [154]. As substitutional vacancies and anti-site defects have to be expected at the respective temperatures, it now becomes clear why, in contrast to experimental evidence, modelling of the "pure" Ti–Al system shows a continuous αTi phase field [154-159]. Another open question is the transition from high-temperature $TiAl_3$ ($D0_{22}$) to the low-temperature $D0_{23}$-polymorph [29]. Recent density functional theory (DFT) calculations by Fang & Fan [160] showed that a series of intermediate stacking configurations of high stability exist. As even annealing for long time at intermediate temperatures may not equilibrate these "wrong" stacking, it becomes clear why $TiAl_3$ compounds of varying stacking sequences have been observed in dependence on individual experimental conditions [161]. Therefore, also the recent update of the system [7] shows only the presence of the two polymorphs $TiAl_3$ (h) and $TiAl_3$ (l), but no transformation temperature.

Table 4.1. Crystallographic data of solid phases

Phase/ (Strukturbericht designation),Temperature Range (°C)	Pearson Symbol/ Space Group/ Prototype	Lattice Parameters (nm)	Comments/References
(Al), (*A1*), <660.452	*cF4* $Fm\bar{3}m$ Cu	$a_0 = 0.40496$	Pure Al at 25°C [162]
βTi, (*A2*), <1670-882	*cI2* $Im\bar{3}m$ W	$a_0 = 0.33065$	[162] Dissolves 44.6 at.% Al at 1491 °C [29]
		$a_0 = 0.3228$ 35.1 at.% Ti, 23.7 at.% Al, 41.2 at.% Zr [55]	Dissolves ~25 at.% Al at ~25 at.% Zr, ~50 at.% Ti at 1000 °C [55]
αTi, (*A3*), 1491-1120 and <1170	*hP2* *P6₃/mmc* Mg	$a_0 = 0.29506$ $c_0 = 0.46835$	Pure Ti at 25°C [162] Dissolves 50.5 at.% Al at 1456 °C [29] Dissolves 5.8 at.% Zr at 1000 °C [55]
(α₂) Ti₃Al, (*D0₁₉*), <1200	*hP8* *P6₃/mmc* Ni₃Sn	$a_0 = 0.5765$ $c_0 = 0.4625$ [96]	<20-38.5 at.% Al [29]
		$a_0 = 0.5783$ $c_0 = 0.4667$ 52.1 at.% Ti, 28.0 at.% Al, 19.9 at.% Zr [55]	Dissolves ~20 at.% Zr at 1000 °C [55]

Phase/ (Strukturbericht designation),Temperature Range (°C)	Pearson Symbol/ Space Group/ Prototype	Lattice Parameters (nm)	Comments/References
(γ) TiAl, ($L1_0$), <1456	$tP4$ $P4/mmm$ AuCu	$a_0 = 0.4000$ $c_0 = 0.4075$ at 50 at.% Al [97] $a_0 = 0.4080$ $c_0 = 0.4087$ ~42 at.% Ti, ~47 at.% Al, ~11 at.% Zr [163] $a_0 = 0.3974$ $c_0 = 0.4072$ 41.5 at.% Ti, 50.6 at.% Al, 7.9 at.% Zr [55]	46.5-~73 at.% Al [29] Dissolves ~7.9 at.% Zr at 1000 °C [55] Dissolves ~13 at.% Zr at 1274 °C [58]
$TiAl_2$, <1215	$tI24$ $I4_1/amd$ $HfGa_2$	$a_0 = 0.3971$ $c_0 = 2.431.2$ [164]	65.5-67.0 at.% Al [29] Dissolves 11.5 at.% Zr at 1000 °C [55] Dissolves 11.2 at.% Zr at 800 °C [56]
1d-APS (Ti_5Al_{11}, Ti_2Al_5) one-dimensional antiphase domain structures which form on cooling in Al-rich TiAl	tetragonal ordered superstructures of AuCu	$a_0 = 0.39230$ $c_0/4 = 0.41337$ [165] $a_0 = 0.39053$ $c_0/7 = 0.41703$ [165]	for Ti_5Al_{11} ($I4/mmm$, $tI16$, $ZrAl_3$ [86]) for Ti_2Al_5 ($P4/mmm$, $tP28$, Ti_2Al_5 [166])
$TiAl_3$ (h), ($D0_{22}$), 1387-?	$tI8$ $I4/mmm$ $TiAl_3$ (h)	$a_0 = 0.3849$ $c_0 = 0.8610$ [100, 167]	74.2-75.5 at.% Al [7, 29]
$TiAl_3$ (l), ($D0_{23}$), ?	$tI32$ $I4/mmm$ $TiAl_3$ (l)	$a_0 = 0.3877$ $c_0 = 3.3832$ [100, 167]	74.2-75.5 at.% Al [7, 29] Dissolves 7.5 at.% Zr at 1000 °C [55]

Phase/ (Strukturbericht designation),Temperature Range (°C)	Pearson Symbol/ Space Group/ Prototype	Lattice Parameters (nm)	Comments/References
βZr, (A2), <1855-863	cI2 $Im\bar{3}m$ W	$a_0 = 0.36090$ [142]	[162] Dissolves 26 at.% Al at 1350 °C [143]
αZr, (A3), <863	hP2 $P6_3/mmc$ Mg	$a_0 = 0.32316$ $c_0 = 0.51475$ [142]	Pure αZr at 25°C [162] Dissolves 8.3 at.% Al at 910 °C [150]
Zr₃Al, (L1₂), <1019 ± 2	cP4 $Pm\bar{3}m$ Cu₃Au	$a_0 = 0.4373$ [142]	[150]
Zr₂Al, (B8₂), <1215 ± 10	hP6 $P6_3/mmc$ Ni₂In	$a_0 = 0.48939$ (5) $c_0 = 0.59283$ (5) [142]	[150] Dissolves 10.6 at.% Ti at 1000 °C [55] Dissolves 13.8 at.% Ti at 800 °C [56]
Zr₅Al₃, (D8ₘ), <1400-1000	tI32 I4/mcm W₅Si₃	$a_0 = 1.1044$ $c_0 = 0.5391$	[142, 168]
Zr₅Al₃, (D8₈), (<1000?)	hP16 $P6_3/mcm$ Mn₅Si₃	$a_0 = 0.8174$ $c_0 = 0.5698$ [142] $a_0 = 0.8217$ $c_0 = 0.5704$ 30.5 at.% Ti, 39.2 at.% Al, 30.3 at.% Zr [55]	[169, 170] Dissolves 32.0 at.% Ti at 1000 °C [55]
Zr₃Al₂, <1480	tP20 $P4_2/mnm$ Zr₃Al₂	$a_0 = 0.763$ (1) $c_0 = 0.6998$ (1) [142]	[142] Dissolves 14.4 at.% Ti at 800 °C [56]
Zr₄Al₃, <1030	hP7 P6/mmm Zr₄Al₃	$a_0 = 0.5433$ (2) $c_0 = 0.539$ (2) [142] $a_0 = 0.5411$ $c_0 = 0.5354$ 5.6 at.% Ti, 43.4 at.% Al, 51.0 at.% Zr [55]	[142] Dissolves 5.6 at.% Ti at 1000 °C [55] Dissolves 13.5 at.% Ti at 800 °C [56]
Zr₅Al₄, <1550-~1120 (?)	hP18 $P6_3/mcm$ Ti₅Ga₄	$a_0 = 0.8448$ $c_0 = 0.5805$ [142]	[142, 171]

Phase/ (Strukturbericht designation),Temperature Range (°C)	Pearson Symbol/ Space Group/ Prototype	Lattice Parameters (nm)	Comments/References
ZrAl, (*B33*), <1225 ± 25	*oC8* *Cmcm* CrB	$a_0 = 0.3359$ (1) $b_0 = 1.0887$ (3) $c_0 = 0.4274$ (1) [142]	[142]
Zr_2Al_3, <1572 ± 3	*oF40* *Fdd2* Zr_2Al_3	$a_0 = 0.9601$ (2) $b_0 = 1.3906$ (2) $c_0 = 0.5574$ (2) [142] $a_0 = 0.9589$ $b_0 = 1.3946$ $c_0 = 0.5578$ 0.3 at.% Ti, 59.8 at.% Al, 40.2 at.% Zr [55]	[148] Dissolves 0.8 at.% Ti at 1000 °C [55] Dissolves 1.3 at.% Ti at 800 °C [56]
$ZrAl_2$, (*C14*), <1624	*hP12* *P6₃/mmc* $MgZn_2$	$a_0 = 0.52824$ (5) $c_0 = 0.87482$ (5) [142] $a_0 = 0.5273$ $c_0 = 0.8827$ 8.7 at.% Ti, 60.1 at.% Al, 31.2 at.% Zr [55]	[148] Dissolves 8.7 at.% Ti at 1000 °C [55]
$ZrAl_3$, ($D0_{23}$), <1579 ± 3	*tI16* *I4/mmm* $ZrAl_3$	$a_0 = 0.39993$ (5) $c_0 = 1.7283$ (2) [142]	[148] Dissolves about 12 at.% Ti at 1000 °C [55]
Ti_2AlZr, (*B2*)	*cP2* $Pm\bar{3}m$ CsCl	$a_0 = 0.333(6)$ [172]	After annealing the stoichiometric composition at 1200 °C [172]
Ti_2AlZr, ($D0_{19}$)	*hP8* *P6₃/mmc* Ni_3Sn	$a_0 = 0.5961(1)$ $c_0 = 0.4793$ (1) [173]	After annealing the stoichiometric composition at 1000 °C [173]
Zr_2TiAl, ($L2_1$)	*cF16* $Fm\bar{3}m$ $AlCu_2Mn$	$a_0 = 0.684$ [174]	After annealing the stoichiometric composition at 1000 °C or 1050 °C [174]

4.1.3. Phases

Some of the binary phases show large solid solubility ranges for the third element and two ternary compounds, Ti_2AlZr [172, 173, 175] and Zr_2TiAl [174], have been reported which actually could be ordered structures within the wide homogeneity range of $\beta Ti,Zr$.

Addition of Zr to Ti or Ti to Zr stabilizes β with respect to α, i.e. in both cases the α/β transformation temperature is lowered [51, 176]. Within the Ti–Al–Zr system $\beta Ti,Zr$ encompasses a wide range of compositions. At high temperatures it includes the stoichiometric compositions Ti_2AlZr and Zr_2TiAl, for which both specific crystallographic structures have been reported (**Table 4.1**).

Al-rich samples of $\beta Ti,Zr$ annealed for 168 h at 900 °C showed B2-ordering [177]. In an as-cast alloy of stoichiometric composition, the two phases Ti_2AlZr and Zr_5Al_3 were observed [172]. In the as-cast condition Ti_2AlZr showed the $D0_{19}$ structure, space group *P6₃/mm*, while after annealing at 1200 °C for 30 min and also after subsequent ageing at 500 °C for 100 h or at 700 °C for 24h single-phase B2-ordered $\beta Ti,Zr$ was obtained [172]. Mechanical deformation lead to the formation of orthorhombic martensite [172, 178]. B2 ordering was also reported for Al-rich $\beta Ti,Zr$ synthesised from hydrides at 1000 °C [179]. Contrary to these observations, Ti_2AlZr with $D0_{19}$ structure was also observed after annealing an arc-melted button of the stoichiometric composition at 1000 °C for 720 h [173]. This is in agreement with ab-initio calculations, which predicted that Ti_2AlZr will have the $D0_{19}$ structure [175, 180, 181]. However, quenching or deformation of Ti-rich compositions of $\beta Ti,Zr$ may lead to formation the hexagonal ω phase and orthorhombic α'' and hexagonal α' martensite [51, 172, 175, 178] like in many other Ti-based alloys, e.g. in the Ti–Al–Nb system. However, details how the formation of the individual crystallographic structures depends on composition and quenching conditions still have to be established. The site occupation within the B2-ordered phase has been modelled by ab-initio calculations [182]. Interdiffusion coefficients for Ti-rich $\beta Ti,Zr$ at 1000 °C and 1200 °C have been determined in [183].

A phase Zr_2AlTi with cubic $L2_1$ structure, space group *Fm3m* was found in an alloy of stoichiometric composition after annealing at 1050 °C for 720 h or 1000 °C for 480 h [174]. The analyzed composition of Zr_2AlTi lies near or at the $\beta Ti,Zr/(\beta Ti,Zr + Zr_5Al_3)$ phase boundary [55, 184]. That Zr_2AlTi was accompanied by two other phases, of which one could

be Zr_5Al_3 or $(Zr,Ti)_2Al$ according to XRD and analyzed composition [174], may indicate that also this structure may result from ordering within βTi,Zr.

All phases originating in the binary Ti–Al system show a marked solid solubility for Zr (**Table 4.1**). At 1000 °C 6 at.% Zr in αTi,Zr, 20 at.% Zr in Ti_3Al, 8 at.% Zr in TiAl, 12 at.% Zr in $TiAl_2$ and 7.5 at.% Zr in $TiAl_3$ may dissolve [55]. The solid solubility in all phases seems to increase with increasing temperature, e.g. at 1274 °C about 13 at.% Zr may dissolve in TiAl [58]. For the site occupation of Zr in TiAl a strong preference for Ti sites was found [58, 137-139, 185, 186]. Also, in Ti_3Al Zr substitutes for Ti [139, 185, 186]. It was also found that the temperature of the αTi,Zr/Ti_3Al phase boundary is only slightly raised by the addition of Zr [121].

The change from $TiAl_3$ with $D0_{22}$-structure to $ZrAl_3$ ($D0_{23}$-structure) along $(Ti,Zr)Al_3$ in dependence of composition and temperature was investigated by high-temperature XRD [130]. Lattice constants for $(Ti,Zr)Al_3$ with $D0_{22}$- and $D0_{23}$-structure have been determined in [122, 124, 130, 179] and for metastable $L1_2$ in [125, 129, 131, 133, 134]. The formation of metastable $(Ti,Zr)Al_3$ with $L2_1$–structure in Al has been investigated in [135] and transformation to stable $D0_{23}$ during aging between 450–600 °C was studied by transmission electron microscopy (TEM) [132].

Also, most phases originating in the binary Zr–Al system show a marked solid solubility for Ti (**Table 4.1**). Solid solubilities of about 12 at.% Ti in $ZrAl_3$, 9 at.% Ti in $ZrAl_2$, and even 32 at.% Ti in Zr_5Al_3 at 1000 °C [55] and about 14 at.% Ti in Zr_4Al_3, Zr_3Al_2 and Zr_2Al at 800 °C have been reported [56].

4.1.4. Isothermal section at 1000 °C

Most data are available for 1000 °C and the most comprehensive investigation was performed by [55], who determined a complete isothermal section (**Figure 4.1**). More than 38 alloys of about 5 grams each were produced by arc-melting. As the weight loss during alloy production did not exceed 1 wt. %, nominal compositions have been considered as ultimate alloy compositions. Heat treatments were performed at 1000 °C for 1440 h for samples encapsulated in quartz tubes back-filled with Ar followed by water quenching. Samples were examined by metallography, XRD and EPMA. Compositions of coexisting phases were established by an average of five EPMA measurements. The standard deviations of the measured concentrations are ± 0.6 at. % and the total mass of Al, Zr, and Ti was in the range of 97–103%. **Figure 4.1** shows the established isotherm from [55]. While no ternary phases were detected, most binary

phases show marked solid solubility ranges for the third component. It is noted that phase boundaries do not match those currently accepted for Ti–Al [29] and that some phase boundaries are not in accordance with thermodynamic rules applying to isothermal sections [187]. Extrapolation of the phase boundaries from the ternary system onto the binary Al–Zr system shows that apparently the "line compounds" Zr_5Al_3 and $ZrAl_2$ have some marked solid solubility ranges in the binary. The phase Zr_3Al, which should be stable at 1000 °C (**Table 4.1**), has not been detected in [55]. As the solid solubility for Ti in this phase could be very small, it may not have been observed, because no alloy of appropriate composition has been investigated. The phase Zr_5Al_4, which might be stable at 1000 °C [142], has also not been detected in [55]. This is in line with an investigation of the Fe–Al–Zr system, which showed that this phase may only become stable above ~1120 °C [171]. For a discussion, whether Zr_5Al_3 with the Mn_5Si_3-type crystal structure is stable in the binary Al–Zr system or not see [170]. However, it is clear that impurities and third alloying elements stabilise the Mn_5Si_3-type structure in favour of W_5Si_3-type Zr_5Al_3, which might be the stable structure in binary Al–Zr at 1000 °C [142]. Therefore, it is plausible that [55] observed the Mn_5Si_3-type structure for $(Zr,Ti)_5Al_3$. The phase Ti_2Al_5 has by now been identified as a one-dimensional antiphase domain structure, which forms from TiAl that becomes supersaturated in Al on cooling [29]. Among other investigations at this temperature, the homogeneity range of TiAl was studied on 24 different arc-melted alloys, heat-treated at 1000 °C for 10 h [188]. Phases were identified by XRD but no compositions of coexisting phases were established. The solid solubility for Zr in TiAl was found to be about 15 at.%, which is much higher than that reported in [55]. Presumably – and as acknowledged by the authors – annealing times in [188] were too short for equilibrating TiAl. Therefore, alloys may have been supersaturated in Zr from the melting process at high temperatures and therefore the reported solid solubility may be too high. The solid solubility range of TiAl has also been examined on 21 alloys heat treated at 1000 °C for 168 hours [163]. Phases were analyzed by XRD and compositions of phases were established by EPMA, but only lattice constants for TiAl are given and compositions can only be read for TiAl from a figure. According to this study the maximum solid solubility for Zr in TiAl could be about 11 at. % at about 47 at. % Al. Also the presence of the three-phase equilibria TiAl + Ti_3Al + ZrAl and TiAl + $ZrAl_2$ + ZrAl at 1000 °C is shown [163], in contradiction to the results by [55]. The occurrence of phase equilibria between TiAl and ZrAl seems unlikely, because the solid solubility for Ti in ZrAl is very limited compared to that in $ZrAl_2$ and Zr_5Al_3, which makes the presence of three-phase equilibria with the latter two phases more likely, as

determined in [55] (**Figures 4.1 and 4.2**). Two alloys investigated in [137] were single-phase TiAl after annealing at 1000 °C for 192 h, in accordance with [55].The width of the TiAl + Ti_3Al two-phase field at 1000 °C was studied in [136] on 10 alloys, which were equilibrated for 168 h. Phases were identified by XRD and for three alloys the compositions of the coexisting phases were established by EPMA. Compared to phase boundaries established in [55] and the current Ti–Al binary system, the results in [136] are somewhat shifted towards higher Ti contents by 2–3 at.%. The two-phase field was again studied in Kainuma, Fujita, Mitsui, Ohnuma and Ishida [115]. Only one tie-line close to the Ti–Al binary system was established at 1000 °C, which fits very well with the binary [29]. The composition 50 ± 2 at.% Ti, 25 at.% Zr, 25 ± 2 at.% Al was found to be single-phase $D0_{19}$, the structure of Ti_3Al, after annealing at 1000 °C for 720 h [173]. Whether this means that Ti_3Al may have a larger solid solubility for Zr than ~20 at. %, as found in [55] or whether $D0_{19}$ forms on cooling at around 1000 °C from B2, as discussed before, cannot be settled based on the existing experimental evidence.

Vertical sections along Ti-14.9 at.% Al/Zr, Ti-25.3 at.% Al/Zr, and Ti-33.3 at.% Al/Zr were investigated in the 1960s by metallography, DTA, and XRD and results were published in a series of overlapping papers [176, 184, 189-192]. At 1000 °C samples were annealed for 100 h and quenched in water. All values for phase boundaries taken from the figures are unreasonable at 1000 °C, as discussed later, except that for the (αTi,Zr + Ti_3Al)/Ti_3Al phase boundary [192]. 9 diffusion couples prepared for a diffusion study in b.c.c. βTi,Zr were apparently all single-phase βTi,Zr after annealing for 48 h at 1000 °C [183], in accordance with the composition range outlined in [55].

Finally, a ternary compound Zr_2TiAl with cubic $L2_1$-structure was identified in an alloy of appropriate composition that had been annealed for 480 h at 1000 °C and 720 h at 1050 °C [174]. As discussed before, it is assumed that the composition may lie within the extended single-phase region of βTi,Zr and therefore ordering may occur on cooling.

Figure 4.1 shows the diagram established in [55] together with all other results from investigations at this temperature. **Figure 4.2** shows the isothermal section as assessed from the results discussed above. It is based on the one established by [55] with the phase boundaries adjusted to match with those of the accepted binaries and to be in accordance with thermodynamic rules. A small phase field for Zr_3Al and respective tentative multi-phase equilibria have been added to comply with the accepted Al–Zr binary system. As it has not

been settled yet, whether the compositions Ti_2AlZr and Zr_2TiAl are separate phases, or indicate B2-ordering at this temperature within Al-rich compositions of $\beta Ti,Zr$ [172, 177, 179], an area where B2-ordering may occur has been outlined in **Figure 4.2**.

The current assessment makes clear that phase equilibria have to be settled more precisely. They have therefore been reinvestigated (**section 4.2.**) and a comparison between the assessed isothermal section at 1000 °C (**Figure 4.2**) and the newly established one (**Figure 4.5**) is given in section **4.2.9**. and shown in **Figure 4.18**.
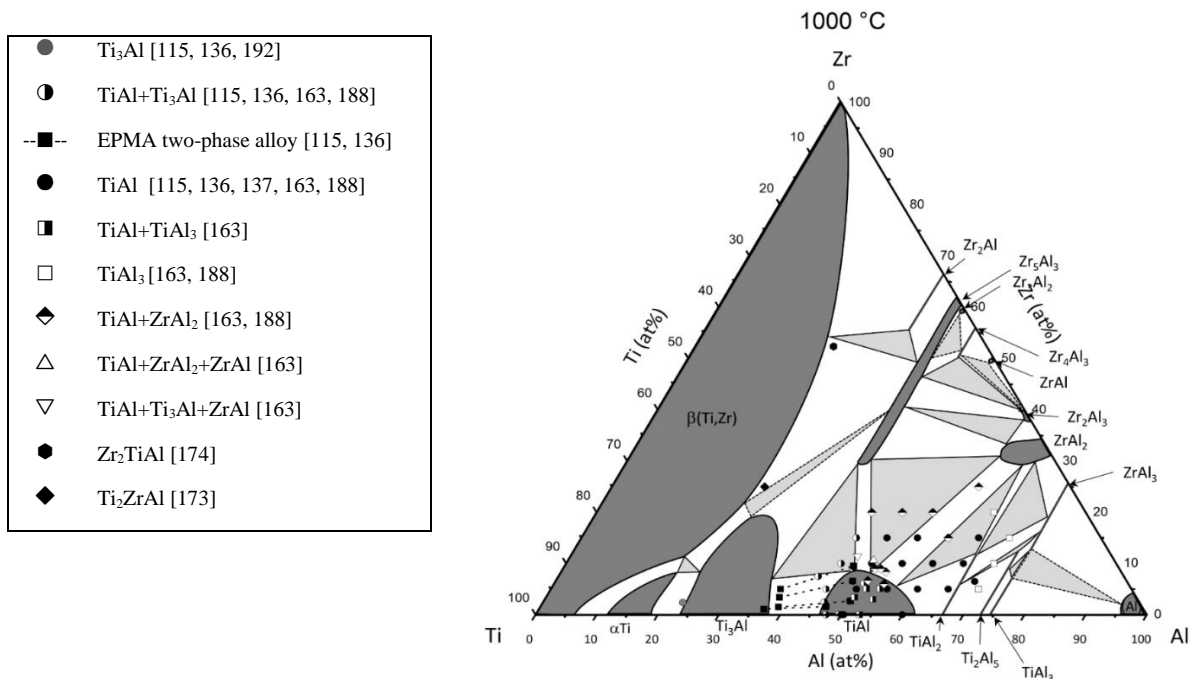
Figure 4.1a. Isothermal section at 1000 °C according to [55] with additional experimental results from the literature.
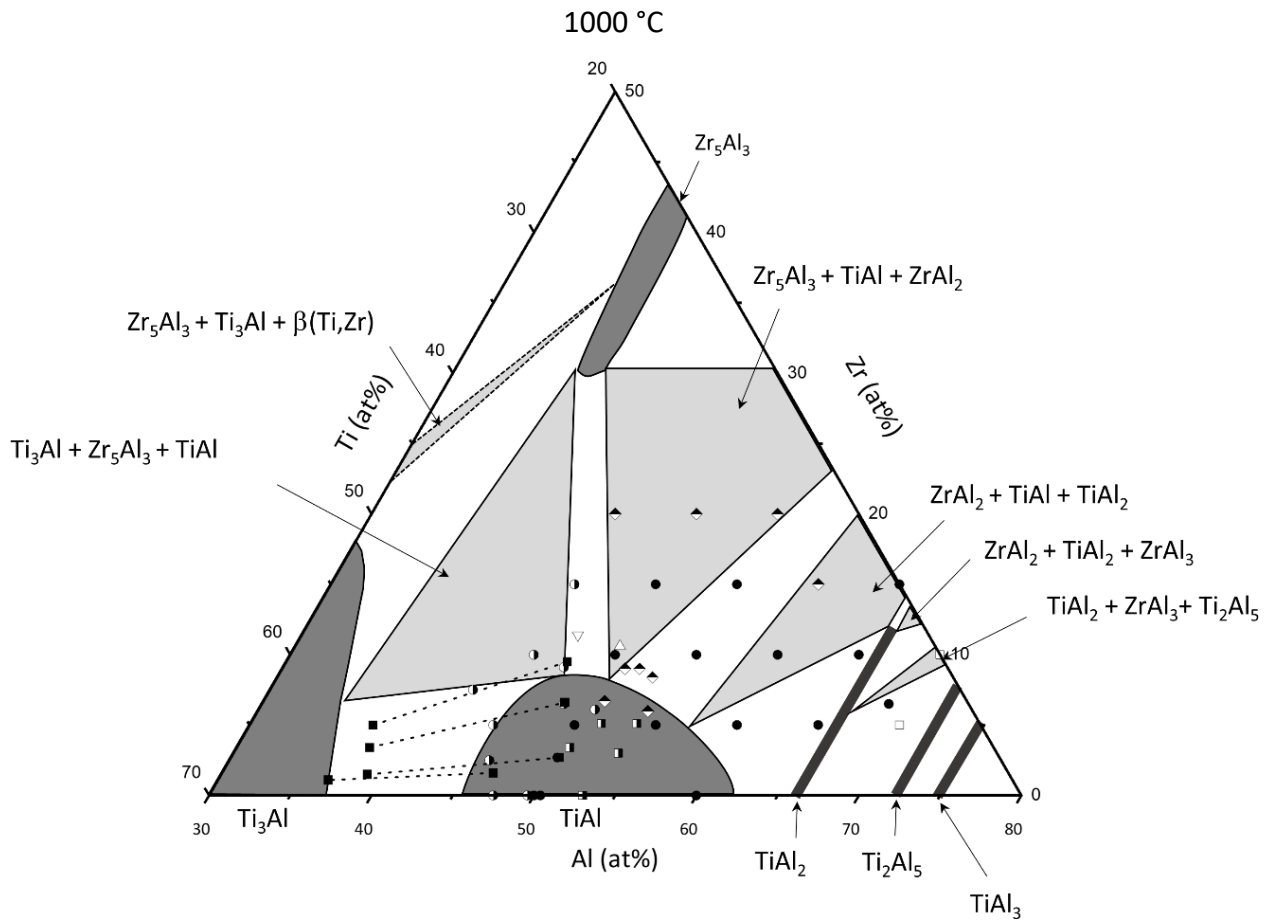
Figure 4.1b. Enlarged area from Figure 1 showing phase equilibria and experimental results for TiAl in more detail.
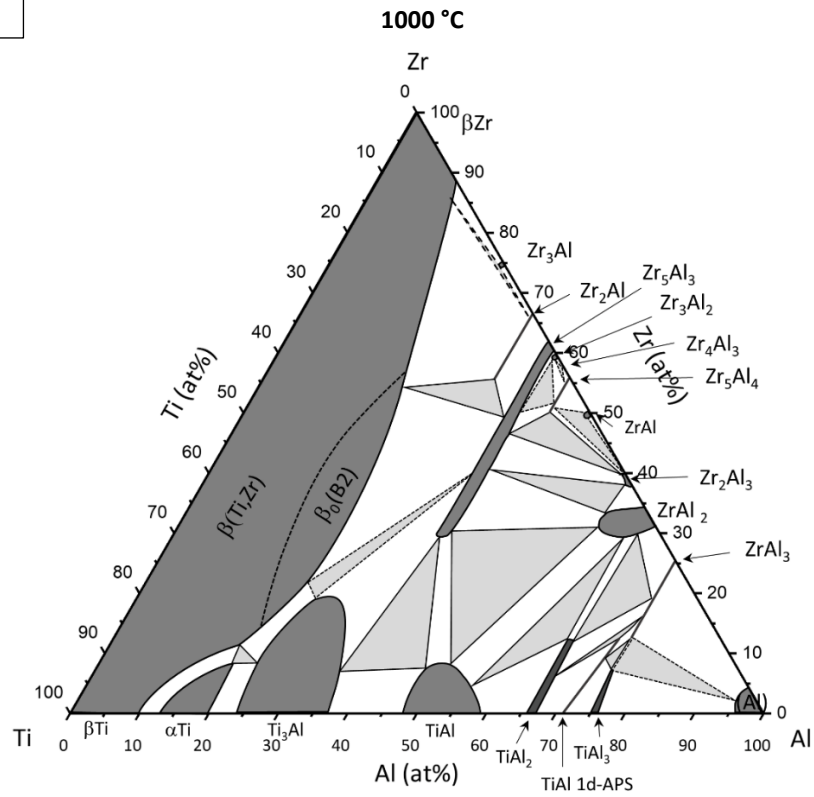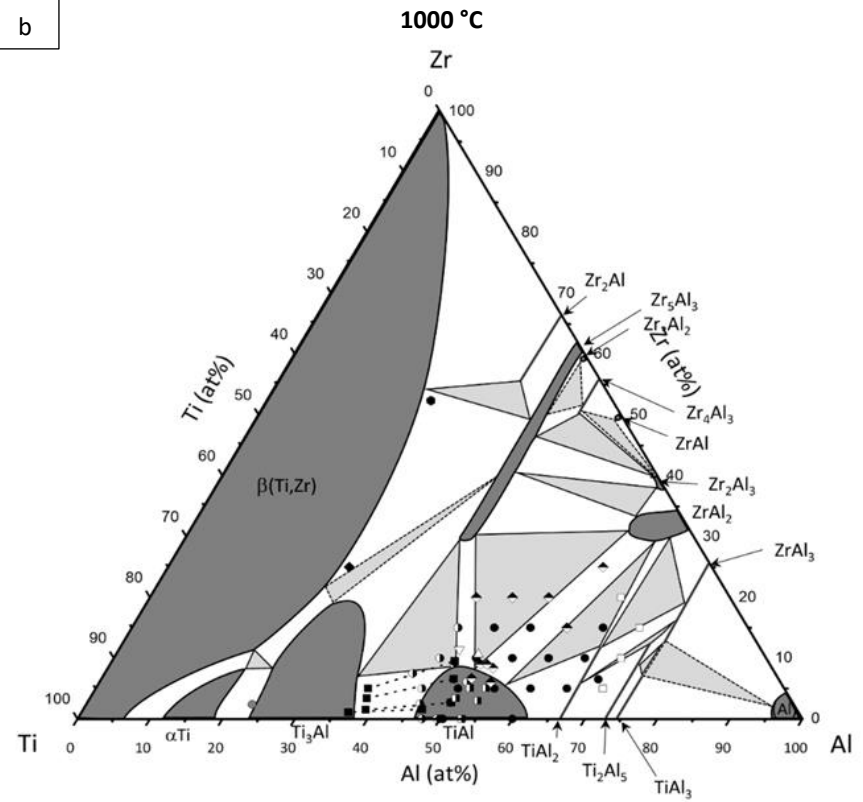
Figure 4.2. a) Critically assessed isothermal section of the Ti–Al–Zr system at 1000 °C and b) in comparison to the one established in [55] with additional previous experiments (for legend see **Figure. 4.1a**).

4.1.5. Isothermal section at 800 °C

A complete isothermal section at 800 °C [56] (**Figure 4.3**) was determined by the same group that established the isotherm at 1000 °C using the same techniques as in [55], except that no XRD has been employed in [56]. In addition, they employed a Ti/TiAl$_3$/Zr diffusion triple and this, like 12 alloys of fixed composition, was heat-treated for 2400 h at 800 °C. Again the isotherm contains some violations concerning thermodynamic rules and determined phase boundaries for the Ti–Al phases are not in good agreement with the accepted binary system [29], particular in showing a much lower solid solubility of Al in αTi. Also, at 800 °C no ternary phases are observed while all binary phases have considerable solid solubility ranges, with the exception of Zr$_2$Al$_3$ and ZrAl. The latter phase was not detected at all, presumably because of its limited homogeneity range in the ternary system. All ternary homogeneity ranges of the binary Zr–Al phases show a pronounced tendency for substitution of Zr by Ti, except ZrAl$_2$, which shows a pronounced tendency for substitution of Al by Ti (**Figure 4.3**). Though a complete isotherm has been established, many three-phase fields have not been experimentally confirmed (dashed triangles in **Figure 4.3**). Therefore it could be theoretically possible that instead of the two-phase equilibrium βTi,Zr + Zr$_4$Al$_3$ the phases ZrAl$_2$ and Zr$_3$Al$_2$ are in equilibrium with each other. The solubility for Zr in TiAl$_2$ is 11.2 at.%, which is about the same value as at 1000 °C [55]. The solubility for Ti in Zr$_2$Al is 13.8 at.%, somewhat higher than at 1000 °C [55]. Solid solubilities of the third element in other binary phases could actually even be higher than indicated in **Figure 4.3**, as the maxima shown there stem either from phase equilibria shown by dashed lines, i.e. experimentally not determined, or from evaluating the diffusion path in the diffusion triple. As the diffusion path will always cross two-phase fields, established compositions can be more or less close to the three-phase equilibrium and therefore do not correspond to a maximum solid solubility in a phase.

Otherwise, there are few other data available for this temperature, mostly for the Ti corner. The effect of Zr addition on the αTi,Zr/(αTi,Zr + Ti$_3$Al) phase boundary was investigated in [120] in the composition range Ti–(8-13)Al–(1-2)Zr at.%. Alloys were produced by arc-melting and rolled prior to annealing at 800 °C for 200 h under flowing Ar. Chemical analyses after heat treatment were in good agreement with the nominal compositions and the amount of oxygen was assumed to be 0.03 to 0.04 wt. %. By light microscopy it was established that all investigated alloys were single-phase αTi,Zr at 800 °C. This shows that αTi,Zr extends to somewhat more Zr-rich and markedly more Al-rich compositions than shown in **Figure 4.3**, in good agreement with the accepted binary Ti–Al system [29].

Quite a couple of vertical sections exist, which include results at 800 °C [184, 189-193]. Though, all of them either missed out some phases and/or phase equilibria, denote data points to other phase boundaries than those shown in **Figure 4.3** or are contradictory in itself (for a detailed discussion see section on Vertical Sections). However, as far as the Ti corner has been investigated, they are inline that αTi,Zr extends further into the ternary system than shown in [56].

Four samples in the Al corner of compositions 0-15Ti–Al-5Zr (at.%) were investigated in [194]. The samples were prepared by annealing pre-cursors pressed from elemental powders at 800 °C for 30 min. Samples were analyzed by observations in a SEM, XRD and EDS. All alloys consist of the two phases Al + (Zr,Ti)Al$_3$. According to the isothermal section by Lü et al. [56], the two Ti-rich compositions should show the three-phase equilibrium Al + (Zr,Ti)Al$_3$ + TiAl$_3$ at 800 °C (Figure 3). One explanation for this discrepancy could be that the annealing time of 30 min was too short to attain equilibrium.

The isothermal section assessed here is shown in **Figure 4.4.** It is based on the results by [56] with an increased solid solubility range for αTi,Zr, in agreement with [120] and the binary Ti–Al system. Phase boundaries have been adjusted to match with those of the accepted binaries and to be in accordance with thermodynamic rules.
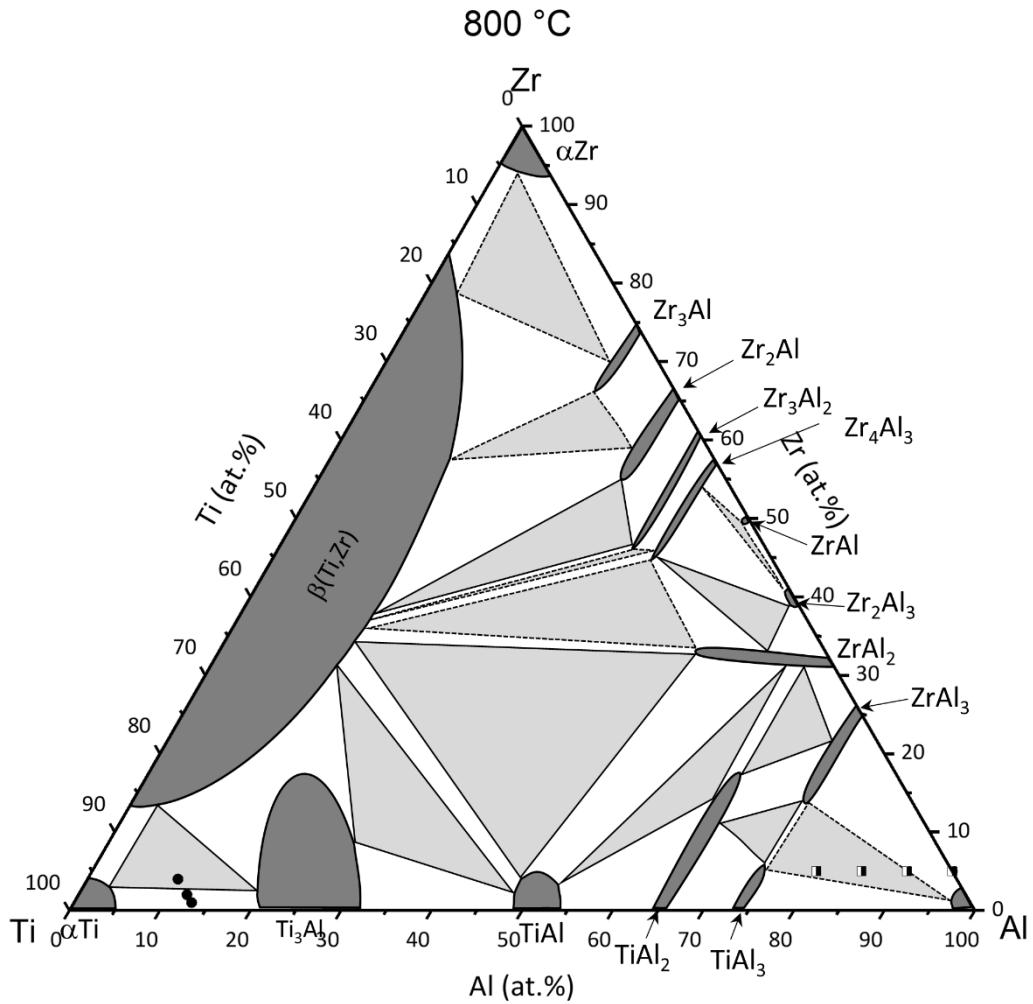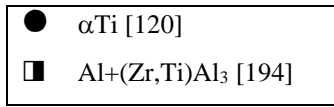
Figure 4.3. Isothermal section at 800 °C according to [56] with additional experimental results from the literature.
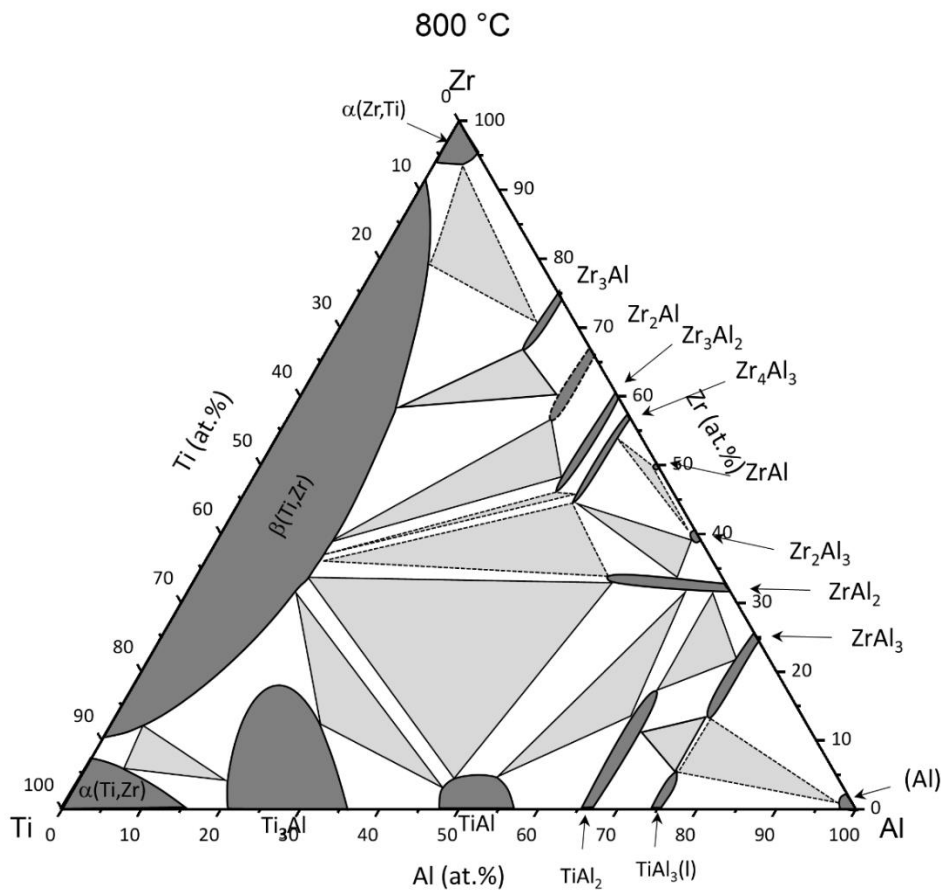
Figure 4.4. Critically assessed isothermal section of the Ti–Al-Zr system at 800 °C.

4.1.6. Data at temperatures below 800 °C

As attaining thermodynamic equilibrium in Ti–Al–Zr alloys at low temperatures becomes more and more difficult, data on phase equilibria below 800 °C are scarce. The effect of Zr addition on the αTi,Zr/αTi,Zr + Ti$_3$Al phase boundary in the temperature range 500–700 °C is shown in [120], which also shows a partial isothermal section at 700 °C. The phase boundary matches well with the accepted binary [29]. From a series of 16 alloys equilibrated for 500 h at 700 °C, the phase boundaries of the two-phase field αTi,Zr + Ti$_3$Al with up to 5 wt.% Zr were determined [192]. Compared to the binary system, the two phase area widens by the addition of Zr, in line with the observation by [120]. The αTi,Zr/αTi,Zr + Ti$_3$Al phase boundary was also studied at 600 °C by equilibrating alloys with 2, 6 and 10 at.% Zr for 400 h [195]. The extrapolated phase boundary matches well with the extrapolated one in the binary Ti–Al system [29]. A partial isothermal section of the Ti-corner at 500 °C showing the αTi,Zr + Ti$_3$Al phase area is included in [192].

4.1.7. Data at temperatures above 1000 °C

Information above 1000 °C is limited to phase equilibria between the phases αTi,Zr, βTi,Zr and TiAl. The phase relations between these phases have been studied by investigating alloys annealed at 1200 °C for 168 h and at 1300 °C for 24 h [115]. Heat treatments were carried out in quartz capsules, which are usually considered not to be any longer gas-tight at these temperatures. However, oxygen and nitrogen contents were below 400 (wt.) ppm after the heat treatments. Compositions of coexisting phases in the quenched samples were determined by EPMA by averaging data from 10 points. At 1200 °C the three-phase equilibrium αTi,Zr + βTi,Zr + TiAl could be determined, showing a maximum solid solubility of 5.1 at.% Zr in αTi,Zr. Though this tie-triangle was not measured directly at 1300 °C, the adjacent tie-lines suggest that the solubility for Zr in αTi,Zr may only slightly increase up to about 5.5 at.% Zr at this temperature.

In the diffusion study of b.c.c. βTi,Zr [183], 11 diffusion couples were annealed for 17 h at 1200 °C. All of them were single-phase βTi,Zr after annealing, in accordance with the βTi,Zr /βTi,Zr + αTi,Zr and βTi,Zr /βTi,Zr + TiAl phase boundaries determined by [115] for lower Zr contents.

 An arc melted alloy of the composition Ti–24.8Al–24.9Zr at. % that was solution treated at 1200 °C for 30 min and water quenched, was found to be single-phase B2-ordered βTi,Zr by TEM [172]. As no anti-phase domains were observed, the authors concluded that the alloy has been B2 at 1200 °C and did not undergo ordering at lower temperatures during quenching.

In a couple of early studies, the extension of the TiAl phase field at 1093 °C [113] and 1274 °C [57, 58] was studied by metallography and XRD. At 1093 °C, 27 different alloys were heat treated for 36–39 h and air cooled [113]. The maximum solid solubility for Zr in TiAl was found to be about 8 at% at 1093 °C [113]. A first partial isothermal section for "1274 °C" was constructed from 19 alloys, which were actually heat treated between 1246–1379 °C for 24–39 h [57]. The partial isothermal section for 1274 °C was updated by 18 alloys, which were wrapped in Ta foil and encapsulated in quartz ampules for the heat treatments and which were quenched in brine after annealing for 24 h [58]. As the determined composition range for TiAl in the binary system is shifted markedly to higher Al contents compared to the currently accepted one [29], the established solid solubility limit of about 13 at.% Zr in TiAl at 1274 °C [58] could be doubted. For establishing various vertical sections, quite a couple of alloys have been studied, which have been equilibrated at 1100 °C [184, 189, 191, 192]. As discussed in more detail in the following section, these results are all considered to be questionable.

4.1.8. Vertical sections

Sections towards the Zr corner

The vertical section Ti–14.9 at.% Al/Zr was investigated between 500–1100 °C by metallography of 19 different annealed alloys and thermal analysis [189]. Established phase boundaries do not match at 800 °C with the current knowledge of the binary Ti–Zr system or the ternary system (**Figure 4.4**) with the sole exception of the βTi,Zr/(αTi,Zr + βTi,Zr) phase boundary. Therefore the location of the minimum in the αTi,Zr/βTi,Zr transformation temperature of about 660 °C and 65 wt.% Zr may be doubtful. A comparable minimum was found in the vertical section Ti–25.3 at.% Al/Zr at about 515 °C and 70 wt.% Zr [176]. In this study, the vertical section has been determined between 500–1900 °C by thermal analysis of 11 alloys and microstructural and XRD investigations of quenched alloys [176]. Beside determination of the solidus temperatures, phase boundaries of the αTi,Zr, αTi,Zr + βTi,Zr, and βTi,Zr phase fields were determined. The melting temperature determined for Zr (1850 °C) and the solidus temperature of Ti_3Al with 24.1 at.% Al (~1650 °C) are very close to the currently accepted values 1855 °C [162] and 1655 °C [29]. Therefore, remaining solidus and liquidus temperatures determined in [176] may be considered as relevant. Though the existence of the compound Ti_3Al has been realized in [176], the phase has not been included in the vertical section. Also, according to the isotherms at 800 °C and 1000 °C shown in **Figures 4.2 and 4.4**, this vertical section should include phase equilibria with quite a number of other phases e.g. TiAl or $Zr(Al,Ti)_2$. As no other phases than αTi,Zr and βTi,Zr are shown in the section, solid phase equilibria from [176] are not further considered here. One more "tentative" section along Ti–33.3 at.% Al/Zr [184] was constructed from 20 samples annealed between 500–1100 °C, which were analyzed by metallography and partly by XRD, supplemented by data from thermal analysis. The section had been considered to be tentative, as many alloys underwent phase transformations during cooling and therefore phase equilibria at the annealing temperature were not clear. Again the section misses out phase equilibria with the phases originating in the Al–Zr binary system, with the exception of Zr_3Al, which according to this section would coexist over a large composition range with αTi,Zr and βTi,Zr [184].

In the vertical sections Ti/Ti–49.4 at.% Zr containing 0, 6.9, and 9.6 at.% Al the phase boundaries for αTi,Zr and βTi,Zr between 600 – ~1100 °C were determined by metallography of annealed samples and additional dilatometry for the binary section [193]. All phase boundaries show a sharp increase in temperature between 0 and about 1 at. % Zr, e.g. about 45K for αTi,Zr/(αTi,Zr + βTi,Zr), and then temperatures decrease steadily to 49.4 at.% Zr. As

far as temperatures can be read from the diagram, they seem not to match phase boundaries shown for 800 °C and 1000 °C in **Figures 4.2 and 4.4** and as a peak in temperature in the αTi,Zr and βTi,Zr phase boundaries is thermodynamically improbable, results of [193] are not further considered here.

Sections towards the Al corner

Based on metallography on heat treated samples quenched from 800 °C, 1000 °C, 1100 °C and 1200 °C, thermal analysis and dilatometry, two vertical sections for Ti–2.7 at.% Zr/Ti–25.3 at.% Al between 700 – 1750 °C and for Ti–2.7 at.% Zr/Ti–25.8 at.% Al, 2.4 at.% Zr between 500 – 1200 °C were determined [191]. Results of the former section were also published in [196] and in some more detail in [190]. The latter section showing additional data for 700 °C was also published in [192]. Though single data points fit well to data shown in **Figures 4.2 and 4.4**, the general sequence of phase equilibria is not correct. While the phase equilibrium αTi,Zr + βTi,Zr + Ti$_3$Al is detected at 1000 °C in the former, i.e. more Zr lean section, it does not show up at this temperature in the latter, i.e. the more Zr-rich one, which only shows the three-phase equilibrium at higher temperatures. According to **Figure 4.2**, the three phase equilibrium should either be present in both sections or only in the more Zr-rich one, but not vice versa as shown in [190-192, 196].

The αTi,Zr/βTi,Zr phase boundaries in the vertical section Ti–2.3 at.% Al/Ti–20 at.% Al, 2.3 at.% Zr were calculated in the temperature range 850–1000 °C and verified by analysing three alloys [197]. Comparison of the αTi,Zr/βTi,Zr phase boundaries at 1000 °C shows that they fit quite well to those shown in **Figure 4.2**. The shift of the αTi,Zr/(αTi,Zr + Ti$_3$Al) phase boundary towards higher temperatures and lower Al contents with increasing Zr content is shown for the temperature range 500 – 700 °C in [120].

4.1.9. Modelling

Recently, CLAPHAD-type and ab-initio calculations were applied to establish isothermal sections at 800 °C and 1000 °C, partial isothermal sections of the Ti-corner at 1000 °C, 1200 °C and 1300 °C and a vertical section along Ti-2.7 at.% Zr/Ti$_3$Al [198]. Thermodynamic parameters from binaries were extracted from [153], [145], and [199] for Ti–Al, Al–Zr, and Ti–Zr, respectively. Experimental data from [55, 56, 115, 172, 190] have been used to optimize thermodynamic parameters using the CALPHAD approach.

According to the modelling, the phase field of αTi,Zr extends much further into the ternary system at 800 °C compared to [56], in line with the discussion of this section above. Also βTi,Zr extends somewhat more into the ternary system at 800 °C, i.e. has a bit higher solid solubility for Al than shown in [56]. The major difference between the isothermal sections for 800 °C are, that the experimental one shows phase equilibria between βTi,Zr and Zr(Al,Ti)$_2$ [56], while the calculations show that TiAl should be in equilibrium with Zr$_4$Al$_3$ [198]. Therefore, multiphase equilibria in a wide range of compositions in the two isotherms are quite different from each other as discussed in [198]. Which of the two versions is correct cannot be decided on the existing evidence.

Modelled [198] and experimentally determined [55] isothermal sections at 1000 °C qualitatively match much better. Though, there are some differences in the solid solubility ranges of individual phases, most notably for Ti$_3$Al, which has less solid solubility for Zr according to the modelling. Otherwise, all multiphase equilibria in the experimental section are reproduced in the modelling. At higher temperatures there is quite some discrepancy at 1200 °C between the modelling [198] and experimental data in the Ti-corner [115], while the match at 1300 °C is somewhat better. Calculated phase boundaries at 800 °C and 1000 °C of the vertical section [198] fit very well with those of the binary accepted here, with the sole exception for the αTi/(αTi + Ti$_3$Al) phase boundary at 800 °C, which according to **Figure 4.4** should be at a somewhat lower Al content.

A vertical section along (Ti,Zr)Al$_3$ has been calculated for 900–1100 °C [200]. In this section the two-phase field D0$_{22}$ + D0$_{23}$ is located much closer to the TiAl$_3$ (D0$_{22}$) side than in the experimentally determined section at 1000 °C (Figure 1) [55]. The relative stability of the L1$_2$, D0$_{22}$ and D0$_{23}$ structures along TiAl$_3$–ZrAl$_3$ was investigated at 0 K by calculating the enthalpy of formation using first principles calculations [201]. The results indicate that the D0$_{23}$ structure is the most stable along the complete section. While this finding is in agreement with

experimental evidence for ZrAl$_3$, it is in contradiction for TiAl$_3$, where D0$_{23}$ is known to be the high-temperature polymorph while at lower temperatures D0$_{22}$ becomes stable. This discrepancy between ab-initio calculations and experiments in case of TiAl$_3$ is well known and also discussed in [201].

.

4.2. Experimental Investigation of Phase Equilibria in Ti–Al–Zr system at 1000-1300°C

4.2.1. Introduction

In a first step a complete assessment of all available literature on phase equilibria in the Ti–Al–Zr system was performed (**section 4.1**). From this assessment it is clear that discrepancies exist, especially between recent CALPHAD modellings [202, 203] and experimentally determined phase equilibria [55, 56, 115, 172, 190]. As pointed out in the assessment (**section 4.1**) as well as in the modellings [202, 203], specifically at 800 °C even the multi-phase equilibria are not settled. Also, at higher temperatures experimental results and modelling are at variance, specifically regarding the extension of the various binary phases into the ternary system and little is known about the stability of β_0. Therefore, the assessment and the modelling came to the conclusion that new reliable experimental data in the Ti–Al–Zr system are needed to resolve these issues [116, 202].

In the present work, as a part of ADVANCE project [33], phase equilibria in the Ti–Al–Zr system were experimentally investigated focusing on the temperature range 1000-1300 °C, to assist the development of TiAl-based alloys for even higher application temperatures and in the temperature range, where the alloys are thermally processed to attain specific microstructures.

4.2.2. Binary systems

Four partial isothermal sections at 1000-1300 °C have been established. Data for the binary systems are taken from the following references: Al–Zr from the assessment by Schuster [142], which is in agreement with all other recent assessments and thermodynamic modellings; Ti–Zr from the latest available assessment by Malfliet et al. [151], and Ti–Al from Palm [7]. For a detailed discussion on the selected binaries see **section 4.1.2**. Compared to [116], the Ti–Al system is taken from a more recent update of the original assessment [29], in which particularly the possibility of B2-ordering in βTi is discussed and which also shows that the previous difference between experiments and modelling for phase equilibria between αTi, βTi and Ti$_3$Al can be settled when vacancies and anti-site defects are included in the modelling. Crystallographic data of all phases observed in the present investigation are listed in **Table 4.1**.

4.2.3. Partial isothermal section at 1000 °C

Figure 4.5 depicts the partial isothermal section at 1000 °C. The compositions of coexisting phases and their lattice parameters are presented in **Table 4.2.**
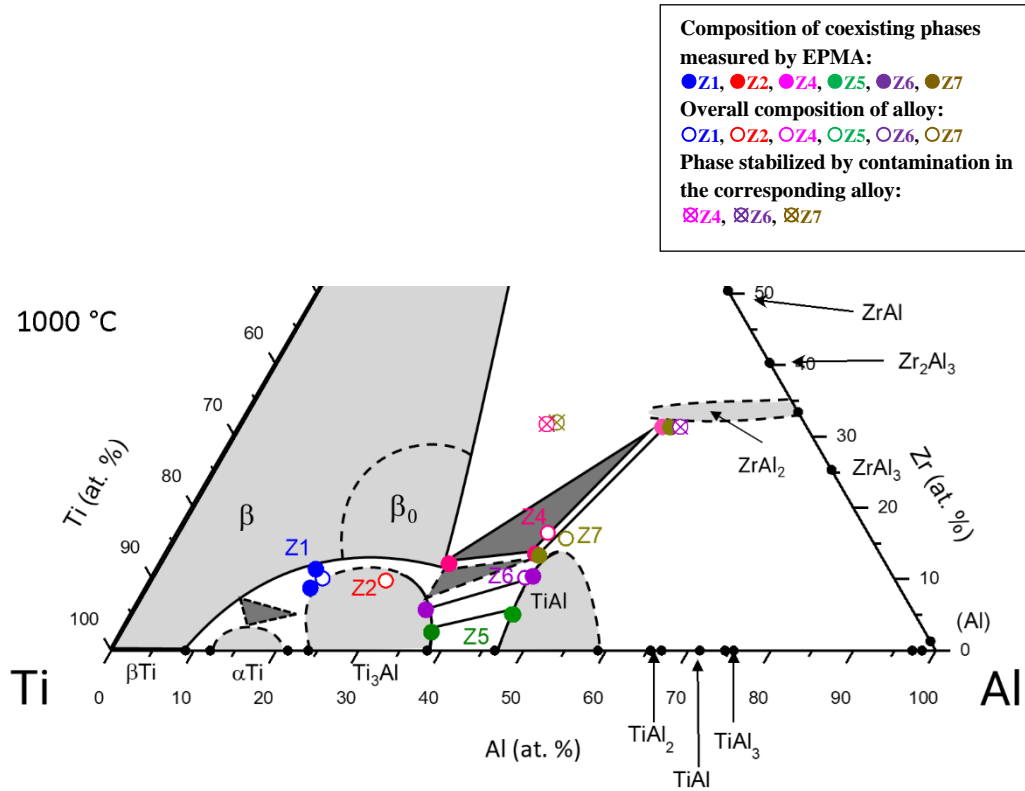
Figure 4.5. Partial Ti–Al–Zr isothermal section at 1000 °C.

Table 4.2. Compositions and lattice parameters of the coexisting phases and impurity contents of samples annealed at 1000 °C. Figures for HT represent the duration of heat treatments; data shown in *italics* are from HE-XRD; lattice parameters marked with an asterisk (*) belong to αTi formed during quenching from βTi,Zr or β_0.

Alloy	HT (h)	Phases	Composition (at. %)			Lattice Parameters (nm)		Impurity (wt. ppm)		
			Ti	Al	Zr	a_0	c_0	C	O	N
Z1	1000	βTi,Zr or β_0	69.5 ± 0.2	19.1 ± 0.3	11.4 ± 0.2	0.29420 (1) * *0.2952**	0.47307(3) * *0.472**			
		Ti₃Al	71.4 ± 0.3	19.8 ± 0.3	8.8 ± 0.2	0.58982 (2) *0.5878*	0.46911 (2) *0.4707*			
Z2	100	Ti₃Al	63.2 ± 0.6	27.4 ± 0.2	9.4 ± 0.5	0.58700(7)	0.46979(5)	147	510	<50
Z4	100	ZrAl₂	17.5 ± 0.7	51.3 ± 0.4	31.2 ± 0.4	0.53756(1) *0.537*	0.87478(3) *0.8745*	111	455	<50
		TiAl	41.8 ± 0.3	44.7 ± 0.2	13.5 ± 0.3	0.40963 (2) *0.411*	0.40976(4) *0.408*			
		β_0	53.0 ± 0.3	34.9 ± 0.2	12.1 ± 0.2	0.327(1) *0.3268*				
Z5	100	TiAl	48.7 ± 0.4	46.2 ± 0.3	5.1 ± 0.3	0.40453(4)	0.40900(7)	100	200	<50
		Ti₃Al	59.9	37.5	2.6	0.5813(4)	0.4651(6)			
Z6	1000	TiAl	43.6 ± 0.9	46.0 ± 0.5	10.4 ± 0.5	0.40737(4)	0.41061(6)			
		Ti₃Al	59.0 ± 0.3	35.3 ± 0.3	5.7 ± 0.1	0.5825 (2)	0.4666 (3)			
Z7	1000	ZrAl₂	16.5 ± 0.4	52.2 ± 0.6	31.3 ± 0.3	0.53688(2)	0.87237(5)			
		TiAl	41.7 ± 0.7	45.1 ± 0.5	13.2 ± 0.3	0.40942(2)	0.40955(2)			

Initial heat treatments at 1000 °C were performed for 100 h. Though samples were in equilibrium after 100 h, grains of individual phases were somewhat small for EPMA. Therefore, the annealing time was increased to 1000 h in sub-sequent heat treatments. Alloy Z4 shows the three-phase equilibrium β_0 + TiAl + ZrAl₂, as established by EPMA, (HE-) XRD

(**Figure 4.6**), and TEM. TEM selected-area diffraction patterns confirm (**Figure 4.7**) that the Zr-rich phase is the hexagonal Laves phase $ZrAl_2$, in agreement with the results by XRD and HE-XRD. The TEM investigations also show that $ZrAl_2$ which contains 17.5 at. % Ti is still the C14-type Laves phase, i.e. the same polymorph as binary $ZrAl_2$. The existence of the equilibrium β_0 + TiAl + $ZrAl_2$ rules out that TiAl is in equilibrium with Zr_5Al_3 at this temperature [55]. However, Zr_5Al_3 is also additionally observed in a few places in Z4, but in contrast to the other three phases it always contains about 2 mass % of impurities, mostly oxygen. The HE-XRD spectrum in **Figure 4.6** shows that Z4 contains only a minor amount of Zr_5Al_3. By HE-XRD the structure of Zr_5Al_3 was identified as hexagonal *P6$_3$/mcm* (D8$_8$, Mn_5Si_3-type). In contrast to Zr_5Al_3 of the tetragonal W_5Si_3-type, the Mn_5Si_3-type is only observed for Zr_5Al_3 when oxygen occupies otherwise empty octahedral sites in this structure [204]. Therefore, this phase is considered only to show up when stabilized by impurities, as already observed in other systems [171, 205]. Phase equilibria between TiAl and adjacent phases have also been studied at 1000 °C by Tanda et al. [188]. For alloys with nominal composition of 45, 50, and 55 at. % Al and 20 at. % Zr as well as for 60 at. % Al and 25 at. % Zr they did observe TiAl in equilibrium with $ZrAl_2$. This is in agreement with the present investigation (**Figure 4.5**) and that Zr_5Al_3 is only observed within this composition range if it stabilized by oxygen.

The TEM investigations also show that B2-ordered β_0 is present in Z4 at 1000 °C. Analysis of the anti-phase boundaries (APBs) showed only presence of a few thermal APBs. If β_0 would have formed by ordering from disordered βTi,Zr during quenching, this would have yielded a large amount of APBs. It is therefore concluded, that B2-ordered β_0 is stable at 1000 °C.
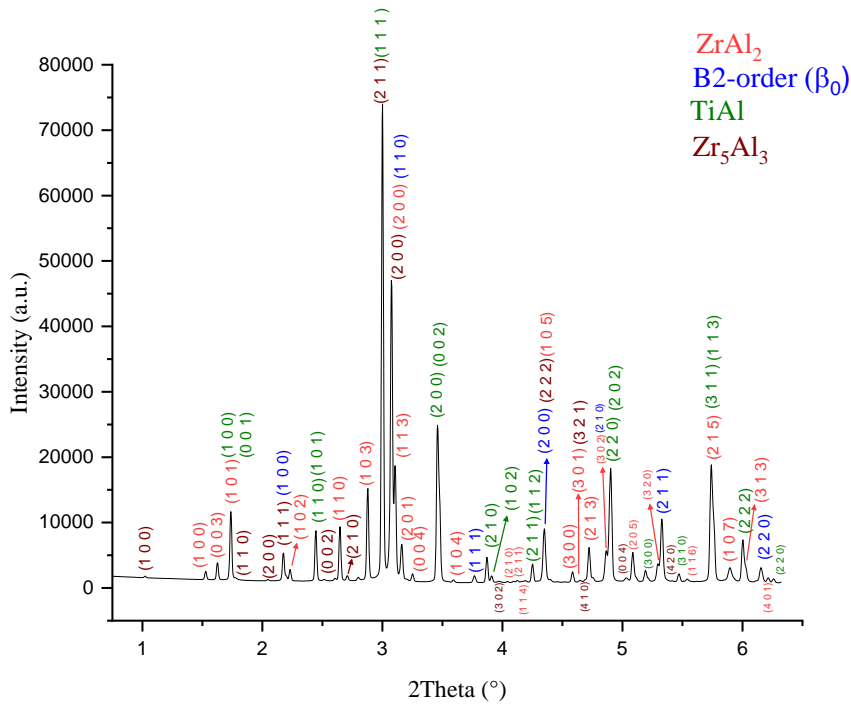
Figure 4.6. HE-XRD analysis of Z4 (Ti-44.7Al-16.5Zr at. %) heat-treated at 1000 °C/ 100 h.
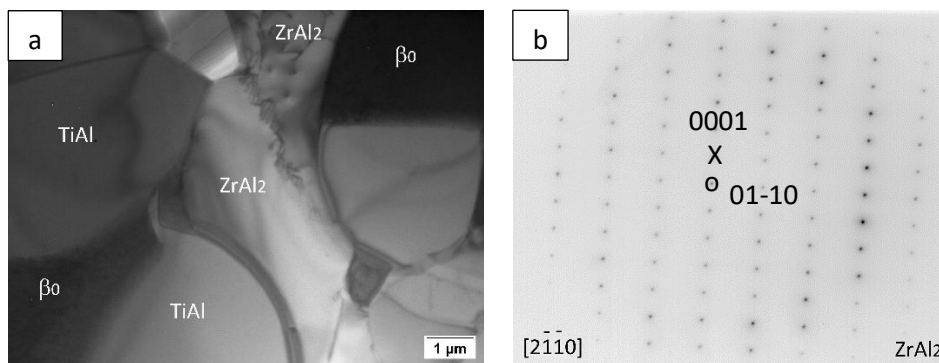
Figure 4.7. Z4 (Ti-44.7Al-16.5Zr at. %), heat treated at 1000 °C/100 h; a) TEM bright field; b) diffraction pattern of ZrAl₂ in [$2\bar{1}\bar{1}0$] zone axis.

The SEM micrograph of Z1 in **Figure 4.8. (a)** shows a two-phase microstructure of Ti₃Al + βTi,Zr or β₀, where the needle- or lath-shaped contrast in the latter phase indicates transformation during quenching. The TEM bright-field image (**Figure 4.8. (b)**) reveals the presence of martensite, which is typical for the transformation from βTi to αTi [206, 207]. Because of this martensitic transformation it is not any longer possible to ascertain whether disordered βTi,Zr or β₀ was present at 1000 °C. Formation of the martensite explains, why αTi is observed at RT in Z1 (**Table 4.2**).

Compared to the assessed data [116], Zr shows a significantly larger solid solubility in TiAl at 1000 °C. The solid solubility of Zr in TiAl was given as 8.5 at.% in the assessment [116], in agreement with [55]. According to **Figure 4.1** the solid solubility of Zr in TiAl is actually about 13.5 at.% at 1000 °C, in satisfactory agreement with about 11 at.% in [163] and 15 at.% in [188]. Data in [55] are for TiAl in equilibrium with Zr_5Al_3 and therefore presumably much lower than otherwise observed. For the solid solubility of Zr in Ti_3Al, data in the assessment [116] are also based on [55], where a solid solubility of nearly 20 at. % Zr has been measured. The present data show that the solid solubility is only about 10 at. % Zr in Ti_3Al at 1000 °C. Again, this discrepancy is attributed to the fact that the much higher solid solubility in [55] is found for Ti_3Al in equilibrium with Zr_5Al_3.

Complete isothermal sections at 1000 °C in [202, 203], which are calculated based on the data in [55, 115], matched qualitatively with the assessed data in [116]. However, as detailed above, the newly established phase equilibria **Figure 4.5** differ from those in [55, 116]. Therefore, also the CALPHAD modellings in [202, 203] show different multiple phase equilibria than the ones established here. This is possibly the reason that also solid solubilities of the third element in the binary phases such as βTi,Zr, Ti_3Al, and $ZrAl_2$ deviate notably in the modellings from those established here.
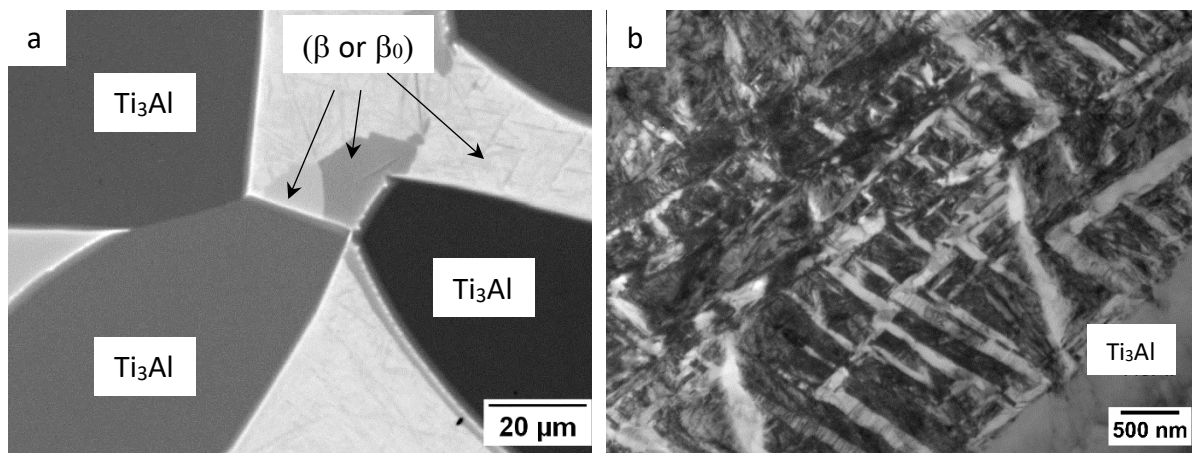
Figure 4.8. Microstructure of Z1 (Ti-20.6Al-10.1Zr at. %), heat treated at 1000 °C/1000 h a) SEM back-scattered electron (BSE) micrograph b) TEM bright field (BF) micrograph.

4.2.4. Partial isothermal section at 1100 °C

The partial isothermal section at 1100 °C is shown in **Figure 4.9**, the compositions of coexisting phases and lattice parameters are presented in **Table 4.3**. Also, in alloys heat-treated at 1100 °C Zr_5Al_3 was sometimes observed (**Figure 4.10**). In those cases, EPMA measurements were performed far away from this phase for minimalizing its influence on the compositions. Phase equilibria are similar to those at 1000 °C. Compared to the partial isothermal section at 1000 °C, alloys Z1 and Z2 locate in the single-phase field of βTi,Zr/β_0 and were therefore not heat-treated at temperatures above 1000 °C. That these two alloys do not undergo phase transformations at higher temperatures is confirmed by DTA (see below).

At 1100 °C alloys Z4 and Z7 comprise β_0 + TiAl + $ZrAl_2$ and alloy Z6 represents the three-phase equilibrium β_0 + Ti_3Al + TiAl. From the overall composition of Z6 it is evident that the sample contains only a minor volume fraction of β_0. Therefore, it was not possible to establish the ordering by XRD, but from the results at 1000 °C (**Figure 4.5**) and 1200 °C (**Figure 4.11**), and the DTA investigation of Z6 (**see below**), it may be concluded that the phase is B2-ordered β_0 In Z6 at 1100 °C.

Data from literature for 1100 °C are scarce and most of them stem from the 1960s, where a series of vertical sections starting from the Ti corner has been established from metallography, DTA and XRD [176, 184, 189-192]. As discussed in detail in [116] most of the results are questionable and they are therefore not considered. The most relevant data stem from an investigation of the homogeneity range of TiAl at 1093 °C [113] (original reference unavailable but data are shown and discussed in [57]). The maximum solid solubility of Zr in TiAl was found to be about 9 at. % at 1093 °C, however, the equilibrium for which this solid solubility was found is not given in [113]. In the present investigation the highest Zr content in TiAl is about 13.5 at. %, observed for the equilibrium β_0 + TiAl + $ZrAl_2$ in alloys Z4 and Z7 (**Table 4.3.**). For the drawing of the dashed βTi,Zr/β_0 phase boundary in **Figure 4.9** the result by Jiang et al. [32] has been considered who found βTi,Zr to be present in Ti-15Al-40Zr at. % solution treated at 1100 °C/2 h.
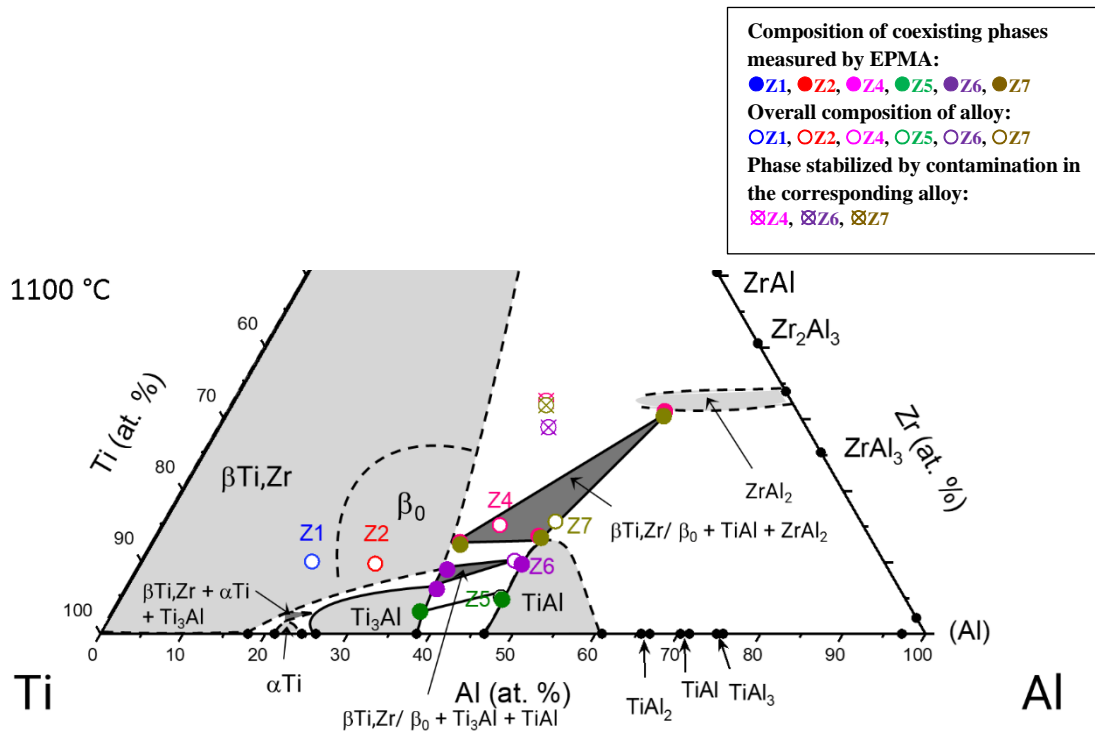
**Figure 4.9.** Partial Ti–Al–Zr isothermal section at 1100 °C.

Table 4.3. Compositions and lattice parameters of the coexisting phases in alloys annealed 1100 °C/200 h; n.d.: not determined but detected

Alloy	Phases	Composition (at. %)			Lattice Parameters (nm)	
		Ti	Al	Zr	a_0	c_0
Z4	ZrAl$_2$	16.0 ± 0.6	52.9 ± 0.3	31.1 ± 0.5	0.53461(1)	0.87451(2)
	TiAl	40.0 ± 0.6	46.3 ± 0.2	13.7 ± 0.5	0.4095(1)	0.4115(4)
	β_0	50.0 ± 0.5	37.2 ± 0.3	12.8 ± 0.3	0.322(8)	
Z5	TiAl	48.9 ± 0.9	46.3 ± 0.6	4.8 ± 0.3	0.40443(3)	0.40845(5)
	Ti$_3$Al	59.7 ± 0.6	37.2 ± 0.5	3.1 ± 0.1	0.5798(1)	0.4665(2)
Z6	TiAl	43.5 ± 0.2	46.8 ± 0.2	9.7 ± 0.2	0.40716(4)	0.41024(6)
	Ti$_3$Al	56.1 ± 0.3	37.6 ± 0.2	6.3 ± 0.1	0.5822(2)	0.4680(3)
	β(or β_0)	53.5 ± 0.3	37.5 ± 0.1	9.0 ± 0.2	n.d.	
Z7	ZrAl$_2$	16.5 ± 0.3	53.1 ± 0.3	30.4 ± 0.3	0.53771(1)	0.87419(3)
	TiAl	39.9 ± 0.4	46.7 ± 0.4	13.4 ± 0.2	0.41051 (2)	0.41094(2)
	β_0	50.1 ± 0.5	37.4 ± 0.4	12.5 ± 0.2	0.327 (1)	
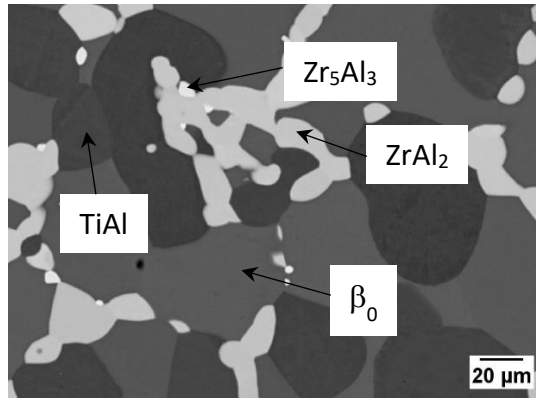
Figure 4.10. BSE micrograph of alloy Z4 (Ti-40.8Al-15.2Zr at. %) heat treated 1100 °C/200 h showing the phase equilibrium β_0 + Ti$_3$Al + TiAl and sporadic small grains of Zr$_5$Al$_3$.

4.2.5. Partial isothermal section at 1200 °C

The partial isothermal section at 1200 °C is shown in **Figure 4.11** and compositions of coexisting phases, lattice parameters, and analyzed impurity contents are presented in **Table 4.4.** Comparison with data for the as-cast alloys (**Table 2.1**) reveals that all samples show only a moderate uptake of oxygen after heat treatment at 1200 °C, with the exception of Z6. Compared to the partial isothermal section at 1100 °C, Ti$_3$Al is no longer present at this temperature and the three-phase equilibrium β_0 + αTi + TiAl is now observed. The reaction observed by DTA at about 1185 °C in Z5 should therefore stem from the reaction αTi + TiAl $\leftrightarrow$ Ti$_3$Al + TiAl. However, Ti$_3$Al was detected by HE-XRD in Z5 at RT after quenching from 1200 °C, showing once more that ordering from αTi to Ti$_3$Al took place during cooling. The presence of β_0 in alloys Z4, Z6 and Z7 is shown by XRD and HE-XRD.

The phase boundary between βTi,Zr and β_0 in **Figure 4.11** is again shown by a dashed line as it has not yet been established. However, in the drawing it is considered that Ti-24.8Al-24.9Zr (at. %) was found to be single-phase B2-ordered β_0 by TEM after solution treating at 1200 °C for 30 min followed by water quenching [172] and that in a diffusion study disordered βTi,Zr was found up to about 20 at. % Al and 39 at. % Zr at 1200 °C [183]. Also, a large number of alloys was annealed at 1200 °C in the βTi,Zr/β_0 phase field by Kornilov and Boriskina [184] and Nartova and Shirokova [192], but most of them underwent martensitic transformation during quenching and therefore no information about the ordering at 1200 °C can be gained from these samples.

None of the investigated alloys locates within the narrow tie triangle β_0 + αTi + TiAl at 1200 °C, which must be positioned in between the tie lines determined for Z5 and Z6. However, this composition range has been studied in detail by Kainuma et al. [115]. Comparison of their results with the present ones in **Figure 4.12** shows an excellent match. Therefore, the position of the dashed three-phase field β_0 + αTi + TiAl in **Figure 4.11** is taken from [115], very slightly adjusted to agree with the binary Ti–Al system accepted here, that differs from the one accepted in [115]. It is noted that in [115] authors did not distinguish between βTi,Zr and β_0, because no structural characterization by e.g. XRD or TEM was performed.

Partial isothermal sections for compositions Ti-(30-60)Al-30Zr at. % Zr were calculated at 1200 °C in [202, 203]. Though both modellings are based on data in [115], comparison of experimental data and modelling in [202, 203] shows an unsatisfactory match. Both modellings differ from phase equilibria shown in **Figure 4.11**, in that they show βTi,Zr in equilibrium with Zr_5Al_3 above about 15 at.% Zr, while the three-phase equilibrium of β_0 + TiAl + $ZrAl_2$ is observed instead.
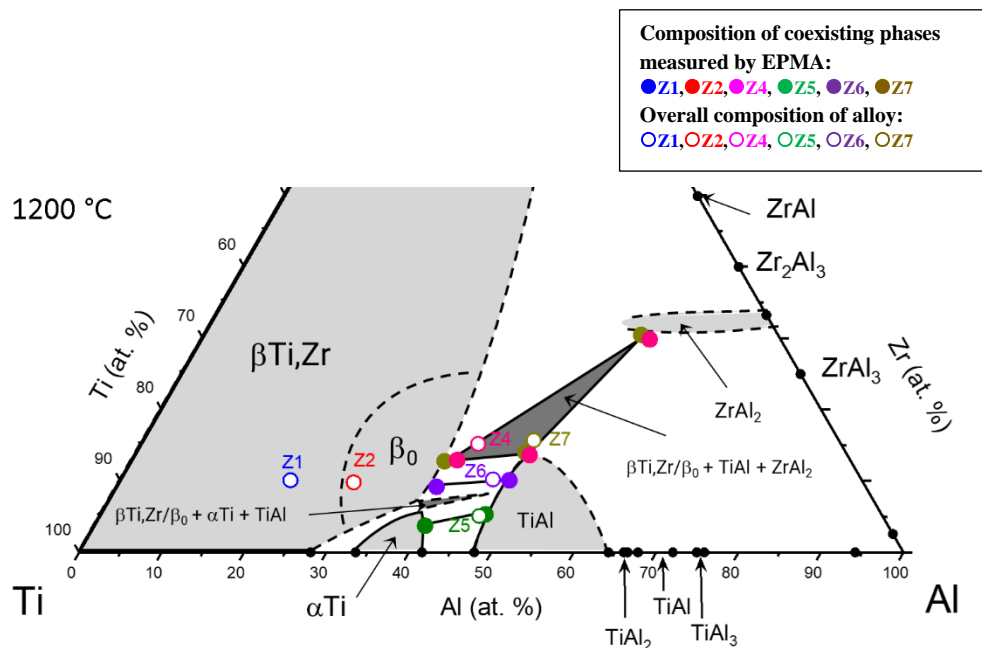
Figure 4.11. Partial Ti–Al–Zr isothermal section of the at 1200 °C.
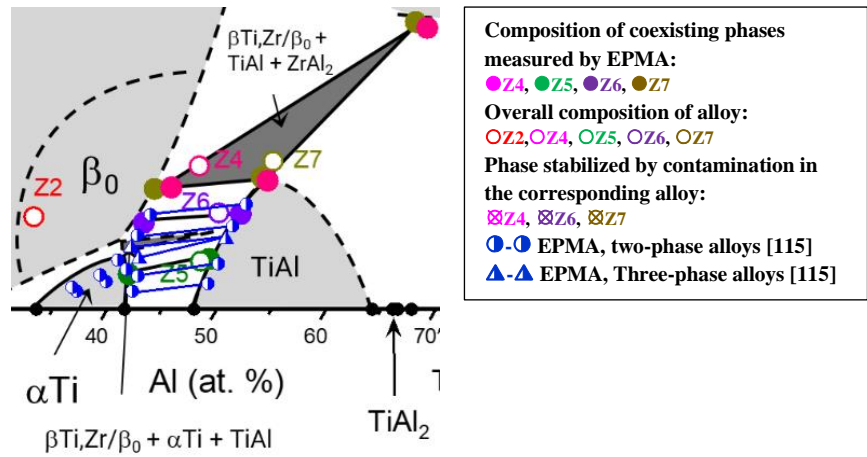
Figure 4.12. Enlarged section of Ti–Al–Zr partial isothermal section at 1200 °C with EPMA data by [115].

Table 4.4. Compositions and lattice parameters of the coexisting phases and impurity contents of samples annealed at 1200 °C/24 h; data shown in *italics* are from HE-XRD.

Alloy	Composition (at. %)				Lattice Parameters (nm)		Impurity (wt. ppm)		
	Phases	Ti	Al	Zr	a_0	c_0	C	O	N
Z4	**ZrAl$_2$**	15.9 ± 0.4	54.3 ± 0.5	29.8 ± 0.2	0.53439(1)	0.87378(2)	140	250	<50
	TiAl	38.5 ± 0.3	47.9 ± 0.3	13.6 ± 0.1	0.40916(7)	0.4119(1)			
	β$_0$	47.7 ± 0.7	39.4 ± 0.6	12.9 ± 0.3	0.327(1)				
Z5	**TiAl**	48.0 ± 0.3	46.7 ± 0.3	5.3 ± 0.2	0.40459(5)	0.40867(8)	120	240	<50
					0.4049	*0.4072*			
	αTi	56.1 ± 0.4	40.1 ± 0.4	3.8 ± 0.1	0.29001(1)	0.4646(4)			
	Ti$_3$Al				*0.579*	*0.4638*			
Z6	**TiAl**	42.7 ± 0.5	47.2 ± 0.7	10.1 ± 0.4	0.40397(4)	0.40868(7)	110	770	<50
					0.4078	*0.4085*			
	β$_0$	52.0 ± 0.7	38.8 ± 0.8	9.2 ± 0.3	0.338(2)				
					0.3253				
Z7	**ZrAl$_2$**	16.6 ± 0.3	53.0 ± 0.4	30.4 ± 0.3	0.53614(5)	0.8742(2)	100	360	<50
					0.5357	*0.873*			
	TiAl	38.9 ± 0.6	47.1 ± 0.5	14.0 ± 0.2	0.40908(3)	0.41162(5)			
					0.410	*0.4095*			
	β$_0$	49.3 ± 0.3	37.9 ± 0.3	12.8 ± 0.2	0.326(5)				
					0.32665				

4.2.6. Partial isothermal section at 1300 °C

Compositions of the coexisting phases measured by EPMA and their lattice parameters are tabulated in **Table 4.5** and the partial isothermal section at 1300 °C based on these data is presented in **Figure 4.13.** In order to check whether preferential evaporation of Al occurred at this high temperature, the overall compositions of alloys Z4, Z6 and Z7 were analyzed after the heat treatment at 1300 °C and results are presented in **Table 2.1**. The results show that, if at all, only a small loss of Al is observed. Measurements of the impurities show that only the oxygen content slightly increased (**Table 4.5**).

Table 4.5. Compositions and lattice parameters of the coexisting phases in alloys annealed at 1300 °C/24 h; n.d.: not determined but detected

Alloy	Phases	Composition (at. %)			Lattice Parameters (nm)		Impurity (wt. ppm)		
		Ti	Al	Zr	a_0	c_0	C	O	N
Z4	ZrAl$_2$	15.9 ± 0.3	54.8 ± 0.3	29.3 ± 0.2	0.53530(1)	0.87245(3)	89	300	<50
	β_0	46.8 ± 0.4	41.0 ± 0.2	12.2 ± 0.3	0.326(1)				
	TiAl	n.d.	n.d.	n.d.	n.d.	n.d.			
Z5	TiAl	45.1 ± 0.4	49.2 ± 0.3	5.7 ± 0.2	0.40383(3)	0.40858(4)	86	220	<50
	αTi	53.6 ± 0.8	42.4 ± 0.6	4.0 ± 0.2	0.28931(4)	0.4639(1)			
Z6	TiAl	41.2 ± 0.3	48.4 ± 0.3	10.4 ± 0.2	0.40689(3)	0.41080(5)	89	480	<50
	β_0 (or β)	51.6 ± 0.9	39.3 ± 0.7	9.1 ± 0.3	0.325(3)				
Z7	ZrAl$_2$	16.2 ± 0.4	54.1 ± 0.6	29.7 ± 0.4	0.53430(1)	0.87287(3)	77	240	<50
	TiAl	37.7 ± 0.3	48.6 ± 0.4	13.7 ± 0.3	0.40852(2)	0.41081(2)			
	β_0	48.7 ± 0.9	38.9 ± 0.9	12.4 ± 0.2	0.325(1)				
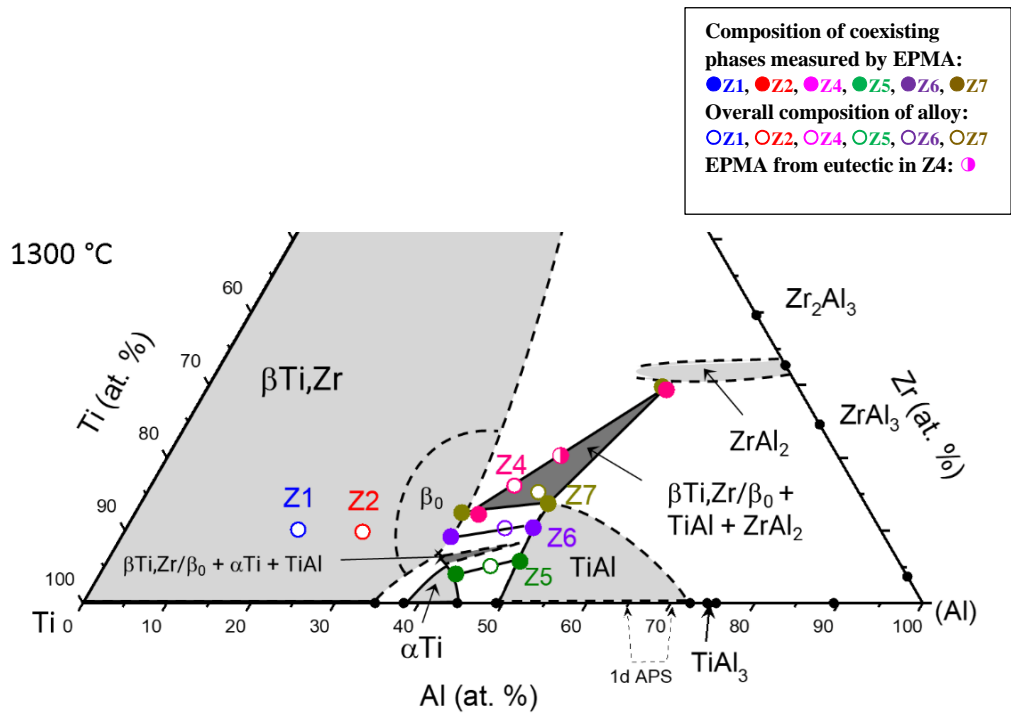
Figure 4.13. The partial Ti–Al–Zr isothermal section at 1300 °C.
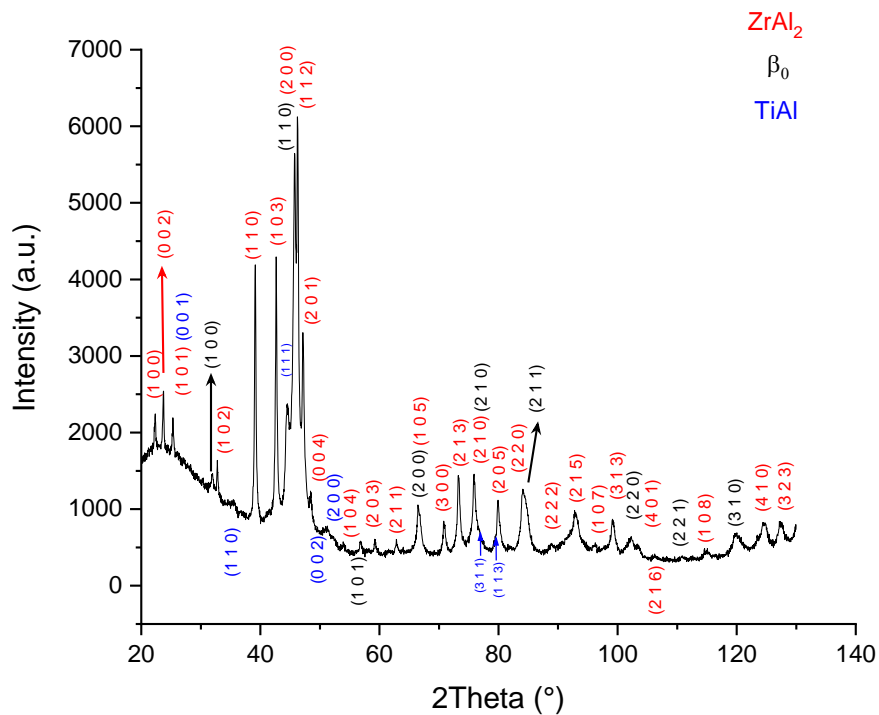
Figure 4.14. XRD analysis of Z4 (Ti-43.3Al-16.1Zr at. %) heat treated at 1300 °C/24 h.
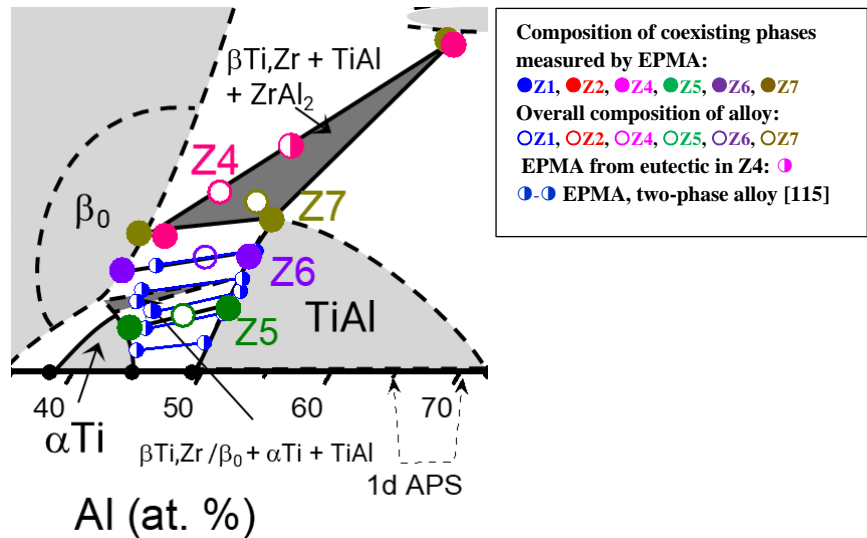
Figure 4.15. Enlarged section of Ti–Al–Zr partial isothermal section at 1300 °C with EPMA data by [115].

Phase equilibria at 1300 °C resemble those at 1200 °C (**Figure 4.11**). The three-phase equilibrium β_0 + TiAl + ZrAl$_2$ is again observed in alloys Z4 and Z7. However, in Z4 TiAl was only detected by XRD, but because the phase fraction of TiAl is only minor, all grains were too small to be measured by EPMA. Alloys Z4 and Z7 show superlattice reflections of β_0, while they are not visible for Z6. This could be due to the low phase fraction of β_0 in Z6 and therefore the ordering cannot be established.

Kainuma et al. [115] investigated phase equilibria among βTi,Zr(β_0), αTi, and TiAl at 1300 °C. They located the position of the narrow βTi,Zr(β_0) + αTi + TiAl three-phase field based on the established compositions of the neighbouring two-phase fields. **Figure 4.15** shows that compositions determined in [115] agree with the current results. The small dashed tie triangles β_0 + αTi + TiAl in **Figure 4.13** and **Figure 4.15** are derived from the combined results shown in **Figure 4.15**.

The solid solubility range of TiAl at 1274 °C was investigated by metallography and XRD of quenched samples [57, 58]. The data by Troup [57] actually stemmed from samples annealed between 1246 to 1379 °C and it is therefore that he gave a range for the maximum solid solubility of 10 to 15 at. % Zr. Spragins et al. [58] found a maximum solid solubility of 13 at. % Zr at 1274 °C, though it was not stated at which equilibrium. As they detected oxides in some of their samples and phase boundaries do not match with the accepted binary Ti–Al system, their values are considered as doubtful [116]. 13.7 at. % Zr have been measured in TiAl in Z7 (**Table 4.5**), but the solid solubility should be somewhat increase at higher Al contents.

Also for 1300 °C partial isothermal sections for the composition range Ti-(30-60)Al-30Zr at. % Zr were calculated in [202, 203], based on data in [115]. Like at 1200 °C, there is again no good match between the experimental data in [115] and both modellings again show phase equilibria between βTi,Zr(β₀) + Zr₅Al₃ instead of β₀ + TiAl + ZrAl₂ determined here.

In a small area near the edge a eutectic is observed in alloy Z4 (**Figure 4.16**), indicating partial melting at 1300 °C. The composition of the eutectic measured with EPMA by employing a widened beam is Ti-46.8Al-20.3Zr at. %. Comparison with the recently established liquidus projection of the Ti–Al–Zr system by Abreu et al. [208] shows that the composition of the eutectic lies on the monovariant line L <-> βTi,Zr + ZrAl₂. While no temperatures are given in [208], DTA analysis of alloy Z4 shows that the eutectic temperature is 1316 ± 2 °C (**Table 4.6 and Figure 4.16**).
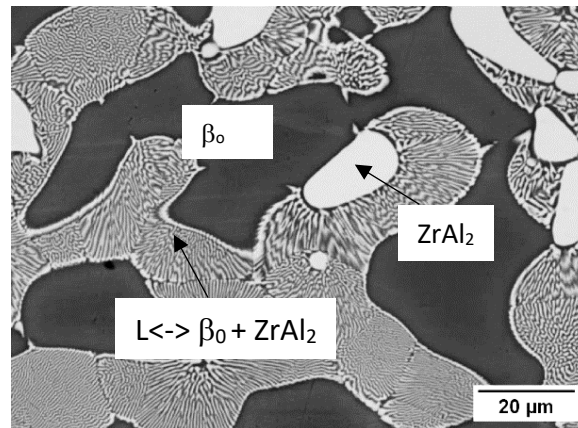
Figure 4.16. Microstructure at the edge of alloy Z4 (Ti-43.3Al-16.1Zr at. %) heat treated at 1300 °C/24h.

4.2.7. DTA analyses

DTA was performed with samples equilibrated at 1000 °C. **Table 4.6** summarizes observed temperatures, allocation to certain reactions, and references for invariant reactions. Temperatures given in **Table 4.6** are evaluated from the first heating, if not noted otherwise, and reactions are listed in the sequence of decreasing temperature.

The peaks in alloy Z1 at 1028 °C and 995 °C are related to the transition from βTi,Zr (or β₀) to Ti₃Al. This would be in full agreement that the alloy Z1 consists of βTi,Zr (or β₀) + Ti₃Al at 1000 °C (**Figure 4.5** and **Table 4.2**), locates in the single-phase field of βTi,Zr/β₀ at 1100 °C (**Figure 4.9**) and in the single-phase field of Ti₃Al at 800 °C [56]. Comparison of the isothermal sections at 1000 °C (**Figure 4.5**) and 1100 °C (**Figure 4.9**) shows that the strong peak observed for alloy Z2 at 1083 °C should also be related to the βTi,Zr/β₀ to Ti₃Al transition. That instead

of two individual peak only one peak is observed is in accordance with **Figure 4.5** which shows that the βTi,Zr/β_0 + Ti$_3$Al two-phase field should be very narrow in that composition range.

The peak at 1316 °C in alloy Z4 is associated with the eutectic L $\leftrightarrow$ βTi,Zr + ZrAl$_2$, as detailed above and in agreement with the liquidus projection [208]. The three peaks at 1219 °C, 890 °C, and 850 °C, all of them only observed during first heating, cannot be allocated to any phase transformation. According to the present results, alloy Z4 consists of βTi,Zr/β_0 + TiAl + ZrAl$_2$ between 1300 °C and 1000 °C and also at 800 °C according to [56]. Therefore, no peak is expected below 1300 °C in this alloy. The weak peak in alloy Z5 at 1185 °C should be associated with the transition from αTi + TiAl to Ti$_3$Al + TiAl, which is observed in Z5 between 1200 °C (**Figure 4.11**) and 1100 °C (**Figure 4.9**). DTA of Z6 shows two distinct peaks above 1300 °C, which are related to the solidification of Z6. According to the liquidus projection [208], the composition of Z6 locates in the field of primary crystallization of βTi,Zr. Therefore the peak at 1353 °C should correspond to the reaction L $\leftrightarrow$ L + βTi,Zr. Due to precipitation of βTi,Zr the composition of the melt enriches in Al, shifting its composition towards the eutectic line L $\leftrightarrow$ βTi,Zr + TiAl [208]. The strong sharp peak at 1314 °C could therefore correspond to this reaction. The weak signal at about 1190 °C may be associated with the transition from the two-phase field β_0 + TiAl at 1200 °C (**Figure 4.11**) to the three-phase field β_0 + TiAl + Ti$_3$Al at 1100 °C (**Figure 4.9**). DTA of Z7 again shows two distinct peaks above 1300 °C (**Table 4.6**). As the composition of Z7 also locates in the field of primary crystallization of βTi,Zr [208], the signal at 1367 °C should correspond to L $\leftrightarrow$ L + βTi,Zr. The signal at 1312 °C could correspond to L $\leftrightarrow$ βTi,Zr + ZrAl$_2$ according to [208], as the Zr content is markedly higher than in alloy Z6 and more comparable to that of alloy Z4 (**Table 2.1**). It is noted, that eutectic temperatures determined in alloys Z4, Z6, and Z7 are very close to each other. As they should stem from two different eutectic lines and as the composition of the ternary eutectic E$_1$ L $\leftrightarrow$ βTi,Zr + TiAl + ZrAl$_2$ in [208], where these two lines meet, must be close by, the temperature of E$_1$ could be at about 1310 °C. There is one more signal at 1219 °C, which is only observed on first heating, which cannot be allocated to any reaction as Z7 consists of βTi,Zr + TiAl + ZrAl$_2$ between 1300 °C to 1100 °C (**Figure 4.9,** and **Figure 4.13**).

Table 4.6. DTA results; reactions are shown and listed with increasing temperature; strength of the peaks is indicated by ss (very strong), s (strong), and w (weak); as the ordering of βTi,Zr is not known when it precipitates from the melt, it is shown as βTi,Zr, though it might B2-ordered β_0.

Alloy	Al (at. %)	Zr (at. %)	Heated to °C	Onset (°C); strength of the peak	Reaction	Ref.
Z1	20.6	10.1	1400	1028; ss	βTi,Zr/β_0 ↔ Ti$_3$Al + βTi,Zr/β_0	
				995; s	Ti$_3$Al + βTi,Zr/β_0 ↔ Ti$_3$Al	
Z2	28.4	9.8	1400	1083 (±3); ss	β(Ti,Zr)/β_0 ↔ Ti$_3$Al	
Z4	44.7	16.5	1400	1316; ss	L ↔ βTi,Zr + ZrAl$_2$	[208]
				1235; s	?	
				890; s	?	
				850; s	?	
Z5	46.1	5.1	1400	~1185; w	αTi + TiAl ↔ Ti$_3$Al + TiAl	
Z6	45.1	10.2	1400	1353; ss	L ↔ L + βTi,Zr	[208]
				1314; s	L ↔ TiAl + βTi,Zr	[208]
				~1190; w	β_0 + TiAl ↔ β_0 + TiAl + Ti$_3$Al	
Z7	47.3	15.7	1400	1367; ss	L ↔ βTi,Zr + ZrAl$_2$	[208]
				1312; ss	L ↔ TiAl + βTi,Zr	[208]
				1219; s	?	

4.2.8. The effect of addition of Zr on the lattice parameters of TiAl

Because it has already been realised in the 1950s that the c/a ratio of TiAl decreases with increasing Zr content, much effort has been spent on this topic [113, 114, 136, 163, 188, 209] (for completeness: in some of the early studies an increase of the c/a ratio with increasing Zr content was reported [57, 58, 210]). As reported data nearly approached unity, it had been expected that possibly a cubic structure could be attained for TiAl by alloying with Zr, which potentially could reduce the brittleness of TiAl. In view of the importance of this topic, the current c/a ratios are shown in **Figure 4.17**. The data once more reveal that the c/a ratio of TiAl markedly decreases in dependence on the Zr content, but does not reach or even exceed a value of 1. As also shown before [163, 188], addition of Zr in TiAl does not change the c/a ratio monotonically and the c/a ratio changes also in dependence on the Al content.
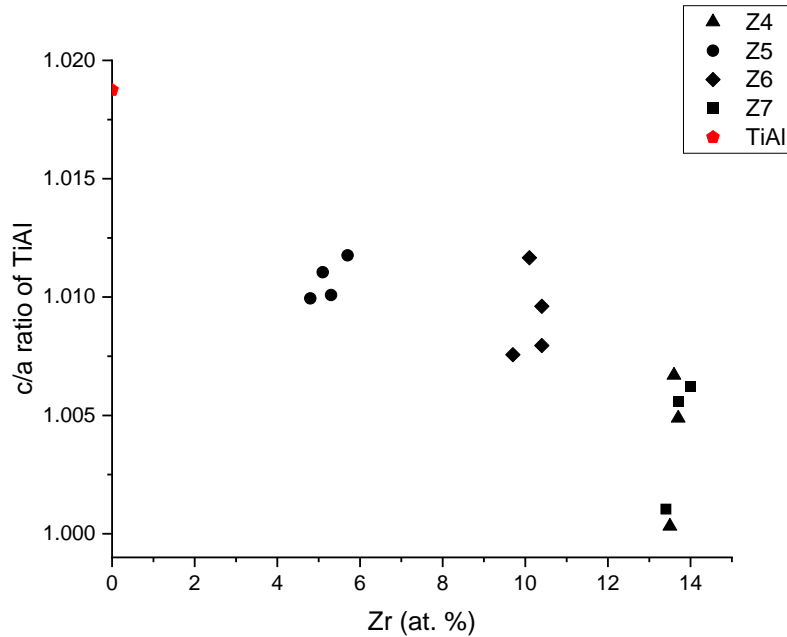
Figure 4.17. c/a ratio of TiAl in dependence on Zr content as determined by EPMA.

4.2.9. Conclusion

The addition of Zr in TiAl-based alloys is beneficial in enhancing the creep resistance and increasing the strength of TiAl through solid solution hardening. Our recent assessment of the Ti–Al–Zr system as well as recent CALPHAD modellings showed the necessity for more experimental data Four partial isothermal sections were experimentally established through SEM, EPMA, (HE-)XRD, TEM, and DTA of six different alloy compositions heat treated at 1000-1300 °C. The results give a new understanding of phase equilibria in the Ti–Al–Zr system between 1000 and 1300 °C. Phase equilibria at all temperatures are different from the ones established before. For instance, **Figure 4.18** shows the established partial Ti–Al–Zr isothermal section at 1000 °C versus the recently assessed version [116], that was primarily based on the experimental investigations of Yang et al. [55] in 2014, which was the most comprehensive experimental study at the time. While previous isothermal sections showed a large solid solubility of Ti in Zr_5Al_3, it is now clear that this phase is stabilized by impurities, most noteworthy oxygen. Therefore, much effort was spent in the present work to keep impurity levels as low as possible. By that, only traces of Zr_5Al_3 were observed and phase equilibria between $\beta Ti,Zr/\beta_0$, TiAl, and $ZrAl_2$ were determined between 1000-1300 °C. Additionally, it is now clear that B2-ordered β_0 already exists at 1000 °C and remains stable up to at least

1300 °C. The new findings can now be implemented for further CALPHAD calculations to anticipate the complete isothermal sections in Ti–Al–Zr system, and to set up the next generation of advanced CALPHAD databases, which could assist the development of TiAl-based alloys with improved properties.
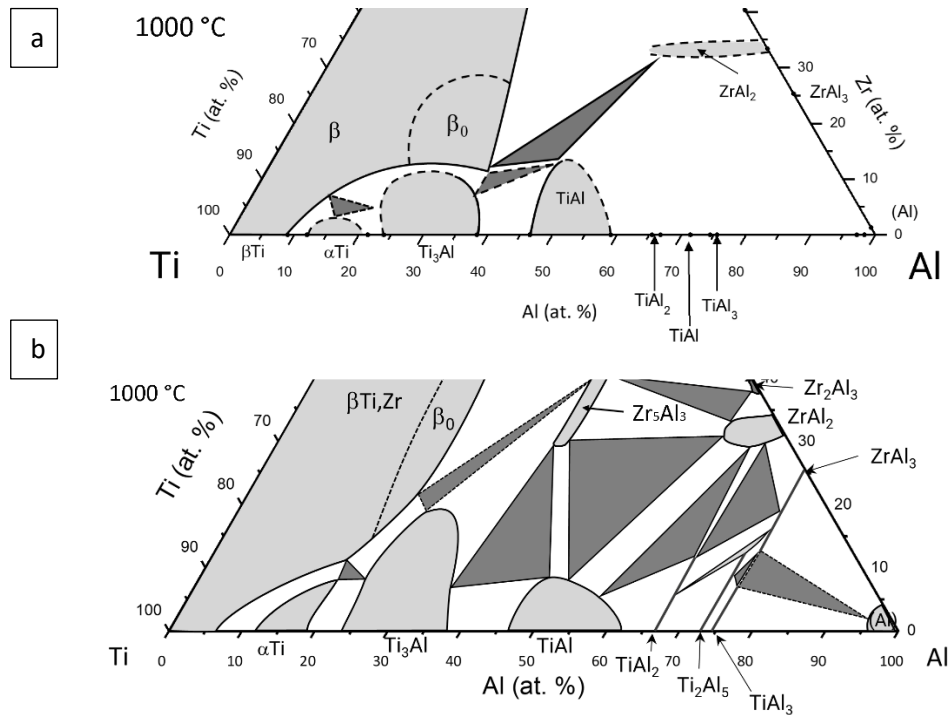
Figure 4.18. Partial Ti–Al–Zr isothermal section at 1000 °C a) from present experimental results b) from assessment in **section 4.1.4** [116].

5. Ti–Al–O system

The investigation of phase equilibria in the Ti–Al–O system is strongly coupled with the interest of the industry in respective materials and can be divided into a "ceramic" and a "metal" part. Due to its exclusive thermal properties such as low thermal expansion combined with low thermal conductivity and excellent thermal shock resistivity above 1500 °C [211, 212], ceramic materials based on the aluminum titanate Al_2TiO_5 (**Table 5.1**) are developed for high-temperature applications, e.g. as diesel particulate filters [213]. Because Al_2TiO_5 decomposes below 1280 °C (**Table 5.1**) and because single-phase Al_2TiO_5 is prone to micro-cracking and rapid coarsening [214], phase equilibria in the oxygen-rich part at temperatures above 1200 °C have been extensively investigated [215].

Due to the high affinity of titanium to oxygen, investigation of the solid solubility of oxygen in Ti started with the development of titanium alloys [31, 216]. Also, in Ti–Al(–X) alloys the presence of oxygen is inevitable. Oxygen induces internal stresses, causes embrittlement and loss of ductility [217] because it promotes the formation of brittle Ti_3Al vs. its less-brittle disordered counterpart αTi [7, 31]. Additionally, the $\beta_0/\beta Ti$ transformation is strongly affected by the presence of oxygen [7], which influences the workability and ductility of the alloy [12]. As it is almost impossible to eliminate oxygen completely from Ti–Al(–X) alloys, the only practical solution would be to set a maximum limit of oxygen content and try to control it [31]. This requires understanding the influence of oxygen on phase equilibria and the resulting consequences on the mechanical properties of the alloys. However, determining the phase equilibria, particularly in the Ti–Al–O system, is challenging. This partially comes from the fact that detection and quantification of oxygen in solid solution is not easily achievable with common techniques such as EPMA/WDS [218, 219]. Though wet-chemical analysis is a precise technique to determine the oxygen content in a bulk material, it cannot be used to analyze individual phases in a multiphase alloy, except they can be separated from each other before analysis. As the latter is usually not possible for Ti–Al(–X) alloys, lack of reliable data for the solid solubility of oxygen in individual phases is the major problem why phase equilibria in the Ti–Al-rich part of the Ti–Al–O system are not well established.

The last assessment of the Ti–Al–O system has been performed in the framework of MSIT [60]. This assessment covers only references up to the year 1990 and showed to be not very complete. By now, more than one hundred new relevant studies have been published, yielding a multitude of new data. Additionally, since the last assessment our understanding of phase

equilibria in the binary Ti–Al system has changed, for instance whether Ti$_3$Al forms at 1200 °C via a peritectoid reaction or congruently could be dependent on the oxygen content.

Hence, it is important to understand the influence of oxygen on phase equilibria in the Ti–Al(–X) systems. If a sound data set would exist for the Ti–Al–O system, CALPHAD modelling of higher order systems would give an idea how phase boundaries will change with respect to oxygen content and what could be the limit of oxygen in practice.

As the last critical assessment of the Ti–Al–O system had been performed thirty years ago, investigation started with a thorough assessment of the literature. **Chapter 5.1** presents the part of the assessment [215] that has been devoted to the "metallic part" at temperatures below 1200 °C and this is the part of the assessment which has been led by the present author. The chapter starts with a literature review of the Ti–Al-rich side of the system (**section 5.1.1**). The accepted binary reference systems i.e., Al–O and Ti–O are discussed in **section 5.1.2**. The Ti–Al system has been discussed before (**section 4.1.2**) and is therefore not addressed again. Various ternary compounds are reported in the literature, which are discussed in detail in **section 5.1.3**, and their stabilities are clarified. From the critical assessment, four (partial) isothermal sections were newly established in the temperature range 945-1200 °C, which are presented in **section 5.1.4**. At the end of this chapter a section has been added (**section 5.1.5**), which was not part of the assessment, where the newly assessed isothermal section at 1100 °C is compared with the one calculated before the start of the ADVANCE project with the then existing CALPHAD database. This section is added to show the differences between the two isotherms, which show the importance of new reliable experimental investigations to update the CALPHAD database.

Chapter 5.2 focuses on the experimental investigations performed within this work, with emphasis on the results for 1100 °C. Investigations start with the SEM and XRD analyses of the samples (**section 5.2.1**). Initially, it was planned to measure the oxygen content in the different phases by EPMA. However, unexpected problems were encountered with measuring oxygen by EPMA. These problems and the efforts to solve them are explained in **section 5.2.2**. Finally, it turned out that the EPMA measurements of O in Ti–Al have a fundamental problem. To confirm this, APT analysis has been performed on one of the samples investigated by EPMA (**section 5.2.3**). In **section 5.2.4**, the own measurements are compared with results of other research groups, who employed different techniques to measure oxygen in Ti–Al alloys. Complementary DTA analyses have been performed on these samples and results are mentioned in **section 5.2.5.** Though beside the single APT measurement no oxygen analysis of

the phases could be performed within this work, the combined results from the metallographic, XRD and DTA investigations give a rough outline of the phase equilibria among αTi, Ti$_3$Al, and TiAl at 1100 °C (**section 5.2.6**). **Section 5.2.6** not only summarizes the outcome of the experimental investigations by comparing it with the assessed isothermal section discussed in **section 5.1.5**, but also gives some directions for future research in this system.

Section 5.1.1 to **5.1.4** is part of the publication by M. Ilatovskaia, Z. Kahrobaee, et al. [215]. The present author led this part of the assessment and has been the main contributor and authored these parts. The figures in [215] had to be simplified for the publication and here the more elaborated versions are shown in **Section 5.1.1** to **5.1.4**. **Section 5.1.5** and investigations done in **chapter 5.2** have not been published yet.

5.1. Critical assessment of the Ti–Al–O system

5.1.1. Literature review of the Ti–Al part of the system

Investigation of the Ti–Al part of the system starts with [220, 221], who investigated the influence of oxygen on phase relationships in the Ti-rich part. Heat treatments between 900-1100°C on alloys with 0-10 wt. % Al and up to 1 wt. % O were performed and samples were analyzed by microscopy and measuring the hardness. Four vertical sections at constant oxygen contents of 0, 0.25, 0.5 and 1 wt. % showing the extension of the αTi + βTi phase field were established and results agree well with the currently accepted Ti–O and Ti–Al binaries. The data show that with increasing oxygen content the αTi + βTi phase field widens and that the αTi $\leftrightarrow$ βTi transformation temperature increases. These observations were confirmed in [222], where about the same composition range has been investigated up to 1250°C. The αTi/(αTi + Ti$_3$Al) phase boundary at 600 and 700°C was established by metallographic investigation of equilibrated alloys with oxygen contents up to 0.35 at.% [120]. This range was later extended at 600°C to about 5 at. % O in [223-225]. The αTi/αTi + Ti$_3$Al phase boundary was again studied by TEM on alloys equilibrated at 600°C for 400 h [195].

In an extensive experimental investigation, compositions of up to 24 at. % Al and 32 at.% O were investigated, yielding partial isothermal sections at 800 and 1000°C [226] and a vertical section Ti–Al$_2$O$_3$ up to 30 wt. % Al$_2$O$_3$ in the temperature range of 200-2000°C [226-228]. However, phase equilibria established in [226-228] do not match with phase boundaries of the current Ti–O and Ti–Al binaries and phase equilibria within the ternary system established by other groups. Waterstrat [31] conducted a comprehensive study on the influence of oxygen on the αTi $\leftrightarrow$ βTi transformation temperature by in-situ neutron diffraction in the temperature range of 650-1200 °C. The established βTi/ (αTi+βTi) phase boundary agrees well with previous studies [220-222]. Misra [229] investigated the reaction between Ti with 25, 43 and 54 at. % Al and Al$_2$O$_3$ by diffusion couples annealed between 900-1300°C and measuring the diffusion profiles by EPMA. No intermediate phase was detected between Al$_2$O$_3$ and TiAl and it was found that oxygen is enriched in Ti$_3$Al compared to TiAl. These results were further on confirmed by the investigation of TiAl/Al$_2$O$_3$ and TiAl/TiO$_2$ diffusion couples annealed at 1000 and 1100°C by EPMA [230].

In [231], five alloys of fixed composition as well as two TiAl/Al$_2$O$_3$ diffusion couples were equilibrated at 1100°C. From the results, a partial isothermal section of the Ti corner has been

derived, though only the diffusion couples' compositions were established by EPMA, while the five alloys were only analyzed regarding their phase content by XRD. A similar approach has been undertaken in [232, 233]. Again, the partial isothermal section at 1100°C seems only to be based on the EPMA results of Ti/Al$_2$O$_3$ diffusion couples, as no details about alloys of fixed compositions, which are mentioned in [232, 233], were reported. However, the partial isothermal sections established in [231-233] agree very well with each other. Another partial isothermal section at 920°C was also established from the investigation of TiAl/Al$_2$O$_3$ diffusion couples [234]. From an unspecified number of arc-melted compositions, which were equilibrated at 945°C for 360 h, a partial isothermal section of the Ti corner was established by EPMA [235]. No results for individual alloys were reported and binary phase boundaries deviate from the accepted binaries and specifically the Ti$_3$Al phase field has an unlikely shape. Ti/Al$_2$O$_3$ diffusion couples investigated by XRD, EPMA and TEM were also employed for the investigation of phase equilibria at 871°C. Because results were not unambiguous, two possible versions of a phase diagram were shown, one showing the three-phase equilibrium TiAl + Ti$_3$Al + TiO, one TiAl + Ti$_3$Al + Ti$_2$O$_3$ instead. However, as phase equilibria for Ti–O deviate markedly from the currently accepted binary, both versions maybe doubtful.

5.1.2. Binary Systems

The Al–O system is accepted from the MSIT evaluation [236]. The phase diagram has been calculated based on the thermodynamic description by [237]. The oxygen solubility in Al is below measurability. α-Al$_2$O$_3$ (alumina) is the only stable compound in this system and it shows no deviation from stoichiometry. Various Al$_2$O$_3$ polymorphs exist (γ, η, δ, θ, λ, σ, κ, χ) which are all metastable, though some of them can persist for long times even at higher temperatures.

The Ti–O system is accepted from the most recent detailed description [238]. This description is in accordance with recent modellings [239, 240]. Besides four phases with notable solid solution ranges αTi, βTi, TiO$_x$, rutile TiO$_{2-\delta}$, the stoichiometric oxides Ti$_3$O$_2$, α-TiO, Ti$_2$O$_3$, Ti$_3$O$_5$ and the sequence of the so-called Magneli phases (Ti$_n$O$_{2n-1}$, n = 4-10, 20) exist.

For Ti–Al the phase diagram is accepted from MSIT [7] and is discussed in **section 4.1.2**.

5.1.3. Solid Phases at the Ti–Al-rich side and ternary compounds

αTi and βTi both show marked solid solubilities for O and Al [7, 238] and both increase the stability of αTi to higher temperatures with respect to βTi. In the Ti–O system this leads to congruent melting of αTi at 1895°C at about 32 at. % O [238]. Both phases also show a marked solid solubility for Al and O, which increases in both phases with increasing temperature [227]. For αTi the c/a-ratio increases by the uptake of O [241]. Ti_3Al has a marked solid solubility for O of about 13 at.% at 1100 °C, while it is less marked in TiAl (3.6 at.% at 1100 °C) [231, 233]. The site occupancy of O in Ti_3Al and TiAl has been calculated by DFT [242] and experimentally determined for Ti_3Al by Rietveld refinement of neutron diffraction patterns [243]. Additionally, [243] measured the increase of the lattice parameters with increasing oxygen content and found a much more pronounced elongation for c than for a, which is a result that oxygen occupies the interstitial octahedral sites formed by 6 Ti atoms. The solid solubility of oxygen in the more Al-rich Ti–Al phases has not been established.

Though a number of ternary phases have been reported over the past decades, Al_2TiO_5 seems to be the only stable ternary compound (crystallographic data for all oxides discussed in the following are summarized in **Table 5.1**). The phase forms from the melt at 1860°C [244, 245], either congruently [244, 246] or by the peritectic reaction L + Al_2O_3 $\leftrightarrow$ Al_2TiO_5 [240, 245] and decomposes by the eutectoid reaction Al_2TiO_5 $\leftrightarrow$ Al_2O_3 + TiO_2 at 1280°C [240, 247, 248]. Al_2TiO_5 possibly undergoes a polymorphic transformation at about 1820°C [245]. Below this temperature, βAl_2TiO_5 (orthorhombic, space group Cmcm) is isomorphous with pseudobrookite [249]. The structure for the high-temperature polymorph has not yet been determined, though XRD patterns have been recorded for αAl_2TiO_5 [245, 250].

$Al_6Ti_2O_{13}$ is a metastable structure [251, 252] which is crystallographically closely related to Al_2TiO_5 and which is often observed together with that phase [252, 253]. The structure has been determined as orthorhombic, space group Cm2m [251]. It has also been shown that intermediate structures between Al_2TiO_5 and $Al_6Ti_2O_{13}$ exist [254]. $Al_2Ti_7O_{15}$ is another orthorhombic phase, space group C2/m, that had been synthesized at 950°C and 1000°C [255, 256]. The phase belongs to a series of $Al_xTi_{3-x}O_5$ compounds, which exist as solid solutions between Al_2TiO_5 and Ti_3O_5 [257, 258], but which only form under reduced p_{O2} [259, 260].
The phase $Al_3Ti_5O_2$ [261, 262] presumably is identical with the Z- or X-phase [263-268], which is frequently observed in scales formed during oxidation of TiAl or Ti_3Al between 800°C and 1100°C [263, 269]. $Al_3Ti_5O_2$ is cubic, space group $P4_232$ [264, 270] and usually identified by

a lattice constant of about 0.69 nm. After oxidation in pure oxygen at 1000 °C for up to 250 h $Al_3Ti_5O_2$ was observed [268] , in accordance with previous studies. However, in alloys of appropriate composition annealed at 1000 °C for 168 h, the phase equilibrium $Ti_3Al + Al_2O_3$ were observed instead [268]. It was therefore concluded that $Al_3Ti_5O_2$ is a metastable phase, finally disintegrating into oxgen-rich $Ti_3Al + Al_2O_3$ [268]. This observation is in line with results from all studies of $TiAl/Al_2O_3$ diffusion couples, where no phase was observed between TiAl and Al_2O_3 at respective temperatures [229-234]. Recent DFT clculations also indicate that $Al_3Ti_5O_2$ is not a stable phase [271].

Al_2Ti_6O was identified by ab-initio calculations as a stable ground state at 0 K. The metal atoms are $D0_{19}$-ordered as in Ti_3Al, with O occupying the octahedral interstitial site formed by 6 Ti atoms [271]. It is noted that this composition lies within the solid solubility range for oxygen in Ti_3Al at higher temepratures [231-233, 268].

At a composition of $Al_{36}Ti_{40}O_{24}$ a phase had been found after sintering at 775 – 1400 °C for up to 500 h [241], designated as τ_5 in the previous assessment [60]. The phase is described as having lattice constants similar to αTi [241], but as it has not been detected in any other investigation which has been performed in the same composition and temperature range and as even after 500 h at 1000 °C the X-ray pattern shown in [241] shows the presence of four phases, which violates the Gibbs phase rule, the phase is herein not considered.

The crystallographic data of the oxide phases discussed above are listed in **Table 5.1.** To avoid redundancy, data for the Ti–Al-rich phases presented in **Table 4.1** are not repeated here. For the complete list of solid phases see [215].

Table 5.1. Crystallographic data of solid phases

Phase/ Temperature Range (°C)	Pearson Symbol/ Space Group/ Prototype	Lattice Parameters (nm)	Comments/References
αAl_2O_3/ <2054	hR30 / R$\bar{3}$m /αAl_2O_3	a_0 = 4.75.86, c_0 = 12.9897	[100, 167]
Ti_3O_2 / <920	hP5 /P6/mmm	a_0 = 4.9915, c_0 = 2.8794	[272]
αTiO/ <939	mC16	a_0 = 9.355, b_0 = 5.868, c_0 = 4.135, β = 107.53°	[273]
TiO_x, γTiO/ 1770-456	cF8 /Fm$\bar{3}$m/ NaCl	a_0 = 4.1766 (x = 1)	[274], halite
Ti_2O_3 / <1838	hR30/ R$\bar{3}$m/ αAl_2O_3	a_0 = 5.4325, α = 56.75°	[275]
TiO_2 <1868	tP6 /P4$_2$/mnm/ TiO_2	a_0 = 4.5937, c_0 = 2.9587	[276], rutile

αAl_2TiO_5/ 1860-1820	?		[245, 250]
βAl_2TiO_5/ 1820-1280	oC32/ Cmcm/ $TiFe_2O_5$	$a_0 = 3.605$, $b_0 = 9.445$, $c_0 = 9.653$	[251], aluminum titanate or tialite
*$Al_6Ti_2O_{13}$ (m)	/ Cm2m/	$a_0 = 3.651$, $b_0 = 9.368$, $c_0 = 12.554$	[251]
*$Al_2Ti_7O_{15}$	/ C2/m/	$a_0 = 17.674$, $b_0 = 2.973$ $c_0 = 9.358$, $\beta = 98.66°$	[255]; forms under reduced p_{O2} [259, 260]
*$Al_3Ti_5O_2$ (m) (Z- or X-phase)	/ P4$_2$32/	$a_0 = 6.90$	[264]; in oxidised samples

5.1.4. Isothermal Sections

Only for 1100-1300°C, complete isothermal sections exist, while partial isothermal sections at higher temperatures are available for the oxide part, for lower temperatures they are available for the Ti corner up to TiAl.

Panda and Jung [277] presented a calculated (predicted) partial isothermal section for Ti_2O_3–TiO_2–Al_2O_3 at 1600°C. It shows the phase equilibria before the last liquid in this part of the Al–Ti–O system solidifies at about 1590°C. Ilatovskaia et al. [240] calculated an isothermal section at 1300°C.

1200°C is the highest temperature for which experimental results are available for the Ti–Al part of the system. A partial isothermal section at 1200 °C based on the results from Schofield and Bacon [222] have been shown in **Figure 5.1.** For the phase boundary of βTi the ternary composition from [222] has been taken, which fits well to those in the accepted binaries. For the Ti-rich phase boundary of αTi, data are available from vertical sections [31, 226-228]. The width of the two-phase field βTi + αTi in the vertical section Ti–Al_2O_3 [226-228] is in agreement with that shown in **Figure 5.1**, but the single-phase region of αTi is too narrow in [226-228], and αTi + Al_2O_3 was already detected at 7.7 at. % O. The location of the αTi phase boundary shown in [31] for 3 and 6 at. % O are at somewhat lower and higher O contents, respectively, than those shown in **Figure 5.1**. Quantitative results from a diffusion couple annealed for 100 h at 1200 °C had been not evaluated in [229], but analysis of the measured profile shows good agreement between the composition of αTi at the (βTi + αTi)/ αTi phase boundary and its position in **Figure 5.1**. Phase equilibria between Ti_3Al and TiAl shown in **Figure 5.1**. have been recently published [278]. Specifically, the oxygen content in the phases was precisely measured by EPMA equipped with soft X-ray emission spectroscopy (SXES).

Results that can be evaluated from the diffusion profile shown in [229] are again in good agreement with [278].
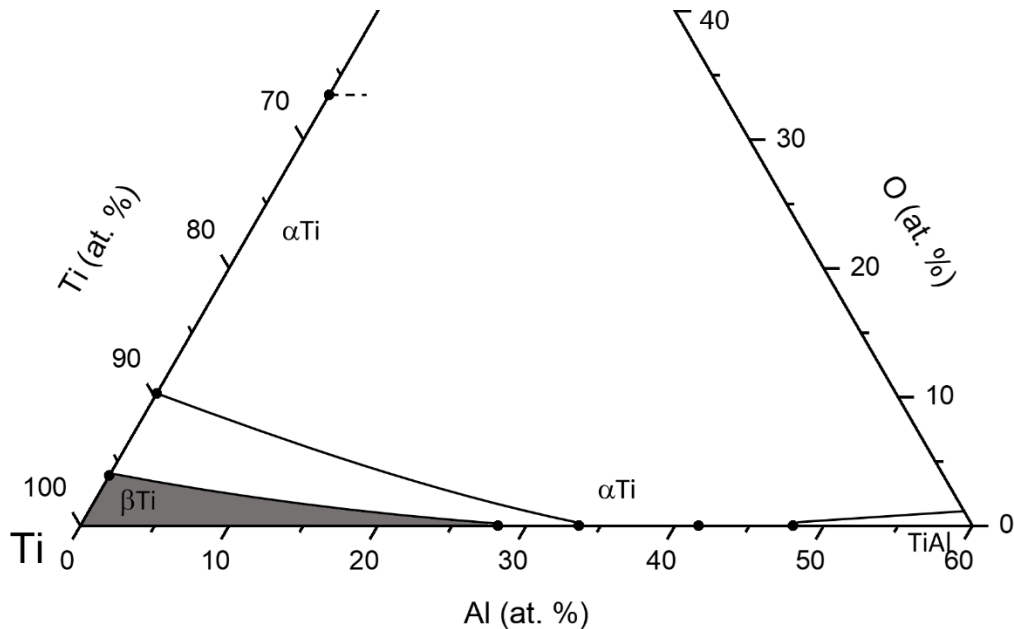
Figure 5.1. Assessed partial Ti–Al–O isothermal section at 1200 °C based on the results from Schofield and Bacon [222].

Figure 5.2 shows the isothermal section at 1100°C. The isotherm is based on experimental data mainly from [233] with additional data from [31, 221, 222, 231, 243] and adjusted to fit to the accepted binaries. The Ti/Al$_2$O$_3$ diffusion couples discussed in [232] are apparently the same as in [233]. Phase equilibria with TiAl$_2$, Al-rich TiAl (= TiAl 1d-APS), and TiAl$_3$ have not been determined and are tentatively shown by dashed lines. In the oxygen-rich part, phase equilibria are taken from the calculated isotherm [240], except of phase equilibria of the Magneli phases and Al$_2$O$_3$, which are not shown in detail for the sake of clarity. The qualitative results of Ti/Al$_2$O$_3$ [279] and TiAl/Al$_2$O$_3$ [230] diffusion couples annealed at 1100°C, which have not been quantified, are in agreement with the phase equilibria shown in **Figure 5.2**. Data from alloys of fixed compositions along Ti–Al$_2$O$_3$ [227, 228] annealed at 1100°C have not been considered herein as the width of the αTi and βTi single-phase fields has been underestimated and the phase Ti$_3$Al has not been taken into account in [227, 228].
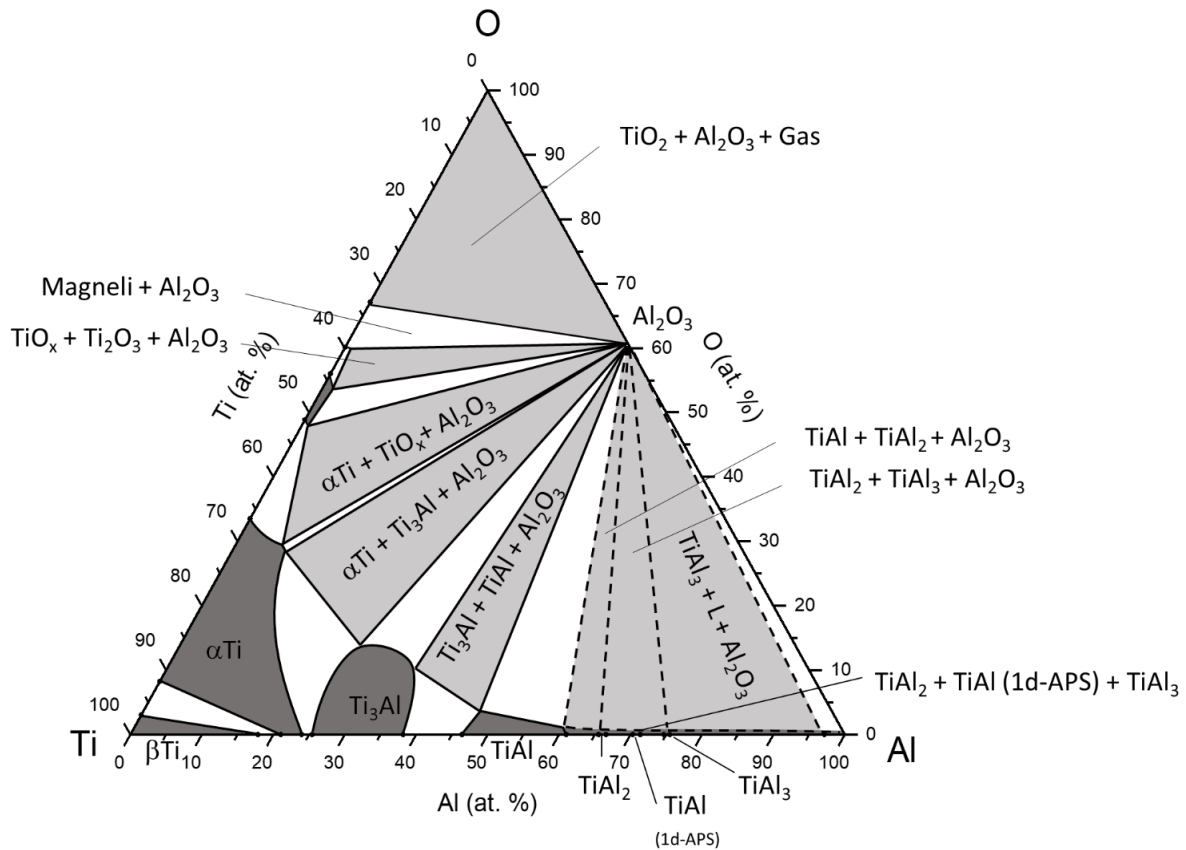
Figure 5.2. Assessed Ti–Al–O isothermal section at 1100 °C mainly based on [233].

Figure 5.3 shows the isothermal section at 1000°C, based on experimental results [31, 221, 222, 226, 231, 263, 268, 280] and complemented by calculated data in the oxygen- and aluminum-rich parts [240]. Data from [227, 228] are again not considered as αTi is shifted to much higher Al and O contents compared to all other data. Many of the experimental data for the partial isothermal section from [226] match the one shown in **Figure 5.3**, but the phase boundaries in [226] are quite different from those in **Figure 5.3**. Reasons for that are that the Ti–Al system employed in [226] is quite different from the one accepted here, with much smaller homogeneity ranges for βTi and Ti$_3$Al. Also, the solid solubility of oxygen in Ti$_3$Al has been underestimated due to lack of respective data and the composition of αTi at the three-phase equilibrium αTi + Ti$_3$Al + Al$_2$O$_3$ is positioned at much lower O and Al contents in [226]. Compared to the partial isothermal section shown in [263], the current section does not include Ti$_3$Al$_{0.9}$O$_{1.1}$ (Al$_3$Ti$_5$O$_2$), which is a metastable phase (**cf. 5.1.3. Solid Phases**).
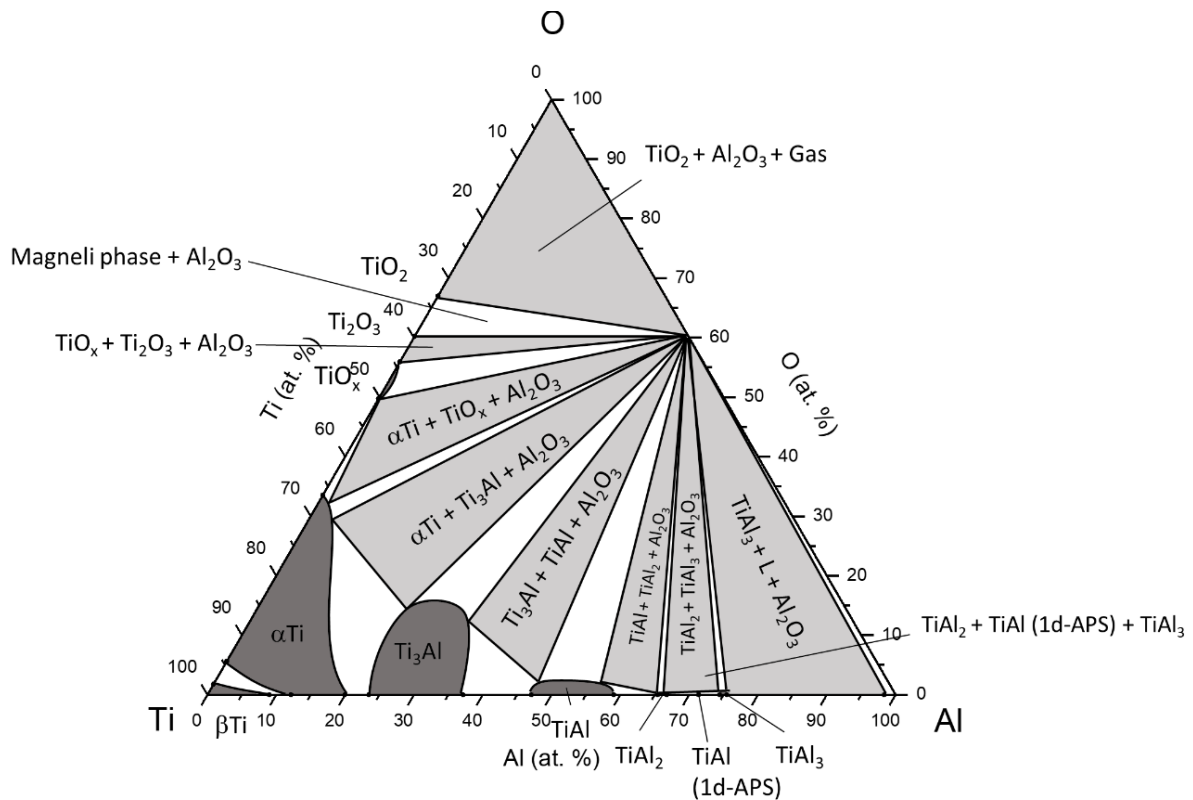
Figure 5.3. Assessed Ti–Al–O isothermal section at 1000 °C.

Figure 5.4 shows the isothermal section at 945°C [235] with αTi + βTi adjusted to fit with the accepted binaries and to experimental values from [220, 222] determined at 950°C. The extension of the Ti$_3$Al single-phase field has been broadened in accordance to that observed at higher temperatures. It is also noted that [235] observed the phase equilibrium αTi + Ti$_3$O$_2$ + Al$_2$O$_3$ at 945°C though Ti$_3$O$_2$ becomes only stable below 920°C according to the accepted binary. αTiO is also included in the isotherm for 945°C in [235], which becomes only stable below 939°C according to the accepted binary [238]. Phase equilibria shown by dashed lines in **Figure 5.4** have not been determined and have been added tentatively.
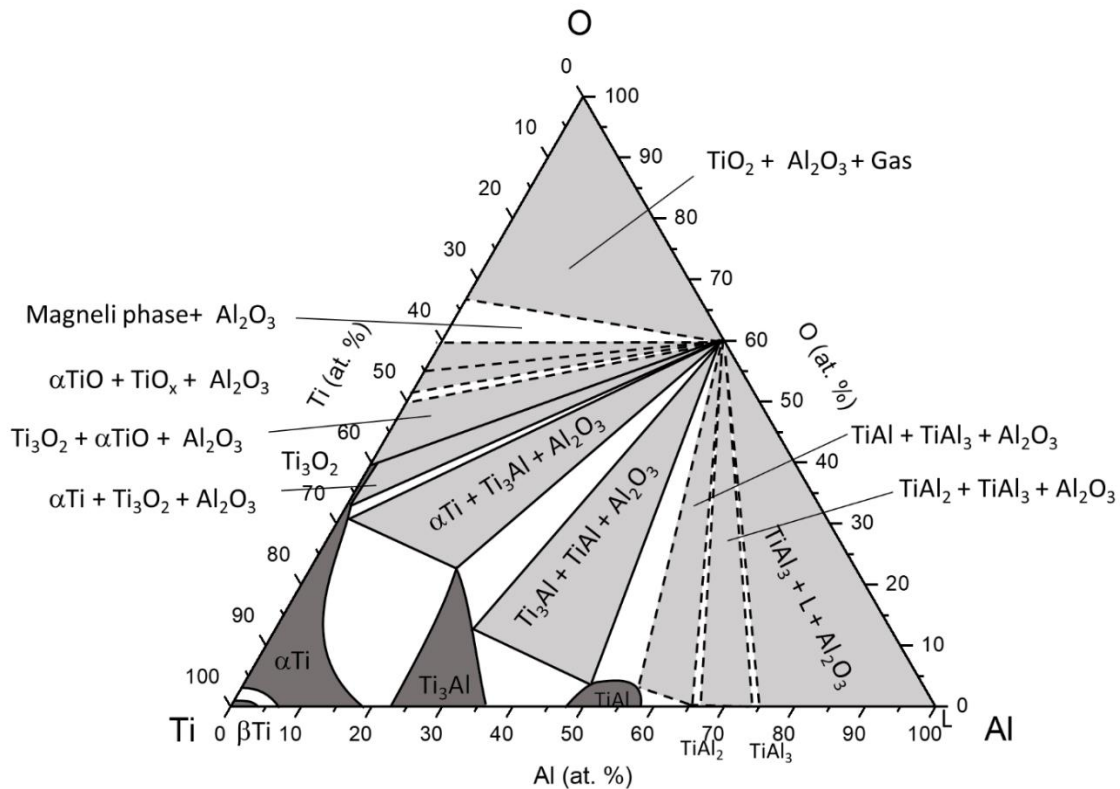
Figure 5.4. Assessed Ti–Al–O isothermal section at 945 °C.

There has been quite a number of investigations focusing on temperatures around 900°C. [271] calculated an isothermal section for 923°C, which shows the phase equilibrium αTi + TiAl₂ + Al₂O₃ in the central part of the system. However, diffusion couple studies showed that instead of this equilibrium the phase equilibria Ti₃Al + Al₂O₃ and TiAl + Al₂O₃ are observed at 920° C [234] and 900°C [229], which are also present at higher temperatures and therefore multi-phase equilibria in the calculated isothermal section for 923°C differ quite prominently from the actual observed ones. A calculated isothermal section at 920°C and 900 °C is presented in [234], and [240] respectively. The results of a Ti₃Al/Al₂O₃ diffusion couple annealed at 900°C for 100 h [229] were not quantified, but the observed sequence of the phases is in agreement with phase equilibria shown in [240]. Other isothermal sections calculated at 900°C [267, 281] included the "X phase" (Al₃Ti₅O₂), which is a metastable phase (**cf. 5.1.3. Solid Phases**). Also, a "simplified" isothermal section, i.e. not showing the homogeneity ranges of the phases, has been calculated for 900°C [282], which is in qualitative agreement with [240]. Another "simplified" isothermal section for 900°C deduced from oxidized samples was presented in [283], which, besides not showing homogeneity ranges, omits the phases αTi and TiAl₂ and

which shows the presence of the three-phase equilibrium TiO + Ti$_3$Al + TiAl, which has not been observed elsewhere at this temperature.

From Ti/Al$_2$O$_3$ diffusion couples annealed for various times up to 940 h and 9 alloys of fixed composition annealed up to 1680 h [284] established two possible versions for an isothermal section at 871°C. Both versions show the equilibrium TiAl + Al$_2$O$_3$ + Ti$_2$O$_3$. They differ in that it is not clear from the experiments whether TiAl is also in equilibrium with TiO at this temperature. In both versions, Ti$_3$Al is in equilibrium with TiO and αTi. Though both versions indicate the solid solubility of oxygen in the Ti–Al phases, this has not been determined. As the phase Ti$_3$O$_2$ has not been considered, actual phase equilibria are doubtful. However, results presented in [284] indicate that below 900°C there is a substantial change in the phase equilibria, in that TiAl and Ti$_3$Al are now in equilibrium with the Ti-oxides, while they are in equilibrium with Al$_2$O$_3$ at 900°C.

Glazova [226] determined a partial isothermal section at 800°C of the Ti corner up to 32 at.% Al and 32 at.% O. Because the isothermal section shows the phases "Ti$_6$Al", "Ti$_6$O" and "Ti$_3$O" within the extended homogeneity range of αTi and respective multi-phase equilibria, though none of these phases exists, this section is not considered. Luthra [285] calculated a complete isotherm for 800°C. In this calculation the phases TiAl$_2$, Ti$_3$O$_2$ and TiO$_x$ were not considered as well as any solid solubility ranges in the binary phases for the third component. The calculated isotherm shows the three-phase equilibrium TiAl + TiO + Al$_2$O$_3$ in the central part of the diagram. In view of the results by [284] at 871°C, this may be possible. Therefore, the experimental results presented in [226-228], which show αTi in equilibrium with Al$_2$O$_3$ at 800°C, and which have also been considered as doubtful for other reasons, are questionable.

Finally, at lower temperatures only the slope of the αTi/αTi + Ti$_3$Al phase boundary has been investigated at 600°C [195, 225] and no phase equilibria below 900°C have been settled by now.

It is worth noting that the complementary figures from above-mentioned references are included in the original manuscript [215].

5.1.5. Comparison between assessed and previously calculated isotherms

TCT1 [34] was the state-of-the-art TCSAB database that was newly developed (October 2017) at the time of the ADVANCE project proposal [33]. Comparing the assessed isothermal

sections with the ones calculated using the TCT1 database reveals substantial discrepancies between them. Even at 1100 °C, the temperature for which the most experimental data exist, the calculated isothermal section does not match the assessed one (**Figure 5.5**) due to the following discrepancies:

- The Al-rich phase boundaries of αTi and Ti$_3$Al are at substantially lower Al contents according to the calculations (**Figure 5.5**).

- According to the assessed isothermal section, complete solid solubility between αTi in the Ti–Al and Ti–O system exists at least between 945-1200 °C (**Figures 5.1 – 5.4**). The calculations predict that with the addition of oxygen, the homogeneity range of αTi will be interrupted by the formation of βTi + Ti$_3$Al near to the Ti–Al system (**Figure 5.5**). This is not supported by any experimental investigation and that αTi becomes unstable by adding less than 1 at. % O and then becomes stable again when it contains about 2 or more at. % O is thermodynamically unlikely.

- The phase Ti$_3$AlO, which is shown in the calculated isothermal section as a dot, i.e. stable only at its stoichiometric composition, is not detected in any of the experimental investigations.

Apart from these discrepancies the calculation shows some violations of thermodynamic rules, which apply to the drawing of phase diagrams [36].

- The Al-lean phase boundary of Ti$_3$Al terminates at around 30 at. % Al and 6 at. % O. CALPHAD predicts the phase boundaries of a ternary system based on the extrapolation of underlying binary systems; in other words, the phase boundaries stem from the established binaries and continue into the ternary system. The current drawing of the Ti$_3$Al phase field requires that the inclination of the Ti$_3$Al + TiAl tie-lines cannot consistently continue towards the binary Ti–Al system, which then would violate the Kornovalov rule. Therefore, the Ti$_3$Al phase boundary has remained unfinished.

- The S-curvature adopted for the Ti-rich phase boundary of Ti$_3$Al between the binary system and the first tie-triangle of βTi + αTi + Ti$_3$Al is thermodynamically unlikely.

- That Ti$_3$AlO is only represented by a dot implies that there is no two-phase field in between the two three-phase fields of αTi + Ti$_3$Al + Ti$_3$AlO and Al$_2$O$_3$ + Ti$_3$Al + Ti$_3$AlO (violation of Gibb´s phase rule) and a violation of Schreinemakers' rule, because the metastable extension of the Al-rich phase boundary of Ti$_3$Al extends into the three-phase field Al$_2$O$_3$ + Ti$_3$Al + Ti$_3$AlO, while the metastable extension of the

Ti-rich phase boundary extends into the two-phase field Al_2O_3 + Ti_3Al. According to Schreinemakers' rule, the metastable extensions of a single-phase field have to extend into phase fields of the same order, i.e. either both into the three-phase field or into the adjacent two-phase fields.

The discrepancies can be resolved if more reliable experimental data of the ternary system are available to adjust/optimize the phase fields. The main difficulty in this system, as was mentioned earlier, is measuring the oxygen content in the Ti–Al-rich phases to determine the compositions of the coexisting phases. The next chapter is dedicated to new experimental results in the Ti–Al–O system at 1100 °C to attain a better understanding of phase equilibria at this temperature and to discuss the attempts to measure the oxygen content in Ti–Al-rich phases.
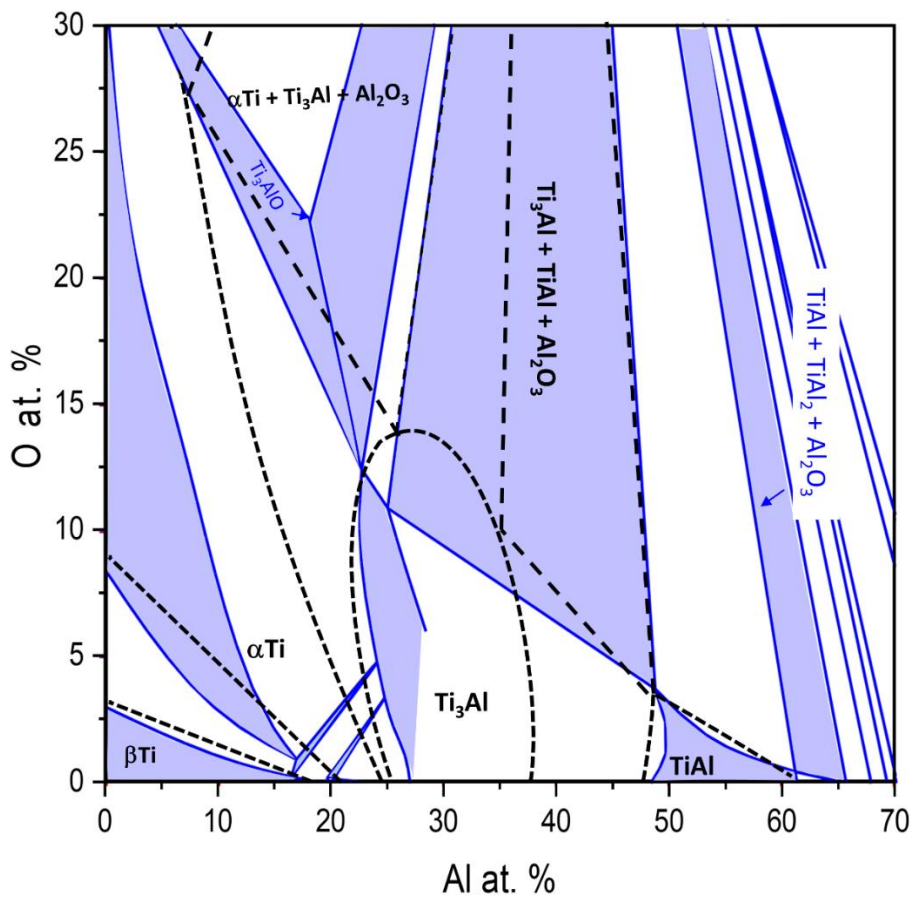
Figure 5.5. Partial Ti–Al–O isothermal section at 1100 °C; the re-drawn isotherm, calculated with the TCT1 database [34] before the start of the ADVANCE project in October 2017 (in blue; courtesy of Thermo-Calc Software AB) is compared with the phase boundaries assessed in **section 5.1.4** and **Figure 5.2** (dashed black lines).

5.2. Experimental investigations of the Ti–Al–O system

In the previous chapter, the need for new reliable experimental data has been shown. In the following, the experimental results on five alloys heat treated at 1100 °C (**see Table 2-1**) are discussed. Utilizing SEM, EPMA, XRD, DTA and APT, attempts have been made to characterize and to measure the chemical composition of the coexisting phases in the annealed alloys. Samples from these alloys were also investigated by XRD and partially by EPMA after annealing at 900 & 1000 °C; however, results are not reported here.

5.2.1. SEM and XRD investigations

Figure 5.6. shows the microstructures of the alloys after annealing at 1100 °C/200 h. Generally, the microstructures even after 200 hours at such high temperature are relatively fine-scaled, however, the coexisting phases are coarse enough for EPMA analysis. XRD analyses of the alloys heat treated at 1100 °C/200 h are presented in **Table 5.2.**

The SEM/BSE images of O3 and O4 show a duplex microstructure consisting of $Ti_3Al + TiAl$, partially showing a coarse, needle-like microstructure. Additionally, few oxides with black contrast are discernible in the SEM-BSE micrographs of O3 and O4. From XRD analyses of these two samples, it is apparent that the oxide phase is Al_2O_3. The XRD of alloy O3 shows the presence of four phases, which indicates that even after 1100 °C/200 h equilibrium has not been attained. $Al_3Ti_5O_2$ was found by XRD (**Figure 5.7**), however, lattice parameters could not be calculated from the few detected peaks. It is due to its low phase fraction that it is also not observed in the microstructure (**Figure 5.6a**). In **section 5.1.3**, it was concluded that $Al_3Ti_5O_2$ may actually not be a ternary phase but that it is stabilized by nitrogen.

Al_2O_3 appears in isolated regions in O4 (**Figure 5.6b**) surrounded with Ti_3Al, and it is not in contact with TiAl. This suggests that Al_2O_3 is not in equilibrium. Al_2O_3 probably formed in the melt, followed by the formation of αTi/or βTi which then transformed to Ti_3Al.

O5-O8 (**Figures 5.6 (c-e)**) display two-phase microstructures. XRD analyses show that the phases are αTi + Ti_3Al, which vary from fine-scaled lamellar structure in O5 to coarse grains in O6 and O8. The αTi grains in O6 and O8 show some disintegration, though no respective signals were observed in the DTA analyses of O6 and O8 (**see section 5.2.5**).
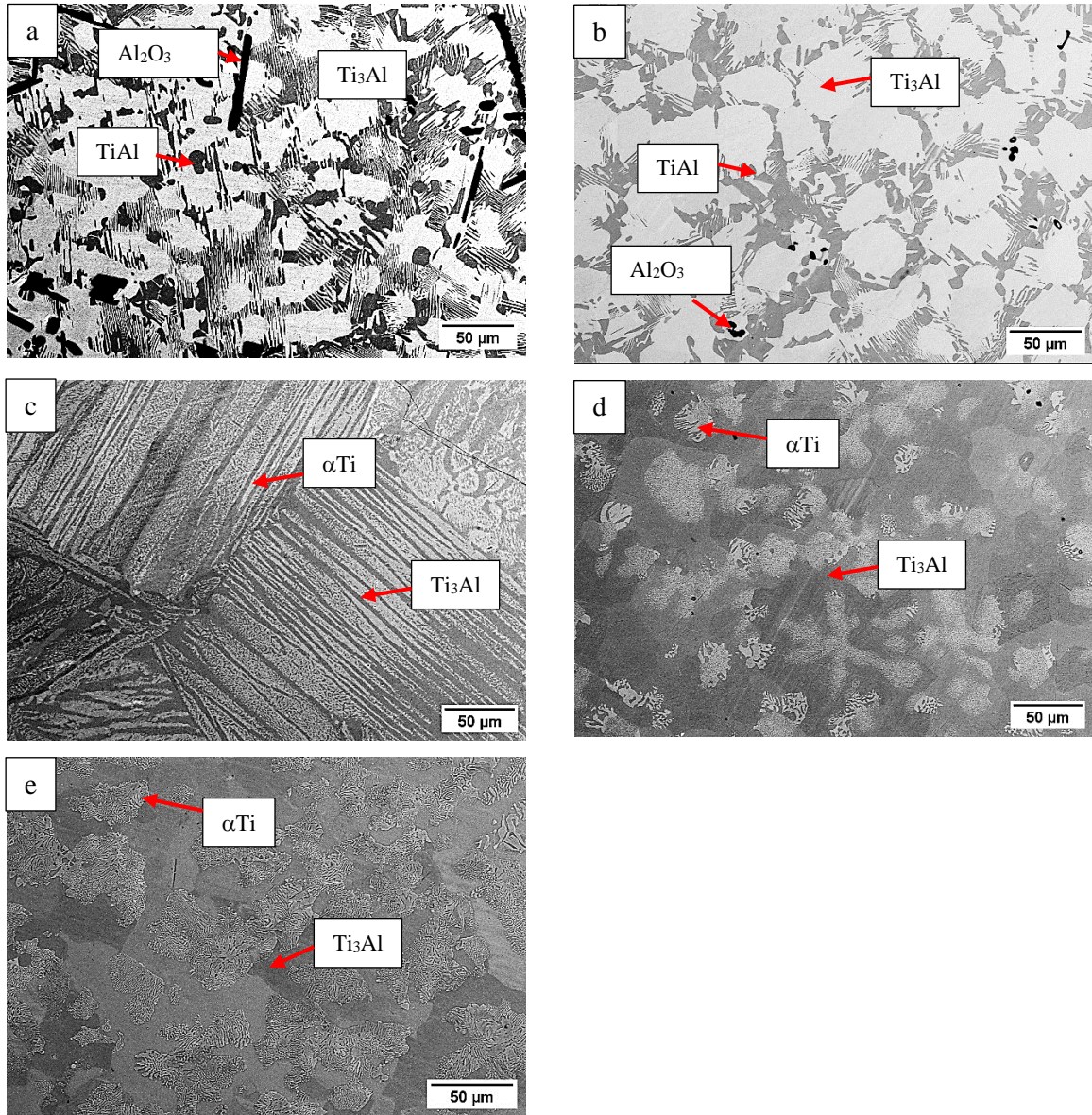
Figure 5.6. BSE micrographs of alloys heat-treated at 1100 °C/ 200 h

a) O3. Ti-42.5Al-12.5O at. %, b) O4: Ti-38.8 Al-5.5 O at. %,

c) O5: Ti-20Al-5O at. %, d) O6: Ti-20Al-10 at. %,

e) O8: Ti-17.5Al-15O at. %.

Table 5.2. Phases in the Ti–Al–O alloys quenched from 1100 °C and their lattice constants and lattice volume (in nm) as determined by XRD compared to the expected phases according to the assessment (**section 5.1.4**); n.d. not determined

Alloy	Phase	Lattice Constants (nm)		Lattice volume (nm³)	Expected at 1100°C
		a_0	c_0		
O3	Ti_3Al	0.57738(2)	0.46526(2)	0.13430	$Ti_3Al + TiAl$
	$TiAl$	0.39952(3)	0.40409(3)	0.06524	
	$Ti_5Al_3O_2$	n.d.		-	
	Al_2O_3	0.47637(5)	1.2993(3)	0.25535	
O4	Ti_3Al	0.57724(2)	0.46540(2)	0.13430	$Ti_3Al + TiAl$
	$TiAl$	0.39945(3)	0.40377(3)	0.06512	
	Al_2O_3	n.d.		-	
O5	αTi	0.29024(1)	0.46772(2)	0.03412	$\alpha Ti\ (+\ Ti_3Al)$
	Ti_3Al	0.58056(2)	0.46737(2)	0.13642	
O6	αTi	0.290148(6)	0.46958(1)	0.03424	$\alpha Ti + Ti_3Al$
	Ti_3Al	0.58001(2)	0.46936 (2)	0.13674	
O8	αTi	0.295583(8)	0.47760(2)	0.03614	$\alpha Ti + Ti_3Al$
	Ti_3Al	0.57962 (1)	0.47037(1)	0.13685	
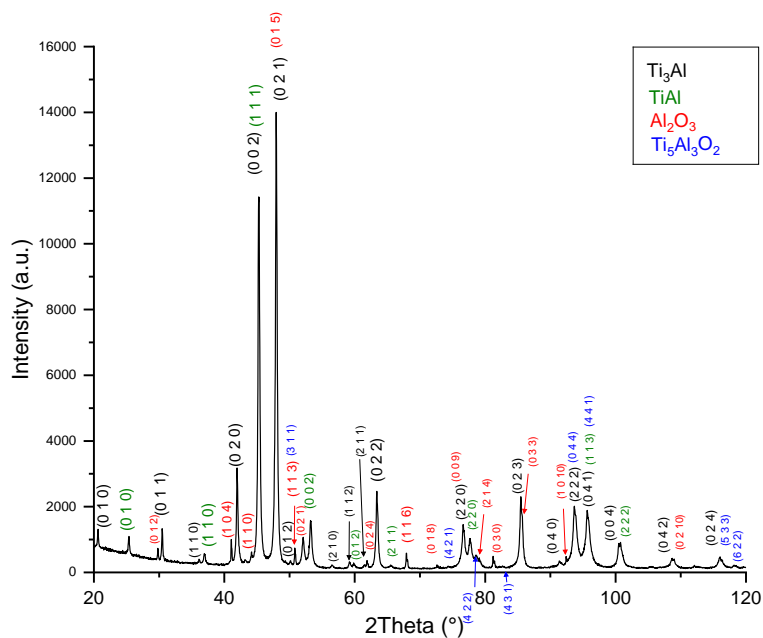
Figure 5.7. XRD analysis of O3. Ti-42.5Al-12.5O at. % heat treated at 1100 °C/200 h.

5.2.2. EPMA analysis of oxygen

As for all the other ternary systems, coexisting phases were to be measured by EPMA. However, EPMA analysis of light elements such as oxygen requires special attention, for instance, light elements have a lower fluorescence yield than heavier elements, resulting in less X-rays being produced (<0.7 keV [286]) in favor of Auger electrons, which makes it troublesome to reach high count rates [219]. This is more challenging when measuring light elements in a compound containing light and heavy elements. Because the count rates of light elements are low, high currents (nA) are employed for measuring the light element. If this high current is used with a pure element standard, the pulse-height analyzer (PHA) can be dramatically reduced by several volts, a phenomenon known as "pulse height depression", therefore, counts can be missed out, and then the quantification will be inaccurate. Also, due to different chemical bonding in the sample and standard, positions of the Kα peak could differ between standard and sample, and if this peak shift is not considered, this again leads to inaccurate analyses [219].

In order to avoid the errors detailed above, the chemical composition of both standard and sample should be as similar as possible [218, 219]. The EPMA analyses of oxygen in the Ti–Al–O alloys have been performed using the oxide standards MgO and ThO$_2$. However, the analyses always gave too high oxygen contents, which could be related to above-mentioned issues. Therefore, new samples were prepared by Dr. Benedikt Distl by oxidizing Ti-30 at. % Al for 1, 4 and 8 hours in air at 1000 °C. The intention was multilateral; these samples contain oxygen only in solid solution, like in the matrix of the samples and therefore no peak shift for O Kα should be present and the oxygen content is closer to that of the phases in the equilibrated samples. Additionally, the oxygen content in these three samples is determined by wet-chemical analysis to establish a calibration curve of the oxygen content vs. emitted X-rays in counts per second (cps) to optimize the EPMA measurements.

Utilizing SEM/BSE it was confirmed that all three samples were still single-phase Ti$_3$Al after oxidation at 1000 °C. Intensities of the elements Ti, Al and O were measured using EPMA/WDS with line scans of about 1500 µm length to ensure that the elements are homogenously distributed. The actual oxygen contents of standards were measured by wet-chemical analysis using NCS Fusion Master ONH and the results are shown in **Table 5.3.** The results show that all three oxidized Ti-30 at. % Al samples have about the same oxygen content of 0.1-0.2 at.%. Therefore, they were not useful to establish a calibration curve.

In a second step, Ti-30 at. % Al and other samples with known oxygen contents have been analyzed using the oxide standards MgO and ThO_2. The results of a number of measurements are presented in **Table 5.4.**

Table 5.3. Oxygen contents as determined by wet-chemical analysis in Ti-30 at. % Al after oxidizing for various times at 1000 °C

Sample	O at. %
Ti-30Al- 1h	0.22
Ti-30Al- 4h	0.12
Ti-30Al- 8h	0.14

Table 5.4. Samples measured with MgO and ThO_2 standard

Sample	Ti (at. %)	Al (at. %)	O (at. %)	Nb (at. %)	Fe (at. %)	Used standard
Ti-30Al (1h)	64.00 ± 1.8	30.00 ± 1.2	**6.0 ± 0.5**			ThO_2 (V=10 kV)
Ti-30Al (1h)	62.4	28.8	**8.8**			ThO_2 (V=15 kV)
Ti-30Al (1h)	65.4 ± 0.6	29.2 ± 1.2	**5.4 ± 0.8**			MgO (V= 15 kV)
TiAlNb[1]	45.9 ± 0.6	24.8 ± 0.5	**6.1 ± 0.7**	23.2 ± 0.1		MgO (V= 15 kV)
FeAlNb [2]	-	26.9 ± 0.2	**0.5 ± 0.1**	1.8 ± 0.4	70.9 ± 0.4	MgO (V= 15 kV)
Ti-30Al as-cast	65.7 ± 0.3	30.3 ± 0.1	**3.9 ± 0.2**			MgO (V= 15 kV)

(1)   Sample is provided by courtesy of Dr. Benedikt Distl.

(2)   Sample is provided by courtesy of Angelika Gedsun.

All measurements on Ti-30 at. % Al utilizing different standards yield at least one order of magnitude higher oxygen contents than measured by wet-chemical analysis. Investigating various samples shows that the problem persists in all the samples containing Ti as the major element.

It has been reported that on reactive metals, such as Zr and Ti a native oxide skin (of 4-10 nm) develops on the surface [286]. On the other hand, due to the large mass absorption coefficient (mac) of O Kα, common EPMA analysis of oxygen is limited mainly to the surface of the sample [287]. Correspondingly, the high oxygen content comes from this superficial oxide skin.

In order to prevent the samples from forming an oxide layer, Ar ion cleaning was done by employing a plasma cleaner (as explained in **chapter 2**). This technique was also implemented to remove hydrocarbon contamination and oxide layers on APT specimens and proved to be successful [288]. However, even after Ar ion cleaning prior to the measurements, almost the same results were achieved.

5.2.3. Oxygen analysis by APT

Because EPMA was not successful, APT was utilized as it provides a high lateral resolution and has been used to analyze oxygen [289]. Furthermore, APT operates at high vacuum and therefore no passive layer can form on the sputtered surface. APT was performed on one sample to evaluate the feasibility of the technique in determining the phase equilibria in the Ti–Al–O system. O4: Ti-38.8 Al-5.5 O (at. %) heat treated at 1100 °C/200 h, has been selected, which shows a two-phase microstructure (**Figure 5.8**). Two needle-like specimens of about 200 nm length were cut out by FIB, containing single-phase Ti_3Al and TiAl and were measured with APT. **Figure 5.9.** shows the reconstruction of the APT analysis of single-phase Ti_3Al, providing the distribution of oxygen in the sample. Analyzed compositions are presented in **Table 5.5.**
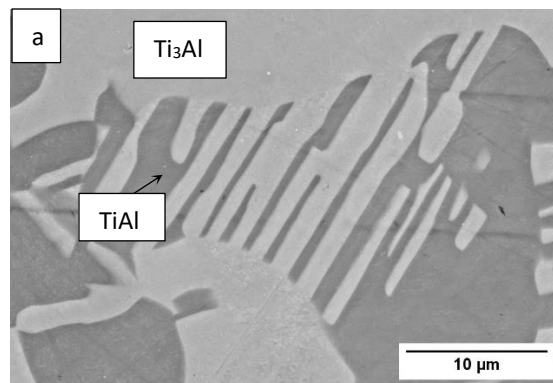
Figure 5.8. Micrograph (BSE contrast) of the sample O4: Ti-38.8 Al-5.5 O (at. %) heat treated at 1100 °C/ 200 h.
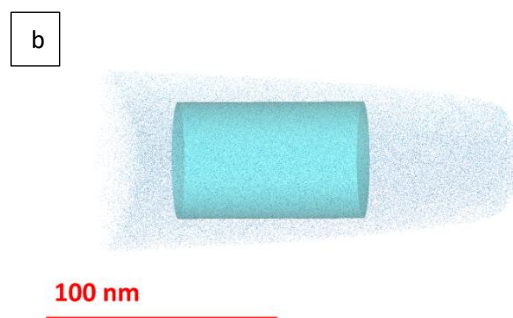
Figure 5.9. APT reconstruction showing the distribution of oxygen in Ti_3Al. The blue cylinder indicates the area, in which chemical composition is analyzed.

Table 5.5. Compositions of coexisting phases established by APT

Phase	Ti (at. %)	Al (at. %)	O (at. %)	N (at. %)
TiAl	50.1 ± 0.01	49.7 ± 0.01	0.167 ± 0.001	-
Ti_3Al	59.9 ± 0.02	34.2 ± 0.02	5.8 ± 0.007	0.123

The results, showed that APT can be used to precisely measure oxygen in Ti-based alloys. In the absence of oxide layer, the oxygen solid solubility between Ti_3Al and TiAl can be distinguished; as expected the oxygen solid solubility in the Ti_3Al is one order of magnitude higher than in ordered TiAl [31]. However, APT sample preparation is time-consuming and measurements of many samples were not foreseen within the ADVANCE project budget and therefore, no further APT measurements were performed.

5.2.4. Comparison with oxygen measurements in Ti–Al alloys by other groups

Goldstein et al. [286] were aware of the formation of a passive oxide layer on Ti-rich samples and therefore utilized a similar approach as in here (**section 5.2.2**) to measure the oxygen content in Ti–Si–O compounds e.g., αTi, βTi and Ti_5Si_3. They measured the Kα ratio of O in a so-called oxygen-free sample and in Fe_2O_3 as standard. Assuming that the oxygen in the so-called oxygen-free sample comes only from the passive oxide layer, they associated the measured oxygen with the oxide layer and subtracted this value when measuring oxygen in other samples. They measured an amount of about 3.4 at. % O in the oxygen-free samples (**Table 5.6**), which is similar to 3.9 at. % measured here for Ti-30 at.% Al in as-cast state (oxygen-free). However, even subtracting this value from our measurements, still yields significantly higher amounts of oxygen.

Table 5.6. Compounds measured by Goldstein et al. [286] using Fe_2O_3 standard

Compound	Measured oxygen content (at. %)	Actual oxygen content (at. %)	Used standard
Ti_3Si	3.7	0	Fe_2O_3 (V=10 kV)
Ti_5Si_3	3.4	0	
Ti_5Si_4	3.2	0	
TiSi	3.3	0	

Very recently, Nakashima et al. [216, 290] used an EPMA equipped with an additional soft X-ray emission spectrometer (SXES). SXES utilizes a variable space grating that allows the

efficient and parallel collection of very low energy-rays, so called "soft" X-rays, thereby providing a high energy resolution of 60-2400 eV. They optimized the analysis condition by measuring the oxygen Kα peak intensities for various probe currents, acceleration voltages, and dwell times for samples with known oxygen contents. Using the optimized conditions, they measured the chemical composition of coexisting phases in Ti-43Al-xO and Ti-48Al-xO (x = 0.1, 0.4, 0.6, 1.0) at. % annealed at 1100 and 1200 °C. Prior to all measurements, sample surfaces were cleaned by the Ar plasma cleaner in the sample exchange chamber. Though apparently quite a number of samples were prepared, only for two alloys heat treated at 1100 °C/2880 h compositions of coexisting phases were presented [216] (**Table 5.7**). Measured oxygen contents are in good agreement with results established here by APT (**Table 5.5**).

Table 5.7. Analyzed data for alloys heat-treated at 1100 °C/2880h using SXES by [216]

	Phase	**Ti (at. %)**	**Al (at. %)**	**O (at. %)**
Alloy 1		56.5	42.5	1
	TiAl	50	49.7	**0.25**
	αTi	61.2	36.7	2
Alloy 2		51.7	47.2	1
	TiAl	53	46.7	**0.25**
	Ti$_3$Al	57.7	36.2	**6**

Li et al. [233] (from the same research group as Goldstein et al. [286]) used EPMA for Ti and Al and created a calibration curve of the lattice expansion due to increasing oxygen contents in solid solution in αTi and Ti$_3$Al. Alloys were prepared by powder metallurgy and arc-melting and heat treated at 800-1000 °C. In their EPMA measurements they employed a thin-film program to compensate the effects caused by the passive oxide skin. In this method, the K-ratios (the ratio between the net X-ray intensities obtained from sample and standard) are determined at various accelerating voltages and then compared with theoretical K-ratios obtained from the $\phi(\rho z)$ model [219], in which the thickness and/or the composition of the layer or substrate are the unknowns. The unknown thicknesses and composition are calculated by repetitive iterations of those values until the theoretical and experimental K-ratios are closely matched [291]. This analysis needs a dedicated program, which mostly are not open source and our EPMA lab does not have it.

Using their XRD data and additional data from literature and assuming that the interstitially dissolved oxygen and the substitutionally dissolved Al do not influence their individual effect on the cell volume, Li et al. [233] constructed a set of calibration curves for the volume of the unit cell of αTi and Ti₃Al in dependence on the amount of oxygen or aluminum (**Figure 5.10**). This plot can be used to estimate the approximate oxygen content if unit cell volume and Al content are known. For O4 with an Al content of 34.2 at. % Al and taking the unit cell volume from **Table 5.2** an oxygen content of about 7 at. % is obtained from **Figure 5.10** and the APT measurement gave a somewhat lower content of 5.8 at. % O. For samples O5-O8 the precise Al content in Ti₃Al is not known. However, **Figure 5.2** shows that the Ti-rich phase boundary of Ti₃Al runs at a more or less constant Al content of about 24.0 at. % Al at 1100 °C. Plotting the cell volumes of O5-O8 in **Figure 5.10** reveals that the sequence is correct. The oxygen content in Ti₃Al increases from O6 to O8 in accordance with increasing oxygen content of these three alloys. However, the actual oxygen contents read from the plot (O5: ~ 6; O6: ~7.5; O8: ~ 9 at. % O) seem to be reasonable, at least in case of O5 and O6. However, the overall compositions of the alloys suggest that the difference in the oxygen contents in Ti₃Al should actually be higher and αTi + Ti₃Al tie-lines, starting at compositions taken from **Figure 5.11** and which must pass the overall composition of the respective alloy, would have to be rather steep. It is therefore inferred, that oxygen contents evaluated from **Figure 5.10** are somewhat too low.
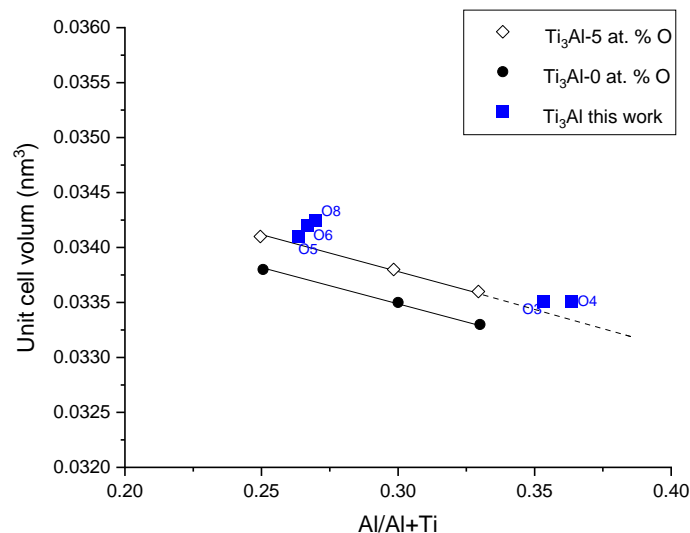
Figure 5.10. Calculated volumes of the hexagonal cell of Ti₃Al in dependence on composition from [233] with data from present work in color (note that for Ti₃Al the volume is unit cell volume/4 as data in [233] are shown for the unit cell volume of αTi).

5.2.5. DTA analyses

Table 5.8. summarizes the results of the DTA analyses. The DTA investigations of alloys O3, O4, O6, and O8 heat treated at 1100 °C show no signal up to about 1200 °C. This is in full agreement with the assessed isothermal sections between 945-1100 °C (**Figure 5.2-4**), according to which no reaction is expected for these alloys within this temperature range. The signals observed in O4 and O5 cannot be allocated straight forward to certain reactions because they occur at temperatures above those studied here.

Table 5.8. DTA results; reactions are shown and listed with decreasing temperature; strength of the peaks is indicated by ss (very strong), s (strong), and w (weak)

Alloy	Al (at. %)	O (at. %)	Heated to °C	Onset (°C); strength of the peak	Reaction
O3	37.2	7.3	1300	No peak	
O4	38.8	5.5	1400	1316, s	αTi $\leftrightarrow$ αTi + TiAl (?)
O5	19.5	5.5	1400	1203, s	βTi + αTi $\leftrightarrow$ Ti$_3$Al (?)
				1178, w	αTi $\leftrightarrow$ Ti$_3$Al + αTi (?)
O6	19.2	11.6	1400	No peak	
O8	16.4	17.8	1400	No peak	

5.2.6. Summary of the results obtained at 1100°C

The combined results of APT and XRD are compared with the assessed Ti–Al–O isothermal section at 1100 °C in **Figure 5.11a** and together with analyzed compositions by SXES [216] in **Figure 5.11b**. Both APT and SXES yield similar oxygen values of about 0.2 at. % in TiAl. It is notable that the oxygen content in TiAl is about one order of magnitude lower than what was expected from the assessed literature (about 4 at. %). Also, the phase boundary of Ti$_3$Al on the Al-rich side should be revised. It should be shifted to lower Al contents as indicated by the blue dashed lines in **Figure 5.11**. This is also supported by the SXES results on samples annealed at 1100 and 1200 °C [216, 290]. As a consequence, the three-phase field Ti$_3$Al + TiAl + Al$_2$O$_3$ will be considerably broader because the composition of Ti$_3$Al in this equilibrium will shift to lower Al contents while the composition of TiAl is not only at lower O contents but also at higher Al contents as the combined APT and SXES [216, 290] results indicate.

Additionally, the microstructure **Figure 5.6(c)** and quantitative XRD analysis of O5 show that the phase fraction of Ti$_3$Al is larger than expected from the assessed isothermal section

Figure 5.11, according to which O5 should be nearly single-phase αTi at 1100 °C**.** Therefore, it can be expected that also the αTi phase boundary shifts to lower Al contents, compared to the assessed one.

These remarks show that the Ti–Al–O system should be further investigated to generate a better understanding of the phase equilibria at the Ti-rich side of the system, for which only scarce experimental investigations are available. One reason for this are the problems in the analysis by EPMA. However, as APT and possibly also SXES are becoming more available, better opportunities exist to study the phase equilibria in this system in the future.
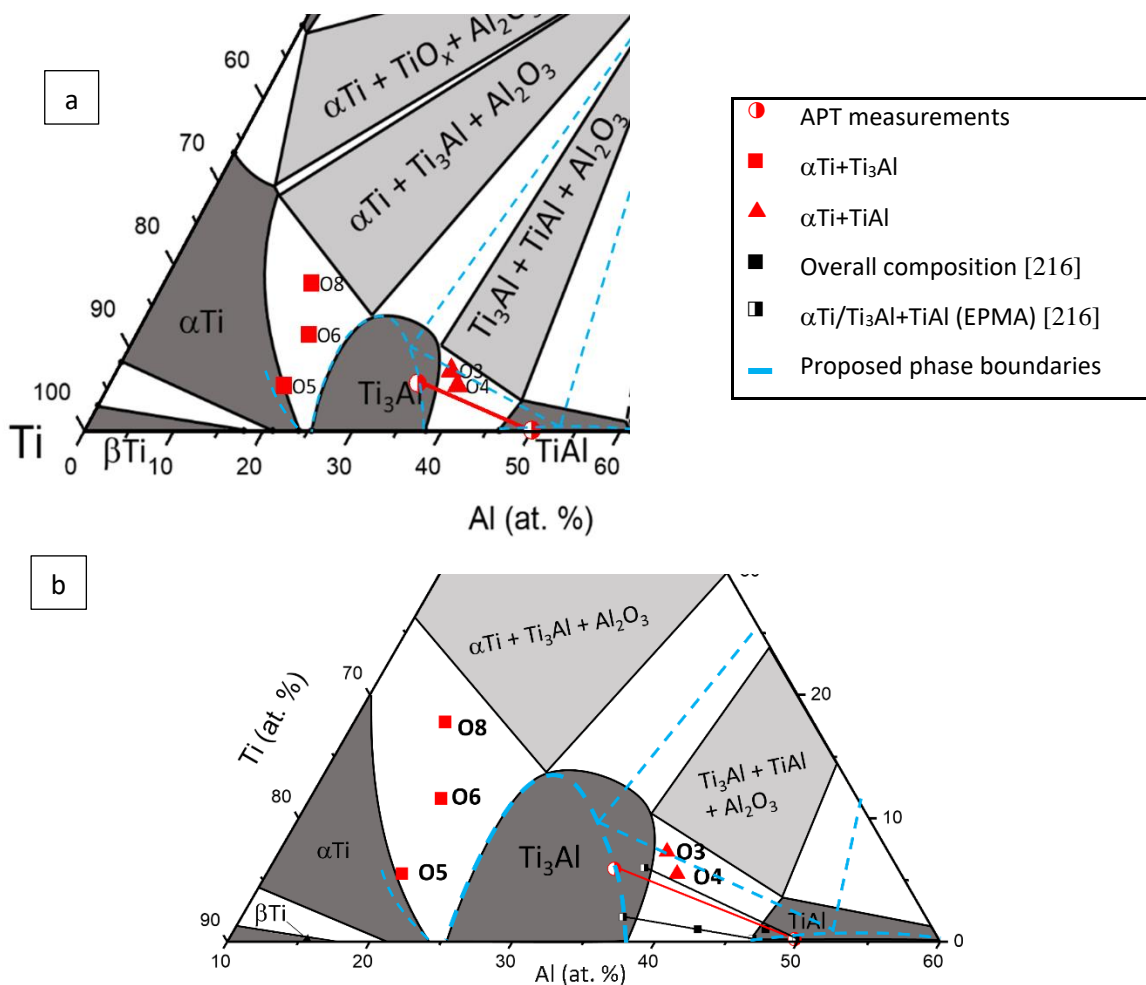
Figure 5.11. a) Partial assessed Ti–Al–O isothermal section at 1100 °C with APT measurements and proposed corrections for the phase boundaries (dashed blue lines) b) Enlarged section of Ti–Al–O system with additional SXES data from [216] .

6. Final conclusion and summary

The current thesis is the outcome of almost four years of investigations to provide a profound understanding of phase equilibria in Ti–Al–X (X= Si, Zr, and O) systems. Demands are growing to significantly reduce aircraft noise, CO_2, and NO_x emissions. Under Clean Sky 2 European joint undertaking, a consortium has been formed between Thermo-Calc Software AB, Max-Planck-Institut für Eisenforschung GmbH, Helmholtz-Zentrum Hereon (formerly known as Helmholtz-Zentrum Geesthacht), and Montanuniversität Leoben; the ADVANCE project was born to serve the research and accelerate the development of TiAl-based alloys to extend their usage in aero engines.

Within the ADVANCE project, the experimental investigations were employed hand-in-hand with the optimisation of CALPHAD database. At the beginning of the project, TCT1 [34] was employed at MTU to develop TNM (Ti–43.5Al–4Nb–1Mo–0.1B at. %) [12] alloys. However, to further develop even more capable alloys, compositions have to be further optimized and new alloying elements will be added. Therefore, it was evident that the CALPHAD database has to be improved to correspond to the new compositions [10].

On the MPIE side, detailed experimental investigations with state-of-the-art equipment have been carried out. Additionally, the team's long-standing experience in the assessment of phase equilibria - also in collaboration with MSIT- allowed for a comprehensive assessment of the literature and existing phase diagrams. The critical assessments and outstanding experimental capabilities at MPIE efficiently led to exploring the inconsistencies and trying to resolve them.

The outcome of the thesis can be summarized as follows:

In the Ti–Al–Si system, isothermal sections between 800-1200 °C from various research groups existed before; however, their results contradict with each other in that data for the solid solubilities of Al in Ti_5Si_3 and for Si in the Ti–Al varies in different investigations. This is partially due to the stability of the microstructure and sluggish diffusion, so that even at very high temperatures reaching equilibrium takes a long time. While this feature essentially makes Si an interesting alloying element, determining the phase equilibria is somewhat challenging. Within this work the following results have been achieved:

➔ It is now clear that the solid solubility of Al in Ti_5Si_3 is about 7 at. % Al at all temperatures. The Si solid solubility in $TiAl_2$ is only about 0.3 at. %, independent of the investigated temperature. The maximum solid solubility of Si in TiAl is about 0.5 at. % Si. The Si solid

solubility in αTi increases from 0.6 at. % at 800 °C to about 1.0 at. % at 1000 °C, while the Si solid solubility in Ti₃Al is about 1.5 at. % at all investigated temperatures.

➔ No ternary phase was found and Ti₃Si was not detected in any of the alloys. In calculated isothermal sections the equilibrium Ti₅Si₃ + αTi is usually interrupted by the formation of Ti₃Si. However, the current investigation shows that at least for alloys with Ti < 81 at. % no phase equilibria with Ti₃Si are observed.

➔ Based on the precise solid solubilities established within this work at five consecutive temperatures at 800-1200 °C, solid solubilities and therefore phase fractions at higher and lower temperatures can be extrapolated by CALPHAD calculations. These data can be implemented to predict processing parameters to achieve the desired microstructure.

In the Ti–Al–Zr system the last assessment of the literature was done in 2004, covering 44 references and the outcome were partial isothermal sections showing equilibria only between βTi, αTi, Ti₃Al and TiAl at 1000-1300 °C. Since then, significant new results have been published. Therefore, a new assessment of the system was necessary. The new assessment covers 98 references and provides two complete assessed isothermal sections at 800 and 1000 °C.

Through the assessment it became clear that the recent CALPHAD modellings show large discrepancies with the available experimental evidence. Especially, data at 1000 °C were questionable. This is due to the general difficulties in establishing phase equilibria in the Ti–Al–(X) system and the high susceptibility of Zr to oxygen. Therefore, it was evident that new experimental data are necessary. Four partial isothermal sections were experimentally determined by means of SEM, EPMA, (HE-)XRD, TEM, and DTA of six alloys heat treated at 1000-1300 °C. The achievements of the experimental investigation on the Ti–Al–Zr system between 1000-1300 °C can be summarized as follows:

➔ The solid solubility of Zr in TiAl is markedly higher than expected. Compared to the assessed data of 8.5 at. % Zr at 1000 °C, the actual solid solubility is about 13.5 at. % at this temperature.

➔ From the assessed isothermal section at 1000 °C, a large solid solubility of more than 30 at. % Ti in Zr₅Al₃ was expected. It became clear that Zr₅Al₃ is stabilized to this extent only by impurities and the Ti solid solubility is far less than what was reported previously.

➔ The Laves phase $ZrAl_2$ is in equilibrium with Ti_3Al, TiAl and with B2-ordered βTi ($β_0$) at 1000 °C. This is an equilibrium that had not been reported before because of the presence of Zr_5Al_3, stabilized by impurities.

➔ That disordered βTi becomes B2-ordered $β_0$ with increasing Zr contents was known before, though previous observations were not consistent with each other. The present investigation shows that $β_0$ is stable within a wider composition range and already exists at 1000 °C and remains stable up to at least 1300 °C.

➔ The c/a ratio of TiAl decreases with increasing Zr content, but does not reach unity. Also, the c/a ratio does not change monotonically by the addition of Zr but also changes in dependence of the Al content.

In the Ti–Al–O system, an assessment of the complete system has been carried out in collaboration with MSIT. The outcome in the Ti–Al-rich side are four partial isothermal sections from 945-1200 °C. However, comparison between the assessed isothermal section with the modelled versions based on the then existing TCSAB (TCT1) database revealed discrepancies among them, showing the need for more reliable experimental data. Five alloys were produced and heat-treated between 800-1100 °C. The oxygen solid solubility in the coexisting phases could not be measured with EPMA, though different approaches were tried out. The instant formation of an oxide skin on the sample surface is the problem, which could be circumvented by measuring with APT. Due to the problem with EPMA, the limited experimental investigations concentrated on alloys heat treated at 1100 °C. With the established results the assessed isothermal section at 1100 °C was partly revised. In that:

➔ The oxygen solid solubility in TiAl is about 0.2 at. %, which is at least one order of magnitude lower than formerly reported values. The current investigation revealed that oxygen analysis by EPMA yields such high contents, caused by the oxide skin on the surface.

➔ The Al-rich phase boundaries of Ti_3Al and αTi should be revised to lower Al contents. As a consequence, the three-phase field Ti_3Al + TiAl + Al_2O_3 will be markedly broader than expected.

The experimental results were implemented into TCSAB´s advanced database ADV_TD2_alpha. The new database shows significant improvements compared to the old TCT1 in predicting phase stability and phase transformation temperatures for TNM alloys. The

ADV_TD2_alpha database will also serve to facilitate the development of new TiAl-based alloys, e.g. strengthened by Zr, and of Ti alloys.

References

[1] A. T. A. G. (ATAG), https://aviationbenefits.org/environmental-efficiency/aviations-impact-on-the-environment/.

[2] F. Appel, J. D. H. Paul, M. Oehring, Gamma Titanium Aluminide Alloys: Science and Technology, John Wiley & Sons, (2011).

[3] H. Clemens, S. Mayer, Design, Processing, Microstructure, Properties, and Applications of Advanced Intermetallic TiAl Alloys, Adv. Eng. Mater., 15 (2013) 191-215.

[4] T. M. Pollock, S. Tin, Nickel-Based Superalloys for Advanced Turbine Engines: Chemistry, Microstructure and Properties, J. Propul. Power, 22 (2006) 361-373.

[5] M. J. Blackburn, M. P. Smith, Titanium Alloys of the TiAl Type, U.S. Patent, United Technologies Corporation, Hartford, Conn., 4,294,615, 1981.

[6] H. Clemens, H. Kestler, Processing and Applications of Intermetallic γ-TiAl-Based Alloys, Adv. Eng. Mater., 2 (2000) 551-570.

[7] M. Palm, Al-Ti binary phase diagram evaluation, G. Effenberg (Ed.) in: MSI Eureka, Materials Science International services GmbH (MSI), Stuttgart, (2020) pp. 1-11.

[8] B. P. Bewlay, S. Nag, A. Suzuki, M. J. Weimer, TiAl Alloys in Commercial Aircraft Engines, Mater. High Temp., 33 (2016) 549-559.

[9] S.-C. Huang, Titanium Aluminum Alloys Modified by Chromium and Niobium and Method of Preparation, in, Google Patents, (1989).

[10] H. Clemens, W. Smarsly, V. Güther, S. Mayer, Advanced Intermetallic Titanium Aluminides, in: Proceedings of the 13th World Conference on Titanium, Wiley Online Library, (2016) pp. 1189-1200.

[11] P. Bartolotta, J. Barrett, T. Kelly, R. Smashey, The Use of Cast Ti−48Al− 2Cr−2Nb in Jet Engines, JOM, 49 (1997) 48-50.

[12] H. Clemens, W. Wallgram, S. Kremmer, V. Güther, A. Otto, A. Bartels, Design of Novel β-Solidifying TiAl Alloys with Adjustable β/B2-Phase Fraction and Excellent Hot-Workability, Adv. Eng. Mater., 10 (2008) 707-713.

[13] H. Z. Niu, X. J. Chen, Y. F. Chen, S. Zhao, G. H. Liu, D. L. Zhang, Microstructural Stability, Phase Transformation and Mechanical Properties of a Fully-Lamellar Microstructure of a Mo-Modified High-Nb γ-TiAl Alloy, Mater. Sci. Eng.: A, 784 (2020) 139313.

[14] B. P. Bewlay, M. Weimer, T. Kelly, A. Suzuki, P. R. Subramanian, The Science, Technology, and Implementation of TiAl Alloys in Commercial Aircraft Engines, MRS Online Proceedings Library, 1516 (2013) 49-58.

[15] MTU Press archive detail, https://www.mtu.de/newsroom/press/press-archive/press-archive-detail/titanium-aluminide-mtu-aero-engines-develops-new-turbine-blade-material/.

[16] P. Janschek, Wrought TiAl Blades, Materials Today: Proceedings, 2 (2015) S92-S97.

[17] T. Tetsui, Development of a TiAl Turbocharger for Passenger Vehicles, Mater. Sci. Eng.: A, 329-331 (2002) 582-588.

[18] T. Tetsui, Application of TiAl in a Turbocharger for Passenger Vehicles, Adv. Eng. Mater., 3 (2001) 307-310.

[19] H. Clemens, S. Mayer, Development Status, Applications and Perspectives of Advanced Intermetallic Titanium Aluminides, in: Materials Science Forum, Trans Tech Publ, (2014) pp. 15-20.

[20] Mitsubishi Turbocharger, https://www.turbocharger.mtee.eu/gasoline-versus-diesel-turbo/.

[21] X. Wu, Review of Alloy and Process Development of TiAl Alloys, Intermetallics, 14 (2006) 1114-1122.

[22] S.-C. Huang, E. L. Hall, Plastic Deformation and Fracture of Binary TiAl-Base Alloys, Metall. Trans. A, 22 (1991) 427-439.

[23] P. J. Spencer, A Brief History of CALPHAD, Calphad, 32 (2008) 1-8.

[24] N. Saunders, A. P. Miodownik, CALPHAD (Calculation of Phase Diagrams): a Comprehensive Guide, Elsevier, (1998).

[25] M. Schloffer, F. Iqbal, H. Gabrisch, E. Schwaighofer, F.-P. Schimansky, S. Mayer, A. Stark, T. Lippmann, M. Göken, F. Pyczak, H. Clemens, Microstructure Development and Hardness of a Powder Metallurgical Multi Phase γ-TiAl Based Alloy, Intermetallics, 22 (2012) 231-240.

[26] H. Clemens, B. Boeck, W. Wallgram, T. Schmoelzer, L. M. Droessler, G. A. Zickler, H. Leitner, A. Otto, Experimental Studies and Thermodynamic Simulations of Phase Transformations in Ti-(41-45) Al-4Nb-1Mo-0.1 B Alloys, MRS Online Proceedings Library (OPL), 1128 (2008).

[27] H. F. Chladil, H. Clemens, H. Leitner, A. Bartels, R. Gerling, F.-P. Schimansky, S. Kremmer, Phase Transformations in High Niobium and Carbon Containing γ-TiAl Based Alloys, Intermetallics, 14 (2006) 1194-1198.

[28] U. R. Kattner, The Calphad Method and Its Role in Material and Process Development, Tecnol. Metal. Mater. Min., 13 (2016) 3-15.

[29] J. C. Schuster, M. Palm, Reassessment of the binary Aluminium-Titanium phase diagram, J. Phase Equilib. Diffus., 27 (2006) 255-277.

[30] B. Distl, G. Dehm, F. Stein, Effect of Oxygen on High-Temperature Phase Equilibria in Ternary Ti-Al-Nb Alloys, Z. anorg. u. allgem. Chem., 646 (2020) 1151-1156.

[31] R. M. Waterstrat, Effect of Interstitial Elements on Phase Relationships in the Titanium-Aluminum System, in: U.S. National Institute of Standards and Technology, Gaithersburg, MD (1988) pp. 1-54.

[32] X. J. Jiang, Y. K. Zhou, Z. H. Feng, C. Q. Xia, C. L. Tan, S. X. Liang, X. Y. Zhang, M. Z. Ma, R. P. Liu, Influence of Zr Content on β-Phase Stability in α-Type Ti–Al Alloys, Mater. Sci. Eng.: A, 639 (2015) 407-411.

[33] Thermo-Calc Software AB, Next Generation TiAl Alloys Advanced by New European Consortium, https://thermocalc.com/blog/next-generation-tial-alloys-advanced-by-new-european-consortium/.

[34] Thermo-Calc Software AB, TCTI1: TCS Ti/TiAl-based Alloys Database, v.1, http://www.thermocalc.com/media/50229/tcti1_extended_info.pdf

[35] Clean Sky, https://www.clean-aviation.eu/clean-sky-2/programme-overview-and-structure/clean-sky-2-structure.

[36] A. Prince, Alloy Phase Equilibria, Elsevier (1966).

[37] P. Perrot, Al-Si-Ti Ternary Phase Diagram Evaluation, G. Effenberg (Ed.) in: MSI Eureka, Materials Science International Services GmbH (MSI), Stuttgart, (2004) pp. 1-18.

[38] P. Perrot, Ti-Al-Si, G. Petzow, G. Effenberg (Eds.) in: Ternary alloys. A comprehensive Compendium of Evaluated Constitutional Data and Phase Diagrams, VIII, VCH, Weinheim, Germany, (1993) pp. 283-290.

[39] V. Raghavan, Al-Si-Ti (aluminum-silicon-titanium), J. Phase Equilibria Diffus., 30 (2009) 82-83.

[40] V. Raghavan, Al-Si-Ti (aluminum-silicon-titanium), J. Phase Equilibria Diffus., 26 (2005) 624-628.

[41] S. Tsuyama, S. Mitao, K.-n. Minakawa, Alloy modification of γ-base titanium aluminide for improved oxidation resistance, creep strength and fracture toughness, Mater. Sci. Eng.: A, (1992) 451-456.

[42] T. Noda, M. Okabe, S. Isobe, M. Sayashi, Silicide precipitation strengthened TiAl, Mater. Sci. Eng.: A, 192 (1995) 774-779.

[43] R. Schmid-Fetzer, Phase Diagrams: The Beginning of Wisdom, J. Phase Equilib. Diffus., 35 (2014) 735-760.

[44] J. Li, S. Hao, Study of $\alpha(\alpha_2)/\gamma$ Phase Equilibria in the Ti-Al-Si Ternary System, Acta Metall. Sin-ENGL, 32 (1996) 1171-1176.

[45] S. Liu, F. Weitzer, J. C. Schuster, N. Krendelsberger, Y. Du, On the reaction scheme and liquidus surface in the ternary system Al–Si–Ti, Int. J. Mater. Res., 99 (2008) 705-711.

[46] S. P. Gupta, Intermetallic Compounds in Diffusion Couples of Ti with an Al-Si Eutectic Alloy, Mater. Charact., 49 (2003) 321-330.

[47] C. R. d. F. Azevedo, H. M. Flower, Microstructure and Phase Relationships in Ti–Al–Si System, Mater. Sci. Technol., 15 (1999) 869-877.

[48] K. Kasraee, A. Tayebifard, E. Salahi, Effect of Substitution of Si by Al on Microstructure and Synthesis Behavior of Ti_5Si_3 Based Alloys Fabricated by Mechanically Activated Self-Propagating High-Temperature Synthesis, Adv. Powder Technol., 25 (2014) 885-890.

[49] M. Zha, H. Y. Wang, S. T. Li, S. L. Li, Q. L. Guan, Q. C. Jiang, Influence of Al Addition on the Products of Self-Propagating High-Temperature Synthesis of Al–Ti–Si System, Mater. Chem. Phys., 114 (2009) 709-715.

[50] Z. Guan, T. Pfullmann, M. Oehring, R. Bormann, Phase formation during ball milling and subsequent thermal decomposition of Ti–Al–Si powder blends, J. Alloys Compd., 252 (1997) 245-251.

[51] X. J. Jiang, Y. K. Zhou, Z. H. Feng, C. Q. Xia, C. L. Tan, S. X. Liang, X. Y. Zhang, M. Z. Ma, R. P. Liu, Influence of Zr Content on β-Phase Stability in α-Type Ti–Al Alloys, Mat. Sci. Eng., A639 (2015) 407-411.

[52] M. Allen, V. Güther, J. Lindemann, S. Kardos, Solid Solution Strengthening of TiAl Alloys with Zirconium, in: Intermetallics Proceedings 2021, Bad Staffelstein, Germany (2021) pp. 73-74.

[53] D. Wimler, J. Lindemann, M. Reith, A. Kirchner, M. Allen, W. G. Vargas, M. Franke, B. Klöden, T. Weißgärber, V. Güther, Designing Advanced Intermetallic Titanium Aluminide Alloys for Additive Manufacturing, Intermetallics, 131 (2021) 107109.

[54] L. Tretyachenko, Al-Ti-Zr Ternary Phase Diagram Evaluation, MSI, Materials Science International Services GmbH, Stuttgart, (2004).

[55] F. Yang, F. H. Xiao, S. G. Liu, S. S. Dong, L. H. Huang, Q. Chen, G. M. Cai, H. S. Liu, Z. P. Jin, Isothermal Section of Al–Ti–Zr Ternary System at 1273 K, J Alloys Compd, 585 (2014) 325-330.

[56] K. L. Lü, F. Yang, Z. Y. Xie, H. S. Liu, G. M. Cai, Z. P. Jin, Isothermal Section of Al−Ti−Zr Ternary System at 1073 K, Trans. Nonferrous Met. Soc. China, 26 (2016) 3052−3058.

[57] D. H. Troup, An Investigation of the Gamma Phase of the Binary Titanium-Aluminum Alloy with Zirconium Additions, in: School of Engineering; Air Force Institute of Technology, Air University, Wright-Patterson Airforce Base, OH (1962) pp. 1-89.

[58] S. V. Spragins, J. R. Myers, R. K. Saxer, Influence of zirconium additions on the epsilon phase of the titanium-aluminium system, Nature Lett., 4993 (1965) 183-184.

[59] J. Dai, J. Zhu, C. Chen, F. Weng, High temperature oxidation behavior and research status of modifications on improving high temperature oxidation resistance of titanium alloys and titanium aluminides: A review, J. Alloys Compd., 685 (2016) 784-798.

[60] M. Hoch, R. Lin, Al-O-Ti Ternary Phase Diagram Evaluation, G. Effenberg (Ed.) in: MSI Eureka, Materials Science International services GmbH (MSI), Stuttgart (1993) pp. 1-12.

[61] K. Das, P. Choudhury, S. Das, The Al-O-Ti (Aluminum-Oxygen-Titanium) System, J. Phase Equilib., 23 (2002) 525.

[62] L. S. T'sai, T. R. Hogness, The Diffusion of Gases Through Fused Quartz, J. Phys. Chem., 36 (2002) 2595-2600.

[63] R. Kainuma, M. Palm, G. Inden, Solid-Phase Equilibria in the Ti-rich Part of the Ti-Al System, Intermetallics, 2 (1994) 321-332.

[64] Powder Diffraction File PDF-2, release 2004, International Center for Diffraction Data, Newtown Square, PA, USA (2004).

[65] N. Schell, A. King, F. Beckmann, T. Fischer, M. Müller, A. Schreyer, The High Energy Materials Science Beamline (HEMS) at PETRA III, in: Materials Science Forum, Trans Tech Publ, (2014) pp. 57-61.

[66] A. Hammersley, FIT2D: a Multi-Purpose Data Reduction, Analysis and Visualization Program, J. Appl. Crystallogr., 49 (2016) 646-652.

[67] L. Lutterotti, Total Pattern Fitting for the Combined Size–Strain–Stress–Texture Determination in Thin Film Diffraction, Nucl. Instrum. Methods Phys. Res., Sect. B, 268 (2010) 334-340.

[68] L. A. Giannuzzi, F. A. Stevie, Introduction to Focused Ion Beams Instrumentation, Theory, Techniques and Practice, Springer, New York (2005).

[69] J. Mayer, L. A. Giannuzzi, T. Kamino, J. Michael, TEM Sample Preparation and FIB-Induced Damage, MRS bulletin, 32 (2007) 400-407.

[70] M. Fiore, F. Beneduce, C. R. d. F. Azevedo, Assessment of the Ti-Rich Corner of the Ti-Si Phase Diagram: the Recent Dispute about the Eutectoid Reaction, Mater. Res., 19 (2016) 942-953.

[71] Z. Kahrobaee, M. Palm, Experimental Investigation of Ti–Al–Si Phase Equilibria at 800–1200 °C, J Alloys Compd, 924 (2022) 166223.

[72] Z. Kahrobaee, M. Palm, Determination of Phase Equilibria in the Ti–Al–Si System at 800–1200 °C, Proceedings Intermetallics 2021, pp. 78 - 79. Intermetallics 2021, Bad Staffelstein, Germany, October 04, 2021 - October 08, (2021).

[73] X. Weihao, Z. Liang, J. Huiren, Effects of Si on High Temperature Oxidation Resistance of TiAl Alloy, Journal-Beijing University of Aeronautics and Astronautics, 32 (2006) 365.

[74] D. Vojtěch, M. Mort'aniková, P. Novák, Kinetic and Thermodynamic Aspects of High-Temperature Oxidation of Selected Ti-Based Alloys, in: Defect and Diffusion Forum, Trans. Tech. Publ. Ltd., (2007) pp. 123-128.

[75] P. Novák, Příprava, vlastnosti a použití intermetalických sloučenin, Chemické listy, 106 (2012) 884-889.

[76] M. Cabibbo, A. Knaislová, P. Novák, F. Průša, C. Paoletti, Role of Si on Lamellar Formation and Mechanical Response of Two SPS Ti–15Al–15Si and Ti–10Al–20Si Intermetallic Alloys, Intermetallics, 131 (2021) 107099.

[77] M. Bulanova, L. Tretyachenko, M. Golovkova, K. Meleshevich, Phase equilibria in the α-Ti-Al-Si region of the Ti-Si-Al system, J. Phase Equilibria Diffus., 25 (2004) 209-229.

[78] M. Bulanova, L. Tretyachenko, M. Golovkova, Phase equilibria in the Ti-rich corner of the Ti-Si-Al system, Z. Metallk., 88 (1997) 256-265.

[79] O. Schob, H. Nowotny, F. Benesovsky, The Ternary Systems (Titanium, Zirconium, Hafnium)-Aluminum-Silicon, Planseeber. Pluvermet., 10 (1962) 65-67.

[80] D. H. Turner, F. A. Crossley, The Titanium-Rich Corner of the Ti-Al-Si System in "Studies of Phase Relationships and Transformation Processes of Titanium-Alloy Systems", D.J. McPherson, W. Rostoker (Eds.), in: Wright Air Development Center, Technical Report, (1954) pp. 52-66.

[81] F. Crossley, D. Turner, Titanium-rich corner of the Ti-Al-Si system, Trans. Met. Soc. AIME, 212 (1958) 60-63.

[82] J. Li, Y. Zong, S. Hao, Effects of Alloy Elements (C, B, Fe, Si) on the Ti-Al Binary Phase Diagram, J. Mater. Sci. Technol. , 15 (1999) 58-62.

[83] C. R. d. F. Azevedo, H. M. Flower, Calculated Ternary Diagram of Ti–Al–Si System, Mater. Sci. Technol., 16 (2000) 372-381.

[84] C. R. d. F. Azevedo, H. M. Flower, Experimental and Calculated Ti-rich Corner of the Al-Si-Ti Ternary Phase Diagram, Calphad, 26 (2002) 353-373.

[85] J. C. Viala, N. Peillon, F. Bosselet, J. Bouix, Phase Equilibria at 1000 °C in the Al-C-Si-Ti Quaternary System: An Experimental Approach, Mater. Sci. Eng.: A, 229 (1997) 95-113.

[86] A. Raman, K. Schubert, The constitution of some alloy series related to TiAl$_3$. II. Investigations in Some T-Al-Si and T$^{4...6}$-In Systems, Z. Metallk., 56 (1965) 44-52.

[87] J. Gröbner, D. Mirković, R. Schmid-Fetzer, Thermodynamic Aspects of Grain Refinement of Al–Si Alloys Using Ti and B, Mater. Sci. Eng.: A, 395 (2005) 10-21.

[88] Z. Li, C. Liao, Y. Liu, X. Wang, Y. Wu, M. Zhao, Z. Long, F. Yin, 700° C isothermal section of the Al-Ti-Si ternary phase diagram, J. Phase Equilibria Diffus., 35 (2014) 564-574.

[89] Y. Li, Q.-F. Gu, Q. Luo, Y. Pang, S.-L. Chen, K.-C. Chou, X.-L. Wang, Q. Li, Thermodynamic investigation on phase formation in the Al–Si rich region of Al–Si–Ti system, Mater. Des., 102 (2016) 78-90.

[90] J. Wang, Y. Liu, Y. Liu, C. Wu, X. Su, The Isothermal Section of the Al-Si-Ti Ternary System at 550 °C, J. Phase Equilib. Diffus., 40 (2019) 810-819.

[91] K. Kamei, T. Ninomiya, S. Hayashi, The Phase Diagram of the Al-Si-Ti Equilibrium System, Metallurgical Abstracts of Light Metal Alloys, 3 (1968) 67-70.

[92] H. L. Lukas, N. Lebrun, Al-Si Binary Phase Diagram Evaluation, in: MSI Eureka, Effenberg, G. (Ed.) by MSI, Materials Science International Services GmbH, Stuttgart, (2004) pp. 1-7.

[93] C. Colinet, J.-C. Tedenac, Structural Stability of Intermetallic Phases in the Si-Ti System. Point Defects and Chemical Potentials in D8$_8$-Si$_3$Ti$_5$ Phase, Intermetallics, 18 (2010) 1444-1454.

[94] S. H. Manesh, H. M. Flower, Liquidus Projection of Ti-Al-Si Ternary System in Vicinity of γ Alloys, Mater. Sci. Technol., 10 (1994) 674-680.

[95] P. Villars, L. D. Calvert, Pearson's Handbook of Crystallographic Data 2ed., ASM International, (1997).

[96] M. J. Blackburn, The Ordering Transformation in Titanium- Aluminum Alloys Containing up to 25 at. % Aluminum Trans. Met. Soc. AIME, 239 (1967) 1200-1208.

[97] J. Braun, M. Ellner, B. Predel, Experimental Investigations of the Structure and Stability of the TiAl Phase, Z. Metall., 86 (1995) 870-876.

[98] E. Illeková, P. Švec, D. Janičkovič, Influence of the Processing on the Ordering Process in the Al-Ti Binary System with Composition Close to Al$_3$Ti, in: J. Phys. Conf. Ser., IOP Publishing Ltd, (2009) pp. 1-6.

[99] H. Mabuchi, T. Asai, Y. Nakayama, Aluminide Coatings on TiAl Compound, Scr. Metall., 23 (1989) 685-689.

[100] J. Braun, M. Ellner, Phase Equilibria Investigations on the Aluminum-Rich Part of the Binary System Ti-Al, Metall. Mater. Trans. A, 32 (2001) 1037-1047.

[101] V. N. Svechnikov, Y. A. Kocherzhinsky, L. M. Yupko, O. G. Kulik, E. A. Shishkin, Phase Diagram of The Titanium-Silicon System, in: Dokl. Akad. Nauk. SSSR, (1970) pp. 393-396.

[102] M. J. Blackburn, Some Aspects of Phase Transformations in Titanium Alloys in: Boeing Scientific Research Labs., Seattle, (1970) pp. 633-643.

[103] A. Hellwig, G. Inden, M. Palm, The Invariant Reaction Between α, α$_2$ and γ in the Ti-Al System, Scr. Mater., 27 (1992) 143-148.

[104] R. Miida, M. Kasahara, D. Watanabe, Long-Period Antiphase Domain Structures of Al-Ti Alloys Near Composition Al$_3$Ti, Jpn. J. Appl. Phys., 19 (1980) L707-L710.

[105] L. Zhang, G. Qiu, J. Wu, A Preliminary Research on the Mechanical Properties of TiAl+ Ti$_5$Si$_3$ Dual Phase Alloys, MRS Online Proceedings Library (OPL), 364 (1995).

[106] F.-S. Sun, S.-E. Kim, C.-X. Cao, Y.-T. Lee, M.-G. Yan, A study of Ti$_5$Si$_3$/γ Interface in TiAl Alloys, Scr. Mater., 45 (2001) 383-389.

[107] T. Takemoto, I. Okamoto, Intermetallic Compounds Formed During Brazing of Titanium with Aluminium Filler Metals, J. Mater. Sci., 23 (1988) 1301-1308.

[108] Q. Luo, Q. Li, J.-Y. Zhang, S.-L. Chen, K.-C. Chou, Experimental investigation and thermodynamic calculation of the Al–Si–Ti system in Al-rich corner, J. Alloys Compd., 602 (2014) 58-65.

[109] J. S. Wu, P. A. Beaven, R. Wagner, The Ti$_3$(Al, Si)+Ti$_5$(Si, Al)$_3$ Eutectic Reaction in the Ti-Al-Si System, Scr. Metall. Mater., 24 (1990) 207-212.

[110] J. Fan, X. Li, Y. Su, J. Guo, H. Fu, The Microstructure Parameters and Microhardness of Directionally Solidified Ti–43Al–3Si Alloy, J. Alloys Compd., 506 (2010) 593-599.

[111] F.-S. Sun, F. S. Froes, Precipitation of Ti$_5$Si$_3$ Phase in TiAl Alloys, Mater. Sci. Eng.: A, 328 (2002) 113-121.

[112] Z. Zhang, H. M. Flower, Composition and Lattice Parameters of Silicide and Matrix in Cast Ti–Si–Al–Zr Alloys, Mater. Sci. Technol., 7 (1991) 812-817.

[113] D. R. Sandlin, H. A. Klung, A Phase Study of a Selected Portion of the Ti-Al-Zr Ternary System Inclucing Lattice Parameter Determination for the Ti-Al Gamma Phase, in: School of Engineering; Air Force Institute of Technology, Air University, Wright-Patterson Airforce Base, OH (1961).

[114] F. C. Davies, The Effects of Ternary Additions on Lattice Parameters in the Gamma Phase of Titanium-Aluminum Alloy System, in: School of Engineering; Air Force Institute of Technology, Air University, Wright-Patterson Airforce Base, OH (1959) pp. cited in (1962 Tro).

[115] R. Kainuma, Y. Fujita, H. Mitsui, I. Ohnuma, K. Ishida, Phase Equilibria Among α (hcp), β (bcc) and γ (L1$_0$) Phases in Ti–Al Base Ternary Alloys, Intermetallics, 8 (2000) 855-867.

[116] Z. Kahrobaee, M. Palm, Critical Assessment of the Al-Ti-Zr System, J. Phase Equilib. Diffus., 41 (2020) 687-701.

[117] Z. Kahrobaee, M. Palm, Experimental Evaluation of the Isothermal Section of the Ti–Al–Zr Ternary System at 1273 K, Proceedings Intermetallics 2019, pp. 174 - 175. Intermetallics 2019, Bad Staffelstein, Germany, September 30, 2019 - October 04, (2019).

[118] Z. Kahrobaee, B. Rashkova, K. Hauschildt, M. Palm, Experimental Investigation of Phase Equilibria in the Ti—Al—Zr System at 1000–1300° C, Crystals, 12 (2022) 1184.

[119] I. I. Kornilov, Physical Metallurgy of Titanium (Metalovideniye Titana), I.I. Kornilov (Eds.), in: 5th Conference on Metallurgy, Physical Metallurgy, and Application of Titanium and Its Alloys, National Aeronautics and Space Administration, Moscow (1963) pp. 1-351.

[120] F. A. Crossley, Effects of the Ternary Additions: O, Sn, Zr, Cb, Mo and V on the α/α+Ti$_3$Al Boundary of Ti-Al Base Alloys, Trans. Metall. Soc. AIME, 245 (1969) 1963-1968.

[121] G. K. Scarr, J. C. Williams, S. Ankem, H. B. Bomberger, The Effect of Zirconium and Oxygen on α_2 Precipitation in Titanium-Aluminum Alloys, G. Lütjering, U. Zwicker, W. Bunk (Eds.), in: 5th Interntional conference on Titanium, DGM, Munich, Germany (1985) pp. 1475-1479.

[122] S. Tsunekawa, M. E. Fine, Lattice Parameters of $Al_3(Zr_xTi_{1-x})$ vs. x in Al-2 at.% (Ti + Zr) Alloys, Scr. Metall., 16 (1982) 391-392.

[123] V. R. Parameswaran, J. R. Weertman, M. E. Fine, Coarsening Behavior of $L1_2$ Phase in an Al-Zr-Ti Alloy, Scr. Metall., 23 (1989) 147-150.

[124] K. M. Lee, J. H. Lee, I. H. Moon, Effects of V and Zr Addition on Lattice Parameters of Al_3Ti Phase in Mechanically Alloyed Al-8 wt.% Ti Alloys, Scr. Metall. Mater., 29 (1993) 737-740.

[125] P. Málek, M. Janecek, B. Smola, P. Bartuska, J. Plestil, Structure and Properties of Rapidly Solidified Al-Zr-Ti Alloys, J. Mater. Sci., 35 (2000) 2625-2633.

[126] A. A. Abdel-Hamid, Crystallization of Complex Aluminide Compounds from Dilute Al-Ti Melts Containing One or Two Other Transition Metals of IVB to VIB Groups, Z. Metallkd., 81 (1990) 601-605.

[127] B. Dubost, Applications industrielles et détermination des diagrammes d'équilibre de phases des alliages légers Progrès et perspectives (Industrial applications and determination of equilibrium phase diagrams for light alloys. Progress and prospects), Rev. Metall. (Paris), 90 (1993) 195-209.

[128] L. Zhang, D. G. Eskin, L. Katgerman, Influence of Ultrasonic Melt Treatment on the Formation of Primary Intermetallics and Related Grain Refinement in Aluminum Alloys, J. Mater. Sci., 46 (2011) 5252–5259.

[129] G. J. Fan, X. P. Song, M. X. Quan, Z. Q. Hu, Mechanical Alloying and Thermal Stability of $Al_{67}Ti_{25}M_8$ (M = Cr, Zr, Cu), Mater. Sci. Eng. A, A231 (1997) 111-116.

[130] M. V. Karpets, Y. V. Milman, O. M. Barabash, N. P. Korzhova, O. N. Senkov, D. B. Miracle, T. N. Legkaya, I. V. Voskoboynik, The Influence of Zr Alloying on the Structure and Properties of Al_3Ti, Intermetallics, 11 (2003) 241-249.

[131] S. S. Nayak, S. K. Pabi, B. S. Murty, High Strength Nanocrystalline $L1_2$-$Al_3(Ti,Zr)$ Intermetallic Synthesized by Mechanical Alloying, Intermetallics, 15 (2007) 26-33.

[132] K. E. Knipling, D. C. Dunand, D. N. Seidman, Precipitation Evolution in Al–Zr and Al–Zr–Ti Alloys During Aging at 450–600 °C, Acta Mater., 56 (2008) 1182-1195.

[133] E. A. Popova, A. B. Shubin, P. V. Kotenkov, E. A. Pastukhov, L. E. Bodrova, O. M. Fedorova, Al–Ti–Zr Master Alloys: Structure Formation, Russ. Metall. (Engl. Transl.), 2012 (2012) 357-361.

[134] E. A. Popova, P. V. Kotenkov, E. A. Pastukhov, A. B. Shubin, Master Alloys Al–Sc–Zr, Al–Sc–Ti, and Al–Ti–Zr: Their Manufacture, Composition, and Structure, Russ. Metall. (Engl. Transl.), 2013 (2013) 590-594.

[135] P. Kotenkov, E. Popova, I. Gilev, Formation of Stable and Metastable Aluminides in Al–Zr–Ti, Al–Ti–Nb Alloys, V.A. Volkovich, S.V. Zvonarev, I.V. Kashin, E.D. Narkhov (Eds.), in: Physics, technologies and innovation (PTI-2018): Proceedings of the V International Young Researchers' Conference, Ekaterinburg, Russia (2018) pp. 020046.

[136] K. Hashimoto, H. Doi, K. Kasahara, T. Tsujimoto, T. Suzuki, Effects of Third Elements on the Structures of TiAl-Based Alloys, Nippon Kinzoku Gakkaishi (Journal of Japan Institute of Metals), 52 (1988) 816-825.

[137] H. Doi, K. Hashimoto, K. Kasahara, T. Tsujimoto, Site Determination of Third Elements in TiAl Compound by X-Ray Diffractometry, Mater. Trans., JIM, 31 (1990) 975-982.

[138] X. F. Chen, R. D. Reviere, B. F. Oliver, C. R. Brooks, The Site Location of Zr Atoms Dissolved in TiAI, Scr. Metall. Mater., 27 (1992) 45-49.

[139] C. T. Forwood, M. A. Gibson, P. R. Miller, C. J. Rossouw, A. J. Morton, Alloying Effects and Deformation Processes in Duplex γ-TiAl Alloys, M.V. Nathal, R. Darolia, C.T. Liu, P.L. Martin, D.B. Miracle, R. Wagner, M. Yamaguchi (Eds.), in: Structural Intermetallics 1997, TMS, Warrendale, PA, Seven Springs, PA (1997) pp. 545-554.

[140] J. L. Murray, Al-Ti System, J.L. Murray (Ed.) in: Phase diagrams of binary titanium alloys, ASM, Metals Park (1987) pp. 12-24.

[141] I. Ansara, B. Grieb, B. Legendre, Al-Ti-Zr Ternary Phase Diagram Evaluation, MSI, Materials Science International Services GmbH, Stuttgart, (1993).

[142] J. Schuster, Al-Zr binary phase diagram evaluation, G. Effenberg (Ed.) in: MSI Eureka, Materials Science International Services GmbH (MSI), Stuttgart, (2004) pp. 1-22.

[143] J. Murray, A. Peruzzi, J. P. Abriata, The AI-Zr System, J. Phase Equilib., 13 (1992) 277-291.

[144] H. Okamoto, Al-Zr, J. Phase Equilib., 23 (2002) 455-456.

[145] T. Wang, Z. P. Jin, J. C. Zhao, Thermodynamic Assessment of the Al-Zr Binary System, J. Phase Equilib. Diffus., 22 (2001) 544-551.

[146] E. Fischer, C. Colinet, An Updated Thermodynamic Modeling of the Al-Zr System, J. Phase Equilib. Diffus., 36 (2015) 404-413.

[147] R. Tamim, K. Mahdouk, Thermodynamic Reassessment of the Al–Zr Binary system, J. Therm. Anal. Calorim., 131 (2018) 1187–1200.

[148] A. Janghorban, A. Antoni-Zdziobek, M. Lomello-Tafin, C. Antion, T. H. Mazingue, A. Pisch, Phase Equilibria in the Aluminium-Rich Side of the Al–Zr System, J. Therm. Anal. Calorim., 114 (2013) 1015–1020.

[149] J. Murray, A. Peruzzi, J. P. Abriata, The AI-Zr (aluminum-zirconium) System, J. Phase Equilib., 13 (1992) 277-291.

[150] A. Peruzzi, Reinvestigation of the Zr-Rich End of the Zr-Al Equilibrium Phase Diagram, J. Nucl. Mater., 186 (1992) 89-99.

[151] A. Malfliet, A. Kozlov, N. Lebrun, Ti-Zr binary phase diagram evaluation, G. Effenberg (Ed.) in: MSI Eureka, Materials Science International services GmbH (MSI), Stuttgart, (2015) pp. 1-8.

[152] B. Batalu, G. Cosmeleata, A. Aloman, Critical Analysis of the Ti-Al Phase Diagrams, UPB. Sci. Bull., Seies B, 68 (2006) 77-90.

[153] V. T. Witusiewicz, A. A. Bondar, U. Hecht, S. Rex, T. Y. Velikanova, The Al-B-Nb-Ti System: III. Thermodynamic Re-Evaluation of the Constituent Binary System Al-Ti, J Alloys Compd, 465 (2008) 64-77.

[154] H. Wang, R. C. Reed, J.-C. Gebelin, N. Warnken, On the Modelling of the Point Defects in the Ordered B2 Phase of the Ti–Al System: Combining CALPHAD with First-Principles Calculations, CALPHAD, 39 (2012) 21-26.

[155] J. L. Murray, Calculation of the Titanium-Aluminum Phase Diagram, Metall. Trans. A, 19 (1988) 243-247.

[156] U. R. Kattner, J.-C. Lin, Y. A. Chang, Thermodynamic Assessment and Calculation of the Ti-Al System, Metall. Trans. A, 23 (1992) 2081-2090.

[157] N. Saunders, System Al-Ti, I. Ansara (Ed.) in: COST507: Thermochemical Database for Light Metal Alloys, ECSC-EEC-EAEC, Brussles and Luxembourg, (1995) pp. 52-56.

[158] F. Zhang, S. L. Chen, Y. A. Chang, U. R. Kattner, A Thermodynamic Description of the Ti-Al System, Intermetallics, 5 (1997) 471-482.

[159] I. Ohnuma, Y. Fujita, H. Mitsui, K. Ishikawa, R. Kainuma, K. Ishida, Phase Equilibria in the Ti-Al Binary System, Acta Mater., 48 (2000) 3113-3123.

[160] C. M. Fang, Z. Fan, An Ab Initio Study on Stacking and Stability of $TiAl_3$ Phases, Comput. Mater. Sci., 153 (2018) 309-314.

[161] E. Illeková, P. Švec, D. Janičkovič, Influence of the Processing on the Ordering Process in the Al-Ti Binary System with Composition Close to Al_3Ti, J. Phys.: Conf. Ser., 144 (2009) 012111.

[162] T. B. Massalski, Binary Alloy Phase Diagrams, 2nd ed., ASM International, Metals Park, OH, (1990).

[163] K. Kasahara, K. Hashimoto, H. Doi, T. Tsujimoto, Crystal Structure and Hardness of TiAl Phase Containing Zirconium, Nippon Kinzoku Gakkaishi (Journal of Japan Institute of Metals), 51 (1987) 278-284.

[164] H. Mabuchi, T. Asai, Y. Nakayama, Aluminide coatings on TiAl compound, Scr. Metall., 23 (1989) 685-689.

[165] J. C. I. Schuster, H., Phases and Phase Relations in the Partial System $TiAl_3$-TiAl, Z. Metallkd., 81 (1990) 389-396.

[166] R. Miida, One Dimensional Antiphase Domain Structures in the Aluminum-rich Al-Ti Alloys, Jap. J. Appl. Phys., 25 (1986) 1815-1824.

[167] F. J. J. van Loo, G. D. Rieck, Diffusion in the Titanium-Aluminium System - I. Interdiffusion Between Solid Al and Ti or Ti-Al Alloys, Acta Metall., 21 (1973) 61-71.

[168] M. Pötzschke, K. Schubert, Zum Aufbau einiger zu T^4-B^3 homologer und quasihomologer Systeme II. Die Systeme Ti-Al, Zr-Al, Hf-Al, Mo-Al und einige ternäre Systeme, Z. Metallkd., 53 (1962) 548-561.

[169] H. Nowotny, H. Auer-Welsbach, J. Bruss, A. Kohl, Ein Beitrag zur Mn_5Si_3-Struktur (D 8_8-Typ), Monatsh. Chem. Verw. Teile Anderer Wiss. Chem. Mon., 90 (1959) 15-23.

[170] J. C. Schuster, J. Bauer, J. Debuigne, Investigation of Phase Equilibria Related to Fusion Reactor Materials: I. The Ternary System Zr-Al-N, J. Nucl. Mater., 116 (1983) 131-135.

[171] F. Stein, G. Sauthoff, M. Palm, Phases and Phase Equilibria in the Fe-Al-Zr System, Z. Metallkd., 96 (2004) 469-485.

[172] M. Premkumar, K. S. Prasad, A. K. Singh, Structure and Stability of the B2 Phase in Ti–25Al–25Zr Alloy, Intermetallics, 17 (2009) 142-145.

[173] D. Sornadurai, B. Panigrahi, V. S. Sastry, Ramani, Crystal Structure and X-Ray Powder Diffraction Pattern of Ti_2ZrAl, Powder Diffr., 15 (2000) 189-190.

[174] D. Sornadurai, V. S. Sastry, V. T. Paul, R. Flemming, F. Jose, R. Ramaseshan, S. Dash, Microstructure, Crystal Structure and Mechanical Properties of the New Ternary Intermetallic Alloy Phase Zr_2TiAl, Intermetallics, 24 (2012) 89-94.

[175] A. Pathak, A. K. Singh, A First Principles Study of Structural and Mechanical Properties of Ti_2AlZr Intermetallic, Intermetallics, 63 (2015) 37-44.

[176] I. I. Kornilov, T. T. Nartova, M. M. Savel`yeva, Phase Equilibrium of Alloys of the Section Ti_3Al-Zr of the Ternary System Ti-Al-Zr, I.I. Kornilov (Eds.), in: Metallovedeniye Titana, Nauka, Moscow (1964) pp. 53-57.

[177] Y. Miyajima, K. Ishikawa, K. Aoki, Hydrogen-Induced Amorphization in Ti–Al–Zr Compounds with $D0_{19}$, B2 and FCC Structures, Mater. Trans., 43 (2002) 1085-1088.

[178] M. Premkumar, A. K. Singh, Deformation Behavior of an Ordered B2 Phase in Ti–25Al–25Zr Alloy, Intermetallics, 18 (2010) 199-201.

[179] G. N. Muradyan, S. K. Dolukhanyan, A. G. Aleksanyan, O. P. Ter-Galstyan, N. L. Mnatsakanyan, Regularities and Mechanism of Formation of Aluminides in the TiH_2–ZrH_2–Al System, Russ. J. Phys. Chem. B, 13 (2019) 86-95.

[180] C. Ravi, P. Vajeeston, S. Mathijaya, R. Asokamani, Electronic Structure, Phase Stability, and Cohesive Properties of Ti_2XAl (X=Nb, V, Zr), Phys. Rev. B, 60 (1999) 15683-15690.

[181] C. Ravi, R. Asokamani, Site Preference of Zr in Ti_3Al and Phase Stability of Ti_2ZrAl, Bull. Mater. Sci., 26 (2003) 97-103.

[182] P. Modak, L. M. Ramaniah, A. K. Singh, Structure of the B2 Phase in the Ti–25Al–25Zr Alloy: A Density Functional Study, J. Phys.: Condens. Matter, 22 (2010) 345502.

[183] F. Fan, Y. Gu, G. Xu, H. Chang, Y. Cui, Diffusion Research in BCC Ti-Al-Zr Ternary Alloys, J. Phase Equilib. Diffus., 40 (2019) 686-696.

[184] I. I. Kornilov, N. G. Boriskina, Study of the Phase Structure of the Alloys of the System Ti-Al-Zr Along the Ti_3Al-Zr Section, I.I. Kornilov (Eds.), in: Metallovedeniye Titana, Nauka, Moscow (1964) pp. 58-66.

[185] Y. L. Hao, D. S. Xu, Y. Y. Cui, R. Yang, D. Li, The Site Occupancies of Alloying Elements in TiAl and Ti_3Al Alloys, Acta Mater., 47 (1999) 1129-1139.

[186] R. Yang, Y. Hao, Y. Song, Z.-X. Guo, Site Occupancy of Alloying Additions in Titanium Aluminides and Its Application to Phase Equilibrium Evaluation, Z. Metallkd., 91 (2000) 296-301.

[187] A. Prince, Alloy Phase Equilibria, Elsevier, Amsterdam (1966).

[188] D. Tanda, T. Tanabe, R. Tamura, S. Takeuchi, Synthesis of Ternary $L1_0$ Compounds of Ti–Al–Zr System and Their Mechanical Properties, Mat. Sci. Eng., A387-389 (2004) 991-995.

[189] Y. N. Pylaeva, M. A. Volkova, Study of the Alloys of the Ternary System Ti-Al-Zr, I.I. Kornilov (Eds.), in: Metallovedeniye Titana, Nauka, Moscow (1964) pp. 38-42.

[190] N. I. Shirokova, T. T. Nartova, I. I. Kornilov, Исследование равновесия и свойств сплавов Ti-Zr-Al (Investigation of the phase equilibrium and properties of Ti-Zr-Al alloys), Izvestia Akademii nauk SSSR. Metally, 1968 (1968) 183-187.

[191] N. I. Shirokova, T. T. Nartova, Investigation of the Phase Equilibrium and Properties of Alloys of the Titanium Corner of the System Ti-Zr-Al, N.P. Sazhin (Eds.), in: Titanovyye Splavy dlya Novoy Tekhniki, Nauka, Moscow (1968) pp. 101-106.

[192] T. T. Nartova, N. I. Shirokova, Phase Equilibria and Heat Resistance of Ti-Zr-Al Alloys, Izvestia Akademii nauk SSSR. Metally, 1970 (1970) 194-198.

[193] Y. N. Borisova, I. I. Shashenkova, Study of the Properties of Alloys of the Sytems Ti-Zr and Ti-Zr-Al, N.P. Sazhin (Eds.), in: Titanovyye Splavy dlya Novoy Tekhniki, Nauka, Moscow (1970) pp. 202-207.

[194] D. Xu, W. Long, X. Zhou, Microstructure and corrosion resistance of $Al_3(Zr, Ti)/Al$ composite prepared by powder metallurgy, Adv. Compos. Lett., 29 (2020) 1-9.

[195] D. Li, Y. Liu, X. Wan, Thermal Stability of Titanium Alloys. I. Electron Concentration Rule for Formation of the Ti_3X Phase, Acta Metall. Sin. (China), 20 (1984) A375-A383.

[196] N. I. Shirokova, T. T. Nartova, I. I. Kornilov, Investigation of the Phase Equilibrium and Properties of Ti-Zr-Al Alloys, Russ. Metall. (Engl. Transl.), 1968 (1968) 115-117.

[197] J. P. Gros, I. Ansara, M. Allibert, Prediction of α/β Equilibria in Titanium-Based Alloys Containing Al, Mo, Zr, Cr (Part II), P. Lacombe, R. Tricot, G. Béranger (Eds.), in: 6th World Conference on Titanium, Les Editions de Physique. Les Ulis Cedex, France, Cannes, France (1988) pp. 1559-1564.

[198] Z. X. Deng, D. P. Zhao, Y. Y. Huang, L. L. Chen, H. Zou, Y. Jiang, K. Chang, Ab Initio and CALPHAD-Type Thermodynamic Investigation of the Ti–Al–Zr System, J. Min. Metall., Sect. B, 55 (2019) 427-437.

[199] H. K. C. Kumar, P. Wollants, L. Delaey, Thermodynamic Assessment of the Ti-Zr System and Calculation of the Nb-Ti-Zr Phase diagram J Alloys Compd, 202 (1994) 121-127.

[200] S. I. Park, S. Z. Han, S. K. Choi, H. M. Lee, Phase Equilibria of $Al_3(Ti,V,Zr)$ Intermetallic System, Scr. Mater., 34 (1996) 1697-1704.

[201] G. Ghosh, S. Vaynman, M. Asta, M. E. Fine, Stability and Elastic Properties of $L1_2$-$(Al,Cu)_3(Ti,Zr)$ Phases: Ab Initio Calculations and Experiments, Intermetallics, 15 (2007) 44-54.

[202] Z. Deng, D. Zhao, Y. Huang, L. Chen, H. Zou, Y. Jiang, K. Chang, Ab initio and CALPHAD-type thermodynamic investigation of the Ti-Al-Zr system, J. Min. Metall., Sect. B, (2019) 39-39.

[203] J. Wang, W. Zheng, G. Xu, X. Zeng, Y. Cui, Thermodynamic Assessment of the Ti–Al–Zr System and Atomic Mobility of Its BCC Phase, Calphad, 70 (2020) 101801.

[204] S. J. Kim, R. J. Kematick, S. S. Yi, H. F. Franzen, On the Stabilization of Zr_5Al_3 in the Mn_5Si_3-Type Structure by Interstitial Oxygen, Journal of the Less Common Metals, 137 (1988) 55-59.

[205] Y. U. Kwon, M. A. Rzeznik, A. Guloy, J. D. Corbett, Impurity Stabilization of Phases with the Manganese Silicide (Mn_5Si_3)-Type Structure: Questions Regarding Lanthanum-Tin (La_5Sn_3) and Zirconium Silicide (Zr_5Si_3), Chem. Mater., 2 (1990) 546-550.

[206] S. Banerjee, P. Mukhopadhyay, Phase Transformations: Examples from Titanium and Zirconium Alloys, Elsevier, (2010).

[207] S. Mayer, M. Petersmann, F. D. Fischer, H. Clemens, T. Waitz, T. Antretter, Experimental and Theoretical Evidence of Displacive Martensite in an Intermetallic Mo-containing γ-TiAl Based Alloy, Acta Mater., 115 (2016) 242-249.

[208] D. A. Abreu, A. A. A. P. Silva, J. C. P. Santos, D. F. Barros, C. S. Barros, N. Chaia, C. A. Nunes, G. C. Coelho, Liquidus Projection of the Al–Ti–Zr System, J. Alloys Compd. , 849 (2020) 156463.

[209] S. Neumeier, J. Bresler, C. Zenk, L. Haußmann, A. Stark, F. Pyczak, M. Göken, Partitioning behavior of Nb, Ta, and Zr in fully lamellar γ/α2 titanium aluminides and its effect on the lattice misfit and creep behavior, Adv. Eng. Mater., 23 (2021) 2100156.

[210] T. Kawabata, H. Fukai, O. Izumi, Effect of Ternary Additions on Mechanical Properties of TiAl, Acta Mater., 46 (1998) 2185-2194.

[211] H. A. J. Thomas, R. Stevens, Aluminium Titanate--a Literature Review. II. Engineering Properties and Thermal Stability, Br. Ceram. Trans. J., 88 (1989) 184-190.

[212] H. A. J. Thomas, R. Stevens, Aluminium Titanate: a Literature Review. I: Microcracking Phenomena, Br. Ceram. Trans. , 88 (1989) 144-151.

[213] M. Backhaus-Ricoult, C. Glose, P. Tepesch, B. Wheaton, J. Zimmermann, Aluminum Titanate Composites for Diesel Particulate Filter Applications, in: Ceram. Eng. Sci. Proc., (2010) pp. 147.

[214] C.-H. Chen, H. Awaji, Temperature Dependence of Mechanical Properties of Aluminum Titanate Ceramics, J. Eur. Ceram. Soc., 27 (2007) 13-18.

[215] M. Ilatovskaia, Z. Kahrobaee, N. Omar, M. Palm, L. Schmitt, Y. Yang, L. Dreval, Al-O-Ti Ternary Phase Diagram Evaluation, A. Watson (Ed.) in: Ternary Evaluations, MSI, Materials Science International Services GmbH, Stuttgart (2022) pp. 1-57.

[216] A. Shaaban, H. Nakashima, M. Ueda, M. Takeyama, Effects of Oxygen Addition on the Microstructure, Phase Transformations, and Oxidation Resistance of TiAl Alloys, J Alloys Compd, (2022) 165716.

[217] X. Wu, A. Huang, D. Hu, M. H. Loretto, Oxidation-Induced Embrittlement of TiAl Alloys, Intermetallics, 17 (2009) 540-552.

[218] J. D. Geller, C. Herrington, High Count Rate Electron Probe Microanalysis, J. Res. Nat. Inst. Stand. Technol., 107 (2002) 503.

[219] X. Llovet, A. Moy, P. T. Pinard, J. H. Fournelle, Reprint of: Electron Probe Microanalysis: A Review of Recent Developments and Applications in Materials Science and Engineering, Prog. Mater Sci., 120 (2021) 100818.

[220] H. D. Kessler, W. Rostoker, R. J. Van Thyne, Titanium Phase Diagrams, in: U. S. Wright Air Develop. Centre Rep. (WADC-TR-52-335), Illinios Intitute of Technology (1953) pp. 1-85.

[221] R. J. Van Thyne, H. D. Kessler, Influence of Oxygen, Nitrogen, and Carbon on the phase relationships of the Ti-Al system, JOM, 6 (1954) 193-199.

[222] T. H. Schofield, A.E. Bacon, The Constitution of the Titanium-Rich Alloys of Ti, Al and Oxygen, J. Inst. Met., (1956) 193-195.

[223] I. Kornilov, F. Tavadze, G. Ronami, The Influence of Stabilizing a- and b-Elements on the Position of Phase Boundaries in the Titanium-Aluminium System, Inst. of Metallurgy, Tbilisi, USSR; and others, (1972).

[224] V. V. Vavilova, A. P. Brynza, I. P. Mnuskin, Phase Equilibrium Diagram and Corrosion Resistance of Ti Alloys with Oxygen, in: Stroenie, Svoistva i Premenenie Metallodov, Nauka Moscow, (1972) pp. 163-168.

[225] V. V. Vavilova, A. P. Brynza, I. P. Mnuskin, Phase Diagram and Electrochemical Properties of Alloys of the Ti-Al-O System Russ. J. Appl. Chem., translated from Zhur. Priklad. Khim. , 48 (1975) 1523-1525.

[226] V. V. Glazova, Investigation of Phase Equilibria in the Ternary System, Dokl. Akad. Nauk SSSR, (1965) 567-570.

[227] I. I. Kornilov, V. V. Glazova, Investigation of the Phase Equilibrium of the Ti-Al$_2$O$_3$ System, Russ. Metall. (Engl. Transl.), 1 (1965) 124-128.

[228] I. I. Kornilov, V. V. Glazova, The Physicochemical Nature of Alloys of the System Ti-Al-O, in: Trans. 6th Conf. Met. Ch., Phys. Met, Moscow (1965) pp. 3-10.

[229] A. K. Misra, Reaction Of Ti And Ti-Al Alloys With Alumina, Metall. Trans. A, 22 (1991) 715-721.

[230] H. Inaba, Y. Murata, Analysis of Interface Reactions of TiAl/Al$_2$O$_3$ and TiAl/TiO$_2$ by the Use of Chemical Potential Diagram, J. Ceram. Soc. Jpn., 105 (1997) 740-745.

[231] M.-X. Zhang, K.-C. Hsieh, J. DeKock, Y. A. Chang, Phase Diagram of Ti-Al-O at 1100 °C, Scr. Metall. Mater., 27 (1992) 1361-1366.

[232] S. Choi, F. Van Loo, R. Metselaar, Reactions and Phase Relations in the Ti-Al$_2$O$_3$ System, (1991).

[233] X. L. Li, R. Hillel, F. Teyssandier, S. K. Choi, F. J. J. Van Loo, Reactions and Phase Relations in the TiAlO System, Acta Metall. Mater., 40 (1992) 3149-3157.

[234] W.-C. Lee, B.J. Lee, O.Y. Kwon, C.S. Kang, A Study on the Identification of Interfacial Reaction Product Between Alumina and Titanium, Journal of the Korean Institute of Metals and Materials, 31 (1993) 1121-1131.

[235] G. P. Kelkar, A. H. Carim, Phase Equilibria in the Ti-AI-O System at 945° C and Analysis of Ti/Al$_2$O$_3$ Reactions, J. Am. Ceram. Soc. , 78 (1995) 572-576.

[236] O. Fabrichnaya, P. Perrot, S. Lakiza, P. Rogl, Al-O Binary Phase Diagram Evaluation, in: MSI Eureka, Effenberg, G. (Ed.) by MSI, Materials Science International Services GmbH, Stuttgart, (2013) pp. 1-21.

[237] B. Hallstedt, Thermodynamic Calculation of Some Subsystems of the Al-Ca-Mg-Si-O System, J. Phase Equilib., 14 (1993) 662-675.

[238] M. Hampl, R. Schmid-Fetzer, Thermodynamic Description of the Ti–O System, Int. J. Mater. Res., 106 (2015) 439-453.

[239] Z. Cao, W. Xie, I.-H. Jung, G. Du, Z. Qiao, Critical Evaluation and Thermodynamic Optimization of the Ti-CO System and Its Applications to Carbothermic TiO_2 Reduction Process, Metall. Mater. Trans. B, 46 (2015) 1782-1801.

[240] M. Ilatovskaia, G. Savinykh, O. Fabrichnaya, Thermodynamic Description of the Ti-Al-O System Based on Experimental Data, J. Phase Equilib. Diffus., 38 (2017) 175-184.

[241] E. S. Zhmudï, A. E. Shmelev, X-Ray Phase Investigation of the Reaction of Titanium with Aluminum Oxide (in English) Translated from Izv. Akad. Nauk SSSR, Neorg. Mater., Inorg. Mater., 9 (1973) 1543-1546.

[242] Y. Wei, H.-B. Zhou, Y. Zhang, G.-H. Lu, H. Xu, Effects of O in a Binary-Phase TiAl–Ti_3Al Alloy: From Site Occupancy to Interfacial Energetics, J. Phys.: Condens. Matter, 23 (2011) 225504.

[243] C. Y. Jones, W. E. Luecke, E. Copland, Neutron Diffraction Study of Oxygen Dissolution in α_2-Ti_3Al, Intermetallics, 14 (2006) 54-60.

[244] E. N. Bunting, Phase Equilibria in the Systems TiO_2, TiO_2–SiO_2, and TiO_2–Al_2O_3, Bur. Standards J. Research, 11 (1933) 719-725.

[245] S. M. Lang, C. L. Fillmore, L. H. Maxwell, The Phase Diagram of the Al_2O_3: TiO_2 System, J. Res. NBS (US), 48 (1952) 298-312.

[246] S. Azimov, Aluminum Titanate Made in a Solar Furnace, Izvestiya Akademii Nauk SSSR, Neorganicheskie Materialy, 20 (1984) 469-471.

[247] E. Kato, K. Daimon, J. Takahashi, Decomposition Temperature of β-Al_2TiO_5, J. Am. Ceram. Soc., 63 (1980) 355-356.

[248] I. M. Low, Z. Oo, In Situ Diffraction Study of Self-Recovery in Aluminum Titanate, J. Am. Ceram. Soc.   , 91 (2008) 1027-1029.

[249] A. Austin, C. Schwartz, The Crystal Structure of Aluminium Titanate, Acta Crystallogr., 6 (1953) 812-813.

[250] D. D. Gulamova, M. Sarkisova, Reaction of Aluminium and Titanium Oxides at High Temperatures, Inorg. Mater., 25 (1989) 671-676.

[251] S. T. Norberg, N. Ishizawa, S. Hoffmann, M. Yoshimura, Redetermination of β-Al_2TiO_5 obtained by melt casting, Acta Crystallogr., Sect. E: Struct. Rep. Online, 61 (2005) i160-i162.

[252] M.-H. Berger, A. Sayir, Directional Solidification of Al_2O_3–Al_2TiO_5 System, J. Eur. Ceram. Soc., 28 (2008) 2411-2419.

[253] L. Mazerolles, V. Bianchi, D. Michel, Intergrowth between Pseudobrookite and Related Phases, C. Nichita, Mori, H., Humphreys, C. J., Tanaka, N., Van Tendeloo, G. (Eds.), in: ICEM-13, 13th International Congress on Electron Microscopy, Vol. 2B, (1994) pp. 905-906.

[254] S. Hoffmann, S. T. Norberg, M. Yoshimura, Structural Models for Intergrowth Structures in the Phase System Al_2O_3-TiO_2 J. Solid State Chem.   , 178 (2005).

[255] O. Monnereau, F. Remy, A. Casalot, Partial Phase Diagram for the TiO_2-Ti_2O_3-Al_2O_3 System at 1223 K and Preparation of a New Double Oxide of Formula $Al_2Ti_7O_{15}$ Compt. Rend. Acad. Sci. Paris, Ser. 2, 301 (1985) 375-378.

[256] F. Remy, O. Monnereau, A. Casalot, F. Dahan, J. Galy, Titane à valence mixte, un nouvel oxyde ternaire: $Al_2Ti_7O_{15}$, J. Solid State Chem., 76 (1988) 167-177.

[257] G. M. Asbrink, A, X-Ray Studies on Some Mixed Oxide Systems of Pseudobrookite Structure, Acta Chem. Scand., 21 (1967).

[258] D. Goldberg, Systems Formed by Alumina with Some Trivalent and Tetravalent Metal Oxides in Particular, Titanium Oxide, ev. Int. Hautes Temp. Refract., (1968) 181-194.

[259] M. Kunugi, A. Konishi, S. Fukutani, Reduction of Aluminium Titanate, J. Soc. Mater. Sci. Jpn., 41 (1966) 517-520.

[260] T. Sperisen, A. Mocellin, On Structures of Mixed Titanium Aluminium Oxides, J. Mater. Sci. Lett., 10 (1991) 831-833.

[261] N. Zheng, W. Fischer, H. Grübmeier, W. J. Quadakkers, V. Shemet, The Significance of Sub-Surface Depletion Layer Composition for the Oxidation Behavior of Y-Titanium Aluminides, Scr. Metall. Mater. , 33 (1995).

[262] V. Shemet, P. Karduck, H. Hoven, B. Grushko, W. Fischer, W. Quadakkers, Synthesis of the Cubic Z-Phase in the Ti-Al-O System by a Powder Metallurgical Method, Intermetallics, 5 (1997) 271-280.

[263] Y. Chen, D. J. Young, B. Gleeson, A New Ti-rich Ternary Phase in the Ti-Al-O System, Mater. Lett., 22 (1995) 125-129.

[264] R. Beye, M. Verwerft, J. De Hosson, R. Gronsky, Oxidation Subscale of γ-Titanium Aluminide, Acta Mater., 44 (1996) 4225-4231.

[265] F. Dettenwanger, E. Schumann, J. Rakowski, G.H. Meier, M. Rühle Development and Microstructure of the Al-depleted Layer of Oxidized TiAl, Mater. Corr., 48 (1996) 23-27.

[266] C. Lang, M. Schütze, The Initial Stages in the Oxidation of TiAl, Mater. Corros., 48 (1997) 13-22.

[267] A. Kussmaul, H.-J. Seifert, J. A. Golczewski, H. L. Lukas, F. Aldinger, Thermodynamic Calculation of Diffusion Paths Applied to the Oxidation of γ-TiAl, Int. J. Mater. Res., 89 (1998) 683-686.

[268] E. Copland, B. Gleeson, D. Young, Formation of Z-$Ti_{50}Al_{30}O_{20}$ in the Sub-Oxide Zones of γ-TiAl-Based Alloys During Oxidation at 1000 °C, Acta Mater., 47 (1999) 2937-2949.

[269] L. Singheiser, L. Niewolak, V. Shemet, W. J. Quadakkers, U. Flesch, Fundamental Considerations for the Development of Oxidation-Resistant Alloys and Coatings Based on γ-TiAl, Metall. Mater. Trans. A, 34 (2003) 2247-2251.

[270] Y. F. Cheng, F. Dettenwanger, J. Mayer, E. Schumann, M. Rühle, Identification of a New Phase Formed During the Oxidation of Y-Titanium Aluminum, Scr. Mater., 34 (1996).

[271] N. H. Gunda, A. Van der Ven, Understanding the Interactions Between Interstitial and Substitutional Solutes in Refractory Alloys: The Case of Ti-Al-O, Acta Mater., 191 (2020) 149-157.

[272] S. Anderson, The Crystal Structure of the So-Called Alpha-Titanium Oxide and Its Structural Relation to the Omega-Phases of Some Binary Alloy Systems of Titanium, Acta Chem. Scand., 13 (1959) 415-419.

[273] E. Hilti, F. Laves, Röntgenographische Untersuchung der Titanmonoxid-Tieftemperatur-Modifikation, Naturwissenschaften, 55 (1968) 131-131.

[274] M. E. Straumanis, H. W. Li, Lattice Constants, Expansion, Coefficients, Densities, Defects, and Structure of the Titanium (II) Oxide Phase, Z. anorg. u. allgem. Chem., 305 (1960).

[275] W. R. Robinson, The Crystal Structures of Ti_2O_3, a Semiconductor, and $(Ti_{0.900}V_{0.100})_2O_3$, a Semimetal, J. Solid State Chem., 9 (1974) 255-260.

[276] C. Howard, T. Sabine, F. Dickson, Structural and thermal parameters for rutile and anatase, Acta Crystallogr., Sect. B: Struct. Sci 47 (1991) 462-468.

[277] S. K. Panda, I.-H. Jung, Coupled Experimental Study and Thermodynamic Modeling of the Al_2O_3–Ti_2O_3–TiO_2 System, ISIJ International, 60 (2020) 31-41.

[278] H. T. Nakashima, M. , Revised Phase Diagram for the Ti-Al-O Ternary System from 35 to 55 at.% Aluminum, M. Heilmaier, Krüger, M., Palm, M., Pyczak, F., Stein, F., (Eds.), in: Intermetallics 2021, Conventus Congressmanagement & Marketing GmbH, Jena, Germany (2021).

[279] J. Kivilahti, E. Heikinheimo, On the Thermodynamics and Microstructural Evolution of the Ti/Al_2O_3 Diffusion Couple, in: Joining Ceramics, Glass and Metal Int. Conf. Bad Nauheim, (1989) pp. 131-138.

[280] A. Menand, A. Huguet, A. Nérac-Partaix, Interstitial Solubility in γ and α$_2$ Phases of TiAl-Based Alloys, Acta Mater., 44 (1996) 4729-4737.

[281] H. J. Seifert, A. Kussmaul, F. Aldinger, Phase Equilibria and Diffusion Paths in the Ti–Al–O–N System, J Alloys Compd, 317 (2001) 19-25.

[282] A. Rahmel, P. J. Spencer, Thermodynamic Aspects of TiAl and $TiSi_2$ Oxidation: The Al-Ti-O and Si-Ti-O Phase Diagrams, Oxid. Met., 35 (1991) 53-68.

[283] S. Becker, A. Rahmel, M. Schorr, M. Schütze, Mechanism of Isothermal Oxidation of the Intel-Metallic TiAl and of TiAl Alloys, Oxid. Met., 38 (1992) 425-464.

[284] R. E. Tressler, T. L. Moore, R. L. Crane, Reactivity and Interface Characteristics of Titanium-Alumina Composites, J. Mater. Sci., 8 (1973) 151-161.

[285] K. L. Luthra, Stability of Protective Oxide Films on Ti-Base Alloys, Oxid. Met., 36 (1991) 475-490.

[286] J. I. Goldstein, S. K. Choi, F. J. J. Van Loo, H. J. M. Heijligers, G. F. Bastin, W. G. Sloof, The Influence of Oxide Surface Layers on Bulk Electron Probe Microanalysis of Oxygen—Application to Ti-Si-O Compounds, Scanning, 15 (1993) 165-170.

[287] S. J. B. Reed, Electron Microprobe Analysis and Scanning Electron Microscopy in Geology, Cambridge university press, (2005).

[288] M. Herbig, A. Kumar, Removal of Hydrocarbon Contamination and Oxide Films from Atom Probe Specimens, Microsc. Res. Tech., 84 (2021) 291-297.

[289] K. Stiller, L. Viskari, G. Sundell, F. Liu, M. Thuvander, H.-O. Andrén, D. J. Larson, T. Prosa, D. Reinhard, Atom probe tomography of oxide scales, Oxid. Met., 79 (2013) 227-238.

[290] H. Nakashima, A. Kinouchi, M. Takeyama, Quantitative Analysis of Oxygen in Solution in the Ti-Al-O Ternary Alloys by Soft X-Ray Emission Spectroscopy, J Alloys Compd, (2022) 165822.

[291] A. Moy, J. Fournelle, ϕ (ρz) Distributions in Bulk and Thin-Film Samples for EPMA. Part 2: Badgerfilm: A New Thin-Film Analysis Program, Microsc. Microanal., 27 (2021) 284-296.

Curriculum vitae

Name: Zahra Kahrobaee

Date of Birth: 28.09.1992

Place of Birth: Semnan, Iran

Nationality: Iranian

2022-NOW   **Research Engineer,** OCAS NV**,** ArcelorMittal R&D**,** Gent, Belgium.

2018- 2022   **Research assistant and Ph.D. student,** Max-Planck-Institut für Eisenforschung GmbH (MPIE), department of Structure and Nano- / Micromechanics of Materials, Intermetallic Materials, Düsseldorf, Germany.

Title of Research:

Critical Assessment and Investigation of the Ti-Al-X (X = Si, Zr, O) Systems.

Within the framework of the European research programme Clean Sky 2 the project ADVANCE is devoted to improve an existing CALPHAD database for the development of more creep and corrosion resistant TiAl-based alloys. ADVANCE is a large-scale collaborative project between the partners Helmholtz-Zentrum Hereon, Germany, Montanuniversität Leoben, Austria, MPIE, and Thermo-Calc Software AB, Sweden. As a part of this project, Ti-Al-rich side of the systems Ti–Al–X with X = Si, Zr and O are studied at temperatures ranging between 700-1300 °C. Through wet-chemical analysis, X-ray diffraction (XRD), electron probe microanalysis (EPMA), differential thermal microanalysis (DTA) and transmission electron microscopy (TEM), phase equilibria in the Ti-Al-rich side of the systems were established. All evaluated data are used to establish isothermal sections for each investigated alloy system and additional vertical sections. Besides experimental work, critical assessments of existing data are performed.

2014- 2017   **M.Sc. in Engineering and Material Sciences**, faculty of engineering at Ferdowsi University of Mashhad (FUM), Iran. GPA: 18.01/20 (the equivalent of 1.6 in German academic grading), ranked the 1st among all the participants. Participated in extracurricular research activities.

Title of thesis:

The Effect of Chemical Component on Mechanical Behavior of Dental Composites.

The main purpose of this research was to improve the mechanical properties of glass ionomer cements (GIC) with specific attention to the chemical composition of glass particles. The base

143

chemical composition which was used in this research was SiO_2-Al_2O_3-P_2O_5-CaO-xZnO. The tests such as Fourier-transform infrared spectroscopy (FTIR), differential thermal analysis (DTA), Raman spectroscopy, Vickers micro hardness (VH), diametral tensile strength (DTS), and fractographic investigation using scanning electron microscopy (SEM) are conducted to evaluate the properties of produced GIC. Moreover, the statistical reliability is calculated using ANOVA and Weibull modulus-m.

2010-2014 **B.Sc. in Engineering and Material Sciences**. Specialization in industrial metallurgy, faculty of engineering at Ferdowsi University of Mashhad (FUM), Iran. GPA: 15.55/20 (the equivalent of 2.34 in German academic grading).

Title of thesis:

An Investigation on Diffusion Bonding of St37 Steel and Gray Cast Iron.

In this study, gray cast iron is welded to St37 steel using diffusion bonding. The achieved joint is investigated using optical microscopy and Vickers micro hardness.

2006-2010 **High School Education on Mathematical Sciences**. Mashhad, Iran. GPA: 19.8/20 (the equivalent of 1.06 in German academic grading).

PROFESSIONAL EXPERIENCE

2022- NOW Working as research engineer at OCAS NV, ArcelorMittal R&D, Gent, Belgium.

2013- 2014 Teaching assistant of two B.Sc. programs in physical chemistry at:

- Ferdowsi University of Mashhad under supervision of Professor Dr.Mehrdad Kashefi.

- Sadjjad University of Technology under supervision of Dr. Saeed Kahrobaee.

2010-2011 Tutoring high school students in mathematics, algebra, chemistry and physics in preparation for entrance exam of universities.

PUBLICATIONS

Talks **Kahrobaee, Z.**; Palm, M.: Determination of phase equilibria in the Ti–Al–Si system at 800–1200 °C, Intermetallics 2021, Bad Staffelstein, Germany, October 04, 2021 - October 08, 2021. (2021)

Kahrobaee, Z.; Stein, F.; Palm, M.: Experimental investigation of phase equilibria in the Ti-Al-Zr system for improvement of a CALPHAD database. 17th Discussion Meeting on Thermodynamics of Alloys (TOFA). Bad Staffelstein, Germany (2020).

Kahrobaee, Z.; Palm, M, ADVANCEs in TiAl based alloy systems - Experimental investigation of phase equilibria in the Ti-Al-Si system at high temperatures. Annual meeting of the technical committee "Intermetallic Phases" of the German Materials Society DGM (2020).

Stein, F.; Distl, B.; **Kahrobaee, Z**.; Palm, M.; Hauschildt, K.; Rackel, M.W.; Pyczak, F.; Mayer, S.; Yang, Y.; Chen, H.-L.; Engström, A.; Improvement of a CALPHAD database for the

development of next generation TiAl alloys by targeted key experiments on high-temperature phase equilibria – The EU project ADVANCE, 149th TMS Annual Meeting & Exhibition, San Diego, California, USA (2020).

Distl, B.; **Kahrobaee, Z.**; Palm, M.; Stein, F.: ADVANCE – New Experimental Data on Ti–Al–X (X = Nb, Mo, W, Zr, Si, B, C, O) Systems to Develop an Improved CALPHAD Database for Next Generation Ti–Al Alloys. French-German Workshop of the DGM Fachausschuss Thermodynamik, Kinetik und Konstitution der Werkstoffe, ICMPE-CNRS-Paris Est, Thiais, France (2019).

Palm, M.; Distl, B.; **Kahrobaee, Z.**; Stein, F.; Mayer, S.; Hauschildt, K.; Rackel, M.; Pyczak, F.; Yang, Y.; Chen, H.-L. et al.: ADVANCE - Advancing a CALPHAD Database for Next Generation TiAl Alloys. 65th Metal Research Colloquium organized by the Department for Metal Research and Materials Testing of the University Leoben, Lech am Arlberg, Austria (2019).

Poster

Kahrobaee, Z.; Stein, F.; Palm, M.: Experimental evaluation of the isothermal section of the Ti–Al–Zr ternary system at 1273 K. Intermetallics 2019, Bad Staffelstein, Germany, September 30, 2019 - October 04, 2019.

Kahrobaee, Z., Mollazadeh, S., Mazinani, M.: Presenting two posters; Investigation of Chemical Components on Mechanical Properties of GICs Reinforced with Aluminosilicate Glass, and Investigation of ZnO on Properties of Aluminosilicate Glass. 6th International Conference & Exhibition on Metallurgy and Materials Engineering, Tehran, Iran, 28-29 October 2017.

Conference paper

Kahrobaee, Z.; Palm, M.: Determination of phase equilibria in the Ti–Al–Si system at 800–1200 °C. In: Proceedings Intermetallics 2021, pp. 78 - 79. Intermetallics 2021, Bad Staffelstein, Germany, October 04, 2021 - October 08, 2021. (2021)

Kahrobaee, Z.; Stein, F.; Palm, M.: Experimental investigation of phase equilibria in the Ti-Al-Zr system for improvement of a CALPHAD database. 17th Discussion Meeting on Thermodynamics of Alloys (TOFA), Bad Staffelstein, Germany, September 28, 2020 - October 02, 2020.

Kahrobaee, Z.; Stein, F.; Palm, M.: Experimental evaluation of the isothermal section of the Ti–Al–Zr ternary system at 1273 K. In: Proceedings Intermetallics 2019, pp. 174 - 175. Intermetallics 2019, Bad Staffelstein, Germany, September 30, 2019 - October 04, 2019.

Journal articles

Kahrobaee, Z.; Rashkova, B., Hauschildt, K., Palm, M.: Experimental Investigation of Phase Equilibria in the Ti–Al–Zr system at 1000-1300 ° C, Crystals 12, pp. 1184 (2022).

145

Kahrobaee, Z.; Palm, M.: Experimental Investigation of Ti–Al–Si Phase Equilibria at 800-1200 °C. Journal of Alloys and Compounds 924, 166223 (2022).

M. Ilatovskaia, **Z. Kahrobaee**, N. A. B. Omar, M. Palm, L.-Y. Schmitt, Yang Yang, L. Dreval: Al–O–Ti Ternary Phase Diagram Evaluation, MSI Eureka, Watson, A. (Ed.) by MSI, Materials Science International Services GmbH, Stuttgart.

Kahrobaee, Z.; Palm, M.: Critical Assessment of the Al–Ti–Zr System. Journal of Phase Equilibria and Diffusion 41, pp. 687 - 701 (2020).